Université de Montréal

Regulation of replication dependent nucleosome assembly

Par

Amogh Gopinathan Nair

Département de biologie moléculaire

Institut de Recherche en Immunologie et en Cancérologie (IRIC)

Faculté de Médecine

Thèse présentée à la Faculté des médecine en vue de l'obtention du grade de

Ph.D. en biologie moléculaire option biologie des systems

April 2021

Résumé de thèse

Chez les cellules humaines, environ 2 mètres d'ADN est compacté dans le noyau cellulaire par la formation d'une structure nucléoprotéique appelée chromatine. La chromatine est composée d'ADN enroulé à la surface d'un octamère de core histones pour former une structure appelée nucléosome. La structure de la chromatine doit être altérée afin d'accéder à l'information génétique pour sa réplication, sa réparation et sa transcription. La duplication de la chromatine lors de la phase S est cruciale pour la prolifération et la survie des cellules. Cette duplication de la chromatine requière une ségrégation des histones parentales, mais aussi une déposition d'histones néo-synthétisées sur l'ADN. Ces deux réactions résultent en formation de chromatine dès qu'une quantité suffisante d'ADNest générée par la machinerie de réplication. De plus, en raison de conditions intrinsèques et extrinsèques, la machinerie de réplication est souvent confrontée à de nombreux obstacles, sous la forme de lésions à l'ADN qui interfèrent avec la réplication de l'ADN. Sous ces conditions, l'assemblage de nucléosomes et la synthèse d'histones sont étroitement régulées afin d'éviter la production d'un excès d'histones et leurs nombreuses conséquences nuisibles à la cellule.

"Chromatin Assembly Factor 1" (CAF-1) est responsable de la déposition initiale des molécules d'H3 et H4 derrière les fourches de réplication. Pour permettre sa fonction d'assemblage de chromatine, CAF-1 est localisée aux fourches de réplication en vertue de sa liaison à une protéine appelée Proliferating Cell Nuclear Antigen (PCNA). Cependant, le mécanisme moléculaire par lequel CAF-1 exerce sa function demeure mal compris.

Dans le deuxième chapitre de ma thèse, j'ai exploré comment CAF-1 se lie à PCNA d'une manière distincte des nombreux autres partenaires de PCNA. Grâce à nos collaborateurs, des études de crystallographie ont démontré que CAF-1 se lie à PCNA grâce à une interaction non-canonique entre le "PCNA Interaction Peptide" (PIP) de CAF-1 et une interaction de type cation-pi (π). Nous avons aussi montré qu'une substitution d'un seul acide aminé, unique au PIP de CAF-1, abolit son interaction avec PCNA et sa capacité d'assemblage de nuclésomes. Nous avons aussi montré que le PIP de CAF-1 est situé à l'extrémité C-terminale d'une très longue hélice alpha qui est conservée à travers l'évolution parmi de nombreux homologues de CAF-1. Nos études biophysiques ont

montré que cette longue hélice alpha forme des structures oligomériques de type "coiled-coil", ce qui suggère certains mécanismes pour dédier un anneau de PCNA à l'assemblage de chromatine et ce, en dépit des nombreux intéracteurs de PCNA présents aux fourches de réplication.

Dans le troisième chapitre de ma thèse, nos collaborateurs et moi-même avons étudié les mécanismes moléculaires par lesquels les cellules parviennent à maintenir un équilibre délicat entre la synthèse d'ADN et la synthèse d'histones et ce, même en présence de lésions à l'ADN qui interfèrent avec la réplication. Chez *Saccharomyces cerevisiae*, nous avons montré que les kinases de réponse au dommage à l'ADN, Mec1/Tel1 et Rad53, inhibent la transcription des gènes d'histones en réponse aux liaisons à l'ADN qui interfèrent avec la réplication. Nous avons montré que la répression des gènes d'histones induite par le dommage à l'ADN est médiée par une phosphorylation extensive de Hpc2, l'une des sous-unités du complexe "Histone Gene Repressor" (HIR). Hpc2 contient un domaine qui se lie à l'histone H3. À partir de la structure d'Hpc2, nous avons généré des mutants qui, d'après la structure, sont incapables de se lier à l'histone H3. Nos résultats montrent que l'accumulation d'histones en excès provoquée par le dommage à l'ADN entraîne la phosphorylation d'Hpc2 and la liaison de l'excès d'histone H3 à Hpc2. Ces résultats suggèrent que la répression transcriptionnelle des gènes d'histones induite par le dommage à l'ADN est médiée, du moins en partie, par une simple rétroaction négative impliquant la liaison des histones en excès à la sous-unité Hpc2 du complexe HIR.

Mots clés : réplication de l'ADN, dommages à l'ADN, nucléosome, histone, assemblage de la chromatine, facteur d'assemblage de la chromatine 1 (CAF-1), antigène nucléaire cellulaire proliférant (PCNA), histones, dommages à l'ADN, complexe HIR, Hpc2, répression du gène des histones

Thesis summary

In human cells, roughly 2 meters of DNA is compacted into the cell nucleus by the formation of a nucleoprotein complex called chromatin. Chromatin is composed of DNA wrapped around an octamer of core histones to form so-called nucleosomes. Chromatin structure needs to be altered to access genetic information for processes like replication, repair and transcription. Duplication of chromatin during S phase is vital for cell proliferation and viability. Chromatin duplication requires segregation of parental histones, but also deposition of newly synthesized histones onto DNA. This process results in packaging all of the synthesized DNA with histones to form nucleosomes as soon as enough nascent DNA has emerged from the replication machinery. Moreover, as a result of intrinsic and extrinsic conditions, the replication machinery often encounters DNA lesions that impede the continuous synthesis of DNA. Under these conditions, nucleosome assembly and histone synthesis are tightly regulated to prevent the production of an excess of histone proteins and their deleterious consequences.

Chromatin Assembly Factor-1 (CAF-1) performs the initial step in chromatin assembly by depositing newly synthesized histone H3-H4 molecules behind replication forks. In order to perform its chromatin assembly function, CAF-1 localizes to DNA replication forks by binding directly to a protein known as the Proliferating Cell Nuclear Antigen (PCNA). However, the exact molecular mechanism by which this is achieved remains poorly understood.

Through the second chapter of my thesis, I have explored how CAF-1 binds PCNA in a manner that is distinct from the numerous other binding partners of PCNA. With the help of our collaborators, crystallographic studies demonstrated that CAF-1 binds to PCNA by virtue of a non-canonical PCNA interaction peptide (PIP) and a cation-pi (π) interaction. We have also shown that a single amino acid substitution, unique to the PIP of CAF-1, disrupts its binding to PCNA and chromatin assembly activity. We found that the CAF-1 p150 PIP resides at the extreme C-terminus of a long alpha helix that is evolutionarily conserved among numerous homologues of CAF-1. Our biophysical studies showed that this long alpha-helix is capable of forming higher-order coiled coils, which suggests

mechanisms to dedicate one PCNA ring for chromatin assembly despite the presence of multiple PCNA interactors at replication forks.

In the third chapter of this thesis, our collaborators and I have addressed the crucial molecular mechanisms by which cells maintain a delicate balance between DNA and histone synthesis despite the presence of DNA lesions that interfere with replication. In *Saccharomyces cerevisiae*, we showed that the DNA damage response kinases Mec1/Tel1 and Rad53 inhibit histone gene transcription when DNA lesions block DNA replication. We also showed that this repression is mediated by phosphorylation of the Hpc2 subunit of the Histone Gene Repressor complex (HIR). Hpc2 contains a domain that directly binds to histone H3. Interestingly, structure-based mutants of Hpc2 predicted to be incapable of binding H3 are defective in DNA damage-induced transcriptional repression of histone genes in response to DNA damage during replication. Our results indicate that the accumulation of excess histones caused by DNA damage during S phase triggers extensive phosphorylation of Hpc2 and binding of excess H3 to Hpc2. This suggests that DNA damage-induced repression of histone genes is mediated, at least in part, by a simple negative feedback triggered by binding of excess histones to the Hpc2 subunit of the HIR complex.

Keywords: DNA replication, DNA damage, nucleosome, histone, chromatin assembly, Chromatin Assembly Factor 1 (CAF-1), Proliferating Cell Nuclear Antigen (PCNA), histones, DNA damage, HIR complex, Hpc2, histone gene repression

Table of contents

List of figures

Chapter 1: General Introduction

Chapter 2:

Supplementary figures

Chapter 3:

Supplementary figures

Chapter 4:

List of tables

Chapter 2:

Chapter 3:

List of abbreviations

µg- Microgram

µl- Microliter

3-MeA- 3-methyl adenine

Å- Angstrom

ACN- Acetonitrile

AEBSF- 4-(2-Aminoethyl)benzene-1-sulfonyl fluoride

AMKL-DS- acute megakaryocytic leukemia with down syndrome

AML- Acute myeloid leukemia

ARS- Autonomously Replicating Sequences

ASF1- Anti-Silencing Factor 1

BER- Base Excision Repair

BSA- Bovine serum albumin

CAF-1- Chromatin Assembly Factor 1

CD- Circular dichroism

CDK- Cyclin-Dependent Kinase

ChIP- Chromatin immunoprecipitation

DAPI- 4′,6-diamidino-2-phenylindole

DDK- Dbf4-Dependent Kinase

DDR- DNA damage response

DNA- Deoxyribonucleic acid

dNTPs- deoxyribonucleoside triphosphates

DTT- Dithiothreitol

EDTA- Ethylenediaminetetraacetic acid

EGF- epidermal growth factor

FA- formic acid

FACT- FAcilitates Chromatin Transcription

FEN1- Flap ENdonuclease 1

FHA- Fork head-associated

GINS- Go-Ichi-Ni-San

GSH- Glutathione

HIR- Histone regulatory

HIRA-Histone repressor complex

HP1- Heterochromatin binding Protein 1

Hpc2- Histone periodic control

HRD- Hpc2-Related Domain

HU- Hydroxyurea

IDCL- Interdomain connecting loop

IPTG- Isopropyl β-D-1-thiogalactopyranoside

ITC- Isothermal titration calorimetry

kDa- Kilo Dalton

MALS- Multi-angle light scattering

MBF- MluI binding factor

MCM- Minichromosome maintenance

mM- millimolar

M-MLV- Moloney Murine Leukemia Virus

M-Molar

MMR- Mismatch repair

MMS- Methyl Methane Sulphonate

MRM- Multiple reaction monitoring

MWCO- Molecular weight cut-off

NaCl- Sodium chloride

NEG- Negative regulatory element

NER- Nucleotide Excision Repair

nm- Nanometer

nM- Nanomolar

NMR- Nuclear magnetic resonance

NuRD- nucleosome remodeling and deacetylase complex

ORC- Origin Recognition Complex

P(r)- particle distribution function

PAGE- Polyacrylamide gel electrophoresis

PBD- PCNA binding domain

PBS- Phosphate buffered saline

PCNA- Proliferating Cell Nuclear Antigen

PIP- PCNA Interaction Peptide

qRT-PCR- quantitative reverse transcriptase PCR

RFC- Replication factor C

Rg- Radius of gyration

RNR- Ribonucleotide reductase

RPA- Replication protein A

RT- Reverse Transcriptase

SAXS- Small-angle X-ray scattering

SBF- SCF binding factor

SDS- Sodium dodecyl sulfate

SEC- Size exclusion chromatography

TCEP- Tris(2-carboxyethyl)phosphine

TEV- Tobacco Etch Virus

TFA- trifluoroacetic acid

UAS- Upstream Activating Sequences

WD40- tryptophan-aspartic acid dipeptide

WHD- Winged helix domain

Acknowledgements

Several people have made significant contributions to my Ph.D. studies including my supervisor, family, and friends. First of all, I would like to sincerely thank my Ph.D. supervisor Dr. Alain Verreault for providing me with the opportunity to conduct research in his lab on outstanding projects. He has been a wonderful teacher and an understanding mentor. He has been very supportive throughout my studies with his advice and motivation through helpful scientific discussions.

I would like to extend my thanks to my Ph.D. committee members Dr. Lea Harrington, Dr. Jim Omichinski and Dr. Rodrigo Reyes for providing constructive comments during committee meetings. I owe my sincere thanks to Dr. Katherine Borden and Dr. Mike Osborne and Dr. Pierre Thibault lab for all their help during my project.

I am grateful to all the past and present members of the Verreault lab for providing me with help when it was necessary. I would like to specially thank Dr Roshan Elizabeth for all her help and support. I would also like to thank the FESP, UdeM, IRIC for their scholarships and SICI tuition fee exemption. I am thankful to the academic affairs staff for their timely assistance and support especially to Dr. Julie Mantovani, Dr. Sebastian Carreno, Dr. Richard Bertrand, and Pascale Le Therizien.

I deeply thank my parents Gopinathan Nair and Geetha Rani and my sister Anagha Adarsh for their constant encouragement to pursue my goals in life. I would like to specially thank my wife Devi Venugopal and my daughter Advika Nair for all their prayers, sacrifices, and continuous encouragement that helped me get through this successfully. Above all, I thank God for everything.

Chapter 1: General Introduction

1. Cell proliferation and DNA replication

"*Omnis cellula e cellula*" - this famous dictum in cell theory introduced by Rudolf Virchow in 1855 is translated as "All cells arise only from pre-existing cells." Though historians dispute and attribute the original observation of "cells originate by the division of pre-existing cells" to Robert Remak, it is now clear that one of the easiest and sustainable ways to produce a living cell is by dividing a pre-existing mother cell into two daughters (Bagot and Arya, 2008).

For a mitotic mother cell to produce two daughter cells, the mother cell's entire genome must be duplicated with high fidelity during S phase. During prophase, the duplicated chromosomes condense with the help of DNA binding proteins known as condensins. During prometaphase, the pairs of sister chromatids that constitute each duplicated chromosome are attached, via their centromeres, to microtubules that are part of the mitotic spindle. At the start of metaphase, the chromosomes align at the equatorial plate that separates the two daughter cells. During the metaphase to anaphase transition, sister chromatids separate by enzymatic breakdown of cohesin and then move in opposite directions to reach the two daughter cells. Telophase entails disassembly of the mitotic spindle, chromosome decondensation and, in organisms with open mitoses (*e.g.* human cells), reassembly of the nuclear envelope around the chromosomes. This is not the case in *S. cerevisiae* where mitosis is closed. In other words, the nuclear membrane is not disassembled at the onset of mitosis. Telophase also includes a process known as cytokinesis, which physically separates the mother cell into two daughter cells by forming a cleavage furrow. Cytokinesis, results in the completion of cell division.

In short, duplication of genomic material through DNA replication is essential for cell proliferation and viability. Hence, it is imperative that the genome copying mechanism be fast, efficient, and error-free. This is achieved in part by the concerted action of multiple enzymes, which form an elaborate DNA replication machinery that will be introduced in section 1.2.1 and section 1.2.2. Defects in DNA replication can either result in daughter cells that are not viable or cells that are viable but carry detrimental mutations. In this thesis, I will be introducing the well-known players of the finely tuned orchestral machinery that promotes eukaryotic DNA replication.

1.1 The DNA replication machinery: Nature's own accurate photocopier of genetic information

As mentioned above, DNA replication is a fundamental biological process where eukaryotic cells in S phase duplicate their entire genome and recreate the pre-existing chromatin structures present in G1 onto nascent sister chromatids [Figure I.1]. To achieve this, cells must perform DNA replication and chromatin assembly onto nascent DNA with high fidelity. Multiple cellular machineries exist to ensure that the entire genome is replicated only once per cell cycle, and there is no incomplete replication of any genomic region. DNA replication also creates an opportunity to assemble the newly replicated DNA into chromatin and transfer the epigenetic information on pre-existing histones faithfully from parental cells to daughter cells.

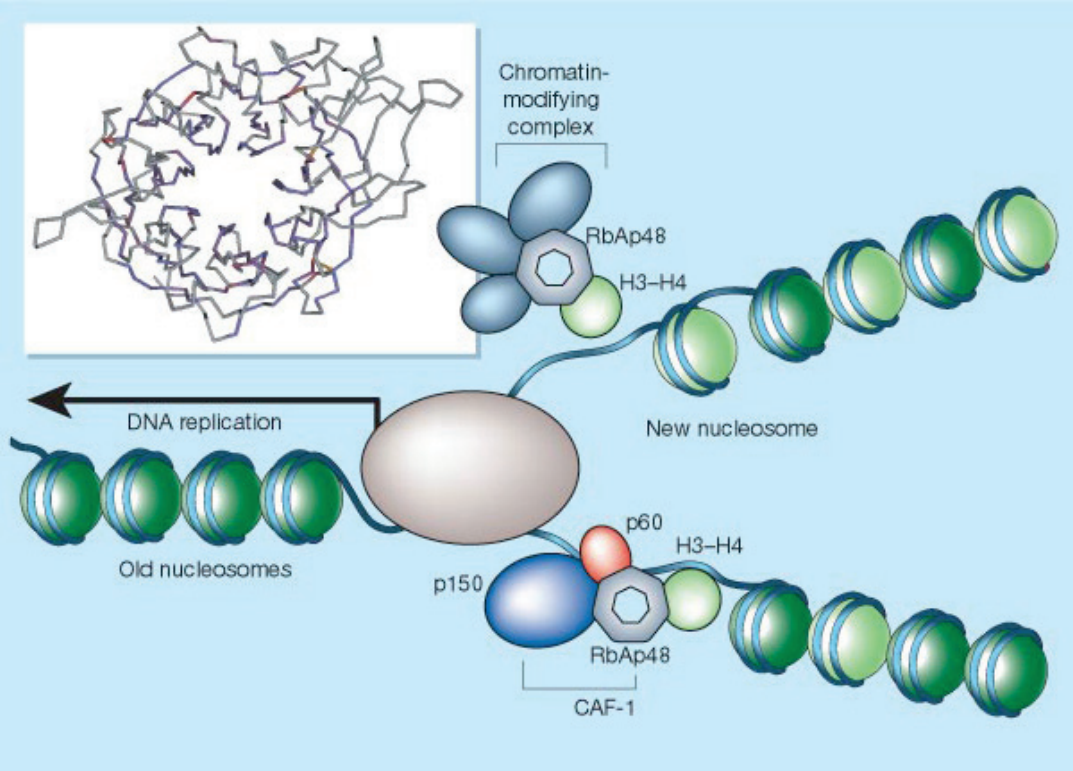

Figure I.1 Schematic representation of chromatin changes that occur during DNA replication (Figure reused with permission from Dr. Michael Buratovich - beyondthedish.wordpress.com). Newly synthesized histones (light green in picture) are deposited rapidly behind replication forks as soon as enough DNA has emerged from the replisome to allow the formation of nucleosome core particles. CAF-1- the only known replication coupled chromatin assembly factor consisting of p150, p60 and RbAp48 subunits are also depicted in the schematic.

The concerted firing of multiple replication origins ensures rapid and efficient duplication of the eukaryotic genome. Cells have also evolved multiple mechanisms to prevent re-replication.

The process of DNA replication occurs in a stepwise fashion.

1) Assembly of *pre-replication* (pre-RCs) and *pre-initiation* complexes (pre-ICs) at replication origins.
2) Origin firing (unwinding of DNA duplex), synthesis of RNA-DNA primers and elongation of DNA synthesis.
3) Replication termination which is poorly understood and not relevant to this thesis.

Termination of DNA replication will not be discussed in this introduction.

1.2 Protein complexes that assemble onto origins of DNA replication

Eukaryotic cells initiate DNA replication at multiple chromosomal locations known as *origins of DNA replication*. *S. cerevisiae* origins consist of consensus *cis*-acting elements known as Autonomously Replicating Sequences (ARS). ARS are recognized in a sequence-specific manner by the Origin Recognition Complex (ORC), which consists of 6 polypeptide subunits known as Orc1 to Orc6 [Figure I.2A, step 1] (Bell and Stillman, 1992). ORC bound to ARS in turn recruits Cdc6, Cdt1 to generate *pre-replication* complexes (pre-RCs). This is followed by recruitment of the MCM DNA helicase [Figure I.2A, steps 1 and 2]. The MCM DNA helicase is a complex that contains six polypeptide subunits known as Mcm2 to Mcm7. These 6 subunits assemble into hexamers and a double hexamer is symmetrically formed around double-stranded DNA. The DNA unwinding activity of the MCM complex is however not active at this stage. Further events are necessary to initiate DNA unwinding at ARS elements (origins).

First, the action of two types of protein kinases is required. These two kinases are responsible known as the Dbf4-Dependent Kinase (DDK) and a Cyclin-Dependent Kinase (CDK). CDK and DDK phosphorylate a number of proteins that are incorporated into *pre-initiation* complexes (pre-ICs) at this stage, namely Cdc45, Sld3-Sld7, Dpb11 and Sld2 [Figure

I.2A, step 2]. Another essential replication factor incorporated into pre-ICs at this stage is known as GINS (Go-Ichi-Ni-San; Japanese for the numbers 5, 1, 2 and 3 respectively). The numbers refer to the fact that GINS is composed of four polypeptide subunits known as Sld**5**, Psf**1**, Psf**2** and Psf**3** (Homesley et al., 2000; Looke et al., 2017; Sawyer et al., 2004); (Gambus et al., 2006; Li and O'Donnell, 2018); (Moyer et al., 2006; Muramatsu et al., 2010; Pacek et al., 2006).

Importantly, phosphorylation of the MCM helicase by DDK activates its DNA unwinding activity shortly after Cdc45 and GINS are incorporated into the replisome [Figure I.2A, steps 2 to 3] (Nougarede et al., 2000). Incorporation of Mcm10 into the replisome ultimately leads to bidirectional unwinding of double-stranded DNA in the vicinity of origins. This generates two strands of single-stranded DNA with 5' to 3' polarity that are coated by replication protein A (RPA) [Figure I.2A, step 4] (Wold, 1997). This creates an opportunity for DNA polymerase α - primase to synthesize short hybrid RNA-DNA primers [Figure I.2A, step 5]. In turn, these origin-proximal primers attract Pol ε, the enzyme that processively synthesizes the leading strands that extend in opposite directions from the origin [Figure I.2A, step 5). The discontinuous synthesis of lagging strands will be described in section 1.2.2.

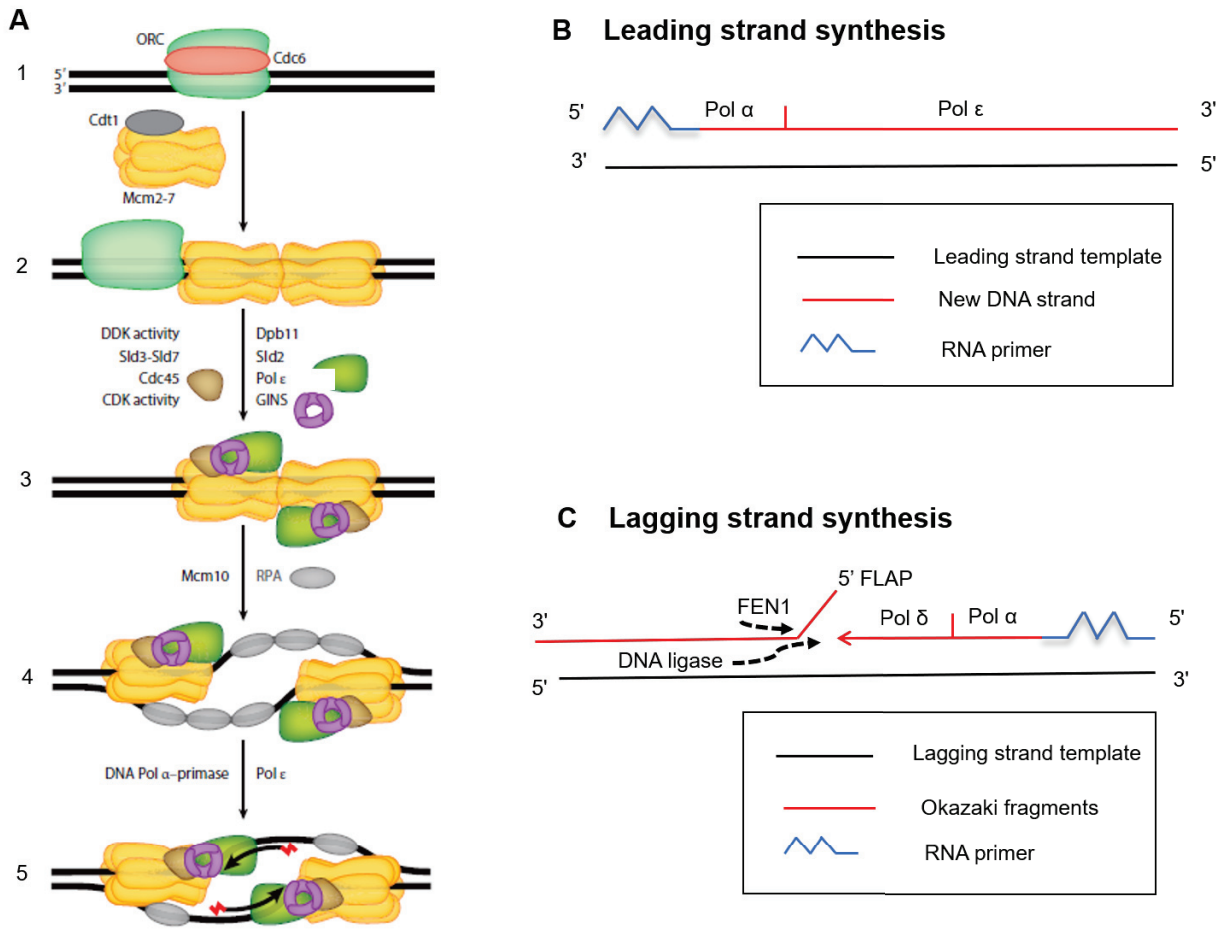

Figure I.2A Schematic showing various stages of replication initiation and formation of a replication fork. (Burgers and Kunkel, 2017 figure reused with permission) Figure I.2B and C shows a simplified version of leading and lagging strand synthesis.

1.2.1 Replicative DNA polymerases and leading strand synthesis

Replicative DNA polymerase alpha (α), delta (δ), and epsilon (ε) all belong to the B family of DNA polymerases and can only synthesize new DNA in the 5' to 3' direction. The strand that is synthesized continuously in the direction of replication fork progression is known as the leading strand [Figure I.2B]. The primase subunit that associates with Pol α synthesizes a short RNA primer that DNA Pol α extends by a short oligonucleotide [Figure I.2B]. The

sequential action of primase and Pol α generates a short RNA-DNA hybrid single strand that, following a switch from Pol α to Pol ε (the leading strand polymerase), leads to the synthesis of a long and continuous leading strand (Lark, 1972b); (Lark, 1972a). The RNA-DNA hybrid is eventually removed by ribonuclease H and other enzymes.

1.2.2 Lagging strand synthesis

The synthesis of the lagging strand is more complicated than that of the leading strand. Although the nascent strand is also synthesized in the 5' to 3' direction, the lagging strand has to be generated as short Okazaki fragments [Figure I.2C] that are synthesized in the direction opposite to that of replication fork progression. These small Okazaki fragments (roughly 150 - 250bp) are then processed by multiple enzymes and finally ligated together to form a continuous lagging strand. As with the initiation of leading strand synthesis, short RNA primers synthesized by Pol α - primase are required to start synthesis of each Okazaki fragment. Pol α has lower fidelity and processivity (O'Donnell et al., 2013) compared with Pol delta (δ), and Pol epsilon (ε). Hence the RNA-DNA hybrid primers synthesized by Pol α - primase need to replaced by DNA synthesized from the main polymerases responsible for either leading [Pol ε] or lagging strand synthesis [Pol δ] (Leonhardt et al., 2000).

In order to enhance their processivity, both leading and lagging strand polymerases associate with a hollow clamp that encircles DNA. The eukaryotic DNA clamp that increases DNA polymerase processivity is a homotrimeric ring known as the Proliferating Cell Nuclear Antigen [PCNA] (Lujan et al., 2016). PCNA is loaded onto and unloaded from the DNA in an ATP - dependent manner by a clamp loader called replication factor C (RFC). In addition to DNA polymerases, PCNA binds to numerous proteins through short motifs known as PCNA Interaction Peptides (PIPs) [Figure I.7; section 1.6]. Among many others, PCNA acts as a

landing platform for enzymes involved in DNA replication, quality control and repair of nascent DNA (mismatch repair), methylation of nascent DNA strands, and chromatin assembly [see section 1.6].

The discontinuous synthesis of the lagging strand requires the concerted action of additional replication enzymes to join Okazaki fragments into a continuous nascent strand [Figure I.2C]. Ribonuclease H removes the RNA primer (Cerritelli and Crouch, 2009) and the error-prone DNA synthesized by Pol α is removed by a DNA exonuclease. Following a switch from Pol α to Pol δ, synthesis proceeds to the 5'-end of the previous Okazaki fragment [Figure I.2C]. Pol δ displaces a short segment of DNA at the 5'-end of that Okazaki fragment to generate a structure known as a flap [Figure I.2C]. This flap is cleaved by a structure-specific endonuclease known as FEN1 (Flap Endonuclease 1). The product of this cleavage is a nick between two Okazaki fragments that is sealed by a DNA ligase [Figure I.2C] (Balakrishnan and Bambara, 2013; Bambara et al., 1997).

1.3 Challenges to propagate chromatin structures during DNA replication

The process of DNA replication poses several challenges for cells to restore chromatin structures behind the replication machinery. During replication fork progression, the nucleosomes in front of the moving fork must be disassembled. However, the pre-existing histones that carry epigenetic marks must be retained near the DNA sequences on which they were present before the fork reaches them (McKnight and Miller, 1977; Sogo et al., 1986).

1) During the passage of replication forks, pre-existing histones located ahead of forks must be recycled and incorporated back onto the nascent sister chromatids

2) The gaps in nucleosome arrays created by DNA duplication need to be filled in by deposition of newly synthesized histones onto the nascent sister chromatids (Bannister and Kouzarides, 2011; Burgess and Zhang, 2013).

1.3.1 Propagation of epigenetic marks carried by pre-existing histones

Pre-existing histones (often referred to as old or parental histones) present in G1 carry epigenetic information (*e.g.* histone H3 K9 or K27 methylation) that is crucial for stable propagation of epigenetic states in proliferating cells (*e.g.* stable gene silencing, X-chromosome inactivation, and many others). Cells employ efficient mechanisms to faithfully transfer this epigenetic information to nascent sister chromatids behind replication forks. Each histone octamer comprises two H3-H4 dimers that assemble into an $(H3\text{-}H4)_2$ tetramer which is flanked by two H2A-H2B dimers. Current evidence strongly suggests that epigenetic marks are confined to H3 and H4, and absent from H2A and H2B.

The epigenetic marks carried by pre-existing histones must be copied onto the newly synthesized histones in order to faithfully propagate epigenetic information from parental cells to daughters.

1.3.2 Hypothetical models for segregation of pre-existing histones during DNA replication

The molecular mechanisms involved in the transfer of epigenetic information from pre-existing to newly synthesized histones are poorly understood but, ultimately, those mechanisms depend upon the mode of segregation of pre-existing histones onto the two nascent sister chromatids. The three segregation models that have been proposed are shown in Figure I.3. Although a single model may be preponderant, those three models are not mutually exclusive provided that they occur during replication of different segments of chromosomes.

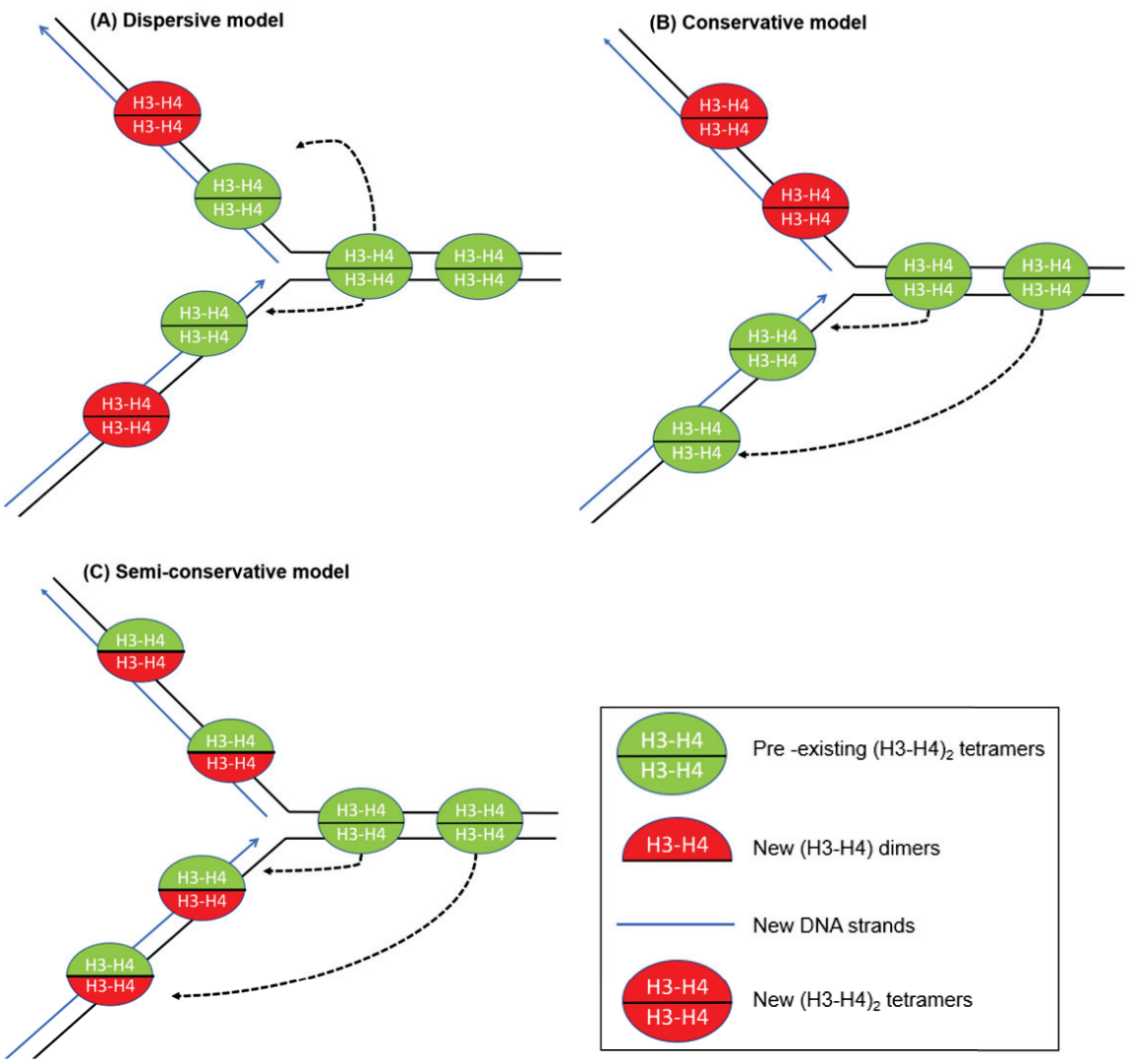

Figure I.3 The three proposed models for segregation of pre-existing histones at replication forks. Namely A) dispersive, B) conservative and C) semi- conservative models of histone segregation is depicted. Parental histones are coloured green and newly synthesized histones shown in red.

The "*dispersive*" model of histone segregation [Figure I.3A] proposes that pre-existing $(H3\text{-}H4)_2$ tetramers remain intact, and are transferred behind the fork onto either the leading strand chromatid or the lagging strand chromatin [Figure I.3A] (Hammond et al., 2017);(Jackson and Chalkley, 1985); (Alabert et al., 2015); (Alabert and Groth, 2012); Hammond *et al.* 2017). The gaps created by DNA duplication are filled in by $(H3\text{-}H4)_2$ tetramers composed of two newly synthesized H3-H4 dimers to restore a normal nucleosomal density [Figure I.3A].

The "*conservative*" model of pre-existing histone segregation [Figure I.3B] posits that $(H3\text{-}H4)_2$ tetramers remain intact [Figure I.3B] but, in contrast to the "dispersive" model, all the parental $(H3\text{-}H4)_2$ tetramers are transferred behind the fork onto only one of the two nascent chromatids, either the lagging strand chromatid [as depicted in Figure I.3B) or the leading strand chromatid [not depicted in Figure I.3B] (Roufa and Marchionni, 1982). In this case, the second chromatid (lagging strand chromatid as depicted in Figure I.3B) is only comprised of $(H3\text{-}H4)_2$ tetramers formed from newly synthesized H3-H4 dimers [Figure I.3B].

The "semi-conservative" model for pre-existing histone segregation [Figure I.3C] requires the separation of parental $(H3\text{-}H4)_2$ tetramers into two H3-H4 dimers, a reaction commonly referred to as "*parental histone tetramer splitting*" (Tagami et al., 2004). Although there is compelling evidence that the majority of pre-existing $(H3\text{-}H4)_2$ tetramers do not split during replication (Leffak, 1984; Prior et al., 1980) this does not rule out the possibility that semi-conservative segregation may occur during replication of specific chromosome segments. In the "semi-conservative" model, the $(H3\text{-}H4)_2$ tetramers that form onto the two nascent chromatids consist of a parental H3-H4 dimer and an H3-H4 dimer that contains only newly synthesized molecules [Figure I.3C].

1.4 Chaperones that promote *de novo* nucleosome assembly of newly synthesized histones

During the S phase, parental DNA is duplicated, and pre-existing histones present in G1 are segregated among the two nascent chromatids. The gaps created by DNA duplication are filled in by deposition of newly synthesized histones onto the two nascent sister chromatids. Histone chaperones play an important role in tightly binding and shielding the large positive charge of core histones to minimize their non-productive (i.e. interactions that cannot result in proper nucleosome assembly) and potentially harmful non-specific interactions of free histones with nucleic acids (RNA and DNA).

Although this is not often emphasized, the term "*histone chaperones*" does not have the same meaning as in the context of molecular chaperones that assist protein refolding in an ATP-*dependent* manner (*e.g. Escherichia coli* GroEL-GroES). For instance, core histones acquire their three-dimensional structure in an ATP-*independent* manner even when they are refolded in the absence of other proteins. The term "*histone chaperones*" was instead coined to reflect the fact that they assist in the formation of nucleosomes in an ATP-*independent* manner, but the histone chaperones do not remain part of the final product, namely nucleosomes or chromatin.

1.4.1 Anti-Silencing Factor 1 (ASF1)

ASF1 is a histone chaperone that is evolutionarily conserved from yeast to humans. Current evidence suggests that ASF1 binds to newly synthesized H3-H4 dimers in the nucleoplasm, possibly as soon as the new H3-H4 dimers dissociate from the karyopherins that import new H3-H4 molecules into the nucleus (Blackwell et al., 2007).

A high-resolution structure has revealed why ASF1 can only bind to H3-H4 dimers, rather than $(H3\text{-}H4)_2$ tetramers (English et al., 2006). The interactions that hold the two H3-H4 dimers within the $(H3\text{-}H4)_2$ tetramer reside within a surface of interaction that resides within the C-

terminal domains of the two H3 molecules (Luger et al., 1997). Because ASF1 also binds to the C-terminal domain of H3 (English et al., 2006). ASF1 binding to H3 sterically hinders the H3-H4 surface of interaction that is the foundation stone of the $(H3\text{-}H4)_2$ tetramer (Luger et al., 1997). In principle, two ASF1-H3-H4 complexes could assemble an $(H3\text{-}H4)_2$ tetramer onto nascent DNA but, because ASF1 lacks a known domain for interaction with the replication machinery, it is generally felt that the role of ASF1 in *de novo* nucleosome assembly is to handover its H3-H4 dimers to CAF-1 (Han et al., 2013) (Liu et al., 2012; Tyler et al., 2001), which directly binds to PCNA at replication forks. Consistent with this, ASF1 binds to the p60 subunit (*S. cerevisiae* Cac2) of CAF-1, and further conformational rearrangements allow the transfer of H3-H4 dimers from ASF1 to CAF-1 (Krawitz et al., 2002; Mello et al., 2002), (Liu et al., 2012; Tyler et al., 2001).

1.4.2 Chromatin Assembly Factor 1 (CAF-1)

CAF-1 is a 3-subunit protein complex that is evolutionarily conserved from yeast to humans. CAF-1 was initially purified from nuclear extracts of human cells by virtue of its ability to promote replication-*dependent* nucleosome assembly in an *in vitro* system for replication of plasmids containing the Simian Virus 40 (SV40) origin of DNA replication (Smith and Stillman, 1989). Despite the fact that CAF-1 was discovered 32 years ago, it thus far remains the only histone chaperone that promotes nucleosome assembly in a replication-dependent manner. CAF-1 mediates the first step in nucleosome assembly behind replication forks, namely the deposition of newly synthesized H3-H4 onto either the leading strand chromatid or the lagging strand chromatid [Figure I.1]. It remains somewhat controversial whether a single 3-polypeptide CAF-1 complex can deposit an intact $(H3\text{-}H4)_2$ tetramer onto DNA or whether two CAF-1 complexes act in concert to deposit two H3-H4 dimers, ultimately resulting in the formation of an $(H3\text{-}H4)_2$

tetramer onto DNA. However, recent biophysical studies showed that a CAF-1 heterotrimer binds to a single H3-H4 (Sauer et al., 2017). Based on their results, the authors favour the view that two CAF-1-H3-H4 complexes need to dimerize in order to deposit onto DNA an $(H3\text{-}H4)_2$, solely composed of new H3 and H4 molecules (Mattiroli et al., 2017b; Sauer et al., 2017). In striking contrast to this model, other authors reported that a single CAF-1 heterotrimer binds to two newly synthesized H3-H4 dimers, but is able to promote $(H3\text{-}H4)_2$ tetramer formation before the histones are deposited onto nascent DNA (Liu *et al*., 2012; Liu *et al*., 2016).

De novo nucleosome assembly occurs in a stepwise manner: H3-H4 are deposited first onto nascent DNA, and subsequently joined by two H2A-H2B dimers (Smith and Stillman, 1991). CAF-1 mediates the first step in nucleosome assembly, namely the deposition of newly synthesized H3-H4 onto DNA. There is currently no evidence that CAF-1 plays any role in the deposition of H2A-H2B onto DNA (Smith and Stillman, 1991; Tagami et al., 2004). The histone chaperone NAP1 has been implicated in the deposition of H2A-H2B (Aguilar-Gurrieri et al., 2016; Andrews et al., 2010), but because Nap1 is not essential for viability in *S. cerevisiae*, it is widely assumed that additional H2A-H2B chaperones remain to be discovered.

In yeast and vertebrate cells, CAF-1 is a three-subunit protein complex. The subunits of vertebrate CAF-1 are known as p150 (CHAF1A), p60 (CHAF1B), and RbAp48 (RBBP6) (Kamakaka et al., 1996). The homologous subunits of *Saccharomyces cerevisiae* CAF-1 are called Cac1 (Rlf2), Cac2, and Cac3 [Msi1] (Kaufman et al., 1997).

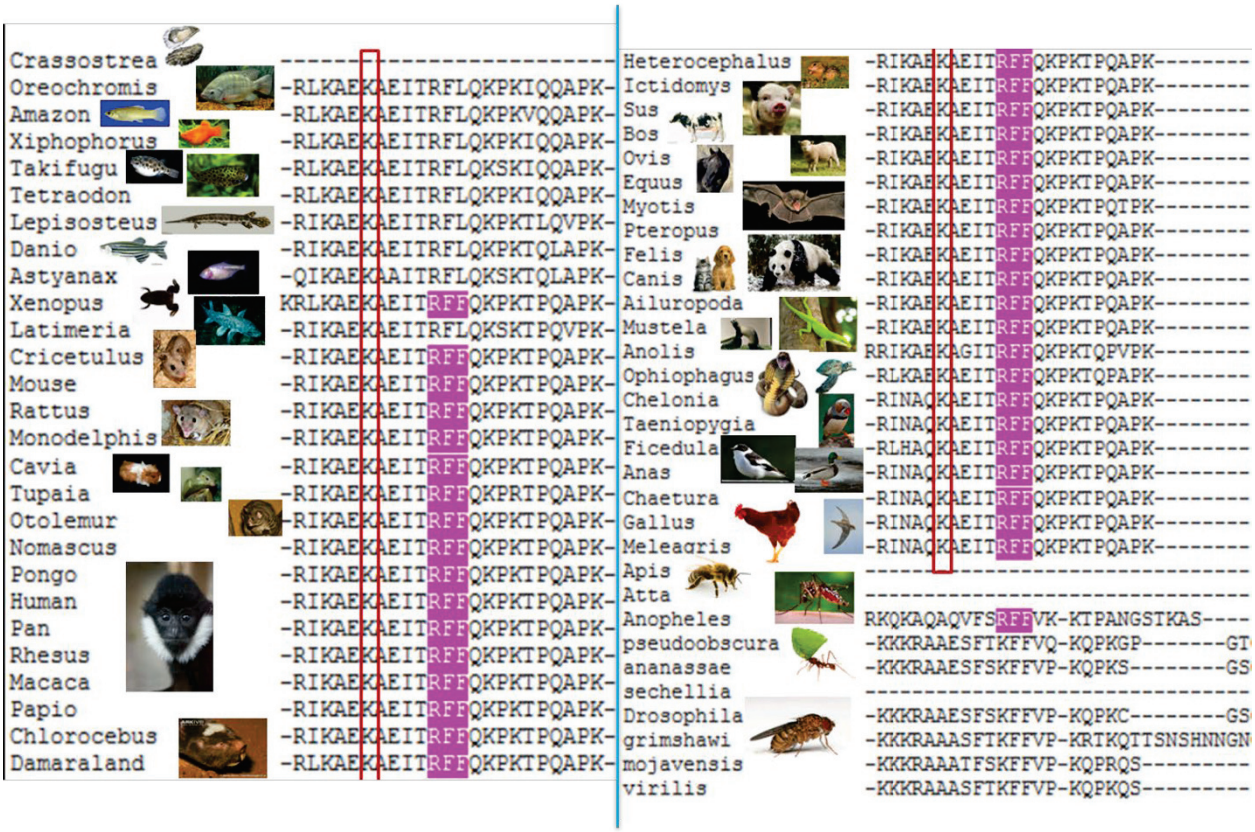

Figure I.4 Multiple sequence alignment of the PIPs of CAF-1 from a wide range of species. The conservation of non-canonical PIP box residue lysine is shown inside a red box. The three residues for which we observed electron density in the crystal structure (RFF) is highlighted in pink.

Throughout S phase, CAF-1 localizes to patterns of nuclear foci that are stereotypical of early-, mid- and late S-phase (O'Keefe et al., 1992). The foci that contain CAF-1 are sites of DNA synthesis based on two criteria. First, these foci contain a locally high density of PCNA and, most importantly, the patterns of PCNA foci coincide with foci of DNA synthesis detected following a short pulse of bromodeoxyuridine (Krude, 1995), (Murzina et al., 1999).

In addition to its prominent role at replication forks, CAF-1 also promotes nucleosome assembly during processes that require PCNA-dependent DNA synthesis. These include DNA strand break repair (Nabatiyan et al., 2006), long-patch base excision repair (Nabatiyan et al., 2006) and nucleotide excision repair (Gaillard et al., 1997), (Martini et al., 1998; Moggs et al., 2000; Polo et al., 2006). CAF-1 - mediated nucleosome assembly during all these processes depends upon the ability of CAF-1 to bind directly to PCNA [section 1.6.2] (Krawitz et al., 2002; Moggs et al., 2000; Shibahara and Stillman, 1999; Zhang et al., 2000).

Because of this PCNA dependency, it is important to emphasize that CAF-1 - mediated histone deposition onto nascent DNA occurs very rapidly behind the sites of DNA synthesis. Strong evidence argues that nucleosomes are formed almost as soon as enough double-stranded DNA has emerged from the replisome to enable the formation of nucleosomes [150 - 250bp]. In addition, there is evidence that CAF-1 - mediated histone deposition on the lagging strand chromatid takes place before ligation of Okazaki fragments has taken place (Smith and Whitehouse, 2012). Thus, CAF-1 likely has access to a PCNA ring localized in close proximity to the enzymes involved in DNA synthesis.

1.4.2.1 CAF-1 domains and subunits

As stated earlier, the three subunits of vertebrate CAF-1 are known as p150, p60, and RbAp48, and are conserved in eukaryotes. The p150 subunit contains domains and motifs that mediate multiple interactions with PCNA and other proteins [Figure I.5]. Previous results demonstrated that the first 296 amino acids of human CAF-1 p150 are not needed for chromatin assembly either *in vitro* or *in vivo* (Kaufman et al., 1995). Instead, this N-terminal domain of p150 plays a role in the spatial organization of nucleolar-associated chromosomal domains such

as repetitive α-satellite DNA elements (Smith et al., 2014) a function that does not depend on the ability of CAF-1 to assemble nucleosomes at sites of DNA synthesis (Smith et al., 2014). The same N-terminal domain of CAF-1 also contains an internal PxVxL motif for interaction with Heterochromatin binding Protein 1 (HP1) [Figure I.5](Murzina et al., 1999). This motif plays a role in the duplication of pericentric heterochromatin in proliferating cells, but it is not required for replication-coupled deposition of new H3-H4 molecules onto nascent DNA (Quivy et al., 2008). In *S.cerevisiae*, HP1 does not exist, but Cac1 nonetheless plays an important role in heterochromatin-mediated silencing of reporter genes (Enomoto et al., 1997; Kaufman et al., 1997); (Huang et al., 2007; Quivy et al., 2008).

CAF-1 p150 also harbors a so-called KER domain that is enriched in the charged amino acids lysine (K), glutamic acid (E), and arginine (R) and devoid of aromatic residues [Figure I.5]. It has been reported that the KER domain directly binds to DNA with high affinity (Sauer et al., 2017).

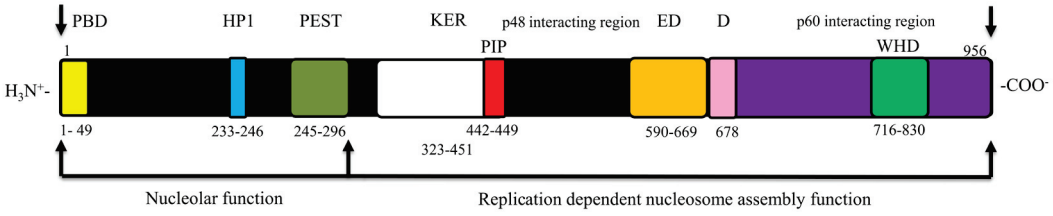

PBD: PCNA binding domain
PIP: PCNA interaction peptide
PEST: Proline Glutamic acid, Serine, Threonine rich domain
HP1: Heterochromatin protein binding motif (PxVxL)
KER: Domain rich in Lysine, Glutamic acid and Arginine residues
ED: Domain rich in Glutamic acid and Aspartic acid residues
D: Dimerization domain
WHD: Winged helix domain

Figure I.5 Domain architecture of the CAF-1 p150 subunit from *Homo sapiens*. Residues (1-296 amino acids) at the N-terminus which is dispensable for chromatin assembly is shown along with residues 297-956 at the C-terminus which is indispensable for chromatin assembly. The PIP region present within the KER domain is highlighted in red.

A short PCNA Interaction Peptide (PIP) resides immediately after the KER domain [Figure I.5]. This PIP is crucial for chromatin assembly (Kaufman et al., 1995; Rolef Ben-Shahar et al., 2009). In fact, previous results from our laboratory have shown that the p150 subunits of human and mouse CAF-1 contain two functionally distinct surfaces for PCNA binding, namely the PCNA binding domain (PBD) and the aforementioned PCNA Interaction Peptide (PIP) (Rolef Ben-Shahar et al., 2009). The PBD is located between residues 12-34 near the extreme N-terminus of p150 [Figure I.5]. The PBD binds strongly to PCNA, but it lacks sequence similarity with canonical PIPs (Rolef Ben-Shahar et al., 2009). Therefore, the PBD likely represents a novel class of surfaces for PCNA binding. However, in spite of its relatively strong binding to PCNA, the PBD was found dispensable for *in vitro* chromatin assembly during SV40 DNA replication (Rolef Ben-Shahar et al., 2009). The function of the PBD has thus far remained unknown.

In contrast to the N-terminal PBD, the PIP that resides internally, and immediately follows the KER domain, binds with relatively weak affinity to PCNA (Figure I.5]. It is nonetheless essential for replication-coupled chromatin assembly (Rolef Ben-Shahar et al., 2009). This internal CAF-1 p150 PIP is a non-canonical motif in which the highly conserved glutamine (Q) of canonical PIPs is substituted by a lysine (K) in CAF-1 p150 homologues from a

wide range of species [Figure I.4]. Two types of argument suggest that this single amino acid substitution contributes to the weak affinity of the CAF-1 p150 PIP for PCNA. In canonical PIPs, the carbonyl and amino groups of the side chain of the highly conserved glutamine make multiple contacts with PCNA and mutating this glutamine into a lysine (the residue conserved in this position of CAF-1 p150 PIPs) nearly abolishes binding of canonical PIPs to PCNA (Rolef Ben-Shahar et al., 2009). Conversely, mutating the lysine of CAF-1 p150 PIPs into a glutamine considerably enhances their affinity for PCNA (Rolef Ben-Shahar et al., 2009). Another intriguing feature of the CAF-1 p150 PIP is that, for most of the proteins that contain canonical PIPs (*e.g.* DNA replication enzymes), the motif is present at either the extreme N-terminus or C-terminus of the protein. In contrast, the non-canonical PIP is always located internally within the primary amino acid sequences of CAF-1- p150 homologues from widely divergent species that range from yeast to humans. This is unlikely a coincidence which, in turn, suggests that an internal location of CAF-1 p150 PIPs may be of physiological importance.

The so-called ED domain of CAF-1 p150 [Figure I.5] is rich in acidic residues (aspartic and glutamic acid) and binds to H3-H4 with high affinity (Liu *et al*., 2016; Mattiroli *et al*., 2017a; Mattiroli *et al*., 2017b; Sauer *et al*., 2017). CAF-1 p150 also contains a p60 binding domain and a poorly defined homo-dimerization domain that are located C-terminal to the ED domain [Figure I.5].

For technical reasons, the precise range of amino acids that are needed for homo-dimerization of p150 is not known. This is because this domain was identified by a single deletion of 36 amino acids (Quivy et al., 2001), and site-directed mutagenesis was not employed to further refine the residues necessary for homo-dimerization. Although the results of this study

are controversial (Gerard et al., 2006), p150 homo-dimerization has been proposed to be regulated by phosphorylation of p150 mediated by Cdc7-Dbf4 (Dbf4-Dependent Kinase or DDK), the protein kinase that participates in the initiation of DNA replication. The cyclic model that emerged from this study is the following. The non-phosphorylated form of p150 forms a homo-dimer that is incapable of binding PCNA. Upon phosphorylation by DDK, CAF-1 p150 is converted into monomers that bind PCNA and promote deposition of H3-H4 onto nascent DNA. To complete the cycle, p150 is dephosphorylated by an unknown phosphatase, which returns p150 to the homo-dimeric state. Many aspects of this model remain nebulous, such as the rationale for the existence and function of the homo-dimeric form that cannot bind PCNA or promote nucleosome assembly.

Structural studies uncovered the presence of a Winged Helix Domain (WHD) in *S. cerevisiae* Cac1 and vertebrate p150 [Figure I.5](Zhang et al., 2016). The WHD domain of the large subunit of CAF-1 homologues binds DNA in a sequence-independent manner (Zhang et al., 2016). Mutations that cripple DNA binding by the WHD confer partial loss-of-function phenotypes compared with the phenotypes of cells that completely lack CAF-1 (Zhang et al., 2016). This is likely because the KER domain also binds DNA regardless of DNA sequence (Sauer et al., 2017). It seems possible that the KER domain may partially compensate for the lack of DNA binding conferred by mutation of the WHD. The fact that the KER domain binds DNA with much greater affinity

The p60 subunit of CAF-1 (*S. cerevisiae* Cac2) is composed of multiple WD40 repeats. As described in section 1.4.2.1, current evidence suggests a mechanism by which ASF1-associated H3-H4 dimers are handed over to CAF-1. This suggests that ASF1 might somehow interact with CAF-1. Consistent with this, biophysical studies performed with *S. cerevisiae* CAF-

1 revealed that the interaction between CAF-1 and ASF1 is mediated through ASF1 binding to a domain of the Cac2 subunit (Liu *et al*., 2012; Malay *et al*., 2008). This domain, known as the B domain, is conserved from yeast to humans and located C-terminal to the WD repeats of the Cac2 subunit (Liu *et al*., 2012; Malay *et al*., 2008).

The so-called HIR complex, which is involved in replication-independent nucleosome assembly in organisms that range from yeast to humans [Section 1.8], contains subunits known as Hir1 and Hir2 in *S. cerevisiae* (homologous to human HIRA, which is a fusion of both yeast Hir1 and Hir2). Even though they are subunits of replication-*independent* chromatin assembly complexes, Hir1, Hir2 and HIRA contain a B domain that is structurally related to that of the Cac2 subunit of CAF-1, a replication-*dependent* chromatin assembly factor (Malay et al., 2008; Tang et al., 2006; Tyler et al., 2001). Some degree of structural similarity between replication-*independent* and replication-*dependent* chromatin assembly complexes is to be expected given that they both act on identical or very similar histone substrates, namely H3-H4 in *S. cerevisiae* [H3.1-H4 and H3.3-H4 in humans] (Section 1.8). It turns out that the B-domains are necessary for ASF1 to handover H3-H4 to either CAF-1 or the HIR complex (Tang et al., 2006).

Human RbAp48 (p48 or RBBP7 ; *S. cerevisiae* Cac3/Msi1) is, like the p60 subunit, composed of WD40 repeats that collectively fold into a 6-bladed β propeller structure. RbAp48 and the nearly identical RbAp46 are core histone-binding subunits (Murzina et al., 2008; Verreault et al., 1998). In fact, at least in part because of their ability to bind H3-H4, RbAp46/RbAp48 are integral subunits of several functionally distinct histone-modifying enzymes. In addition to CAF-1, these include HAT1, an enzyme that acetylates newly synthesized H4 molecules, HDAC1/HDAC2-dependent histone deacetylases such as the

nucleosome remodeling and deacetylase complex (NuRD), and several others. Intriguingly RbAp46/RbAp48 bind to a structurally distorted form of histone H4 in which the α-helix 1 of the histone-fold is peeled off and rotated away from the histone-fold;(Murzina et al., 2008); (Zhang et al., 2013). The functional significance of this partially unfolded histone-fold is not known, but the highly irregular conformation of histone H4 when bound to RbAp46/RbAp48 suggests that this may represent an important intermediate along the path leading to the formation of mature $(H3\text{-}H4)_2$ tetramers onto DNA. Although RbAp48 is clearly an histone H4-binding subunit, a paradox has recently emerged. However, within the 3-subunit CAF-1 complex from *S. cerevisiae*, the Cac3 subunit only makes a minor contribution to H3-H4 binding (Mattiroli et al., 2017a). The main contribution to histone binding is provided by the Cac1 and Cac2 subunits and, in particular, the aforementioned ED domain of Cac1 [Figure I.5] (Liu et al., 2016; Mattiroli et al., 2017a). This is paradoxical because, *in vivo*, the *CAC3* gene is as essential for CAF-1 function as the *CAC1* and *CAC2* genes (Kaufman et al., 1997). A possible resolution of this paradox may be that the essential role of Cac3 for CAF-1 function *in vivo* is unrelated to its ability to bind histone H4 *in vitro*. For instance, Cac3 may need to bind an as yet unidentified non-histone protein to confer activity to CAF-1.

1.5 Histone chaperones involved in transient nucleosome disruption and recycling of pre-existing histones

1.5.1 FACT (FAcilitates Chromatin Transcription)

The histone-binding complex FACT (FAcilitates Chromatin Transcription) plays important roles in the disruption of pre-existing nucleosomes ahead of replication forks and/or the recycling of pre-existing histones onto nascent DNA. FACT consists of three polypeptides known as Spt16, Pob3 and Nhp6 in *S. cerevisiae*. The latter two are replaced by a single

polypeptide known as SSRP1 in humans. The Spt16 subunit, also known as Cdc68, was identified through genetic screens designed to uncover transcriptional regulators in *S. cerevisiae* (Prendergast et al., 1990; Rowley et al., 1991; Winston et al., 1984)

The human FACT complex, which consists of SPT16 and SSRP1, was later purified by virtue of its ability to disassemble and reassemble nucleosomes during transcriptional elongation through chromatin *in vitro* (Belotserkovskaya et al., 2003). However, there are three lines of evidence indicating that, independently of its role in transcription, FACT also plays a role in DNA replication through chromatin. First, the Spt16 and Pob3 subunits of FACT interact with the catalytic subunit of DNA polymerase α (Wittmeyer and Formosa, 1997). Second, hypomorphic mutations in genes that encode FACT subunits greatly exacerbate the phenotypes of mild loss-of-function mutations off genes encoding DNA replication enzymes (Formosa, 2003). Third, mildly hypomorphic alleles of *SPT16* and *POB3* confer sensitivity to conditions that impede DNA replication, such as the depletion of dNTPs caused by hydroxyurea (Formosa, 2003). In addition to DNA polymerase α (Wittmeyer and Formosa, 1997). FACT interacts with Replication Protein A [RPA] (VanDemark et al., 2006) and the CMG complex [Cdc45, Mcm, Gins] (Gambus et al., 2006), the active form of the helicase that unwinds double-stranded DNA during the elongation phase of DNA replication. This suggests that FACT may be continuously present at DNA replication forks throughout the entire genome and S-phase. FACT is therefore present at the heart of the replisome and current evidence suggests that Spt16 binding to H2A-H2B and H3-H4 promotes nucleosome disassembly and reassembly at replication forks (Belotserkovskaya et al., 2003; Hondele et al., 2013; Kemble et al., 2015). FACT engages in extensive contacts with DNA while maintaining multiple components of a partially disassembled

nucleosome in close proximity (Formosa and Winston, 2020; Liu et al., 2020; Wang et al., 2018).

Based on biochemical and structural studies, it is not far-fetched to propose that FACT may be capable of two seemingly opposite activities: disassembly of pre-existing nucleosomes located ahead of replication forks and their reassembly onto the nascent sister chromatids (Formosa and Winston, 2020). This transient disruption of histone-DNA interactions facilitates MCM activity *in vitro* as well as replication fork progression *in vivo* (Kurat et al., 2017; Tan et al., 2006)

Since evidence from both yeast and mammalian cells indicates that FACT and Pol α interact with H2A-H2B (Belotserkovskaya et al., 2003; Evrin et al., 2018; Hondele et al., 2013; Kemble et al., 2015), it also seems plausible that FACT and Pol α might contribute to recycling H2A-H2B during replication. Intriguingly, FACT activity is dispensable for viability in fission yeast (Lejeune et al., 2007) and in certain types of vertebrate cells (Shen et al., 2018), implying that this complex is not absolutely essential for either replication or transcription. Since other proteins have been shown to promote replication through nucleosomal substrates [*e.g.* T antigen, the simian virus 40 DNA helicase] (Ramsperger and Stahl, 1995) it seems plausible that other replisome components might allow nucleosome disruption and replication fork progression through chromatin in the absence of FACT.

1.5.2 MCM2

The primary barrier to replication fork progression through chromatin is the separation of DNA strands when the DNA is wrapped around the surface of histone octamers. The wrapping of DNA around histone octamers likely represents a general barrier to DNA strand separation because both viral [*e.g.* SV40 T antigen] (Ramsperger and Stahl, 1995) and cellular DNA

helicases [*e.g.* the Cdc45-MCM-GINS helicase] have evolved mechanisms to contend with the nucleosomal DNA barrier. In the case of the MCMs, one of the subunits of the hexameric complex, known as MCM2, contains an evolutionarily conserved N-terminal acidic surface (approximately 200 residues of which 30% are acidic residues) that binds histones (Foltman et al., 2013; Huang et al., 2015; Ishimi et al., 1996; Richet et al., 2015). It has been reported that FACT and MCM2 bind pre-existing histones in a cooperative manner (Foltman et al., 2013). *S. cerevisiae* mutant cells where the only source of Mcm2 contains a truncation of the acidic N-terminal tail are viable (Foltman et al., 2013). Therefore, this domain is not absolutely essential for DNA replication. This may be because the two subunits of FACT, Spt16 and Pob3, contain histone-binding C-terminal acidic domains that may act in a partially redundant manner with the acidic domain in the N-terminal tail of Mcm2 (Foltman et al., 2013). Nonetheless, cells that lack the acidic N-terminal tail of Mcm2 have a defect in the maintenance of the 2-micron minichromosome (Foltman et al., 2013), which is known to be packaged into nucleosomes.

1.6 PCNA

PCNA belongs to a family of DNA sliding clamps that are structurally and functionally conserved [Figure I.6]. In eukaryotes, PCNA is a homotrimeric ring (87kDa) with a central cavity, which allows the PCNA ring to close around DNA. As a result, PCNA is topologically linked to DNA. The PCNA ring slides along the DNA without dissociating and, thereby, increases the processivity of replicative DNA polymerases.

Structural studies of PCNA homologues from multiple species have shown that the PCNA homotrimer has in fact 6-fold symmetry [Figure I.6A] (Krishna et al., 1994). Each PCNA monomer contains two structurally related globular domains that are connected by a long flexible

loop called the interdomain connecting loop [IDCL, Figure I.6A]. The inner surface of PCNA comprises twelve α-helices, whereas the outer ring surface comprises six β sheets [Figure I.6A]. The presence of many lysine and arginine residues on the inner surface α-helices results in an inner surface with a high positive charge. The rationale behind the high positive charge density within the inner surface of the PCNA ring is far from obvious and counterintuitive. One might be tempted to reason that the high density of positive charges within the inner might result in non-specific interactions with the phosphate groups of DNA, which might be expected to interfere with PCNA sliding and processivity. Thus, the molecular function of the high positive charge density remains unknown.

DNA polymerases and other PCNA-binding proteins bind to the so-called front face of the PCNA ring [Figure I.6B]. This is the face of the PCNA ring that points in the direction of DNA synthesis. The other face of the PCNA ring, known as the rear face or the back face of PCNA [Figure I.6B] points in the direction opposite to that of DNA synthesis. The back face of the PCNA ring is the site of attachment of SUMO and ubiquitin which are important to control DNA synthesis when the DNA template strands are damaged [section 1.6] (Kelch, 2016).

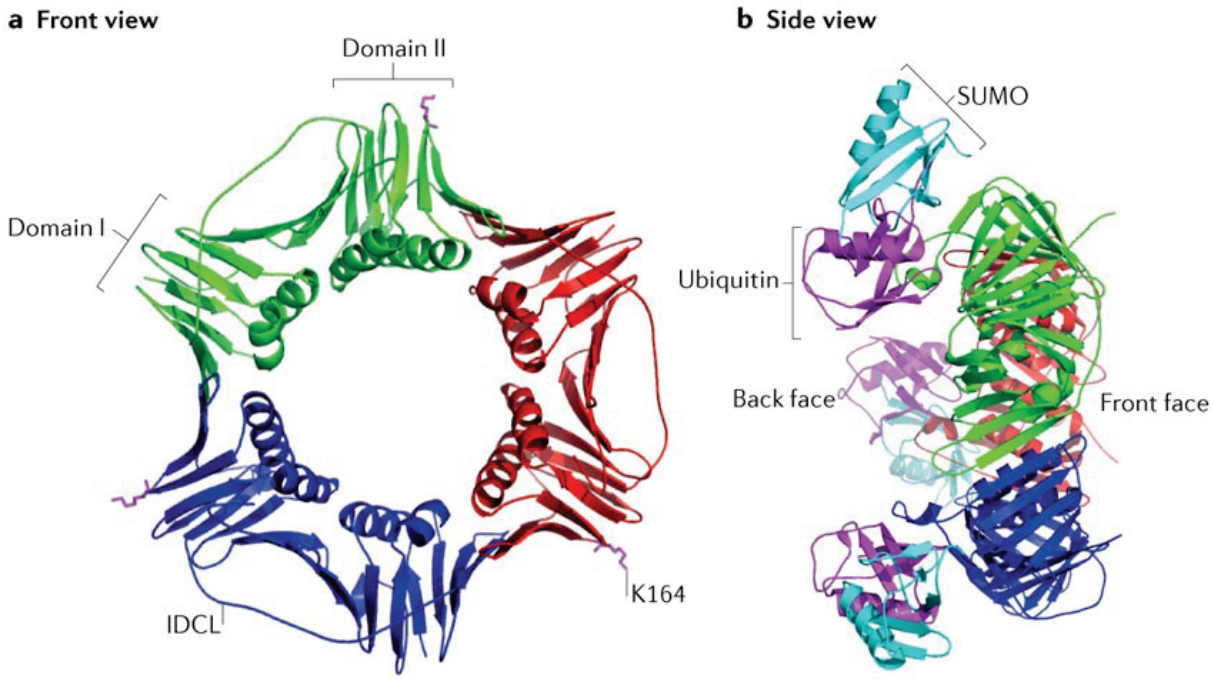

Figure I.6 Front and side views of the structure of PCNA from *Saccharomyces cerevisiae.* (Mailand et al., 2013 figure reused with permisssion). The individual PCNA monomers are represented in three different colours (red, blue, and green). Two domains in each monomers are connected by the inter domain connecting loop (IDCL). Side view shows binding sites for bulkier Ubiquitin and SUMO motifs through the back face of PCNA.

Numerous PCNA binding proteins, such as the cyclin-dependent kinase inhibitor p21, DNA polymerase pol δ, DNA ligase 1 (Lig1), Flap Endonuclease 1 (FEN1), and many others, bind to a hydrophobic surface that is formed by the IDCL and the underlying β-sheet [Figure I.6A] (Freudenthal et al., 2009). Among PCNA binding proteins, the most common motif that binds to the hydrophobic surface of PCNA is the so-called PCNA Interaction Peptide [PIP] (De

Biasio and Blanco, 2013; Hingorani and O'Donnell, 2000; Jonsson et al., 1998; Maga and Hubscher, 2003; Mailand et al., 2013; Moldovan et al., 2007; Naryzhny, 2008). Although many variations exist among individual proteins, the most common PIPs (canonical PIPs) have the consensus sequence Q-X-X-h-X-X-a-a, where 'h' represents an aliphatic hydrophobic amino acid (isoleucine, leucine, valine or methionine) and 'a' represents amino acids with an aromatic side chain (phenylalanine, tyrosine, or tryptophan). X can be any amino acid (Moldovan et al., 2007). Some PCNA binding proteins contain PIPs whose sequences significantly depart from the consensus (De Biasio and Blanco, 2013); (Pedley et al., 2014).

1.6.1 PCNA and DNA replication

During DNA replication, the CMG helicase unwinds the DNA, Pol α - primase subsequently synthesizes an RNA primer, and Pol ε and Pol δ respectively extend the primer for leading and lagging strand synthesis (Figure I.2B and Figure I.2C. On the leading strand only one PCNA ring needs to encircle DNA for processive DNA synthesis. In contrast, even though the segments of DNA synthesized by Pol δ are relatively short (approximatively 100 - 200 nucleotides), Pol δ requires a PCNA ring to synthesize each Okazaki fragment (Stodola and Burgers, 2016).

The 3'-end of so-called primer-template junctions, which are junctions where the 3'-end of the RNA-DNA primer is base-paired to the template strand, are the sites of PCNA loading. The junctions are recognized in a structure-specific manner by Replication Factor C [RFC], which is often referred to as a clamp loader because RFC opens the hollow PCNA clamp and closes it around the primer-template DNA junction (Bowman et al., 2004)

In addition to promoting DNA synthesis by Pol δ, PCNA also plays other prominent roles during Okazaki fragment maturation in concert the enzymes Flap ENdonuclease 1 (FEN1) and DNA ligase 1. Pol δ is an enzyme capable of limited strand displacement, which enables synthesis of short DNA segments without the need for strand separation by a helicase [Figure I.2C] (Stodola and Burgers, 2016). When Pol δ reaches the 5'-end of the previous Okazaki fragment, it displaces its 5'-end, which creates a DNA structure known as a 5'-flap [Figure I.2C]. FEN1 is involved in cleaving off the flap structure formed by the displacement of the RNA-DNA primer [Figure I.2C]. DNA ligase then catalyzes the sealing off of the nick between adjacent Okazaki fragments. For efficient and rapid synthesis of the lagging strand, the activities of Pol δ, FEN1 and Lig1 must be tightly coordinated, and the enzymes must act on DNA according to a strict sequence (Pol δ must act first, FEN1 second and Lig1 last). Three classes of models have been proposed to account for at least part of these requirements.

The first class of models, which one might term distributive models, entails dynamic binding and dissociation of each of the three enzymes (Pol δ, FEN1 and Lig1) from a single homo-trimeric PCNA ring. This model emerged from *an in vitro* inability, likely because of steric hindrance, to force Pol δ, FEN1 and Lig1 to simultaneously bind to the three monomers of the same PCNA ring. Distributive models, however, are not without their own shortcomings. For instance, it is not clear how processive lagging strand synthesis could occur when the three enzymes responsible for Okazaki fragment maturation continuously dissociate from a single PCNA ring and rebind to the very same PCNA ring in a mutually exclusive manner and according to a very specific sequence (Pol δ first, followed by FEN1 and then Lig1).

The second class of models to achieve rapid and accurate maturation of Okazaki fragments are known as tool belt models. Tool belt models have also been invoked to account for

the ability of different error-prone DNA polymerases to bypass specific DNA lesions in the template strands (section 1.6.3). A tool belt consists of a PCNA ring in which each of the three monomers binds a functionally distinct enzyme. Interestingly, PCNA from the archaeal *S. solfataricus* is a heterotrimer in which each subunit binds to a specific partner, namely PolB1, Fen1 or Lig1 (Beattie and Bell, 2012). However, the three monomers of eukaryotic PCNA have the same amino acid sequence and, therefore, it is far from clear how the eukaryotic PCNA ring could simultaneously accommodate one molecule each of Pol δ, FEN1 and Lig1, as opposed to three molecules of any one enzyme or other permutations that would not be compatible with efficient Okazaki fragment maturation or processive DNA synthesis.

The third class of models to achieve rapid and accurate maturation of Okazaki fragments invokes the presence of "*multiple"* PCNA rings on the lagging strand. In this model, at least three PCNA rings need to encircle DNA at each Okazaki fragment: the front ring is proposed to bind Pol δ, the middle ring FEN1 and the third ring DNA ligase 1. One problem with this model is that it requires functionally distinct enzymes (Pol δ, FEN1 and Lig1) to access identical PCNA rings according to a specific sequence. In other words, identical PCNA rings need to acquire distinct functions. There is very little information on how this could be achieved, except in one case. The structure of the Lig1 holoenzyme bound to PCNA shows that, through steric hindrance, Lig1 precludes functionally unrelated enzymes from accessing the PCNA ring to which Lig1 is bound [Figure I.8] (Pascal et al., 2004). This obviously does not solve the numerous problems raised by the "multiple PCNA ring" hypothesis, but the mode of Lig1 binding to PCNA nicely illustrates one of the mechanisms by which a PCNA ring may become "*dedicated*" to a specific enzyme activity. Nevertheless, this model is highly speculative,

unsubstantiated by compelling evidence and, as far as we know, has never been rigorously tested.

1.6.2 PCNA and replication-coupled chromatin assembly

Although the CAF-1 protein complex was first described 31 years ago, it has thus far remained the only chromatin assembly factor (histone chaperone) that preferentially deposits H3-H4 onto nascent DNA to promote replication-coupled nucleosome assembly even in the presence an excess of unreplicated DNA (Smith and Stillman, 1989). This has prompted interest in uncovering the molecular mechanism by which CAF-1 had this unique property to promote nucleosome assembly preferentially onto replicating DNA. Several lines of genetic and biochemical evidence eventually converged to provide a compelling case that PCNA was the linchpin that enabled CAF-1 to preferentially assemble histones onto replicating DNA (Shibahara and Stillman, 1999 ; Zhang *et al*., 2000 ; Sharp *et al.*, 2001 ; Krawitz *et al.*, 2002 ; Rolef Ben-Shahar *et al*., 2009). The genetic evidence emerged from two experimental approaches in the budding yeast *Saccharomyces cerevisiae*. First, *S. cerevisiae* cells that lack CAF-1 exhibit a defect in transcriptional silencing of reporter genes integrated into sub-telomeric heterochromatin. Screens of separation-of-function alleles of PCNA resulted in the identification of a subset of PCNA hypomorphic alleles that were not defective in DNA replication, but whose silencing defect was epistatic with the sub-telomeric heterochromatin silencing defect of cells lacking CAF-1 (Zhang *et al*., 2000 ; Sharp *et al.*, 2001). Second, an elegant genetic screen for loss-of-function alleles in the *S. cerevisiae CAC1* gene uncovered a point mutation in the Cac1 subunit that resided in a PIP-like motif (Krawitz *et al.*, 2002). Further biochemical studies with purified proteins confirmed that the mutation indeed crippled the binding of *S. cerevisiae* CAF-1 to PCNA (Krawitz *et al.*, 2002). Visual inspection of the mouse and human p150 sequences

revealed the presence of a PIP-like sequence which, when mutated, abolished the targeting of p150 to PCNA-containing DNA replication foci *in vivo*, and crippled the ability of CAF-1 p150 to promote replication-coupled nucleosome assembly *in vitro* (Rolef Ben-Shahar et al., 2009). Collectively, these studies firmly established PCNA as a partner of CAF-1 that is essential for replication-dependent nucleosome assembly in organisms ranging from yeast to vertebrates.

1.6.3 PCNA and translesion synthesis

In addition to playing roles in DNA replication, PCNA also promotes DNA damage tolerance mediated by error-prone DNA polymerases. DNA is continuously subjected to DNA lesions. These include numerous spontaneous lesions created by reactive metabolites and lesions caused by exposure to DNA damaging agents present in the environment. When present in the template strands, a subset of DNA base lesions blocks the progression of replicative polymerases (*e.g.* 3-methyl adenine). In this case, the replicative polymerase is transiently replaced by an "*emergency*" polymerase that is capable of synthesizing DNA despite the lesion in the template strand. This process is therefore known as either translesion synthesis or DNA lesion bypass. Because the DNA lesion is not removed, this is a form of DNA damage tolerance, rather than DNA repair (Cipolla et al., 2016; Jansen et al., 2015).

A number of "*emergency*" polymerases, such as Pol eta (Pol η), Pol kappa (Pol κ), Pol zeta (Pol ζ), Pol iota (Pol ι) and Rev1 specialize in bypassing different types of adducts in the DNA template strands (Boehm *et al*., 2016). However, the synthesis of DNA across a damaged template strand comes at the price of a considerably higher frequency of mutations compared

the mutation rate of replicative polymerases (Pol ε or Pol δ). Because of this, "*emergency*" polymerases are referred to as error-prone polymerases. One might be inclined to believe that, in contrast to replicative polymerases (Pol ε and Pol δ), error-prone polymerases should not be processive and, therefore, should not associate with PCNA. Counterintuitively, this is not the case. Error-prone polymerases require PCNA binding to execute their roles in translesion synthesis but their association with PCNA is transient. There are mechanisms to dissociate error-prone polymerases from PCNA shortly following DNA lesion bypass.

Furthermore, the binding of error-prone polymerases to PCNA is tightly regulated in order to prevent these enzymes from interfering with Pol ε and Pol δ when there is no lesion in the template strand. This tight regulation is achieved through two mechanisms. The first is that the PIPs of error-prone polymerases are quite divergent from canonical PIPs. Consistent with this, the PIPs of error-prone polymerases bind to PCNA very weakly and adopt PCNA-bound conformations that are very different than those adopted by canonical PIPs (Hishiki et al., 2009).

The second determinant of specificity is that, due to the low affinity of their unusual PIPs for PCNA, error-prone polymerases require a second surface for stable and productive interaction with PCNA. The second determinant of specificity is a ubiquitin binding domain of error-prone polymerases that engages a PCNA ring that has acquired a DNA damage inducible ubiquitin moiety (Bienko et al., 2005; Guo et al., 2006; Hoege et al., 2002; Kannouche et al., 2004; Plosky et al., 2006; Watanabe et al., 2004). In this case, the DNA damage-inducible ubiquitylation of PCNA is clearly part of the mechanism that "*dedicates*" a PCNA ring to error-prone polymerases and DNA lesion bypass. In addition, even though the non-canonical PIPs of error-prone

polymerases exhibit very low affinity for PCNA on their own, they are nonetheless essential for DNA lesion bypass (Boehm *et al.*, 2016). Therefore, the high selectivity and affinity necessary for productive engagement of ubiquitylated PCNA, which is necessary for translesion synthesis, depends upon a bipartite interaction surface of error-prone polymerases that implicates both their non-canonical PIPs and their ubiquitin-binding domains.

1.6.4 PCNA and DNA excision repair mechanisms

There exist three major and evolutionarily conserved DNA excision repair mechanisms. They are known as Nucleotide Excision Repair (NER), Base Excision Repair (BER), and Mismatch repair (MMR). NER removes lesions that grossly distort the DNA double helix structure. These include intra-strand crosslinks [*e.g.* the cyclobutane pyrimidine dimers caused by ultraviolet radiation]. (Marteijn et al., 2014). In order to remove the lesion, endonucleases cleave the phosphodiester backbone of DNA both 5' and 3' of the lesion and the 24-34 nucleotide long oligonucleotide containing the lesion is excised by PCNA- and Polδ-dependent synthesis of lesion-free DNA.

BER removes adducts to DNA bases caused by, for example, oxidation, alkylation, or spontaneous deamination of cytosine into uracil (Krokan and Bjoras, 2013). The first step is catalyzed by DNA glycosylases that have specificity for different types of DNA base adducts. The site where the base lesion was initially present is now lacking a base, a structure often referred to as an abasic site. In the so-called long patch BER pathway, an endonuclease (AP endonuclease) cleaves the phosphodiester backbone 5' of the abasic site, which generates a 3'-hydroxyl from which PCNA- and Pol δ-dependent synthesis can synthesize a pristine new strand. The oligonucleotide containing the abasic site(s) is excised by the flap endonuclease FEN1.

MMR acts on the nascent strands, either the leading or the lagging strand that emerge from replicative polymerases. When the inappropriate base is incorporated into the nascent strands, it can be removed by the MMR excision repair pathway. The MMR machinery scans the nascent strands for misincorporated bases. Misincorporated bases are excised through a mechanism analogous to the one that operates during NER. Endonucleases cleave the phosphodiester backbone of DNA both 5' and 3' of the misincorporated base and a short oligonucleotide containing the inappropriate is excised by PCNA- and Polδ-dependent synthesis.

The three major excision repair pathways attract CAF-1, which is not in itself surprising given that PCNA-dependent DNA synthesis by Pol δ is involved in each pathway (Martini et al., 1998; Moggs et al., 2000; Nabatiyan et al., 2006; Rodriges Blanko et al., 2016)

However, the length of DNA synthesized in each repair pathway is much shorter than the length of DNA in the nucleosome core particle (147 bp). This may suggest that nucleosome remodelling and/or histone dissociation may precede PCNA-dependent DNA synthesis, which in turn would create a demand for CAF-1-mediated deposition of new H3-H4 molecules onto the nascent DNA. At least for NER, this scenario is supported by experimental evidence showing that, in a CAF-1-dependent manner, histones tagged with fluorescent epitopes localized to foci of UV-induced DNA lesions in (Polo et al., 2006). Among many remaining puzzles is the recurring issue of how CAF-1 and Pol δ can both exert their functions through PCNA, without mutually interfering with each other, at sites of NER, BER and MMR.

From the multitude of functions PCNA participates in, researchers have an unarguable notion that PCNA is a global interaction hub for many proteins involved in DNA replication processes and repair processes. This is depicted in the following picture.

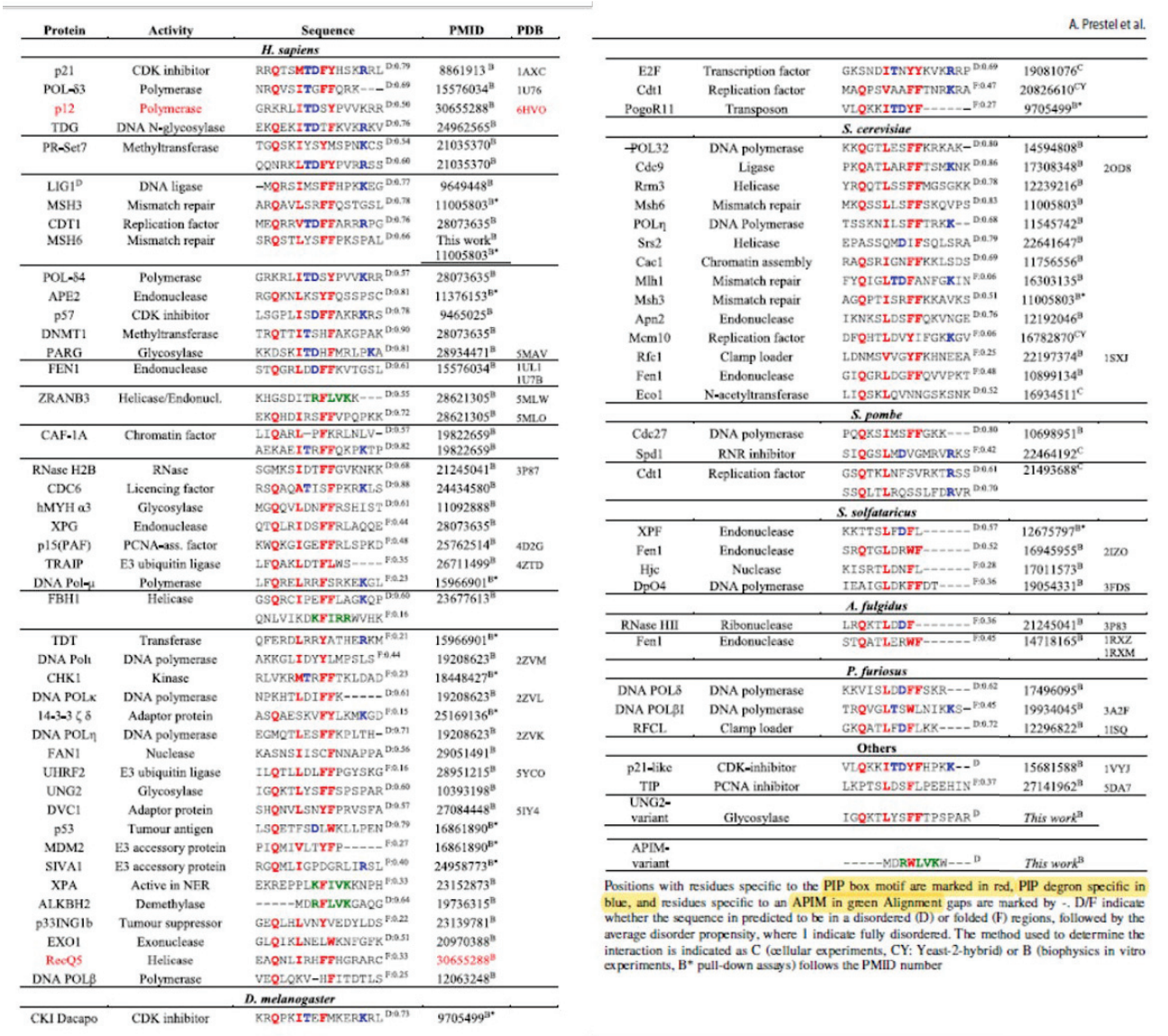

Protein	Activity	Sequence	PMID	PDB
		H. sapiens		
p21	CDK inhibitor	RRQTSMTDFYHSKRRL D:0.79	8861913 B	1AXC
POL-δ3	Polymerase	NRQVSITGFFQRK--- D:0.69	15576034 B	1U76
p12	Polymerase	GRKRLITDSYPVVKRR D:0.56	30655288 B	6HVO
TDG	DNA N-glycosylase	EKQEKITDTFKVKRKV D:0.76	24962565 B	
PR-Set7	Methyltransferase	TGQSKIYSYMSPNKCS D:0.54	21035370 B	
		QQNRKLTDFYPVRRSS D:0.60	21035370 B	
LIG1 D	DNA ligase	-MQRSIMSFFHPKKEG D:0.77	9649448 B	
MSH3	Mismatch repair	ARQAVLSRFFQSTGSL D:0.78	11005803 B*	
CDT1	Replication factor	MEQRRVTDFFARRRPG D:0.76	28073635 B	
MSH6	Mismatch repair	SRQSTLYSFFPKSPAL D:0.66	This work B 11005803 B*	
POL-δ4	Polymerase	GRKRLITDSYPVVKRR D:0.57	28073635 B	
APE2	Endonuclease	RGQKNLKSYFQSSPSC D:0.81	11376153 B*	
p57	CDK inhibitor	LSGPLISDFFAKRKRS D:0.78	9465025 B	
DNMT1	Methyltransferase	TRQTTITSHFAKGPAK D:0.90	28073635 B	
PARG	Glycosylase	KKDSKITDHFMRLPKA D:0.81	28934471 B	5MAV
FEN1	Endonuclease	STQGRLDDFFKVTGSL D:0.61	15576034 B	1UL1 1U7B
ZRANB3	Helicase/Endonucl.	KHGSDITRFLVKK--- D:0.55	28621305 B	5MLW
		EKQHDIRSFFVPQPKK D:0.72	28621305 B	5MLO
CAF-1A	Chromatin factor	LIQARL-PFKRLNLV- D:0.57	19822659 B	
		AEKAEITRFFQKPKTP D:0.82	19822659 B	
RNase H2B	RNase	SGMKSIDTFFGVKNKK D:0.68	21245041 B	3P87
CDC6	Licencing factor	RSQAQATISFPKRKLS D:0.88	24434580 B	
hMYH α3	Glycosylase	MGQQVLDNFFRSHIST D:0.61	11092888 B	
XPG	Endonuclease	QTQLRIDSFFRLAQQE D:0.64	28073635 B	
p15(PAF)	PCNA-ass. factor	KWQKGIGEFFRLSPKD D:0.48	25762514 B	4D2G
TRAIP	E3 ubiquitin ligase	LFQAKLDTFLWS---- D:0.35	26711499 B	4ZTD
DNA Pol-μ	Polymerase	LFQRELRRFSRKEKGL D:0.23	15966901 B*	
FBH1	Helicase	GSQRCIPEFFLAGKQP D:0.60	23677613 B	
		QNLVIKDKFIRRWVHK D:0.16		
TDT	Transferase	QFERDLRRYATHERKM D:0.21	15966901 B*	
DNA Poh	DNA polymerase	AKKGLIDYYLMPSLS D:0.44	19208623 B	2ZVM
CHK1	Kinase	RLVKRMTRFFTKLDAD D:0.23	18448427 B*	
DNA POLκ	DNA polymerase	NPKHTLDIFFK----- D:0.61	19208623 B	2ZVL
14-3-3 ζ δ	Adaptor protein	ASQAESKVFYLKMKGD D:0.15	25169136 B*	
DNA POLη	DNA polymerase	EGMQTLESFFKPLTH- D:0.71	19208623 B	2ZVK
FAN1	Nuclease	KASNSIISCFNNAPPA D:0.56	29051491 B	
UHRF2	E3 ubiquitin ligase	ILQTLLDLFFPGYSKG D:0.16	28951215 B	5YCO
UNG2	Glycosylase	IGQKTLYSFFSPSPAR D:0.60	10393198 B	
DVC1	Adaptor protein	SHQNVLSNYFPRVSFA D:0.57	27084448 B	5IY4
p53	Tumour antigen	LSQETFSDLWKLLPEN D:0.79	16861890 B*	
MDM2	E3 accessory protein	PIQMIVLTYFP----- D:0.27	16861890 B*	
SIVA1	E3 accessory protein	RGQMLIGPDGRLIRSL D:0.40	24958773 B*	
XPA	Active in NER	EKREPPLKFIVKKNPH D:0.33	23152873 B	
ALKBH2	Demethylase	-----MDRFLVKGAQG D:0.64	19736315 B	
p33ING1b	Tumour suppressor	GEQLHLVNYVEDYLDS D:0.22	23139781 B	
EXO1	Exonuclease	GLQIKLNELWKNFGFK D:0.51	20970388 B	
RecQ5	Helicase	EAQNLIRHFFHGRARC D:0.33	30655288 B	
DNA POLβ	Polymerase	VEQLQKV-HFITDTLS D:0.25	12063248 B	
		D. melanogaster		
CKI Dacapo	CDK inhibitor	KRQPKITEFMKERKRL D:0.73	9705499 B*	

A. Prestel et al.

E2F	Transcription factor	GKSNDITNYYKVKRRP D:0.69	19081076 C	
Cdt1	Replication factor	MAQPSVAAFFTNRKRA F:0.47	20826610 CY	
PogoR11	Transposon	VLQKKITDYF------ F:0.27	9705499 B*	
		S. cerevisiae		
-POL32	DNA polymerase	KKQGTLESFFKRKAK- D:0.80	14594808 B	
Cdc9	Ligase	PKQATLARFFTSMKNK D:0.86	17308348 B	2OD8
Rrm3	Helicase	YRQQTLSSFFMGSGKK D:0.78	12239216 B	
Msh6	Mismatch repair	MKQSSLLSFFSKQVPS D:0.83	11005803 B	
POLη	DNA Polymerase	TSSKNILSFFTRKK-- D:0.68	11545742 B	
Srs2	Helicase	EPASSQMDIFSQLSRA D:0.79	22641647 B	
Cac1	Chromatin assembly	RAQSRIGNFFKKLSDS D:0.69	11756556 B	
Mlh1	Mismatch repair	FYQIGLTDFANFGKIN F:0.06	16303135 B	
Msh3	Mismatch repair	AGQPTISRFFKKAVKS D:0.51	11005803 B*	
Apn2	Endonuclease	IKNKSLDSFFQKVNGE D:0.76	12192046 B	
Mcm10	Replication factor	DFQHTLDVYIFGKKGV F:0.06	16782870 CY	
Rfc1	Clamp loader	LDNMSVVGYFKHNEEA F:0.25	22197374 B	1SXJ
Fen1	Endonuclease	GIQGRLDGFFQVVPKT F:0.48	10899134 B	
Eco1	N-acetyltransferase	LIQSKLQVNNGSKSNK D:0.52	16934511 C	
		S. pombe		
Cdc27	DNA polymerase	PQQKSIMSFFGKK--- D:0.80	10698951 B	
Spd1	RNR inhibitor	SIQGSLMDVGMRVRKS F:0.42	22464192 C	
Cdt1	Replication factor	GSQTKLNFSVRKTRSS D:0.61	21493688 C	
		SSQLTLRQSSLFDRVR D:0.70		
		S. solfataricus		
XPF	Endonuclease	KKTTSLFDFL------ D:0.57	12675797 B*	
Fen1	Endonuclease	SRQTGLDRWF------ D:0.52	16945955 B	2IZO
Hjc	Nuclease	KISRTLDNFL------ F:0.28	17011573 B	
DpO4	DNA polymerase	IEAIGLDKFFDT---- F:0.36	19054331 B	3FDS
		A. fulgidus		
RNase HII	Ribonuclease	LRQKTLDDF------- F:0.36	21245041 B	3P83
Fen1	Endonuclease	STQATLERWF------ F:0.45	14718165 B	1RXZ 1RXM
		P. furiosus		
DNA POLδ	DNA polymerase	KKVISLDDFFSKR--- D:0.62	17496095 B	
DNA POLβI	DNA polymerase	TRQVGLTSWLNIKKS- D:0.45	19934045 B	3A2F
RFCL	Clamp loader	GKQATLFDFLKK---- D:0.72	12296822 B	1ISQ
		Others		
p21-like	CDK-inhibitor	VLQKKITDYFHPKK-- D	15681588 B	1VYJ
TIP	PCNA inhibitor	LKPTSLDSFLPEEHIN F:0.37	27141962 B	5DA7
UNG2-variant	Glycosylase	IGQKTLYSFFTPSPAR D	*This work* B	
APIM-variant		-----MDRWLVKH--- D	*This work* B	

Positions with residues specific to the PIP box motif are marked in red, PIP degron specific in blue, and residues specific to an APIM in green Alignment gaps are marked by -. D/F indicate whether the sequence in predicted to be in a disordered (D) or folded (F) regions, followed by the average disorder propensity, where 1 indicate fully disordered. The method used to determine the interaction is indicated as C (cellular experiments, CY: Yeast-2-hybrid) or B (biophysics in vitro experiments, B* pull-down assays) follows the PMID number

Figure I.7 PCNA interaction partners (Prestel et al., 2019, figure reused with permisssion). Figure depicts proteins involved in various cellular processes with distinct PCNA interaction peptides from multiple species. The residues of the conserved canonical PIP box region are

highlighted in red. In the case of most of these proteins, the exact molecular binding mechanism is not known. But in the following example, researchers have shown how functional interference is prevented between PIP-box-containing proteins.

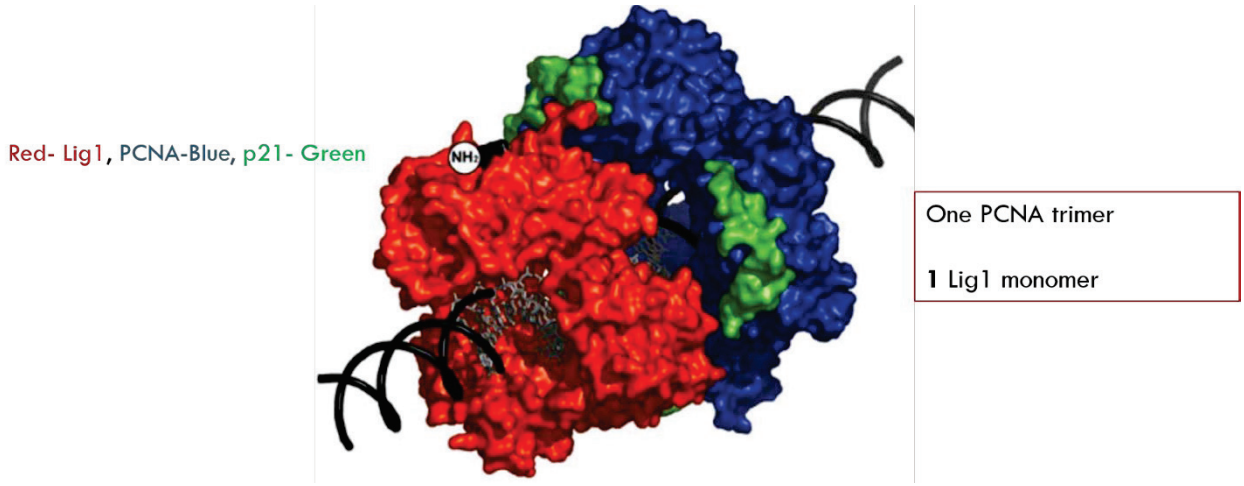

Figure I.8 Schematic showing DNA ligase I monomer in complex with PCNA (Pascal et al., 2004 figure reused with permission). One monomer of DNA ligase I monomer (shown in red) occludes the other two PIP binding sites on the surface of PCNA (shown in blue).

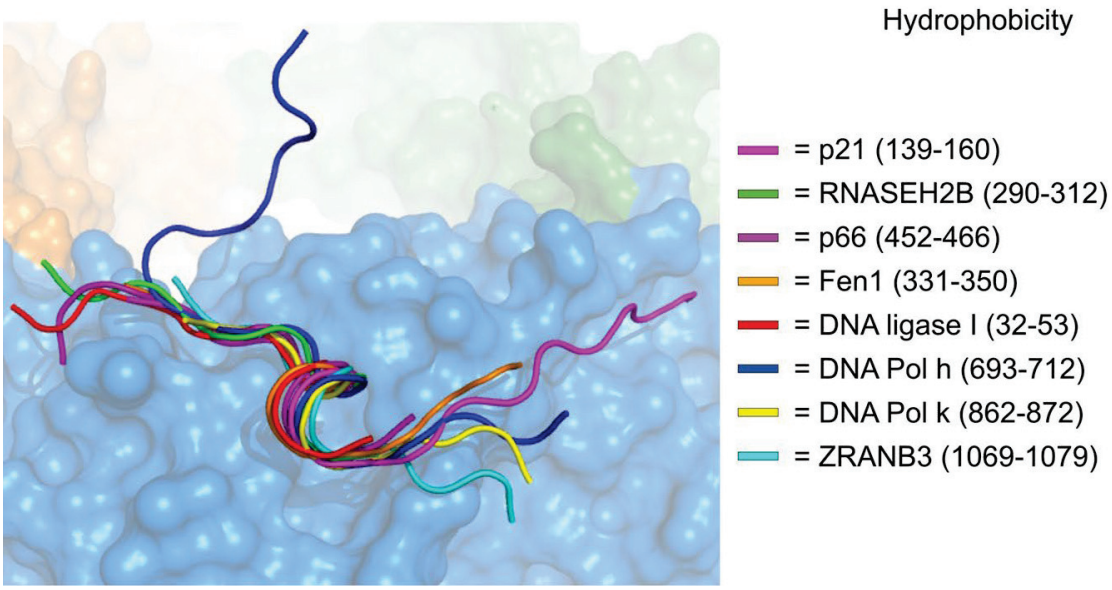

Figure I.9 Overlay of published crystal structures with human PCNA (Prestel et al., 2019, figure reused with permission). Most of the replication enzymes bind to the surface of PCNA in a similar conformation.

A recent report from Prestel *et al.* 2019 has collated the published PIP-box and PIP-degron-containing peptides. The overlay depicts that most of them adopt a similar conformation when bound to PCNA. The above picture also shows an extended N-terminal region and hydrophobic residues that form a 3_{10} helix. p21 also has additional C-terminal residues that interact with the hydrophobic pocket and IDCL of PCNA (Gulbis et al., 1996). Since different proteins with PIPs bind PCNA differently, we were curious to find out how CAF-1 was mediating its interaction with PCNA. Our results are further described in subsequent chapters.

1.6.5 PCNA post translational modifications

PCNA had been reported to be ubiquitylated on the back face (*i.e.* the face opposite to the direction of DNA synthesis) and these modifications help the cells cope with DNA lesions that interfere with DNA synthesis. Sumoylation of lysines at 164 and 127 by UBC9 (E2) and SIZ1 (E3) prevents ubiquitylation of the same residues (Hoege et al., 2002) and attracts an enzyme known as Srs2, which dismantles Rad51 filaments (Veaute et al., 2003) and, thereby, prevents illegitimate recombination between sister chromatids. Mono-ubiquitylation of lysine 164 by UBC2 (E2) and RAD18 (E3) attracts enzymes that promote error-prone DNA lesion bypass (Hoege et al., 2002); (Daigaku et al., 2010), which is a form of DNA damage tolerance that is not accompanied by immediate repair of the lesion (Daigaku et al., 2010). Attachment of a ubiquitin

chain held by lysine 63-linked isopeptide bonds leads to DNA damage tolerance mediated by template switching (Daigaku et al., 2010).

In *S. cerevisiae*, Eco1 acetylates several lysine residues located within the α-helices that line the inner cavity of the PCNA ring (Billon et al., 2017). The exact molecular function of this acetylation is not known but, because the inner cavity is lined by numerous positively charged that might interact non-specifically with DNA, it has been suggested that charge neutralization by acetylation may serve to enhance PCNA sliding and polymerase processivity.

1.6.6 Role of PCNA and CAF-1 in cancer therapy

PCNA is widely known as a cell proliferation marker, mainly because of its association with replicative DNA polymerases, however in addition to this PCNA plays a much bigger role in coordinating various cellular processes. Because of this same reason, though PCNA looks like a lucrative target for various cancers they are not been widely employed yet as a therapeutic option. But more and more researchers are exploiting the potential of targeting the regions of inter domain connecting loop (IDCL) together with the DNA replication and repair function of PCNA in combination with existing chemotherapeutic drugs.

Currently, approaches to treat cells with agents targeting PCNA rely on the use of small molecules or on peptides that either bind to PCNA, or act as a binding competitor for its interacting partners. Since PCNA is subjected to several post translational modifications (PTMs) which help regulate its function by various binding partners; researchers have identified PCNA post translational modifications as a viable therapeutic target for controlling over proliferation in cancer cells. This concept is further strengthened by the fact that PCNA tyrosine (Y) 211 phosphorylation has been shown to be stimulated by the concerted action of growth factors: for

instance, epidermal growth factors (EGF) and protein kinases (c-Abl). Hence, in addition to EGF and EGFR inhibitors already being used in treatment, researchers have successfully used small molecular inhibitors and peptides that specifically inhibit Y211 phosphorylation (Wang et al., 2006; Zhao et al., 2012; Zhao et al., 2011). These PCNA targeting peptides are designed to either prevent downstream protein-protein interactions or block the phosphorylation on tyrosine 211 site.

In addition to this, several studies have tried using the possibility of blocking the inter domain connecting loop (IDCL) binding sites to prevent its interaction with multiple PIP containing proteins. T2AA is a small molecule derivative of the thyroid hormone 3,3,5- triiodothyronine (T3) that targets PCNA-PIP interaction and is experimentally shown to inhibit interaction of PCNA with DNA polymerase delta. Treatment with T2AA is shown to cause replication stress, fork stalling and inhibition of DNA synthesis which eventually promote S phase arrest and apoptosis (Actis et al., 2013; Punchihewa et al., 2012).

Recent research also identified the presence of an isoform of PCNA which is acidic and expressed exclusively in breast, prostrate and esophageal adenocarcinoma cancer cells with an elevated rate of metastasis, but this isoform is absent in normal cells (Bechtel et al., 1998; Hammoud et al., 2007; Malkas et al., 2006; Wang et al., 2011). It is still unclear how their regulation is maintained selectively in cancer cells versus normal cells. Also, general targeting of PCNA could lead to cytotoxic effects in normal cells as highlighted by mouse studies that show early embryonic lethality in the absence of PCNA (Peled et al., 2008; Roa et al., 2008). Specifically targeting the cancer associated isoform of PCNA and targeting specific signaling pathways and post translational modifications that are more prominent in cancer cells could be a beneficial future approach. In addition, more targeted studies using animal models are necessary

to assess the safety and specificity of PCNA inhibitors. Another avenue that needs further research is in the targeted delivery of these small molecular inhibitors or peptides specifically to the cancer cells. A thorough understanding and combinatorial use of novel inhibitors with current chemotherapeutic agents will enhance their benefits.

Researchers have recently reported success in treating higher grade pancreatic ductal adenocarcinomas which are notorious to treat solely using traditional chemotherapeutic drugs (Smith et al., 2020). Studies have shown that pancreatic ductal adenocarcinomas show a higher level of PCNA expression and in addition show somatic mutations in major DNA damage response pathways and DNA repair genes. Authors created a synthetic peptide that mimic a specific region within the IDCL of PCNA that is important for protein-protein interaction specifically in cancer cells. They report that the synthetic R9-caPeptide they created is capable of causing DNA damage, replication fork progression and promoting apoptosis specifically in pancreatic cancer cells (Smith et al., 2020).

Chromatin assembly factor on the other hand, in addition to facilitating nucleosome assembly soon after DNA replication, plays major roles in all major DNA repair pathways (Martini et al., 1998; Nabatiyan and Krude, 2004; Zhu et al., 2009). Dysregulation or overexpression of CAF-1 namely the large two subunits are also observed in genome wide screens of multiple cancer types (Gevaert and Plevritis, 2013; Shah et al., 2014) and in several hematologic malignancies. Increased CAF-1 expression positively correlates with the tumor proliferation marker Ki-67 and is marked with late stage cancers that have poor clinical outcome. Thus, researchers are exploring the possibility of using CAF-1 as a prognostic and predictive tool for advanced stage cancers.

Over expression of CHAF1B is observed in several solid tumors like in cervical cancers, gliomas (de Tayrac et al., 2011), melanomas (Mascolo et al., 2010), prostrate cancers (Staibano et al., 2009) and in human acute myeloid leukemias (AML) (Volk et al., 2018) and acute megakaryocytic leukemia with down syndrome (AMKL-DS). Researchers have shown that the second large subunit of CAF-1 known as CHAF1B or p60 is implicated in progression of normal hematopoiesis, while its over expression causes leukemia (Volk et al., 2018).

Increased expression of CHAF1A and CHAF1B in cervical and lung cancers are associated with advanced clinical stage of the disease, increased metastasis, and higher recurrence (Liu et al., 2017; Yang et al., 2020). Overexpression of CHAF1A mRNA and protein along with CHAF1B and RBBP4 is also observed in high grade colon cancers (Wu et al., 2014).

Recent *in vitro* experiments also suggest that higher expression of CAF-1 promotes tumorigenesis and increased apoptosis (Sykaras et al., 2021). Even though higher expression of CAF-1 subunits in most of solid tumors makes it a promising potential target for prognostic purposes, more studies are needed to understand the complex molecular mechanism of CAF-1 that promotes tumorigenesis. Hence for the successful development of novel chemotherapeutic agents, it is important to understand and differentiate the mechanistic details of both PCNA and CAF-1 in promoting normal cellular DNA replication and its role in promoting tumorigenesis.

1.7 Histone gene organization and regulation in *Saccharomyces cerevisiae*

Eukaryotic cells contain numerous copies of core histone genes. In contrast, our favorite model organism to study histone gene expression, *Saccharomyces cerevisiae,* has only two copies of each gene encoding the canonical replication-dependent histones (H2A, H2B, H3, H4). The genes encoding the core histone variants (e.g. H2A.Z or CENP-A) are not regulated in the same

manner as the genes expressing canonical histones and, therefore, will not be discussed further. Canonical histone mRNAs are produced from four divergent histone gene pairs in *S. cerevisiae* [Figure I.10]. The two divergent gene pairs encoding H3-H4 are *HHT1-HHF1* and *HHT2-HHF2* [HHT = Histone H Three; HHF = Histone H Four] (Smith and Murray, 1983) [Figure I.10]. The two divergent gene pairs encoding H2A-H2B are known as *HTA1-HTB1* and *HTA2-HTB2* [HTA = Histone Two A; H2B = Histone Two B (Hereford et al., 1979) [Figure I.10].

1.7.1 Transcriptional activation of *S. cerevisiae* histone genes

The four canonical core histone gene pairs are tightly regulated during the cell cycle. They are maximally transcribed during S phase and repressed at other stages of the cell cycle. The core histone gene promoters contain specialized *cis-acting* DNA elements that either activate or repress histone gene transcription [Figure I.10]. The Upstream Activating Sequences (*UAS*), the negative regulatory element (*NEG*) and the proteins that bind to those sequences will be discussed separately in the following sections.

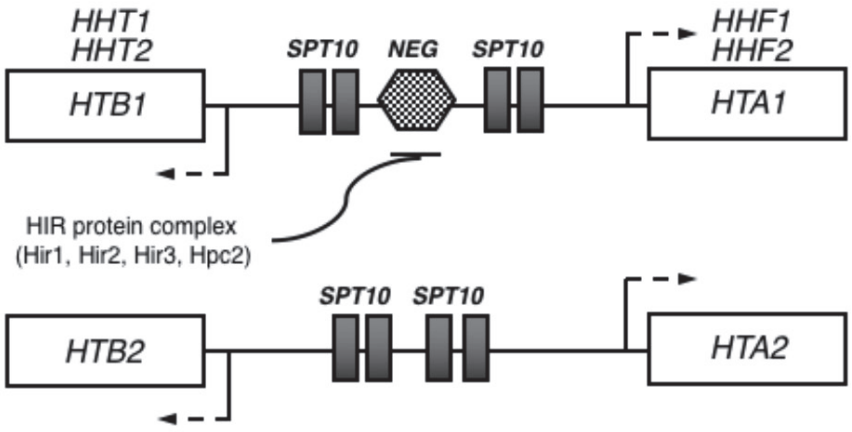

Figure I.10. *S. cerevisiae* histone mRNAs expressed from divergent promoters. The promoters of three divergent histone gene pairs shown above except HTA2-HTB2, contains specialized NEG region required for histone gene repression.

1.7.2 Upstream activating sequence (*UAS*)

The divergent promoters of the four core histone gene pairs each contain at least four 16-base pair UAS elements (Eriksson et al., 2005a; Osley, 1991) [Figure I.10]. They are required for activation of histone gene transcription during the G1-S transition and the S phase of the cell cycle. As described below, the *UAS* elements activate transcription by binding to transcription factors such as Spt10 and the SBF and MBF complexes.

1.7.3 Spt10

Unlike histone proteins, Spt10 is not absolutely essential for viability, but deletion of the *SPT10* gene results in a severe proliferation defect and alters, positively or negatively, the expression of a very large number of non-histone genes (Dollard et al., 1994; Eriksson et al., 2012; Eriksson et al., 2005a). Spt10 is an unusual transcription factor that possesses an acetyltransferase domain that is essential for its role in promoting histone gene transcription. However, despite numerous studies from several laboratories, the direct substrate(s) of the acetyltransferase domain of Spt10 has remained elusive. Spt10 is an activator of transcription dedicated to the canonical replication-dependent histone genes. For instance, the presence of Spt10 at histone gene promoters, but no other yeast promoters, was demonstrated by chromatin immunoprecipitation combined with microarrays [ChIP - chip] (Eriksson et al., 2005b; Mendiratta et al., 2006). This striking specificity of Spt10 has been attributed to the following. Spt10 is a homodimer that contains a highly site-specific zinc finger DNA binding domain that recognizes *UAS* elements that are

uniquely found in the promoters of canonical histone genes, and nowhere else in the yeast genome (Mendiratta et al., 2006). The abundance of all the canonical histone mRNAs is greatly reduced in cells lacking Spt10 (Eriksson et al., 2005b); (Xu et al., 2005). On the other hand, the abundance changes of a multitude of non-histone mRNAs in cells lacking Spt10 has been attributed to reduced histone protein abundance. Consistent with this interpretation, the phenotypes of cells lacking Spt10 are suppressed, and the abundance of most mRNAs restored, by co-overexpression of H2A, H2B, H3 and H4 (Eriksson et al., 2005a). These results suggest that Spt10 is a very important, but not an essential activator dedicated to transcription of canonical replication-dependent histone genes.

1.7.4 The SCF binding factor (SBF) and the MluI binding factor (MBF)

The SCF Binding Factor (SBF) is composed of a heterodimer of the Swi4 and Swi6 proteins, whereas the MluI Binding Factor (MBF) is composed of a heterodimer of Mbp1 and Swi6. The Swi4 and Mbp1 subunits are, respectively, the site-specific DNA binding subunits of SBF and MBF (Iyer et al., 2001). Individually deleting the *SWI4* or the *MBP1* gene, showed reduced expression of canonical histone mRNAs and many other histone RNAs. Unlike Spt10, which is dedicated to histone gene transcription, SBF and MBF promote transcription of many cell cycle-regulated genes in addition to histone genes. In spite of this, two lines of evidence indicate that SBF and MBF directly activate histone gene transcription. First, the specific DNA binding sequences recognized by SCF and MBF are present within the *UAS* elements of all the promoters of canonical histone genes (Eriksson et al., 2012). Second, based on chromatin immunoprecipitation (ChIP), SBF and MBF are located at those *UAS* elements *in vivo*. Single mutants lacking either Swi4 (SCF) or Mbp1 (MBF) are viable and show reduced abundance of histone RNAs (Eriksson et al., 2012). However, because cells lacking both Swi4 and Mbp1 are

inviable, it is not possible to determine whether SCF and MBF are collectively essential for transcription of canonical histone genes. The mechanism through which SBF and MBF activate histone gene transcription is not known.

1.7.5 *cis*-acting DNA sequences required for histone gene repression in *S. cerevisiae*

The *cis*-acting DNA sequence that is crucial for transcriptional repression of all canonical histone gene promoters is known as the negative regulatory (*NEG*) region [Figure I.10]. *NEG* was defined as a 54 bp *cis*-acting DNA sequence that, when deleted from the *HTA1-HTB1* promoter, prevented transcriptional repression of the *HTA1* and *HTB1* gene during the cell cycle and in response to DNA damage (Osley *et al*., 1986). Three out of the four core histone gene pairs: *HTA1-HTB1*, *HHT1-HHF1*, and *HHT2-HHF2* contain a *NEG cis*-acting element (Figure I.10) that is required for histone gene repression. In contrast, the *NEG* element is absent from the promoter of the *HTA2-HTB2* gene pair [Figure I.10] (Marino-Ramirez *et al*., 2006; Osley, 1991). Nonetheless, the *HTA2* and *HTB2* genes are also transcriptionally repressed during early G1, G2/M and in response to DNA damage during S-phase (Eriksson *et al*., 2012).

1.7.6 *trans*-acting factors that repress histone gene transcription

The *S. cerevisiae* histone regulatory (HIR) complex is composed of four polypeptide subunits known as Hir1, Hir2, Hir3, and Hpc2 (histone periodic control). This complex is evolutionarily conserved from yeast to humans. The subunits of the human complex are known as HIRA (a protein that includes both *S. cerevisiae* Hir1 and Hir2), CABIN (a homologue of *S. cerevisiae*

Hir3), and UBINUCLEIN (UBN1 and UBN2, two homologues of *S. cerevisiae* Hpc2). The genes encoding the four subunits of the *S. cerevisiae* HIR complex were identified in genetic screens designed to uncover mutants that cannot repress histone gene transcription in early G1 or in response to DNA damage during S-phase (Lycan et al., 1987; Xu et al., 1992a). The HIR complex represses three of the four histone gene pairs, namely *HTA1-HTB1*, *HHT1-HHF1*, and *HHT2-HHF2*, but not *HTA2-HTB2* which lacks the *NEG* element (Kurat et al., 2014). Nonetheless, the *HTA2* and *HTB2* genes are repressed during early G1 or in response to DNA damage (Lycan et al., 1987; Xu et al., 1992b), but the mechanism of *NEG*- and HIR-independent repression of *HTA2-HTB2* is not known.

Interestingly, the *NEG* element and HIR proteins are necessary for transcriptional repression of histone gene promoters fused to non-histone reporter genes [*e.g.* the genes that encode β-galactosidase and neomycin resistance](Osley, 1991). Because those reporter genes lack the 3'-untranslated histone mRNA sequences that post-translationally regulate mRNA abundance, the reporter gene experiments demonstrate that the action of the *NEG* element and the HIR complex are exerted through transcriptional repression of histone gene promoters. *In vitro* studies with partially purified HIR complexes have suggested that the HIR proteins do not directly bind to canonical histone gene promoters *in vitro* (Osley, 1991), but this remains to be firmly established. It is formally possible that non-HIR proteins that were not present *in vitro* may facilitate direct binding of the HIR complex to the *NEG* element *in vivo*. However, this hypothesis has not yet been confirmed since no protein that facilitates recruitment of HIR to *NEG* elements has thus far been identified (DeSilva et al., 1998; Prochasson et al., 2005); (Mendiratta et al., 2007). Nonetheless, chromatin immunoprecipitation (ChIP) studies revealed

that the four subunits of the HIR complex localize to histone gene promoters (Eriksson et al., 2012).

Although the four HIR subunits (Hir1, Hir2, Hir3 and Hpc2) are essential for transcriptional repression of histone genes in *S. cerevisiae*, the subunit that is best studied and most tightly regulated is Hpc2. We will therefore confine this introduction to the properties of Hpc2 (the homologue of human UBN1 and UBN2), an important focal point in this thesis. Human UBN1 and UBN2 contain a 50-amino acid domain that, based on its homology with yeast Hpc2 was termed the Hpc2-Related Domain (HRD) of UBN1 and UBN2. Interestingly, the HRD of human UBN1/UBN2, and the HRD of their *S. cerevisiae* homologue Hpc2, directly bind to histone H3. Human UBN1/UBN2 bind to the replication-independent variant H3.3 (Ricketts et al., 2015) which contains a few residues that distinguish H3.3 from the replication-dependent H3.1/H3.2. Structures of UBN1 bound to H3.3 have identified only a few residues that enable UBN1 to discriminate between H3.3 and H3.1/H3.2 (Ricketts et al., 2015; Ricketts and Marmorstein, 2017). Importantly, the residues of UBN1 that directly contact H3.3 are identical in *S. cerevisiae* Hpc2. This raises the exciting possibility of creating structure-based mutants of Hpc2 that may prove to be unable to bind yeast H3. This is exciting because it may open the possibility to address whether cell cycle and/or DNA damage-induced repression of histone genes depends upon a negative feedback by which excess histones are sensed through their direct binding to the Hpc2 subunit of the HIR complex. If this proves to be the case, Hpc2 might serve a sensor of the presence of excess histones.

1.8 The HIR complex and its role in replication-independent nucleosome assembly

All the canonical H3 molecules derived from the *HHT1* and *HHT2* genes have exactly the same amino acid sequence. Unexpectedly, the sequence of *S. cerevisiae* H3 is identical to that of the replication-independent H3.3 variant in human cells (Baxevanis and Landsman, 1998). Intriguingly, this suggests that *S. cerevisiae* H3 can serve as substrate for both replication-dependent and replication-independent nucleosome assembly, unlike in human cells. For replication-dependent nucleosome assembly, *S. cerevisiae* H3, which is identical to human H3.3, binds to CAF-1. In contrast, *S. cerevisiae* H3 promotes replication-independent nucleosome assembly by binding to the Hpc2 subunit of the HIR complex. Consistent with this, the 4-subunit HIR complex has been purified from *S. cerevisiae* in association with H3 (equivalent to human H3.3) - H4 (Green et al., 2005); (Prochasson et al., 2005). Importantly, in a system that consists only of purified proteins, the HIR-H3-H4 complex was capable of depositing H3-H4 onto a non-replicating plasmid DNA, thus providing strong evidence for its replication-independent nucleosome activity (Prochasson et al., 2005); (Green et al., 2005)

1.9 DNA damage response and prevention of excess histone synthesis

1.9.1 Methyl Methane Sulphonate (MMS)

MMS is an alkylating agent whose main cytotoxic lesion is the alkylation of the N3 position of adenine, a lesion often referred to as 3-methyl adenine (3-MeA). The primary reason why 3-MeA is cytotoxic is that it blocks the synthesis of DNA by replicative polymerases (Pol δ and Pol ε). Thus, the main consequence of the presence of 3-MeA ahead of replication forks is to slow down the rates of DNA replication fork elongation. This occurs when replicative DNA polymerases encounter 3-MeA in the template strands for DNA synthesis.

1.9.2 Hydroxyurea (HU)

Unlike MMS, HU does not completely block replicative DNA polymerases, but nonetheless dramatically slows down all the polymerases involved in DNA synthesis throughout the genome. This is because HU is an inhibitor of ribonucleotide reductase (RNR), the enzyme that catalyzes the reduction of ribonucleoside triphosphates (NTPs) into deoxyribonucleoside triphosphates (dNTPs). As a result, HU decreases the pools of dNTPs below the threshold concentration required for optimal DNA synthesis by replicative polymerases.

1.9.3 The response to genotoxic agents that interfere with replication fork progression

The genetic material is constantly bombarded by extrinsic (genotoxic agents from the environment) and intrinsic (metabolites that react with DNA) sources of DNA damage. Cells have evolved numerous surveillance and protective mechanisms that promote DNA repair and preserve genome integrity. Some of those mechanisms are collectively known as DNA damage checkpoints. For instance, once persistent DNA lesions have been detected, the so-called G2/M DNA damage checkpoint of yeast cells blocks the transition from metaphase to anaphase until DNA lesions have been repaired. This ensures that cytotoxic or mutagenic DNA lesions are not transferred to daughter cells. In contrast to the G2/M DNA damage checkpoint, the intra S-phase DNA damage response operates in a fundamentally distinct manner. Rather than completely blocking a cell cycle transition, the intra S-phase DNA damage response merely extends the duration of S-phase to facilitate the repair of DNA lesions ahead of incoming replicative polymerases. The *biological rationale* is that, by prolonging S-phase duration, several repair machineries can remove DNA lesions ahead of incoming DNA polymerases. In turn, this minimizes the probability that replicative polymerases will

encounter cytotoxic or mutagenic DNA lesions. Based on this fundamental difference with, for instance the G2/M checkpoint that completely arrests cell cycle progression, we prefer the term intra S-phase DNA damage response, rather the more commonly used term intra S-phase checkpoint.

1.9.4 The intra S-phase DNA damage response as a source of excess histones

In response to conditions that interfere with DNA replication, the intra S-phase DNA damage response is activated by two protein kinases known as Mec1 and Rad53 in *S. cerevisiae*. In response to many forms of DNA damage, Mec1 phosphorylates and activates the kinase activity of Rad53. Mec1 and Rad53 also phosphorylate many proteins that act in concert to delay S-phase progression and promote DNA repair. The key role of the intra S-phase DNA damage response in delaying S-phase progression is to suddenly block the firing of new DNA replication origins upon detection of DNA lesions. In order to block the firing of new DNA replication origins, Mec1 and Rad53 phosphorylate replication proteins that were present at origins that had not yet fired at the time when DNA damage was detected. Activation of the intra S-phase DNA damage response therefore results in a sudden and abrupt decline in the total rate of DNA synthesis because the total number of active replication forks is much lower than in the absence of DNA damage. In turn, this abrupt decline in the total rate of DNA synthesis provokes the accumulation of excess histones.

Previous studies from our laboratory have reported the importance of maintaining a delicate balance between histone synthesis and DNA synthesis using S. cerevisiae as a model organism (Gunjan and Verreault, 2003). Excess histones are toxic because they bind tightly and non-specifically to nucleic acids (DNA and RNA), and even properly assembled chromatin. S. cerevisiae cells that contain excess histones exhibit defects in DNA repair, gene expression,

mitotic chromosome segregation, and likely other processes that were not investigated. Yeast cells have evolved the use of at least three partially redundant strategies to attenuate the deleterious effects of excess histones, including transcriptional repression of histone genes, degradation of excess histone mRNAs in the nucleus, and degradation of excess histone proteins. The focus of this thesis (Chapter 3) is to study the transcriptional repression of histone genes under conditions that produce excess histones, namely DNA lesions that activate the intra S-phase DNA damage response.

1.10 Thesis objectives and main results

My Ph.D. research work was focused on understanding the molecular mechanisms of two distinct processes related chromatin assembly. First, I studied the mode of PCNA binding by CAF-1 (see rationale below). Second, I studied the repression of histone gene transcription in response to DNA lesions that delay S-phase progression, and the role of this mechanism in preventing the accumulation of excess histone proteins (chapter 3).

The long-term goal related to the work that I initiated in chapter 2 is to understand the following conundrum. Figure I.11 shows a simplified diagram of some, but not all the PCNA-binding enzymes that continuously exert their activities at or very close behind all replication forks. The fact that most of these functionally distinct PCNA-binding enzymes contain "*seemingly*" similar PIPs raises the fascinating question of how all these enzymes perform their functions without mutually interfering with each other. This is a multifaceted question because one is led to hypothesize that there are several potential types of functional interference. For instance, the different replication enzymes (Pol ε, Pol δ, FEN1 and DNA ligase) should not

compete for binding to any given PCNA ring. In other words, the different PCNA rings must "*somehow*" acquire specificity for different aspects of DNA replication and post-replicative functions (see below). Furthermore, the PCNA-binding proteins that need to act on nascent double-stranded DNA behind the sites of synthesis (*e.g.* the DNA methyltransferase DNMT1, the mismatch repair enzymes and CAF-1) should obviously not compete with the DNA replication enzymes that also bind PCNA. Last, but not least, some PCNA-binding enzymes obviously have to act sequentially. For instance, DNMT1 cannot methylate many CpG dinucleotides when the nascent hemi-methylated DNA is wrapped around histone octamers (Felle et al., 2011; Okuwaki and Verreault, 2004). This suggests that DNMT1 must bind PCNA and methylate the nascent strand before CAF-1 binding to PCNA enables the deposition of histones onto nascent DNA. How the sequential action of functionally distinct PCNA-binding enzymes is orchestrated is not known at all.

As a first step to elucidate this intricate jigsaw puzzle, my first objective (chapter 2) was to determine how CAF-1 binds to PCNA by comparison to the mode of PCNA binding determined for DNA replication enzymes.

Based on structural and biophysical evidence, we found that CAF-1 binding to PCNA is unorthodox, and thus far unique among PCNA-binding enzymes. Tentatively, our results suggest hypothetical mechanisms to dedicate one PCNA ring for CAF1-mediated chromatin assembly, despite the presence of multiple other PCNA-binding proteins at replication forks.

For my second objective (chapter 3), I investigated the crucial molecular mechanism by which cells maintain a delicate balance between DNA and histone synthesis despite the presence of DNA lesions that interfere with replication. Our results suggest that DNA damage-induced repression of histone genes is mediated, at least in part, by a simple negative feedback triggered by binding of excess histones to the Hpc2 subunit of the HIR complex.

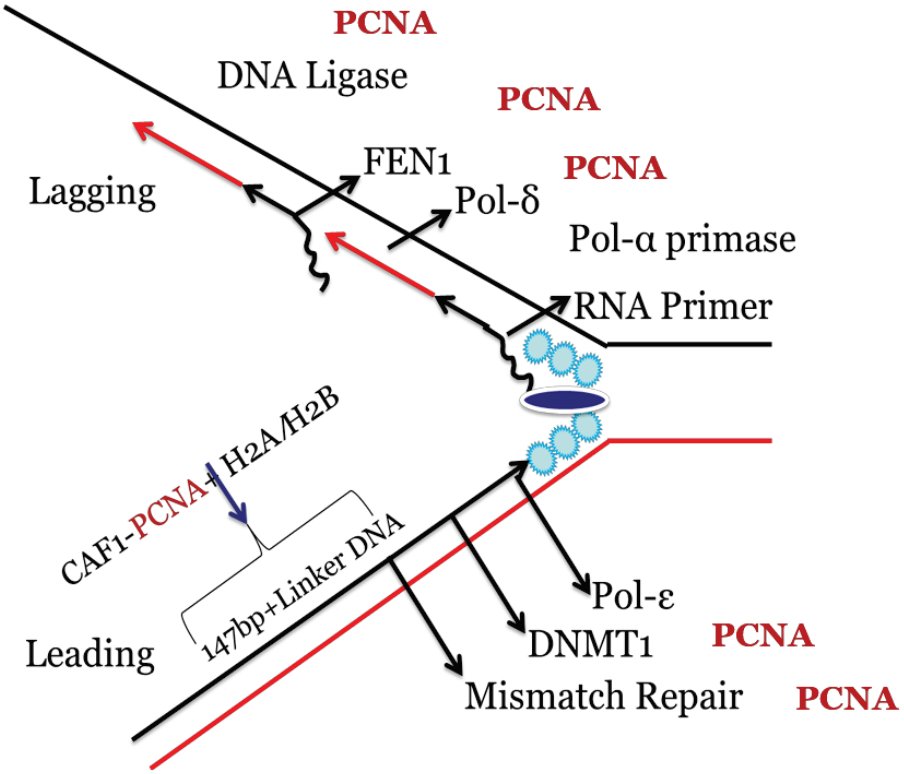

Figure I.11. Simplified representation of PCNA-binding enzymes at replication forks. Pol α - primase is not processive and, therefore, does not need to bind PCNA. For clarity, this is not shown here but some proteins (*e.g.* DNMT1, Mismatch Repair enzymes and CAF-1) must act on both the leading strand chromatid and the lagging strand chromatid.

References Introduction

Actis, M., A. Inoue, B. Evison, S. Perry, C. Punchihewa, and N. Fujii. 2013. Small molecule inhibitors of PCNA/PIP-box interaction suppress translesion DNA synthesis. *Bioorg Med Chem*. 21:1972-1977.

Aguilar-Gurrieri, C., A. Larabi, V. Vinayachandran, N.A. Patel, K. Yen, R. Reja, I.O. Ebong, G. Schoehn, C.V. Robinson, B.F. Pugh, and D. Panne. 2016. Structural evidence for Nap1-dependent H2A-H2B deposition and nucleosome assembly. *EMBO J*. 35:1465-1482.

Alabert, C., T.K. Barth, N. Reveron-Gomez, S. Sidoli, A. Schmidt, O.N. Jensen, A. Imhof, and A. Groth. 2015. Two distinct modes for propagation of histone PTMs across the cell cycle. *Genes Dev*. 29:585-590.

Alabert, C., and A. Groth. 2012. Chromatin replication and epigenome maintenance. *Nature reviews. Molecular cell biology*. 13:153-167.

Andrews, A.J., X. Chen, A. Zevin, L.A. Stargell, and K. Luger. 2010. The histone chaperone Nap1 promotes nucleosome assembly by eliminating nonnucleosomal histone DNA interactions. *Mol Cell*. 37:834-842.

Bagot, C.N., and R. Arya. 2008. Virchow and his triad: a question of attribution. *Br J Haematol*. 143:180-190.

Balakrishnan, L., and R.A. Bambara. 2013. Okazaki fragment metabolism. *Cold Spring Harbor perspectives in biology*. 5.

Bambara, R.A., R.S. Murante, and L.A. Henricksen. 1997. Enzymes and reactions at the eukaryotic DNA replication fork. *J Biol Chem*. 272:4647-4650.

Bannister, A.J., and T. Kouzarides. 2011. Regulation of chromatin by histone modifications. *Cell Res*. 21:381-395.

Baxevanis, A.D., and D. Landsman. 1998. Histone Sequence Database: new histone fold family members. *Nucleic Acids Res*. 26:372-375.

Beattie, T.R., and S.D. Bell. 2012. Coordination of multiple enzyme activities by a single PCNA in archaeal Okazaki fragment maturation. *EMBO J*. 31:1556-1567.

Bechtel, P.E., R.J. Hickey, L. Schnaper, J.W. Sekowski, B.J. Long, R. Freund, N. Liu, C. Rodriguez-Valenzuela, and L.H. Malkas. 1998. A unique form of proliferating cell nuclear antigen is present in malignant breast cells. *Cancer Res*. 58:3264-3269.

Bell, S.P., and B. Stillman. 1992. ATP-dependent recognition of eukaryotic origins of DNA replication by a multiprotein complex. *Nature*. 357:128-134.

Belotserkovskaya, R., S. Oh, V.A. Bondarenko, G. Orphanides, V.M. Studitsky, and D. Reinberg. 2003. FACT facilitates transcription-dependent nucleosome alteration. *Science*. 301:1090-1093.

Bienko, M., C.M. Green, N. Crosetto, F. Rudolf, G. Zapart, B. Coull, P. Kannouche, G. Wider, M. Peter, A.R. Lehmann, K. Hofmann, and I. Dikic. 2005. Ubiquitin-binding domains in Y-family polymerases regulate translesion synthesis. *Science*. 310:1821-1824.

Billon, P., J. Li, J.P. Lambert, Y. Chen, V. Tremblay, J.S. Brunzelle, A.C. Gingras, A. Verreault, T. Sugiyama, J.F. Couture, and J. Cote. 2017. Acetylation of PCNA Sliding Surface by Eco1 Promotes Genome Stability through Homologous Recombination. *Mol Cell*. 65:78-90.

Blackwell, J.S., Jr., S.T. Wilkinson, N. Mosammaparast, and L.F. Pemberton. 2007. Mutational analysis of H3 and H4 N termini reveals distinct roles in nuclear import. *J Biol Chem*. 282:20142-20150.

Boehm, E.M., M. Spies, and M.T. Washington. 2016. PCNA tool belts and polymerase bridges form during translesion synthesis. *Nucleic Acids Res*. 44:8250-8260.

Bowman, G.D., M. O'Donnell, and J. Kuriyan. 2004. Structural analysis of a eukaryotic sliding DNA clamp-clamp loader complex. *Nature*. 429:724-730.

Burgers, P.M.J., and T.A. Kunkel. 2017. Eukaryotic DNA Replication Fork. *Annu Rev Biochem*. 86:417-438.

Burgess, R.J., and Z. Zhang. 2013. Histone chaperones in nucleosome assembly and human disease. *Nat Struct Mol Biol*. 20:14-22.
Cerritelli, S.M., and R.J. Crouch. 2009. Ribonuclease H: the enzymes in eukaryotes. *The FEBS journal*. 276:1494-1505.
Cipolla, L., A. Maffia, F. Bertoletti, and S. Sabbioneda. 2016. The Regulation of DNA Damage Tolerance by Ubiquitin and Ubiquitin-Like Modifiers. *Front Genet*. 7:105.
Daigaku, Y., A.A. Davies, and H.D. Ulrich. 2010. Ubiquitin-dependent DNA damage bypass is separable from genome replication. *Nature*. 465:951-955.
De Biasio, A., and F.J. Blanco. 2013. Proliferating cell nuclear antigen structure and interactions: too many partners for one dancer? *Adv Protein Chem Struct Biol*. 91:1-36.
de Tayrac, M., M. Aubry, S. Saikali, A. Etcheverry, C. Surbled, F. Guenot, M.D. Galibert, A. Hamlat, T. Lesimple, V. Quillien, P. Menei, and J. Mosser. 2011. A 4-gene signature associated with clinical outcome in high-grade gliomas. *Clin Cancer Res*. 17:317-327.
DeSilva, H., K. Lee, and M.A. Osley. 1998. Functional dissection of yeast Hir1p, a WD repeat-containing transcriptional corepressor. *Genetics*. 148:657-667.
Dollard, C., S.L. Ricupero-Hovasse, G. Natsoulis, J.D. Boeke, and F. Winston. 1994. SPT10 and SPT21 are required for transcription of particular histone genes in Saccharomyces cerevisiae. *Mol Cell Biol*. 14:5223-5228.
English, C.M., M.W. Adkins, J.J. Carson, M.E. Churchill, and J.K. Tyler. 2006. Structural basis for the histone chaperone activity of Asf1. *Cell*. 127:495-508.
Enomoto, S., P.D. McCune-Zierath, M. Gerami-Nejad, M.A. Sanders, and J. Berman. 1997. RLF2, a subunit of yeast chromatin assembly factor-I, is required for telomeric chromatin function in vivo. *Genes Dev*. 11:358-370.
Eriksson, P.R., D. Ganguli, V. Nagarajavel, and D.J. Clark. 2012. Regulation of histone gene expression in budding yeast. *Genetics*. 191:7-20.
Eriksson, P.R., G. Mendiratta, N.B. McLaughlin, T.G. Wolfsberg, L. Marino-Ramirez, T.A. Pompa, M. Jainerin, D. Landsman, C.-H. Shen, and D.J. Clark. 2005a. Global regulation by the yeast Spt10 protein is mediated through chromatin structure and the histone upstream activating sequence elements. *Mol Cell Biol*. 25:9127-9137.
Eriksson, P.R., G. Mendiratta, N.B. McLaughlin, T.G. Wolfsberg, L. Marino-Ramirez, T.A. Pompa, M. Jainerin, D. Landsman, C.H. Shen, and D.J. Clark. 2005b. Global regulation by the yeast Spt10 protein is mediated through chromatin structure and the histone upstream activating sequence elements. *Mol Cell Biol*. 25:9127-9137.
Evrin, C., J.D. Maman, A. Diamante, L. Pellegrini, and K. Labib. 2018. Histone H2A-H2B binding by Pol alpha in the eukaryotic replisome contributes to the maintenance of repressive chromatin. *EMBO J*. 37.
Felle, M., H. Hoffmeister, J. Rothammer, A. Fuchs, J.H. Exler, and G. Langst. 2011. Nucleosomes protect DNA from DNA methylation in vivo and in vitro. *Nucleic Acids Res*. 39:6956-6969.
Foltman, M., C. Evrin, G. De Piccoli, R.C. Jones, R.D. Edmondson, Y. Katou, R. Nakato, K. Shirahige, and K. Labib. 2013. Eukaryotic replisome components cooperate to process histones during chromosome replication. *Cell reports*. 3:892-904.
Formosa, T. 2003. Changing the DNA landscape: putting a SPN on chromatin. *Current topics in microbiology and immunology*. 274:171-201.
Formosa, T., and F. Winston. 2020. The role of FACT in managing chromatin: disruption, assembly, or repair? *Nucleic Acids Res*. 48:11929-11941.
Freudenthal, B.D., L. Gakhar, S. Ramaswamy, and M.T. Washington. 2009. A charged residue at the subunit interface of PCNA promotes trimer formation by destabilizing alternate subunit interactions. *Acta Crystallogr D Biol Crystallogr*. 65:560-566.

Gaillard, P.H.L., J.G. Moggs, D.M. Roche, J.P. Quivy, P.B. Becker, R.D. Wood, and G. Almouzni. 1997. Initiation and bidirectional propagation of chromatin assembly from a target site for nucleotide excision repair. *EMBO J*. 16:6281-6289.

Gambus, A., R.C. Jones, A. Sanchez-Diaz, M. Kanemaki, F. van Deursen, R.D. Edmondson, and K. Labib. 2006. GINS maintains association of Cdc45 with MCM in replisome progression complexes at eukaryotic DNA replication forks. *Nat Cell Biol*. 8:358-366.

Gerard, A., S. Koundrioukoff, V. Ramillon, J.C. Sergere, N. Mailand, J.P. Quivy, and G. Almouzni. 2006. The replication kinase Cdc7-Dbf4 promotes the interaction of the p150 subunit of chromatin assembly factor 1 with proliferating cell nuclear antigen. *EMBO reports*. 7:817-823.

Gevaert, O., and S. Plevritis. 2013. Identifying master regulators of cancer and their downstream targets by integrating genomic and epigenomic features. *Pac Symp Biocomput*:123-134.

Green, E.M., A.J. Antczak, A.O. Bailey, A.A. Franco, K.J. Wu, J.R. Yates, and P.D. Kaufman. 2005. Replication-independent histone deposition by the HIR complex and Asf1. *Curr Biol*. 15:2044-2049.

Gulbis, J.M., Z. Kelman, J. Hurwitz, M. O'Donnell, and J. Kuriyan. 1996. Structure of the C-terminal region of p21(WAF1/CIP1) complexed with human PCNA. *Cell*. 87:297-306.

Gunjan, A., and A. Verreault. 2003. A Rad53 kinase-dependent surveillance mechanism that regulates histone protein levels in S. cerevisiae. *Cell*. 115:537-549.

Guo, C., T.S. Tang, M. Bienko, J.L. Parker, A.B. Bielen, E. Sonoda, S. Takeda, H.D. Ulrich, I. Dikic, and E.C. Friedberg. 2006. Ubiquitin-binding motifs in REV1 protein are required for its role in the tolerance of DNA damage. *Mol Cell Biol*. 26:8892-8900.

Hammond, C.M., C.B. Stromme, H. Huang, D.J. Patel, and A. Groth. 2017. Histone chaperone networks shaping chromatin function. *Nature reviews. Molecular cell biology*. 18:141-158.

Hammoud, Z.T., S. Badve, R. Saxena, K.A. Kesler, K. Rieger, L.H. Malkas, and R.J. Hickey. 2007. A novel biomarker for the detection of esophageal adenocarcinoma. *J Thorac Cardiovasc Surg*. 133:82-87.

Han, J., H. Zhang, H. Zhang, Z. Wang, H. Zhou, and Z. Zhang. 2013. A Cul4 E3 ubiquitin ligase regulates histone hand-off during nucleosome assembly. *Cell*. 155:817-829.

Hereford, L., K. Fahrner, J. Woolford, M. Rosbash, and D.B. Kaback. 1979. Isolation of yeast histone genes H2A and H2B. *Cell*. 18:1261-1271.

Hingorani, M.M., and M. O'Donnell. 2000. Sliding clamps: a (tail)ored fit. *Curr Biol*. 10:R25-29.

Hishiki, A., H. Hashimoto, T. Hanafusa, K. Kamei, E. Ohashi, T. Shimizu, H. Ohmori, and M. Sato. 2009. Structural basis for novel interactions between human translesion synthesis polymerases and proliferating cell nuclear antigen. *J Biol Chem*. 284:10552-10560.

Hoege, C., B. Pfander, G.L. Moldovan, G. Pyrowolakis, and S. Jentsch. 2002. RAD6-dependent DNA repair is linked to modification of PCNA by ubiquitin and SUMO. *Nature*. 419:135-141.

Homesley, L., M. Lei, Y. Kawasaki, S. Sawyer, T. Christensen, and B.K. Tye. 2000. Mcm10 and the MCM2-7 complex interact to initiate DNA synthesis and to release replication factors from origins. *Genes Dev*. 14:913-926.

Hondele, M., T. Stuwe, M. Hassler, F. Halbach, A. Bowman, E.T. Zhang, B. Nijmeijer, C. Kotthoff, V. Rybin, S. Amlacher, E. Hurt, and A.G. Ladurner. 2013. Structural basis of histone H2A-H2B recognition by the essential chaperone FACT. *Nature*. 499:111-114.

Huang, H., C.B. Stromme, G. Saredi, M. Hodl, A. Strandsby, C. Gonzalez-Aguilera, S. Chen, A. Groth, and D.J. Patel. 2015. A unique binding mode enables MCM2 to chaperone histones H3-H4 at replication forks. *Nat Struct Mol Biol*. 22:618-626.

Huang, S., H. Zhou, J. Tarara, and Z. Zhang. 2007. A novel role for histone chaperones CAF-1 and Rtt106p in heterochromatin silencing. *EMBO J*. 26:2274-2283.

Ishimi, Y., S. Ichinose, A. Omori, K. Sato, and H. Kimura. 1996. Binding of human minichromosome maintenance proteins with histone H3. *J Biol Chem*. 271:24115-24122.
Iyer, V.R., C.E. Horak, C.S. Scafe, D. Botstein, M. Snyder, and P.O. Brown. 2001. Genomic binding sites of the yeast cell-cycle transcription factors SBF and MBF. *Nature*. 409:533-538.
Jackson, V., and R. Chalkley. 1985. Histone segregation on replicating chromatin. *Biochemistry*. 24:6930-6938.
Jansen, J.G., A. Tsaalbi-Shtylik, and N. de Wind. 2015. Roles of mutagenic translesion synthesis in mammalian genome stability, health and disease. *DNA repair*. 29:56-64.
Jonsson, Z.O., R. Hindges, and U. Hubscher. 1998. Regulation of DNA replication and repair proteins through interaction with the front side of proliferating cell nuclear antigen. *EMBO J*. 17:2412-2425.
Kamakaka, R.T., M. Bulger, P.D. Kaufman, B. Stillman, and J.T. Kadonaga. 1996. Postreplicative chromatin assembly by Drosophila and human chromatin assembly factor 1. *Mol Cell Biol*. 16:810-817.
Kannouche, P.L., J. Wing, and A.R. Lehmann. 2004. Interaction of human DNA polymerase eta with monoubiquitinated PCNA: a possible mechanism for the polymerase switch in response to DNA damage. *Mol Cell*. 14:491-500.
Kaufman, P.D., R. Kobayashi, N. Kessler, and B. Stillman. 1995. The p150 and p60 subunits of chromatin assembly factor I: a molecular link between newly synthesized histones and DNA replication. *Cell*. 81:1105-1114.
Kaufman, P.D., R. Kobayashi, and B. Stillman. 1997. Ultraviolet radiation sensitivity and reduction of telomeric silencing in Saccharomyces cerevisiae cells lacking chromatin assembly factor-I. *Genes Dev*. 11:345-357.
Kelch, B.A. 2016. Review: The lord of the rings: Structure and mechanism of the sliding clamp loader. *Biopolymers*. 105:532-546.
Kemble, D.J., L.L. McCullough, F.G. Whitby, T. Formosa, and C.P. Hill. 2015. FACT Disrupts Nucleosome Structure by Binding H2A-H2B with Conserved Peptide Motifs. *Mol Cell*. 60:294-306.
Krawitz, D.C., T. Kama, and P.D. Kaufman. 2002. Chromatin assembly factor I mutants defective for PCNA binding require Asf1/Hir proteins for silencing. *Mol Cell Biol*. 22:614-625.
Krishna, T.S., X.P. Kong, S. Gary, P.M. Burgers, and J. Kuriyan. 1994. Crystal structure of the eukaryotic DNA polymerase processivity factor PCNA. *Cell*. 79:1233-1243.
Krokan, H.E., and M. Bjoras. 2013. Base excision repair. *Cold Spring Harbor perspectives in biology*. 5:a012583.
Krude, T. 1995. Chromatin assembly factor 1 (CAF-1) colocalizes with replication foci in HeLa cell nuclei. *Experimental cell research*. 220:304-311.
Kurat, C.F., J. Recht, E. Radovani, T. Durbic, B. Andrews, and J. Fillingham. 2014. Regulation of histone gene transcription in yeast. *Cellular and molecular life sciences : CMLS*. 71:599-613.
Kurat, C.F., J.T.P. Yeeles, H. Patel, A. Early, and J.F.X. Diffley. 2017. Chromatin Controls DNA Replication Origin Selection, Lagging-Strand Synthesis, and Replication Fork Rates. *Mol Cell*. 65:117-130.
Lark, K.G. 1972a. Evidence for the direct involvement of RNA in the initiation of DNA replication in Escherichia coli 15T. *J Mol Biol*. 64:47-60.
Lark, K.G. 1972b. Genetic control over the initiation of the synthesis of the short deoxynucleotide chains in E. coli. *Nat New Biol*. 240:237-240.
Leffak, I.M. 1984. Conservative segregation of nucleosome core histones. *Nature*. 307:82-85.
Lejeune, E., M. Bortfeld, S.A. White, A.L. Pidoux, K. Ekwall, R.C. Allshire, and A.G. Ladurner. 2007. The chromatin-remodeling factor FACT contributes to centromeric heterochromatin independently of RNAi. *Curr Biol*. 17:1219-1224.
Leonhardt, H., H.P. Rahn, P. Weinzierl, A. Sporbert, T. Cremer, D. Zink, and M.C. Cardoso. 2000. Dynamics of DNA replication factories in living cells. *J Cell Biol*. 149:271-280.

Li, H., and M.E. O'Donnell. 2018. The Eukaryotic CMG Helicase at the Replication Fork: Emerging Architecture Reveals an Unexpected Mechanism. *BioEssays : news and reviews in molecular, cellular and developmental biology*. 40.

Liu, T., J. Wei, C. Jiang, C. Wang, X. Zhang, Y. Du, J. Li, and H. Zhao. 2017. CHAF1A, the largest subunit of the chromatin assembly factor 1 complex, regulates the growth of H1299 human non-small cell lung cancer cells by inducing G0/G1 cell cycle arrest. *Exp Ther Med*. 14:4681-4686.

Liu, W.H., S.C. Roemer, A.M. Port, and M.E. Churchill. 2012. CAF-1-induced oligomerization of histones H3/H4 and mutually exclusive interactions with Asf1 guide H3/H4 transitions among histone chaperones and DNA. *Nucleic Acids Res*. 40:11229-11239.

Liu, W.H., S.C. Roemer, Y. Zhou, Z.J. Shen, B.K. Dennehey, J.L. Balsbaugh, J.C. Liddle, T. Nemkov, N.G. Ahn, K.C. Hansen, J.K. Tyler, and M.E. Churchill. 2016. The Cac1 subunit of histone chaperone CAF-1 organizes CAF-1-H3/H4 architecture and tetramerizes histones. *eLife*. 5.

Liu, Y., K. Zhou, N. Zhang, H. Wei, Y.Z. Tan, Z. Zhang, B. Carragher, C.S. Potter, S. D'Arcy, and K. Luger. 2020. FACT caught in the act of manipulating the nucleosome. *Nature*. 577:426-431.

Looke, M., M.F. Maloney, and S.P. Bell. 2017. Mcm10 regulates DNA replication elongation by stimulating the CMG replicative helicase. *Genes Dev*. 31:291-305.

Luger, K., A.W. Mader, R.K. Richmond, D.F. Sargent, and T.J. Richmond. 1997. Crystal structure of the nucleosome core particle at 2.8 A resolution. *Nature*. 389:251-260.

Lujan, S.A., J.S. Williams, and T.A. Kunkel. 2016. DNA Polymerases Divide the Labor of Genome Replication. *Trends Cell Biol*. 26:640-654.

Lycan, D.E., M.A. Osley, and L.M. Hereford. 1987. Role of transcriptional and posttranscriptional regulation in expression of histone genes in Saccharomyces cerevisiae. *Mol Cell Biol*. 7:614-621.

Maga, G., and U. Hubscher. 2003. Proliferating cell nuclear antigen (PCNA): a dancer with many partners. *Journal of cell science*. 116:3051-3060.

Mailand, N., I. Gibbs-Seymour, and S. Bekker-Jensen. 2013. Regulation of PCNA-protein interactions for genome stability. *Nature reviews. Molecular cell biology*. 14:269-282.

Malay, A.D., T. Umehara, K. Matsubara-Malay, B. Padmanabhan, and S. Yokoyama. 2008. Crystal structures of fission yeast histone chaperone Asf1 complexed with the Hip1 B-domain or the Cac2 C terminus. *J Biol Chem*. 283:14022-14031.

Malkas, L.H., B.S. Herbert, W. Abdel-Aziz, L.E. Dobrolecki, Y. Liu, B. Agarwal, D. Hoelz, S. Badve, L. Schnaper, R.J. Arnold, Y. Mechref, M.V. Novotny, P. Loehrer, R.J. Goulet, and R.J. Hickey. 2006. A cancer-associated PCNA expressed in breast cancer has implications as a potential biomarker. *Proc Natl Acad Sci U S A*. 103:19472-19477.

Marino-Ramirez, L., I.K. Jordan, and D. Landsman. 2006. Multiple independent evolutionary solutions to core histone gene regulation. *Genome biology*. 7:R122.

Marteijn, J.A., H. Lans, W. Vermeulen, and J.H. Hoeijmakers. 2014. Understanding nucleotide excision repair and its roles in cancer and ageing. *Nature reviews. Molecular cell biology*. 15:465-481.

Martini, E., D.M. Roche, K. Marheineke, A. Verreault, and G. Almouzni. 1998. Recruitment of phosphorylated chromatin assembly factor 1 to chromatin after UV irradiation of human cells. *J Cell Biol*. 143:563-575.

Mascolo, M., M.L. Vecchione, G. Ilardi, M. Scalvenzi, G. Molea, M. Di Benedetto, L. Nugnes, M. Siano, G. De Rosa, and S. Staibano. 2010. Overexpression of Chromatin Assembly Factor-1/p60 helps to predict the prognosis of melanoma patients. *BMC Cancer*. 10:63.

Mattiroli, F., Y. Gu, J.L. Balsbaugh, N.G. Ahn, and K. Luger. 2017a. The Cac2 subunit is essential for productive histone binding and nucleosome assembly in CAF-1. *Scientific reports*. 7:46274.

Mattiroli, F., Y. Gu, T. Yadav, J.L. Balsbaugh, M.R. Harris, E.S. Findlay, Y. Liu, C.A. Radebaugh, L.A. Stargell, N.G. Ahn, I. Whitehouse, and K. Luger. 2017b. DNA-mediated association of two histone-bound

complexes of yeast Chromatin Assembly Factor-1 (CAF-1) drives tetrasome assembly in the wake of DNA replication. *eLife*. 6.
McKnight, S.L., and O.L. Miller, Jr. 1977. Electron microscopic analysis of chromatin replication in the cellular blastoderm Drosophila melanogaster embryo. *Cell*. 12:795-804.
Mello, J.A., H.H. Sillje, D.M. Roche, D.B. Kirschner, E.A. Nigg, and G. Almouzni. 2002. Human Asf1 and CAF-1 interact and synergize in a repair-coupled nucleosome assembly pathway. *EMBO reports*. 3:329-334.
Mendiratta, G., P.R. Eriksson, and D.J. Clark. 2007. Cooperative binding of the yeast Spt10p activator to the histone upstream activating sequences is mediated through an N-terminal dimerization domain. *Nucleic Acids Res*. 35:812-821.
Mendiratta, G., P.R. Eriksson, C.-H. Shen, and D.J. Clark. 2006. The DNA-binding domain of the yeast Spt10p activator includes a zinc finger that is homologous to foamy virus integrase. *J Biol Chem*. 281:7040-7048.
Moggs, J.G., P. Grandi, J.P. Quivy, Z.O. Jonsson, U. Hubscher, P.B. Becker, and G. Almouzni. 2000. A CAF-1-PCNA-mediated chromatin assembly pathway triggered by sensing DNA damage. *Mol Cell Biol*. 20:1206-1218.
Moldovan, G.L., B. Pfander, and S. Jentsch. 2007. PCNA, the maestro of the replication fork. *Cell*. 129:665-679.
Moyer, S.E., P.W. Lewis, and M.R. Botchan. 2006. Isolation of the Cdc45/Mcm2-7/GINS (CMG) complex, a candidate for the eukaryotic DNA replication fork helicase. *Proc Natl Acad Sci U S A*. 103:10236-10241.
Muramatsu, S., K. Hirai, Y.S. Tak, Y. Kamimura, and H. Araki. 2010. CDK-dependent complex formation between replication proteins Dpb11, Sld2, Pol (epsilon}, and GINS in budding yeast. *Genes Dev*. 24:602-612.
Murzina, N., A. Verreault, E. Laue, and B. Stillman. 1999. Heterochromatin dynamics in mouse cells: interaction between chromatin assembly factor 1 and HP1 proteins. *Mol Cell*. 4:529-540.
Murzina, N.V., X.Y. Pei, W. Zhang, M. Sparkes, J. Vicente-Garcia, J.V. Pratap, S.H. McLaughlin, T.R. Ben-Shahar, A. Verreault, B.F. Luisi, and E.D. Laue. 2008. Structural basis for the recognition of histone H4 by the histone-chaperone RbAp46. *Structure*. 16:1077-1085.
Nabatiyan, A., and T. Krude. 2004. Silencing of chromatin assembly factor 1 in human cells leads to cell death and loss of chromatin assembly during DNA synthesis. *Mol Cell Biol*. 24:2853-2862.
Nabatiyan, A., D. Szuts, and T. Krude. 2006. Induction of CAF-1 expression in response to DNA strand breaks in quiescent human cells. *Mol Cell Biol*. 26:1839-1849.
Naryzhny, S.N. 2008. Proliferating cell nuclear antigen: a proteomics view. *Cellular and molecular life sciences : CMLS*. 65:3789-3808.
Nougarede, R., F. Della Seta, P. Zarzov, and E. Schwob. 2000. Hierarchy of S-phase-promoting factors: yeast Dbf4-Cdc7 kinase requires prior S-phase cyclin-dependent kinase activation. *Mol Cell Biol*. 20:3795-3806.
O'Donnell, M., L. Langston, and B. Stillman. 2013. Principles and concepts of DNA replication in bacteria, archaea, and eukarya. *Cold Spring Harbor perspectives in biology*. 5.
O'Keefe, R.T., S.C. Henderson, and D.L. Spector. 1992. Dynamic organization of DNA replication in mammalian cell nuclei: spatially and temporally defined replication of chromosome-specific alpha-satellite DNA sequences. *J Cell Biol*. 116:1095-1110.
Okuwaki, M., and A. Verreault. 2004. Maintenance DNA methylation of nucleosome core particles. *J Biol Chem*. 279:2904-2912.
Osley, M.A. 1991. The regulation of histone synthesis in the cell cycle. *Annu Rev Biochem*. 60:827-861.
Osley, M.A., J. Gould, S. Kim, M.Y. Kane, and L. Hereford. 1986. Identification of sequences in a yeast histone promoter involved in periodic transcription. *Cell*. 45:537-544.

Pacek, M., A.V. Tutter, Y. Kubota, H. Takisawa, and J.C. Walter. 2006. Localization of MCM2-7, Cdc45, and GINS to the site of DNA unwinding during eukaryotic DNA replication. *Mol Cell*. 21:581-587.

Pascal, J.M., P.J. O'Brien, A.E. Tomkinson, and T. Ellenberger. 2004. Human DNA ligase I completely encircles and partially unwinds nicked DNA. *Nature*. 432:473-478.

Pedley, A.M., M.A. Lill, and V.J. Davisson. 2014. Flexibility of PCNA-protein interface accommodates differential binding partners. *PloS one*. 9:e102481.

Peled, J.U., F.L. Kuang, M.D. Iglesias-Ussel, S. Roa, S.L. Kalis, M.F. Goodman, and M.D. Scharff. 2008. The biochemistry of somatic hypermutation. *Annu Rev Immunol*. 26:481-511.

Plosky, B.S., A.E. Vidal, A.R. Fernandez de Henestrosa, M.P. McLenigan, J.P. McDonald, S. Mead, and R. Woodgate. 2006. Controlling the subcellular localization of DNA polymerases iota and eta via interactions with ubiquitin. *EMBO J*. 25:2847-2855.

Polo, S.E., D. Roche, and G. Almouzni. 2006. New histone incorporation marks sites of UV repair in human cells. *Cell*. 127:481-493.

Prendergast, J.A., L.E. Murray, A. Rowley, D.R. Carruthers, R.A. Singer, and G.C. Johnston. 1990. Size selection identifies new genes that regulate Saccharomyces cerevisiae cell proliferation. *Genetics*. 124:81-90.

Prestel, A., N. Wichmann, J.M. Martins, R. Marabini, N. Kassem, S.S. Broendum, M. Otterlei, O. Nielsen, M. Willemoes, M. Ploug, W. Boomsma, and B.B. Kragelund. 2019. The PCNA interaction motifs revisited: thinking outside the PIP-box. *Cellular and molecular life sciences : CMLS*. 76:4923-4943.

Prior, C.P., C.R. Cantor, E.M. Johnson, and V.G. Allfrey. 1980. Incorporation of exogenous pyrene-labeled histone into Physarum chromatin: a system for studying changes in nucleosomes assembled in vivo. *Cell*. 20:597-608.

Prochasson, P., L. Florens, S.K. Swanson, M.P. Washburn, and J.L. Workman. 2005. The HIR corepressor complex binds to nucleosomes generating a distinct protein/DNA complex resistant to remodeling by SWI/SNF. *Genes Dev*. 19:2534-2539.

Punchihewa, C., A. Inoue, A. Hishiki, Y. Fujikawa, M. Connelly, B. Evison, Y. Shao, R. Heath, I. Kuraoka, P. Rodrigues, H. Hashimoto, M. Kawanishi, M. Sato, T. Yagi, and N. Fujii. 2012. Identification of small molecule proliferating cell nuclear antigen (PCNA) inhibitor that disrupts interactions with PIP-box proteins and inhibits DNA replication. *J Biol Chem*. 287:14289-14300.

Quivy, J.P., A. Gerard, A.J. Cook, D. Roche, and G. Almouzni. 2008. The HP1-p150/CAF-1 interaction is required for pericentric heterochromatin replication and S-phase progression in mouse cells. *Nat Struct Mol Biol*. 15:972-979.

Quivy, J.P., P. Grandi, and G. Almouzni. 2001. Dimerization of the largest subunit of chromatin assembly factor 1: importance in vitro and during Xenopus early development. *EMBO J*. 20:2015-2027.

Ramsperger, U., and H. Stahl. 1995. Unwinding of chromatin by the SV40 large T antigen DNA helicase. *EMBO J*. 14:3215-3225.

Richet, N., D. Liu, P. Legrand, C. Velours, A. Corpet, A. Gaubert, M. Bakail, G. Moal-Raisin, R. Guerois, C. Compper, A. Besle, B. Guichard, G. Almouzni, and F. Ochsenbein. 2015. Structural insight into how the human helicase subunit MCM2 may act as a histone chaperone together with ASF1 at the replication fork. *Nucleic Acids Res*. 43:1905-1917.

Ricketts, M.D., B. Frederick, H. Hoff, Y. Tang, D.C. Schultz, T. Singh Rai, M. Grazia Vizioli, P.D. Adams, and R. Marmorstein. 2015. Ubinuclein-1 confers histone H3.3-specific-binding by the HIRA histone chaperone complex. *Nat Commun*. 6:7711.

Ricketts, M.D., and R. Marmorstein. 2017. A Molecular Prospective for HIRA Complex Assembly and H3.3-Specific Histone Chaperone Function. *J Mol Biol*. 429:1924-1933.

Roa, S., E. Avdievich, J.U. Peled, T. Maccarthy, U. Werling, F.L. Kuang, R. Kan, C. Zhao, A. Bergman, P.E. Cohen, W. Edelmann, and M.D. Scharff. 2008. Ubiquitylated PCNA plays a role in somatic

hypermutation and class-switch recombination and is required for meiotic progression. *Proc Natl Acad Sci U S A*. 105:16248-16253.

Rodriges Blanko, E., L.Y. Kadyrova, and F.A. Kadyrov. 2016. DNA Mismatch Repair Interacts with CAF-1- and ASF1A-H3-H4-dependent Histone (H3-H4)2 Tetramer Deposition. *J Biol Chem*. 291:9203-9217.

Rolef Ben-Shahar, T., A.G. Castillo, M.J. Osborne, K.L. Borden, J. Kornblatt, and A. Verreault. 2009. Two fundamentally distinct PCNA interaction peptides contribute to chromatin assembly factor 1 function. *Mol Cell Biol*. 29:6353-6365.

Roufa, D.J., and M.A. Marchionni. 1982. Nucleosome segregation at a defined mammalian chromosomal site. *Proc Natl Acad Sci U S A*. 79:1810-1814.

Rowley, A., R.A. Singer, and G.C. Johnston. 1991. CDC68, a yeast gene that affects regulation of cell proliferation and transcription, encodes a protein with a highly acidic carboxyl terminus. *Mol Cell Biol*. 11:5718-5726.

Sauer, P.V., J. Timm, D. Liu, D. Sitbon, E. Boeri-Erba, C. Velours, N. Mucke, J. Langowski, F. Ochsenbein, G. Almouzni, and D. Panne. 2017. Insights into the molecular architecture and histone H3-H4 deposition mechanism of yeast Chromatin assembly factor 1. *eLife*. 6.

Sawyer, S.L., I.H. Cheng, W. Chai, and B.K. Tye. 2004. Mcm10 and Cdc45 cooperate in origin activation in Saccharomyces cerevisiae. *J Mol Biol*. 340:195-202.

Shah, M.A., E.L. Denton, C.H. Arrowsmith, M. Lupien, and M. Schapira. 2014. A global assessment of cancer genomic alterations in epigenetic mechanisms. *Epigenetics Chromatin*. 7:29.

Shen, Z., T. Formosa, and D. Tantin. 2018. FACT Inhibition Blocks Induction But Not Maintenance of Pluripotency. *Stem Cells Dev*. 27:1693-1701.

Shibahara, K., and B. Stillman. 1999. Replication-dependent marking of DNA by PCNA facilitates CAF-1-coupled inheritance of chromatin. *Cell*. 96:575-585.

Smith, C.L., T.D. Matheson, D.J. Trombly, X. Sun, E. Campeau, X. Han, J.R. Yates, 3rd, and P.D. Kaufman. 2014. A separable domain of the p150 subunit of human chromatin assembly factor-1 promotes protein and chromosome associations with nucleoli. *Mol Biol Cell*. 25:2866-2881.

Smith, D.J., and I. Whitehouse. 2012. Intrinsic coupling of lagging-strand synthesis to chromatin assembly. *Nature*. 483:434-438.

Smith, M.M., and K. Murray. 1983. Yeast H3 and H4 histone messenger RNAs are transcribed from two non-allelic gene sets. *J Mol Biol*. 169:641-661.

Smith, S., and B. Stillman. 1989. Purification and characterization of CAF-I, a human cell factor required for chromatin assembly during DNA replication in vitro. *Cell*. 58:15-25.

Smith, S., and B. Stillman. 1991. Stepwise assembly of chromatin during DNA replication in vitro. *EMBO J*. 10:971-980.

Smith, S.J., C.M. Li, R.G. Lingeman, R.J. Hickey, Y. Liu, L.H. Malkas, and M. Raoof. 2020. Molecular Targeting of Cancer-Associated PCNA Interactions in Pancreatic Ductal Adenocarcinoma Using a Cell-Penetrating Peptide. *Mol Ther Oncolytics*. 17:250-256.

Sogo, J.M., H. Stahl, T. Koller, and R. Knippers. 1986. Structure of replicating simian virus 40 minichromosomes. The replication fork, core histone segregation and terminal structures. *J Mol Biol*. 189:189-204.

Staibano, S., M. Mascolo, F.P. Mancini, A. Kisslinger, G. Salvatore, M. Di Benedetto, P. Chieffi, V. Altieri, D. Prezioso, G. Ilardi, G. De Rosa, and D. Tramontano. 2009. Overexpression of chromatin assembly factor-1 (CAF-1) p60 is predictive of adverse behaviour of prostatic cancer. *Histopathology*. 54:580-589.

Stodola, J.L., and P.M. Burgers. 2016. Resolving individual steps of Okazaki-fragment maturation at a millisecond timescale. *Nat Struct Mol Biol*. 23:402-408.

Sykaras, A.G., A. Pergaris, and S. Theocharis. 2021. Challenging, Accurate and Feasible: CAF-1 as a Tumour Proliferation Marker of Diagnostic and Prognostic Value. *Cancers (Basel)*. 13.

Tagami, H., D. Ray-Gallet, G. Almouzni, and Y. Nakatani. 2004. Histone H3.1 and H3.3 complexes mediate nucleosome assembly pathways dependent or independent of DNA synthesis. *Cell*. 116:51-61.

Tan, B.C., C.T. Chien, S. Hirose, and S.C. Lee. 2006. Functional cooperation between FACT and MCM helicase facilitates initiation of chromatin DNA replication. *EMBO J*. 25:3975-3985.

Tang, Y., M.V. Poustovoitov, K. Zhao, M. Garfinkel, A. Canutescu, R. Dunbrack, P.D. Adams, and R. Marmorstein. 2006. Structure of a human ASF1a-HIRA complex and insights into specificity of histone chaperone complex assembly. *Nat Struct Mol Biol*. 13:921-929.

Tyler, J.K., K.A. Collins, J. Prasad-Sinha, E. Amiott, M. Bulger, P.J. Harte, R. Kobayashi, and J.T. Kadonaga. 2001. Interaction between the Drosophila CAF-1 and ASF1 chromatin assembly factors. *Mol Cell Biol*. 21:6574-6584.

VanDemark, A.P., M. Blanksma, E. Ferris, A. Heroux, C.P. Hill, and T. Formosa. 2006. The structure of the yFACT Pob3-M domain, its interaction with the DNA replication factor RPA, and a potential role in nucleosome deposition. *Mol Cell*. 22:363-374.

Veaute, X., J. Jeusset, C. Soustelle, S.C. Kowalczykowski, E. Le Cam, and F. Fabre. 2003. The Srs2 helicase prevents recombination by disrupting Rad51 nucleoprotein filaments. *Nature*. 423:309-312.

Verreault, A., P.D. Kaufman, R. Kobayashi, and B. Stillman. 1998. Nucleosomal DNA regulates the core-histone-binding subunit of the human Hat1 acetyltransferase. *Curr Biol*. 8:96-108.

Volk, A., K. Liang, P. Suraneni, X. Li, J. Zhao, M. Bulic, S. Marshall, K. Pulakanti, S. Malinge, J. Taub, Y. Ge, S. Rao, E. Bartom, A. Shilatifard, and J.D. Crispino. 2018. A CHAF1B-Dependent Molecular Switch in Hematopoiesis and Leukemia Pathogenesis. *Cancer cell*. 34:707-723 e707.

Wang, S.C., Y. Nakajima, Y.L. Yu, W. Xia, C.T. Chen, C.C. Yang, E.W. McIntush, L.Y. Li, D.H. Hawke, R. Kobayashi, and M.C. Hung. 2006. Tyrosine phosphorylation controls PCNA function through protein stability. *Nat Cell Biol*. 8:1359-1368.

Wang, T., Y. Liu, G. Edwards, D. Krzizike, H. Scherman, and K. Luger. 2018. The histone chaperone FACT modulates nucleosome structure by tethering its components. *Life Sci Alliance*. 1:e201800107.

Wang, X., R.J. Hickey, L.H. Malkas, M.O. Koch, L. Li, S. Zhang, G.E. Sandusky, D.J. Grignon, J.N. Eble, and L. Cheng. 2011. Elevated expression of cancer-associated proliferating cell nuclear antigen in high-grade prostatic intraepithelial neoplasia and prostate cancer. *Prostate*. 71:748-754.

Watanabe, K., S. Tateishi, M. Kawasuji, T. Tsurimoto, H. Inoue, and M. Yamaizumi. 2004. Rad18 guides poleta to replication stalling sites through physical interaction and PCNA monoubiquitination. *EMBO J*. 23:3886-3896.

Winston, F., D.T. Chaleff, B. Valent, and G.R. Fink. 1984. Mutations affecting Ty-mediated expression of the HIS4 gene of Saccharomyces cerevisiae. *Genetics*. 107:179-197.

Wittmeyer, J., and T. Formosa. 1997. The Saccharomyces cerevisiae DNA polymerase alpha catalytic subunit interacts with Cdc68/Spt16 and with Pob3, a protein similar to an HMG1-like protein. *Mol Cell Biol*. 17:4178-4190.

Wold, M.S. 1997. Replication protein A: a heterotrimeric, single-stranded DNA-binding protein required for eukaryotic DNA metabolism. *Annu Rev Biochem*. 66:61-92.

Wu, Z., F. Cui, F. Yu, X. Peng, T. Jiang, D. Chen, S. Lu, H. Tang, and Z. Peng. 2014. Up-regulation of CHAF1A, a poor prognostic factor, facilitates cell proliferation of colon cancer. *Biochemical and biophysical research communications*. 449:208-215.

Xu, F., K. Zhang, and M. Grunstein. 2005. Acetylation in histone H3 globular domain regulates gene expression in yeast. *Cell*. 121:375-385.

Xu, H., U.J. Kim, T. Schuster, and M. Grunstein. 1992a. Identification of a new set of cell cycle-regulatory genes that regulate S-phase transcription of histone genes in Saccharomyces cerevisiae. *Mol Cell Biol*. 12:5249-5259.

Xu, H., U.J. Kim, T. Schuster, and M. Grunstein. 1992b. Identification of a new set of cell cycle-regulatory genes that regulate S-phase transcription of histone genes in Saccharomyces cerevisiae. *Mol Cell Biol*. 12:5249-5259.

Yang, S., Q. Long, M. Chen, X. Liu, and H. Zhou. 2020. CAF-1/p150 promotes cell proliferation, migration, invasion and predicts a poor prognosis in patients with cervical cancer. *Oncol Lett*. 20:2338-2346.

Zhang, K., Y. Gao, J. Li, R. Burgess, J. Han, H. Liang, Z. Zhang, and Y. Liu. 2016. A DNA binding winged helix domain in CAF-1 functions with PCNA to stabilize CAF-1 at replication forks. *Nucleic Acids Res*. 44:5083-5094.

Zhang, W., M. Tyl, R. Ward, F. Sobott, J. Maman, A.S. Murthy, A.A. Watson, O. Fedorov, A. Bowman, T. Owen-Hughes, H. El Mkami, N.V. Murzina, D.G. Norman, and E.D. Laue. 2013. Structural plasticity of histones H3-H4 facilitates their allosteric exchange between RbAp48 and ASF1. *Nat Struct Mol Biol*. 20:29-35.

Zhang, Z., K. Shibahara, and B. Stillman. 2000. PCNA connects DNA replication to epigenetic inheritance in yeast. *Nature*. 408:221-225.

Zhao, H., P.C. Ho, Y.H. Lo, A. Espejo, M.T. Bedford, M.C. Hung, and S.C. Wang. 2012. Interaction of proliferation cell nuclear antigen (PCNA) with c-Abl in cell proliferation and response to DNA damages in breast cancer. *PloS one*. 7:e29416.

Zhao, H., Y.H. Lo, L. Ma, S.E. Waltz, J.K. Gray, M.C. Hung, and S.C. Wang. 2011. Targeting tyrosine phosphorylation of PCNA inhibits prostate cancer growth. *Mol Cancer Ther*. 10:29-36.

Zhu, Q., G. Wani, H.H. Arab, M.A. El-Mahdy, A. Ray, and A.A. Wani. 2009. Chromatin restoration following nucleotide excision repair involves the incorporation of ubiquitinated H2A at damaged genomic sites. *DNA repair*. 8:262-273.

Chapter 2

Unorthodox PCNA binding by Chromatin Assembly Factor 1

Amogh Gopinathan Nair [1,2], Nick Rabas [3], Sara Lejon [3], Caleb Homiski [4], Michael J. Osborne [1], Normand Cyr [5], Alexander Sverzhinsky [6], Thomas Melendy [4], John M. Pascal [6], Ernest D. Laue [3], Katherine L.B. Borden [1,7], James G. Omichinski [5] and Alain Verreault [1,7*]

[1] Institute for Research in Immunology and Cancer, Université de Montréal, QC, Canada

[2] Programme de Biologie Moléculaire, Université de Montréal, QC, Canada

[3] Department of Biochemistry, University of Cambridge, 80 Tennis Court Road, Cambridge, CB2 1GA, UK

[4] University at Buffalo Jacobs School of Medicine & Biomedical Sciences, 3435 Main Street, Buffalo, NY 14214-3000, USA

[5] Département de Biochimie et Médecine Moléculaire, Université de Montréal, C.P. 6128 Succursale Centre-Ville, Montréal, QC, H3C 3J7, Canada

[6] Université de Montréal, Department of Biochemistry and Molecular Medicine, 2900 Boulevard Édouard-Montpetit, Roger-Gaudry Pavilion, Montréal, QC, H3T 1J4, Canada

[7] Département de Pathologie et Biologie Cellulaire, Université de Montréal, QC, Canada

* To whom correspondence should be addressed: Alain Verreault, IRIC, Université de Montréal, P.O. Box 6128, Succursale Centre-Ville, Montreal, QC, Canada, H3C 3J7;

E-mail: alain.verreault@umontreal.ca

This manuscript is "under preparation".

Contributions:

A.G.N and A.V designed experiments. A.G.N performed experiments and analyzed data. N.R and S.L helped with X-ray crystallography studies. N.C helped with SAXS instrument, A.S helped with SEC-MALS instrument. M.J.O helped with NMR, CD and fluorescence quenching experiments. A.V supervised studies. A.G.N and A.V wrote the manuscript.

Abstract

The eukaryotic DNA replication fork is a hub of enzymes that continuously act to synthesize DNA, propagate DNA methylation and other epigenetic marks, perform quality control, repair nascent DNA, and package this DNA into chromatin. Many of the enzymes involved in these spatiotemporally correlated processes perform their functions by binding to the proliferating cell nuclear antigen (PCNA). A long-standing question has been how the plethora of PCNA-binding enzymes can exert their activities without mutually impeding each other. As a first step towards deciphering this complex regulation, we studied how Chromatin Assembly Factor 1 (CAF-1) binds to PCNA. We demonstrate that CAF-1 binds to PCNA in an unprecedented manner that depends upon a cation-pi (π) interaction. An arginine residue, conserved among CAF-1 homologs but absent from other PCNA-binding proteins, invades the hydrophobic pocket normally occupied by proteins that contain canonical PCNA interaction peptide (PIPs). We show that point mutation of this arginine disrupts PCNA binding and chromatin assembly by CAF-1. The PIP of the p150 subunit of CAF-1 likely resides at the extreme C-terminus of a long α-helix (119 amino acids) that has been reported to bind DNA. Remarkably, the length of that helix, and the presence of the PIP at its C-terminus are evolutionarily conserved among numerous species ranging from yeast to humans. Our results suggest that the long helix forms a three-helix coiled-coil that may bind to the three monomers of a PCNA ring. This arrangement of a very long DNA binding coiled-coil that terminates in PIPs may serve to coordinate DNA and PCNA binding by CAF-1.

Introduction

Ahead of the replication fork, pre-existing nucleosomes are dismantled and temporarily dissociated into $(H3\text{-}H4)_2$ tetramers and H2A-H2B dimers (Jackson, 1988; Sogo et al., 1986). The tetramers are segregated to the two nascent sister chromatids in a quasi-stochastic manner (Jackson, 1988; Sogo et al., 1986). The gaps generated by duplication of DNA are almost immediately filled in by newly synthesized H3-H4 deposited onto DNA by a sophisticated histone chaperone known as Chromatin Assembly Factor 1 (CAF-1). Despite the existence of several histone chaperones, CAF-1 is thus far unique in its ability to mediate chromatin assembly in a manner that is tightly coupled to DNA synthesis (Krude, 1995b; Shibahara and Stillman, 1999; Verreault et al., 1996). This unique property of CAF-1 depends upon its ability to bind the proliferating cell nuclear antigen (PCNA), a hollow homo-trimeric ring that encircles DNA and serves as a processivity factor for DNA polymerases (Moggs et al., 2000; Quivy et al., 2001; Shibahara and Stillman, 1999; Zhang et al., 2016; Zhang et al., 2000). In addition, at each DNA replication fork, the same surface of PCNA also engages in numerous interactions with replication enzymes, CAF-1, as well as enzymes that methylate DNA [DNMT1] (Iida et al., 2002), perform mismatch repair [Msh3 and Msh6] (Clark et al., 2000), and many others (Boehm et al., 2016; Maga and Hubscher, 2003; Moldovan et al., 2007; Tsurimoto, 1999).

CAF-1 is composed of three subunits in species that range from yeast to human. In humans, mouse, and *Xenopus*, the three subunits of CAF-1 are p150 (CHAF1A), p60 (CHAF1B), and RbAp48 (RBBP4) (Kaufman et al., 1995; Kim et al., 2016; Quivy et al., 2001). p150 contains two regions that bind PCNA. The first is a motif located within the N-terminal domain of p150 that we previously referred to as PCNA binding domain (PBD) (Figure 1A)

(Rolef Ben-Shahar et al., 2009). Although PBD binds strongly to PCNA *in vitro*, it does not bear obvious similarity to the large family of PCNA interaction peptides (PIPs), and it is dispensable for replication-coupled chromatin assembly (Rolef Ben-Shahar et al., 2009). In contrast, the PIP located internally within the amino acid sequence of p150 [Figure 1A] is unusual because canonical PIPs are generally located at the extreme N- or C-terminus of the polypeptides they are found within. The PIP of p150 only has a modest affinity for PCNA, but is nonetheless essential for chromatin assembly (Rolef Ben-Shahar et al., 2009). In general, PCNA binding proteins that contain canonical PIPs interact with the front face of PCNA [*i.e.,* the face of the PCNA ring oriented in the direction of DNA synthesis] (De March et al., 2017; Dieckman et al., 2012; Gonzalez-Magana and Blanco, 2020; Kelch, 2016).

The consensus sequence for canonical PIPs is composed of eight residues, Q x x h x x a a, wherein a conserved glutamine is present at position 1, an aliphatic residue at position 4 (leucine, isoleucine, valine or methionine), and two aromatic residues at positions 7 and 8 (phenylalanine, tyrosine or tryptophan) [Figure 1B] (Moldovan et al., 2007). Several structures have revealed recurring features of the interaction between canonical PIPs and PCNA (Bruning and Shamoo, 2004; Dieckman et al., 2012; Gulbis et al., 1996; Sakurai et al., 2003; Tsutakawa et al., 2011; Vijayakumar et al., 2007). The carbonyl and amino groups of the glutamine side chain of canonical PIP-containing proteins contribute to binding by making several hydrogen bonds with residues in a small surface cavity of PCNA termed the "Q-pocket" (Bruning and Shamoo, 2004; Dieckman et al., 2012; Gulbis et al., 1996; Jimenji et al., 2019; Sakurai et al., 2003; Tsutakawa et al., 2011; Vijayakumar et al., 2007). This is illustrated by the binding of PCNA to the canonical PIP of human p21 (Figure 1C). The side chain of Q144 is anchored in the so-called Q pocket of PCNA, whereas M147, F150 and Y151 form the three prongs of a hydrophobic plug

that binds to PCNA (Figure 1C). The aliphatic and the aromatic residues of canonical PIPs form a short 3_{10} helix, and generally interact with PCNA in a manner analogous to that of a plug fitting into a three-pin electrical socket (Gulbis et al., 1996; Krishna et al., 1994).

We previously reported that the PIP of CAF-1 p150 possesses non-canonical properties. For instance, the CAF-1 PIP has an intrinsic ability to preferentially inhibit nucleosome assembly preferentially over DNA synthesis in a replication coupled nucleosome assembly assay. In order to probe this further, we determined the structure of the CAF-1 p150 PIP bound to PCNA. We found that the CAF-1 PIP binds to PCNA in an unprecedented manner. Our structure revealed that a cation-π interaction formed between PCNA and a conserved arginine of the CAF-1 p150 PIP that is absent from the PIPs of other PCNA-binding proteins. We show that point mutation of this arginine disrupts PCNA binding and chromatin assembly by CAF-1. The CAF-1 PIP is located at the extreme C-terminus of the KER domain, which an unusually long α-helix that binds DNA. The length of that helix, and the location of the PIP at its C-terminus are evolutionarily conserved from yeast to humans. Our results suggest that the long helix is part of a three-helix coiled-coil that may bind to the three monomers of a PCNA ring. We speculate that the very long DNA binding coiled-coil ending in PIPs may serve to coordinate DNA and PCNA binding by CAF-1.

Materials and Methods

Constructs for expression of mouse CAF-1 p150 in the rabbit reticulocyte lysate

A cDNA fragment for expression of wild-type mouse CAF-1 p150 was present between the *Not*I and *Bam*HI/*Bgl*II sites of the pCITE-4a$^+$ vector (Novagen) (Murzina et al., 1999). The

PIP sequences in human and mouse are identical: 421 - K A E I T R F F - 428 (mouse numbering). Using site-directed mutagenesis, the following PIP mutants were generated within the context of the full-length mouse p150 (CHAF1A) protein: pCITE4a p150 R426D (D is present at that position in several canonical PIPs), pCITE4a p150 R426S (S is present at that position in several canonical PIPs) and pCITE4a p150 R426L (a long aliphatic side chain that cannot form the cation-π interaction, but may nonetheless shelter within the hydrophobic surface of PCNA with which canonical PIPs interact). Wild-type CAF-1 p150 and PIP mutants were expressed, following the manufacturer's instructions, in the rabbit reticulocyte lysate using the T_NT quick system for coupled transcription and translation (L1170-Promega). The expressed proteins were labeled with [^{35}S]-methionine and subsequently used for nucleosome assembly assays.

Generation of lentiviral vectors for doxycycline-inducible expression of GFP CAF-1 p150

To study the localization of GFP CAF-1 p150 wild-type and mutants relative to that of PCNA, cDNAs encoding mouse p150 were cloned into a doxycycline-inducible lentiviral vector, the pCW-Cas9 plasmid encoding a Tet_{ON} (minimal CMV) promoter (pCW-Cas9 Addgene plasmid 50661). The Cas9 insert was replaced by wild-type or mutant mouse CAF-1 p150 using the restriction enzymes *Nhe*I and *Bam*HI. GFP-p150 wild-type and mutant fusion proteins were excised from EGFP-C1 vector (Clonetech) using Nhe1 and BamH1 restriction enzymes as previously reported (Rolef Ben-Shahar et al., 2009). Nhe1 and BamH1 digested fragments were run on 0.8% agarose gel and corresponding DNA bands: vector - pCW-Cas9 (7036 bp) and inserts - wild-type mp150, R426D (3983 bp) were gel purified using Qiagen DNA extraction spin prep columns. Purified DNAs were ligated using the Takara DNA ligase enzyme, following manufacturer's recommended protocol. Positive clones were selected on Luria-Bertani medium

containing 100 µg/ml ampicillin and after DNA isolation, the clones were verified by DNA sequencing.

Cell culture and transfection

HEK-293T and NIH3T3 cells were cultured in Dulbecco's modified Eagle medium (DMEM) with 10% foetal bovine serum without antibiotics. HEK-293T cells were used for co-transfection of the lentiviral packaging plasmids and gene of interest plasmids for viral packaging whereas NIH3T3 cells were used for transduction of the individual viruses and subsequent immunofluorescence analysis. HEK-293T cells, seeded in 100 mm dishes at 80% confluency were transfected with psPAX2 and pMD2G along with plasmids expressing wild-type and mutant mp150 using TransIT – Lenti transfection reagent (Mirus) as per the manufacturer's recommendations. Lentiviral supernatants were harvested at 48 h and 72 h after transfection, filtered using a 0.45-micron filter to remove the cell debris, and used to transduce target NIH3T3 cells seeded on glass bottom 35 mm dishes coated with poly-l-lysine. Polybrene was added at a final concentration of 8 µg/ml to the viral supernatant to aid viral transduction. After 24 h of transduction, viral supernatant containing media was removed from NIH3T3 cells and fresh media containing doxycycline at a final concentration of 2 µg/ml was added to the cells. Turbo GFP was used as a positive control for monitoring transduction efficiency and the cells were verified mycoplasma free using Mycoalert mycoplasma detection kit (Lonza).

Immunofluorescence detection of DNA replication foci in S-phase cells

NIH3T3 cells seeded on glass bottom 35 mm dishes were fixed with 2% paraformaldehyde in PBS at room temperature for 15 min. The cells were then treated with -20ºC methanol to expose the PC10 epitope. The cells after fixation, were washed three times with 1X PBS containing 1% BSA. PC10 primary monoclonal antibody was added to the cells at 1:80 dilution and incubated for 2 h at room temperature. Cells were again washed three times with 1X PBS containing 1% BSA to remove unbound primary antibody and incubated with secondary goat anti-mouse IgG antibody at 1:400 dilution for 2 h at room temperature. After three washes in 1X PBS containing 1% BSA; 4′,6-diamidino-2-phenylindole (DAPI) stain was added at 0.1 µg/ml to the cells and the images were acquired as a Z stack on Zeiss LSM 880, inverted confocal microscope using a plan apochromat 40x/1.4 NA oil immersion objective (scale bars=10 µm). The single images of the Z stacks were analysed and merged using the proprietary ZEN software from Zeiss.

Expression and purification of GST-PIP fusion proteins in *Escherichia coli*

Wild- type p150 PIP WT and R426D peptides were constructed as GST-fusion proteins with a tyrosine at the C-terminus of the peptide. The C-terminal tyrosine was added to aid in peptide detection during the purification by measuring the absorbance at 280 nm. The DNA fragments encoding the GST fusion proteins were inserted into a pGEX-TEV vector, which is essentially a modified pGEX-2T vector where the thrombin cleavage site was replaced with a TEV cleavage site. The pGEX-TEV plasmid was digested with *Bam*HI and *Eco*RI and ligated to DNA fragments encoding either the p150 PIP wild-type and R426D. The final plasmid sequence

is pGEX-TEV-GS-PIP-Y-STOP. The plasmids, pGEX-TEV-PIP wild type and pGEX-TEV-PIP R426D were confirmed by DNA sequencing and then expressed in *Escherichia coli* host strain TOPP2 (Stratagene) with 100 µg/ml ampicillin to saturation at 37°C. The next day, the saturated cells were diluted to 0.05 OD measured at A_{600} nm and the cells were grown at 37°C until the cells reach the mid-exponential phase of 0.6-0.8 at OD A_{600} nm. The cells were then induced with 1 mM isopropyl-D-thiogalactopyranoside (IPTG) for 4 h. 8 litres of cell culture were grown each for the wild-type and R426D mutant. The cells were then harvested by centrifugation in an Avanti J-26XP high-performance centrifuge from Beckman Coulter with a fixed angle rotor (JLA-8.1000) at 9000 x g for 30 min at 4°C. The pellet from 1 litre cells equivalent was lysed in 10 ml of lysis buffer containing 20 mM Tris, pH 7.5, 1 M NaCl, 0.2 mM EDTA, 1 mM DTT, 50 µg/ml lysozyme, 1 mM AEBSF and one tablet of cOmplete™ Mini EDTA-free Protease Inhibitor Cocktail Tablets (Roche). The cell pellet was sonicated in the lysis buffer on ice, at power output level 4 with 10 seconds pulse on and 30 seconds off at 6 watts using a Misonix 3000 Ultrasonic cell disruptor and wider probe. The lysate was clarified by centrifugation for 30 min in an Avanti J-26XP with a fixed angle rotor 25.50 at 30966 x g at 4°C. The clarified supernatant was incubated on a nutator for 6 h at 4°C with 10 ml of glutathione-Sepharose (GSH) resin (Amersham) pre-washed and equilibrated with lysis buffer. After incubation the GSH resin was pelleted, the unbound supernatant was removed, and the resin was washed thrice with lysis buffer and twice with Tobacco Etch Virus (TEV) protease buffer (20 mM sodium phosphate, pH 6.5, 50 mM NaCl, 2 mM DTT). The peptide was cleaved from the GSH resin by incubating in the presence of TEV protease overnight at 4°C. The next day, the supernatant was harvested by centrifugation, and the GSH resin was washed twice with 20 mM sodium phosphate, pH 6.5 buffer. The fractions were run on a 15% polyacrylamide gel to track the

purification and TEV cleavage efficiency. The gel was stained with Coomassie brilliant blue G-250 with 50% (v/v) methanol, 10% (v/v) glacial acetic acid and destained with distilled water with 0.1% (v/v) acetic acid. The supernatant after GSH purification and TEV cleavage contains the purified peptide, and this peptide was further purified to remove the TEV enzyme on an SP-Sepharose (GE Healthcare) ion-exchange chromatography column. After elution from SP-Sepharose columns, pure fractions of the peptide were dialyzed against 4 litres of water overnight using a 1 kDa MWCO dialysis membrane. The dialyzed pure peptide was further quantified, lyophilized, and stored at -80°C until used for ITC experiments.

The protocol had to be modified to purify the mutant peptide of pGEX-TEV-PIP R426D. Even though the mutant protein was expressed at a similar level as the wild-type, the mutant peptide pGEX-TEV-PIP R426D after GSH purification did not bind efficiently to the SP-Sepharose column. This problem was circumvented by modifying the protocol for pGEX-TEV-PIP R426D by carrying out the TEV cleavage followed by performing an additional gel filtration step (gel filtration buffer 20 mM Tris, pH 7.5, 150 mM NaCl, 1 mM DTT) using HiLoad 26 /600 Superdex™ 75 pg column instead of SP-sepharose ion exchange. The eluted peak fractions corresponding to pGEX-TEV-PIP R426D from gel filtration were pooled and lyophilized and stored at -80°C until used for ITC experiments.

Expression and purification of p150L-His6 in *Escherichia coli*

A DNA fragment encoding human p150 residues 342-475 was cloned into the pET28a vector (kanamycin resistant) in-frame with a C-terminal 6-histidine tag. For p150L expression, this plasmid was transformed into *Escherichia coli* BL21(DE3) RIL cells (Stratagene). Single

colonies were inoculated and grown overnight to saturation at 37°C in 2X YT medium containing 50 µg/ml kanamycin. The next day, cells were diluted and grown to mid-exponential phase (A_{600nm} = 0.6 - 0.8) at 37°C and protein expression was induced at 20°C with 0.5 mM isopropyl-β-D-thiogalactopyranoside (IPTG) for 16 h.

After 16h, the cells were harvested in an Avanti J-26XP centrifuge from Beckman Coulter with a fixed angle rotor (JLA-8.1000) at 9000 x g for 30 min at 4°C. The pellets from 1 litre of cell culture were resuspended in 50 ml of lysis buffer containing 50 mM sodium phosphate, pH 7.2, 2.5 M NaCl, 75 mM imidazole, 100 µg/ml lysozyme, 1mM AEBSF, one tablet of cOmplete Mini EDTA-free Protease Inhibitor Cocktail (Roche) and 0.1 mM TCEP. The cells were lysed in a cold room on a nutator for 30 min, followed by sonication at power output level 4 with 10-second pulses on and 30-second off at 6 watts using a Misonix 3000 Ultrasonic cell disruptor and their wider probe. The lysate was clarified by centrifugation for 30 min in an Avanti J-26XP with a fixed angle rotor 25.50 at 30966 x g at 4°C. The supernatant was incubated overnight at 4°C with nickel-nitrilotriacetic acid agarose beads (Qiagen) that were pre-equilibrated in the lysis buffer. After incubation with the beads, the supernatant was removed after centrifugation and the beads were washed thrice in wash buffer containing 50 mM sodium phosphate, pH 7.2, 2.5 M NaCl, 75 mM imidazole, and 0.1 mM TCEP. The p150L-His6 protein was eluted with a buffer containing 50 mM sodium phosphate, pH 7.2, 2.5 M NaCl, 500 mM imidazole, and 0.1 mM TCEP. After elution, p150L-His6 was concentrated using a 3 kDa MWCO amicon concentrator. The presence of 2.5 M NaCl was to prevent the p150L-His6 protein, which is rich in K/E/R residues, from co-purifying with non-specifically bound nucleic acids. After concentration, 500µl to 1ml of p150L-His6 protein was dialysed in a 7 kDa MWCO

Snakeskin dialysis membrane (Thermo Fisher Scientific) in 4 litres of dialysis buffer compatible with biophysics experiments for 3-4 h, repeated thrice. The protein was harvested the next day and the protein stored at -80°C until used. The concentration of p150L-His6 was estimated by measuring A205 (p150L is devoid of Trp or Tyr).

For NMR experiments, CAF-1 p150L-His6 was isotopically labeled by growing *Escherichia coli* in M9 minimal medium containing ^{15}N-ammonium chloride (Sigma) and/or ^{13}C-glucose (Sigma) as the sole nitrogen and carbon sources. A 10X ^{15}N minimal medium (1L) was prepared by dissolving 130 g KH_2PO_4, 100 g K_2HPO_4, 90 g Na_2HPO4, and 24 g K_2SO_4. The pH was adjusted to 7.2 with NaOH before adding 10 g of ^{15}N-NH_4Cl. The 200X trace elements stock solution (1L) was prepared by dissolving 60 g $CaCl_2.2H_20$, 60 g $FeSO_4.7H_20$, 115 g $MnCl_2.4H_20$, 0.8 g $CoCl_2.6H_20$, 0.7 g $MnSO_4.7H_20$, 0.3 g $CuCl_2.2H_20$, 0.02 g H_3BO_3, 0.25 g $(NH_4)_6Mo_7O_{24}.4H_20$, 50 g EDTA.2NaCl in 750 ml H_2O and once dissolved the volume was made up to 1L, which was sterilized through a 0.2micron filter. Regular glucose or ^{13}C glucose was made as 8% (w/v) 40X stock and filter sterilized. 25ml of this solution was used per litre of culture medium. 5g of yeast extract was dissolved in 50ml ddH_20 (10% w/v final) and was autoclaved. To make the 1X (1L) minimal medium, 10X ^{15}N solution was diluted with ddH_20 and added with 25 ml 40X glucose, 5 ml 1M $MgCl_2$, 5 ml 200X trace elements, 100 µl 10% (w/v) yeast extract, 1 ml of antibiotic (kanamycin ; 1000X stock was 50 mg/ml). The cells were grown as an overnight 50 mL primary culture, which was used to inoculate 1L of M9 medium, and induction with IPTG was performed as mentioned above for the rich media.

Crystallography of PIP bound to PCNA

A CAF-1 p150 synthetic peptide with the sequence *IKAE**KAEITRFF***QKPKTPQA (PIP residues are highlighted in bold italics) was synthesized at the University of Cambridge in-house protein and nucleic acid facility (PNAC). For use in crystallization trials, the synthetic peptide was dissolved in demineralized water to a concentration of 23 mM. Initial crystallization conditions were further refined and optimized with the help of the PACT suite (Qiagen) and Additive Screen (Hampton research) that contain multiple reagent libraries that enhance solubility and crystallization of biological macromolecules. Crystal yield was greatly improved under these conditions and we obtained crystals that exhibited flat surfaces and sharp edges indicating regular lattice plane formation. Well conditions were 0.1M MMT buffer pH 5, 22% (w/v) PEG 1,500, 1.0 M Guanidine hydrochloride. These crystals were subsequently used for diffraction studies. The diffraction data was collected by Dr Tomasso Moschetti and Dr Andrew Thompson at the Proxima 1 beamline of the SOLEIL synchrotron (Saint-Aubin, France).

Human PCNA expression and purification for crystallography

pT7-hsPCNA plasmid (kindly donated by Prof. Malcolm Walkinshaw, University of Edinburgh) was introduced into chemically competent *Escherichia coli* strains, Overexpress C41 (DE3) and Overexpress C43 (DE3) cells (Lucigen), which were grown overnight on selective agar plates with 100 µg/ml ampicillin. Transformed C43 (DE3) cells were grown in 3 ml 2X YT (100 µg/ml carbenicillin) pre-cultures to OD_{600} > 0.6. These were added to 450 ml 2X YT (100 µg/ml carbenicillin), cells were grown by shaking incubation (37°C, 250 rpm) until an OD at 600 nm of 0.6-0.8. Cells were induced with 1 mM IPTG and incubated at 37°C for 3 h. Cells were

harvested by centrifugation (4000 x g, 30 min, 4°C) and resuspended in 45 ml Sepharose Buffer-A (15.5 mM 1-methyl-piperazine, 15.5 mM Bis-Tris, 7.8 mM Tris-buffer, pH 8.5 containing Complete EDTA-free protease inhibitor cocktail (Roche). Cells were lysed by multiple passes through an Emulsiflex C5 instrument (Avestin), at variable pressure. Successful PCNA purification was achieved by manual correction of stroke pressure to < 750 kPsi. The lysate was clarified by centrifugation (48000 x g, 45 min, 4°C). The supernatant was applied to two 1 ml HiTrap Q FF (GE Healthcare) connected in series, pre-equilibrated in Buffer-A (15.5 mM 1-methyl-piperazine, 15.5 mM Bis-Tris, 7.8 mM Tris-buffer, pH 8.5) on an ÄKTA Explorer chromatography system (GE Healthcare). After loading, the column was washed with 30 ml 20% Buffer-B (15.5 mM 1-methyl-piperazine, 15.5 mM Bis-Tris, 7.8 mM Tris-buffer, pH 8.5, 1M NaCl), followed by a 20 ml gradient 20-57% Buffer-B and a 10 ml gradient of 57-100% Buffer-B. Relevant fractions (as judged by SDS-PAGE) were concentrated to 2.5 ml using a Vivaspin20 centrifugal concentrator (GE Healthcare) before loading for buffer exchange on a PD-10 Desalting Column (GE Life Sciences) pre-equilibrated in Buffer-C (5.1 mM Na_2HPO_4, 5.1 mM Sodium formate, 10.2 mM Sodium acetate, pH 5.5). Fractions were loaded onto a 5 ml HiTrap Heparin HP column (GE Healthcare) pre-equilibrated in Buffer-C. The column was washed with 25 ml 15% Buffer-D (5.1 mM Na_2HPO_4, 5.1 mM Sodium formate, 10.2 mM Sodium acetate, pH 5.5, 1M NaCl), followed by a 50 ml gradient of 15-100% Buffer-D. Relevant fractions were pooled and concentrated using a Vivaspin20 centrifugal concentrator to 400 µl. This was split into 2 x 200 µl each, injected separately onto a Superdex™ 200 gel filtration column (GE Healthcare) pre-equilibrated in Buffer-E (25 mM Tris-buffer, 25 mM NaCl, 0.5 mM EDTA, 10% glycerol, pH 7.5) at 1.5 ml/min. Relevant fractions were pooled and concentrated to ~10 mg/ml before use in crystallisation trials.

Expression and purification of wild-type and mutant PCNA-His6 proteins in *Escherichia coli*

PCNA-His6 wild-type and mutants were expressed and purified as previously reported (Rolef Ben-Shahar et al., 2009). In short, wild-type or mutant plasmids in pET23-C-His6-PCNA vectors were transformed and expressed in Codon Plus BL21(DE3) pLysS *Escherichia coli* (Stratagene) cells. Single colonies were inoculated and grown overnight in the Luria-Bertani medium containing 100 μg/ml ampicillin to saturation at 37°C. The next day the cells were diluted and grown to mid-exponential phase (0.6-0.8) at OD_{600} and the expression was induced with 1 mM isopropyl-D-thiogalactopyranoside (IPTG) for 4 h. PCNA mutants were transformed and expressed in a similar way.

Cells were spun in an Avanti J-26XP high performance centrifuge from Beckman Coulter with a fixed angle rotor (JLA-8.1000) at 9000 x g for 30 min at 4°C and the pellets from 1 litre of cell culture were resuspended in 50 ml of lysis buffer containing 50 mM sodium phosphate, pH 8.0, 150 mM NaCl, 10% glycerol, 20 mM imidazole, 0.02% nonidet P-40, 2 mM DTT. The cell pellet was sonicated at power output level 4 with 10 seconds pulse on and 30 seconds off at 6 watts using a Misonix 3000 Ultrasonic cell disruptor and wider probe in the lysis buffer. The lysate was clarified by centrifugation for 30 min in an Avanti J-26XP with a fixed angle rotor 25.50 at 30966 x g at 4°C. The supernatant was incubated overnight at 4°C with pre-equilibrated nickel-nitrilotriacetic acid agarose beads (catalogue number - 30230, Qiagen) in the lysis buffer. After incubation, the beads were washed three times with wash buffer and PCNA-His6 wild-type or mutants were eluted with an elution buffer containing 500 mM imidazole.

The eluate was subsequently purified with a Superdex™ 200 gel filtration column (GE Healthcare) in gel filtration buffer 20 mM Tris, pH 7.5, 150 mM NaCl, 1 mM DTT. The fractions corresponding to PCNA homotrimer were pooled, concentrated with an amicon concentrator with 3 kDa MWCO, quantified using absorbance at A280 nm, and stored at -80°C until used.

Isothermal titration calorimetry (ITC)

Recombinant PCNA-His6, PCNA-Y250I-His6 mutant, and the PIP peptides (wild-type, R426D with a C-terminal tyrosine) were expressed and purified as described above. The proteins were dialyzed against three 4-litre changes of ITC buffer containing 10 mM sodium phosphate, pH 7.0, 10 mM NaCl at 4°C overnight. The concentrations of PCNA-His6 and PIP peptides were determined by measuring tyrosine absorption at 280nm. ITC titrations of peptides into PCNA were performed at 23°C in the ITC buffer (10 mM sodium phosphate, pH 7.0, 10 mM NaCl) using a MicroCal VP-ITC system. The concentrations of injected wild-type and mutant PIP in the syringe varied from 200 to 500 μM, whereas PCNA in the ITC sample cell varied, depending on the experiment from 20 to 50 μM PCNA monomer. The protein and peptide samples were degassed before the ITC run. Data analysis was performed using the MicroCal Origin software and all experiments fit the single binding site model with nearly 1:1 stoichiometry of CAF-1 PIP to PCNA monomer.

Replication-dependent nucleosome assembly assays

Replication reactions were assembled as previously reported (Smith and Stillman, 1989; Smith and Stillman, 1991b). The chromatin assembly reactions contained a final concentration of 40 mM Hepes-KOH, pH 7.5, 8 mM $MgCl_2$, 0.5 mM dithiothreitol, 0.2 mM each of dTTP, dCTP, dGTP, 25 µM of dATP, 3 mM ATP, 0.1 mM each of TTP, CTP, GTP, 25 µM [α-32 P] dATP (3000 Ci/mmol; 10 µCi/µl), 40 mM creatine phosphate, 0.05 units/µl creatine phosphokinase, 100 ng of $pSV011^+$ origin containing plasmid, 25 ng/µl T-antigen (T antigen was a kind gift from Dr. Bruce Stillman at Cold Spring Harbor Laboratory), 0.75 units/µl Topoisomerase I, 0.16 units/µl Topoisomerase II.

Each 12.5 µl reaction had purified full-length recombinant CAF-1 as a positive control for nucleosome assembly reaction. The experimental tubes contained *in vitro* translated [^{35}S]-methionine labelled either with wild-type p150 or p150 R426D in increasing amounts. The replication reactions were incubated for 45 min at 37°C and further resumed for an additional 45 min after the addition of 0.25 µl of 1 mg/ml purified H2A.H2B dimers. After incubation, the reaction was stopped by the addition of a stop solution containing 10 mM EDTA and 0.5% SDS. The reaction mixture was first digested with ribonuclease A (20 µg/ml) for 15 min at 37°C and then with 1 mg/ml of pronase for 1 h at 37°C.

The replicated DNA was extracted initially using phenol: chloroform: isoamyl alcohol (25: 24:1) and subsequently with sodium acetate and ethanol. The pellet was rinsed with 70% ethanol and dissolved in 15 µl of 1X TE buffer, pH 8.0 and mixed with 3 µl of 6X bromophenol blue sample buffer. The products of replication were analysed using a native 1.25% agarose gel

in 1 X TAE buffer with 1 mM $Mgcl_2$, without the addition of ethidium bromide. After gel run, the gel was stained with ethidium bromide for 10 min, destained, and imaged. The ethidium bromide stained gel was fixed for 30 min in a fixation solution containing 10% acetic acid and 10% methanol. The gel was rinsed once in water to remove the acid and dried using a gel dryer with Whatman filter papers and covered in saran wrap, without heat for 30 min followed by heating at 70°C for additional 30 min. After the gel was completely dry, it was transferred to an autoradiography cassette with an imaging plate for 1-2 days. The gel was subsequently imaged and analysed using a phosphor imager (Typhoon FLA 7000) to visualize the replicated DNA.

Circular dichroism (CD)

Purified CAF-1 p150L protein was dialyzed overnight against 10 mM sodium phosphate buffer, pH 7.2, 10 mM NaCl, 0.1 mM TCEP. Due to the absence of tyrosine and tryptophan residues in the CAF-1 p150L protein, the protein concentration was measured after dialysis using a spectrophotometer at 205 nm (Anthis and Clore, 2013). The protein was used in the CD experiment at a final concentration of 4.68 μM. Far-UV CD spectra were collected at room temperature using a 0.02 cm path length cuvette on a JASCO J810 CD spectropolarimeter. Effects of buffer were subtracted out by performing a control spectrum on the dialysis buffer alone. CD spectra were acquired with a data pitch of 0.5 nm over a range of 260 nm to 190 nm, with a 1-nm bandwidth, a scan speed of 20 nm/min, a response time of 4 seconds and 4 scans per spectrum. The cut-off voltage for the photo multiplier tube was 600V; we used the data below this range and avoided the region where the noise was too high. Relative ellipticity was converted to mean residue molar ellipticity according to published literature (Fasman, 1996).

Intrinsic tryptophan fluorescence spectroscopy

Fluorescence experiments were performed on an Agilent Cary Eclipse fluorimeter at room temperature. Buffer conditions were identical for all protein components (10 mM sodium phosphate, pH 7.2, 10 mM NaCl, 0.1 mM TCEP). Samples were excited at 280 nm with a 5-nm bandwidth and the emission spectra between 295 nm and 420 nm were collected. Measurements were made for 5 μM PCNA monomer (1 tryptophan residue), 20 μM CAF-1 p150L (0 tryptophan residue), and a complex containing 5 μM PCNA monomer and 20 μM CAF-1 p150L. Both samples were extensively dialyzed against the same buffer and prepared from stock samples to ensure identical conditions.

SEC-MALS

Size exclusion chromatography coupled to multi-angle light scattering (SEC-MALS) was used to determine the molecular mass and oligomerization status of CAF-1 p150L. Samples were injected onto a Superdex 200 Increase 10/300 GL column at 0.35 ml/min using an AKTAmicro (GE Healthcare). The running buffer contained 10 mM sodium phosphate, pH 7.2, 150 mM NaCl, 0.1 mM TCEP. Samples were passed through a Dawn HELEOS II MALS and OptiLab T-rEX online refractive index detectors (Wyatt Technology) after calibration with the BSA monomer. Data were processed with ASTRA Version 6.1.6.5 (Wyatt Technology).

SEC-SAXS

SEC-SAXS data were collected using an ÄKTAmicro FPLC and a Superdex 200 Increase 10/300 column (GE Healthcare), coupled inline to a BioXolver SAXS system (Xenocs) equipped with a MetalJet D2+ 70 kV X-ray source (Excillum) and a PILATUS3 R 300K detector (Dectris). Five hundred microliters of sample were injected into the SEC-SAXS system and the chromatography was developed at a flow rate of 0.05 ml/min. X-ray scattering images corresponding to 60 seconds of exposure were collected continuously at 20°C during the elution and an average scattering profile of all frames within the elution peak was calculated. Buffer scattering was then subtracted from the average scattering profile of the elution peak to yield the sample's scattering curve.

Nuclear magnetic resonance

NMR experiments were carried out on a 600 MHz Bruker Avance III spectrometer equipped with a 5 mm QCIP cryoprobe with Z gradients. All experiments were carried out at 293K. 2D ^{1}H-^{15}N BEST HSQC (Lescop et al., 2007) experiments were carried out using the sequences downloaded from the NMRlib suite (Favier and Brutscher, 2019) of pulse sequences. Selective shaped pulses were used to excite a ^{1}H sweep width of 4.5 ppm, centred at 8.75 ppm, with a recycle delay of 0.2 s. ^{1}H and ^{15}N sweep widths were set to 8417.509 Hz (14 ppm) and 1920.466 Hz (31.6 ppm) respectively, typically 240 t_1 increments were acquired.

NMR samples were prepared in 10 mM sodium phosphate buffer, pH 7.2, 10 mM NaCl, 90% H_2O/10% D_2O. Uniformly ^{15}N labelled CAF-1 p150L and unlabelled PCNA were prepared in

identical buffers and added together from stock samples. Final sample concentrations were at 50 μM for CAF-1 p150L and 400 μM PCNA monomer. NMR spectra were processed with NMRpipe, a multidimensional spectral system based on UNIX pipes (Delaglio et al., 1995).

Results

In order to better understand the molecular basis of CAF-1 binding to PCNA, we determined the crystal structure of a complex between a synthetic peptide encompassing the p150 PIP and PCNA. The crystal structure was solved (Table 1 and Materials and Methods) using molecular replacement from a previously published PCNA structure (Kontopidis et al., 2005). PCNA samples were incubated with a 20-amino acid PCNA interaction peptide (PIP) derived from CAF-1 p150. The PIP used for crystallization, IKAE***KAEITRFF***QKPKTPQA (PIP residues in italics), spanned the entire PIP region.

The crystal structure revealed that there were two PCNA homotrimers per asymmetric unit (Figure 2A). Electron density that could not be accounted for by molecular replacement arose from PIPs bound to each monomer in the asymmetric unit. The initial R_{work} and R_{free} values were considerably reduced by modelling in three residues, RFF, of the PIP used for crystallization: IKAEKAEIT***RFF***QKPKTPQA (PIP residues for which electron density was attributed shown in bold italics). To assess the quality of the model, an F_o - F_c difference density map was generated (Figure 2B). The map was calculated by omitting the peptide and showed that the modelled RFF was consistent with the electron density unaccounted for by that of PCNA alone. The peptide model was therefore sufficiently accurate to account for the diffraction data.

Structure of CAF-1 p150 PIP bound to PCNA

Our model was consistent with the following general orientation of the PIPs relative to PCNA (Figure 2A). As expected from previous structures of PIPs bound to PCNA, there was one CAF-1 p150 PIP bound to each PCNA monomer. As is for many other PIPs (canonical and non-canonical), the CAF-1 p150 PIPs were bound between the interdomain connector loop (IDCL) and the underlying β-sheet (Figure 2A). An enlarged view of how the p150 PIP is bound to PCNA is illustrated in Figure 2B. The side chains of the arginine and phenylalanine residues of RFF were oriented towards PCNA and occupied a surface of PCNA that was essentially the same as that observed in structures of other PCNA-binding peptides. The arginine and first phenylalanine of RFF resided within a hydrophobic pocket on the surface of PCNA, while the second phenylalanine is contacting the edge of the hydrophobic pocket and is, therefore, less sheltered from solvent (Figure 2C). Given the hydrophilic nature of the arginine side chain, its insertion within a hydrophobic pocket was unanticipated. However, an inspection of PCNA residues in close proximity to the arginine side chain suggested that the CAF-1 p150 arginine participated in a cation-π interaction with the electron density on the tyrosine ring of PCNA Tyr250 (Figure 3A). Figure 3B shows other residues that contribute to the hydrophobic environment in which the arginine side chain is anchored by the cation-π interaction.

Structure-based mutagenesis of CAF-1 p150

Given the 20-residue peptide that was used for crystallization, and the 8-residue length of most PIPs, the fact that only three residues (RFF) of the CAF-1 PIP were identified in the crystal structure was not anticipated. The RFF peptide binds to the same surface of PCNA as canonical and non-canonical PIPs. However, the orientation of RFF in the PCNA-bound form is different

from those of the PIPs of p21, FEN1, p66 subunit of Pol δ, and the error-prone DNA polymerase Pol κ [non-canonical PIP] (Figure 3C and 3D).

These two phenylalanine residues of RFF were previously shown to be essential for PCNA binding and the nucleosome assembly activity of intact CAF-1 p150 (Rolef Ben-Shahar et al., 2009). The novel feature is the arginine, which is not conserved in the PIPs of other PCNA-binding proteins, but seemingly plays an important role in the CAF-1 p150 PIP. In fact, the structures of other PIPs bound to PCNA show that the residues corresponding to the arginine of CAF-1 p150 never contact PCNA. Furthermore, an arginine or a lysine is conserved in that position among CAF-1 p150 homologs from numerous species whose common ancestors lived at least 736 million years ago (Figure 1B). We therefore focused our attention on the arginine residue of CAF-1 p150 involved in a cation-π interaction with PCNA, which is unprecedented among PCNA-binding proteins.

CAF-1 PIP binding to PCNA requires Arg426 of mouse p150

We mutated Arg426 of mouse p150 (equivalent to Arg447 in human p150) into either an Asp or Ser. The rationale behind selecting those two residues is that proteins with canonical PIPs often contain an Asp or a Ser at the position occupied by the Arg in CAF-1 p150 (Figure 1B). In addition, neither Ser nor Asp can participate in the cation-π interaction formed by the Arg.

The wild-type and R426D peptides were expressed as GST fusions in *Escherichia coli*, purified to homogeneity (see Materials and Methods) and used in binding assays with human PCNA purified from *Escherichia coli*. When calorimetry experiments were performed in 10 mM sodium phosphate, pH 7.0, and 10 mM NaCl, we observed binding between the wild-type CAF-1

PIP and PCNA with a K_d^{app} equivalent to 24 μM and stoichiometry of 0.83 PIP per PCNA monomer (Figure 4A and Table 2). In contrast, we did not observe any heat exchange when we used the CAF-1 PIP R426D mutant (Figure 4A and Table 2). This suggests that the R426D mutation severely abrogates binding to PCNA. This interpretation is consistent with several other lines of evidence described below. We mutated the tyrosine involved in the cation-π interaction with CAF-1 p150 Arg426. The resulting mutant, PCNA-Y250I-His6 was expressed in and purified from *Escherichia coli*. Based on size exclusion chromatography, there was no evidence of aggregation that might suggest inappropriate folding of PCNA-Y250I-His6. The wild-type PIP was titrated into PCNA-Y250I-His6, but there was no detectable heat exchange. Taken together, the results obtained with the PIP R426D mutant and the PCNA-Y250I were consistent with the cation-π interaction observed in the crystal structure.

Arginine 426 is important for CAF-1 p150 targeting to DNA replication foci that contain PCNA

We determined if the wild-type CAF-1 p150 and the R426D mutant localize to replication foci containing PCNA. Previous research from several laboratories has documented stereotypical patterns of PCNA foci that are characteristic of the different stages of S-phase (Liberti et al., 2011; O'Keefe et al., 1992) (Casas-Delucchi and Cardoso, 2011).

Cells in early S-phase show numerous small PCNA foci distributed throughout the nucleus. These foci can be resolved from each other using super-resolution microscopy, but are difficult to resolve from each other by confocal microscopy (Casas-Delucchi and Cardoso, 2011). This makes protein localization to early S-phase PCNA foci difficult to assess using conventional tools for microscopy. Mid S-phase is the stage when perinuclear and perinucleolar

chromatin are replicated. The corresponding PCNA foci are relatively large and distant from each other, which makes co-localization of a protein of interest with PCNA straightforward. Late S-phase is the stage when pericentric heterochromatin replicates. In mouse cells, this stage shows striking patterns of large and well-resolved PCNA foci but, because CAF-1 contains both a PIP and a PXVXL motif for binding to Heterochromatin Protein 1 [HP1] (Murzina et al., 1999; Thiru et al., 2004), CAF-1 p150 localization to late S-phase PCNA foci persists even if the PIP is mutated because p150 retains the ability to bind to HP1 (Rolef Ben-Shahar *et al*., 2009). Because of these constraints, we focused our attention on cells with patterns of PCNA foci characteristic of mid S-phase. As reported in previous studies (Krude, 1995a; Shibahara and Stillman, 1999), we obtained a distinct immunostaining pattern for PCNA with the monoclonal antibody PC10. During mid S-phase, staining of PCNA with that antibody occurred within foci located around the periphery of the nuclear envelope (Figure 4B, top panel, PC10). However, these cells also showed numerous PCNA foci around the periphery of nucleoli as well as many small foci within the interior of the nucleus (Figure 4B, top panel, PC10). Asynchronously proliferating mouse NIH 3T3 cells were transduced with lentiviral vectors, and expression of wild-type and mutant forms GFP-p150 was induced with doxycycline. Cells were fixed and permeabilized for PCNA detection with the PC10 monoclonal antibody. Mid-S phase cells were identified based upon their stereotypical pattern of PCNA staining at the nuclear periphery. In this subset of S-phase cells, GFP-p150 co-localized with most, and perhaps all the PCNA foci located at the nuclear periphery (Figure 4B, upper panel). In mid S-phase cells, wild-type GFP-p150 was not present in the large foci of heterochromatin that can be detected by DAPI staining of mouse cells. In striking contrast, GFP-p150 R426D did not co-localize with PCNA foci at the nuclear periphery and was anomalously found in large amounts within the nuclear interior and

the large heterochromatic foci (Figure 4B, lower panel). This is consistent with previous observations (Rolef Ben-Shahar *et al*., 2009) that, when CAF-1 is unable to bind to PCNA, it is prematurely associated with pericentric heterochromatin in early and mid S-phase.

Arginine 426 is important for DNA replication-dependent nucleosome assembly

We next sought to compare the activities of CAF-1 p150 wild-type, and the R426D mutant in a replication coupled chromatin assembly assay (Kaufman et al., 1995; Smith and Stillman, 1991a; Smith and Stillman, 1991b). As a first step to perform this assay, we expressed CAF-1 p150 wild-type and the R426D mutant in a rabbit reticulocyte lysate coupled transcription and translation system and labelled the proteins with [^{35}S]-methionine. The wild-type and R426D mutant proteins were present at comparable levels (Figure 4C, left panel). In the replication coupled chromatin assembly system, an S100 extract from human HEK-293T cells provides all the DNA replication enzymes and histones but lacks CAF-1 p150 (Smith and Stillman, 1989). To this extract, a plasmid containing an SV40 origin of replication, and the SV40 large T antigen, were added to initiate DNA replication. Radiolabelled dATP was also added to visualize the replication products by autoradiography.

In the absence of nucleosome assembly, the plasmid is replicated and radiolabelled, but the products of replication are topologically relaxed naked DNA molecules. In contrast, when the recombinant CAF1 protein (p150, p60, p48) or the p150 subunit alone is added, they bind to histones in the S100 extract and promote nucleosome assembly coupled with DNA replication. DNA topoisomerase enzyme I, which is present in the S100 extract and supplemented as well, removes the positive supercoiling in the linker DNA that connects nucleosomes, but not the

negative supercoiling of DNA wrapped around the surface of histone octamers. Thus, efficient nucleosome assembly in the presence of CAF-1 results in the formation of plasmid DNA that is replicated (hence radiolabeled) and negatively supercoiled, thus highlighting the interdependency of chromatin assembly, plasmid supercoiling and DNA replication.

Equal amounts of CAF-1 p150 wild-type and R426D mutant were added to the chromatin assembly assay system. After the replication and chromatin assembly reactions were completed, the DNA was purified and run through an agarose gel. The gel was stained with ethidium bromide to visualize the total DNA, and subsequently dried down and subjected to autoradiography to specifically look at the replicated DNA. Our results indicate that in the absence of recombinant CAF-1, the replicated DNA was not extensively supercoiled (Figure 4C rightmost panel, lane 1). However, when recombinant CAF-1 was added, the replicated DNA was supercoiled (Figure 4C rightmost panel, lane 2), indicative of nucleosome assembly. Similarly, when increasing amounts of the *in vitro* translated wild-type CAF-1 p150 were added, the replication products were supercoiled (Figure 4C, rightmost panel, lanes 3-5). In striking contrast, when increasing amounts of the R426D mutant were added, no supercoiling was observed (Figure 4C, rightmost panel, lanes 6-8). Therefore, we concluded that this mutant was defective in nucleosome assembly. Due to the presence of some residual CAF-1 activity present in the S100 extract, we also observed a small amount of supercoiling in the negative control (Figure 4C rightmost panel, lane 1) and to a similar degree in the other lanes.

A predicted long α-helix of CAF-1 p150 abruptly ends with the PIP

Earlier studies have shown that the KER domain of p150 was essential for nucleosome assembly by CAF-1 (Kaufman et al., 1995). However, it was not clear how the KER domain, named because of its high content in lysine, glutamic acid and arginine residues, exerted its role in CAF-1-mediated nucleosome assembly. We were interested in domains adjacent to the CAF-1 p150 PIP that might modulate its affinity for PCNA. Much to our surprise, several secondary structure algorithms predict the presence of a very long α-helix that included the KER domain. The prediction for human CAF-1 p150 was for a 119-residue helix (Figure 5, from Thr330 to Phe448). At 3.6 residues per turn, this would represent a 33-turn α-helix. We applied the secondary structure prediction algorithms to p150 homologues from several species ranging from yeast to humans. We made two striking observations. First, despite species-specific variations in the length of the helix (100 - 120 amino acids; Supplementary Figure 1), a very long α-helix was predicted in each species. Second, it was most striking that in every species the long α-helix was predicted to terminate after the first aromatic residue of the PIP (Phe448 in Figure 5 and Figure 1B, CAF-1 p150 PIPs). In other words, in each species seven of the eight residues that constitute the PIP were predicted to be part of the helix. In many, but not all species, the C-terminal end of the predicted helix was dictated by the presence of an helix breaking proline a few residues after the PIP (Pro452 in Figure 5).

We decided to address this surprising prediction. To this end, we expressed CAF-1 p150 fragments that contained the long α-helix and the PIP in *Escherichia coli*, and studied their biochemical and biophysical properties. We performed our experiments with a fragment from human p150 (Figure 5, residues 342 - 474, ERL...FEIK) that was highly expressed as a His6-

tagged fusion protein. This fragment is hereafter referred to as CAF-1 p150L. The p150L-His6 protein was soluble and showed no sign of forming aggregates based on size exclusion chromatography.

CAF-1 p150L is highly helical

The first question we sought to answer was whether the purified p150L-His6 protein is in fact an α-helix, as predicted by secondary structure algorithms. We used circular dichroism (CD) to answer this question. When we analyzed p150L by CD, the spectrum clearly showed the features typical of a protein that mostly consists of α-helices (Figure 6A, upper panel), specifically the strong negative ellipticity at 222 nm and 208 nm.

CAF-1 p150L forms oligomers

Panne and colleagues (Sauer et al., 2017) showed that the KER domain of *S. cerevisiae* Cac1 (the yeast homologue of human p150) is in fact the most important DNA binding domain of the CAF-1 protein. They also observed that the KER domain was predicted to form coiled-coil, which are bundles of two to seven α-helices coiled around each other (Rose and Meier, 2004) ; (Cohen and Parry, 1990; Lupas et al., 1991). α-helices that form short coiled-coils (30-40 residues) are relatively common in eukaryotic transcription factors that form domains known leucine zippers (Newman and Keating, 2003). But proteins that form long coiled-coil domains have thus far only been identified in cytoskeletal motor protein families such as myosin, kinesin, and dynein (Kato et al., 2018; Taniguchi et al., 2010). Most of these proteins contain a repetitive pattern of seven amino acids (heptad) that function to bury their hydrophobic surfaces between hydrophilic amino acids. This motif is not present in the CAF-1 p150 KER domain. Nonetheless,

we felt it necessary to investigate the possibility that p150L-His6 might form oligomers by size exclusion chromatography coupled with multiple angle light scattering (SEC - MALS).

So, we asked if p150L could indeed form higher oligomers such as coiled coils. We decided to answer this using another biophysical tool that combined the power of traditional size exclusion chromatography (SEC) coupled to a multi-angle light scattering (MALS) detector. SEC-MALS is a powerful technique known for absolute characterization of molar mass, size, and conformation of biomolecules.

We observed two peaks of p150L-His6 that were well-resolved by SEC. A very prominent first peak that eluted approximately between 12 and 12.5 ml and a much smaller peak that eluted between 14 and 14.5 ml (Figure 6B, blue trace, peaks 1 and 2). Based on the MALS detector, peaks 1 and 2 had molar masses of 44kDa and 29kDa, respectively, corresponding to trimers and dimers of p150L-His6 (Figure 6B, blue trace and Figure 6C). The trimeric form was clearly the most prevalent form (Figure 6B, blue trace).

The elution profile of CAF-1 p150L-His6 was different from that of a typical globular protein. For instance, the elution profile of BSA (Figure 6B, red) showed two peaks, peak 1 eluted between 11.5 and 12.5 ml had a molar mass of 134 kDa, corresponding to a dimer of BSA, and peak 2 eluted between 13.5 and 14.25 ml corresponded to a monomeric molar mass of 67 kDa. In general, during SEC larger proteins elute first from the column, and smaller proteins elute later. However, we found out that the trimeric form of CAF-1 p150L-His6 (44 kDa) eluted

before monomeric BSA (67 kDa), despite having a smaller size (Figure 6B). This suggests that p150L-His6 adopts a non-globular shape.

CAF-1 p150L adopts an elongated rod-like structure

Based on the anomalous elution of p150L-His6 during SEC, we were curious to find out the overall shape of p150L. For that purpose, we used size exclusion chromatography coupled to small-angle X-ray scattering (SEC-SAXS) to determine its approximate shape.

Small-angle X-ray scattering (SAXS) measures the intensities of X-rays scattered by a sample. The scattering angle thus provides low resolution information on the shape, assembly, and conformation of the analyzed protein. The raw SAXS data corresponding to the intensity of p150L elution peak is shown in Figure 7A and 7B. An average scattering profile of all frames within the SEC elution peak was calculated. Next, the particle distribution function P(r) curve was obtained after raw data processing using the pair distribution function GNOM (Figure 7C). This P(r) curve gives information about the shape of the sample by comparing the experimental curve with different standard shapes (Figure 7D ; adapted from (Mertens and Svergun, 2010). Based on this, the P(r) curve of the p150L-His6 protein (Figure 7C) is most similar to that of an oblong rod-shaped protein (cyan in Figure 7D).

Consistent with this, dummy atom modeling of our SAXS results (Figure 7E) suggests that the protein adopts an elongated form with a shape related to that of "beads on a string", with 5 or 6 spherical beads, each with a diameter of 20 - 25 Å. This would roughly amount to 4-5 α-helical turns per "bead" (pitch of an alpha helix is ~5.4 Å), or 13-16 residues (3.6 residues per α-

helical turn), considering that the secondary structure is mostly α-helical in nature which is consistent with the CD data (Figure 6A). The overall length of the particle (D max) is in the 150-160 Å range (Rg ~45-50 Å). Based on the beads (dummy atoms) model, the beads-on-a-string model of p150L adopts a slightly screw-like twisted shape as shown in the surface representation (Figure 7E). The fit of the dummy atom model to the experimental data is shown in (Figure 7F).

CAF-1 p150L may bind directly to PCNA

Secondary structure prediction algorithms included the PIP residues observed in the crystal structure, except the last aromatic residue of RFF, within the last turn of the predicted long helix. Given this, it was far from clear that p150L would bind PCNA when held in an α-helical conformation and/or when part of a three-membered coiled-coil. We attempted to determine whether p150L-His6 bound directly to PCNA by performing nuclear magnetic resonance (NMR) and fluorescence quenching experiments.

The appearance of the 1H-15N BEST HSQC for 15N-labelled p150L alone (Figure 8A) suggested that p150L-His6 was not a well-folded, globular protein with a distinct three-dimensional structure. This did not come as a surprise because p150L is devoid of Trp or Tyr residue. The visible peaks are heterogenous, poorly dispersed, and reduced in number (we should see ~ 139 peaks for a well-folded p150L protein). Overall, the spectrum agrees with SEC and SAXS data, with broad and non-visible peaks likely a consequence of multiple conformations on the intermediate timescale, although further analysis is required to confirm this. The PCNA-His6 homo-trimer (88.7 kDa) is a relatively large protein from an NMR standpoint. PCNA-His6 is sufficiently large that it tumbles slowly in solution which, in turn, results in very few NMR peaks

being detected (Figure 8B ; PCNA-His6 alone). When we mixed CAF-1 p150L-His6 with PCNA-His6, some of the well-resolved peaks corresponding to CAF-1 p150L disappeared or were significantly shifted, which is observed clearly from the overlay of CAF-1 p150L in the presence or absence of PCNA in 2.5-fold molar excess PCNA monomer : p150L (Figure 8C). This is consistent with CAF-1 p150L binding to a PCNA, thus generating a complex (minimal size of p150L-His6 + PCNA-His6 homotrimer = 107 kDa) with slow tumbling time, which results in a loss of signal. The strong visible peaks, many of which undergo chemical shift perturbations, are most likely in regions of p150L-His6 that are unfolded.

To test the hypothesis that there is an interaction between p150L and PCNA more rigorously, we performed a complementary experiment, namely fluorescence quenching, which exploits the inherent absence of tryptophan residues in CAF-1 p150L-His6 and the presence of only one Trp per PCNA-His6 monomer. The intrinsic fluorescence of the PCNA-His6 signal is shown in the absence or presence of a 4-fold molar of excess of p150L over PCNA monomer (Figure 9A, red and black traces respectively). As expected, the emission spectrum of CAF-1 p150L-His6 alone is very small due to the absence of tryptophan residue (blue trace ; Figure 9A). Clearly, the addition of CAF-1 p150L-His6 to PCNA quenched a small portion of the tryptophan signal derived from PCNA-His6, which is consistent with complex formation (Figure 9A). Using PyMOL and our PIP-PCNA structure, we measured the distance between tryptophan 28 (W28) in *Homo sapiens* PCNA and the aromatic residues (the two phenylalanines of the RFF sequence of the PIP) was approximately 20-23 Å. The distance between tryptophan 28 (W28) of PCNA and tyrosine 250 (Y250, the residue involved in the cation-π interaction with the PIP Arg residue) of PCNA was around 18 Å. We also found out that in the 3D protein structure of PCNA,

tryptophan 28 lies in the vicinity of the inter-domain connecting loop (IDCL), where the PIP was shown to bind to PCNA in the crystal structure with the 3 residues RFF (Figure 9B). All these distances are consistent with the possibility that the fluorescence quenching reflects genuine binding of p150L-His6 to PCNA-His6. However, the fact that only a small portion of the PCNA-derived fluorescence emission was quenched upon addition of a four-fold molar excess of p150L-His6 may suggest weak binding. Although the NMR and fluorescence quenching experiments suggest that p150L directly binds to PCNA, further experiments are needed to address this issue and determine the binding affinity.

Discussion

In this manuscript, we showed that the PIP of CAF-1 binds to PCNA in a manner that is unprecedented among the numerous structures of PIPs bound to PCNA. The non-canonical PIP of CAF-1 p150 binds to PCNA in a manner that is unprecedented among other PCNA-binding proteins. Among other features, the positive charge of Arg 426 is involved in forming a cation-π interaction with the electron density on the side chain of PCNA Tyr 250 (Figure 2 and 3). Arg426 is not conserved among other PCNA-binding proteins and, consequently, the cation-π interaction can, thus far, only be formed by CAF-1 homologues from a number of species, but not *S. cerevisiae* or *S. pombe* (Figure 1B). Consistent with this interaction being physiologically relevant, the arginine involved in the cation-π interaction is required for PIP binding to PCNA and for DNA replication coupled nucleosome assembly *in vitro* (Figure 4A and Figure 4C). *In vivo*, Arg426 was needed for targeting CAF-1 p150 to PCNA-containing DNA replication foci during mid S-phase (Figure 4B).

Within the context of the full-length p150 protein, the CAF-1 PIP occurred within the C-terminal turn of a very long α-helix (100 - 120 residues depending on species) that encompasses the entire KER domain (Figure 5 and 6A), which is one of two DNA-binding domains within CAF-1 p150. In solution, the long α-helix that spans the KER domain and PIP forms oligomers, mainly trimers (Figure 6B), and adopts an oblong shape (Figure 7), likely a 3-helix bundle that forms a structure similar to that of coiled-coils. Despite its presence at the end of a long α-helix that forms a higher-order oligomeric structure, we provided preliminary evidence suggesting that juxtaposition of the KER domain and the PIP is not an irremediable obstacle to PCNA binding (Figure 8 and 9).

Is there a PCNA ring dedicated to nucleosome assembly?

One argument that is often invoked to explain how functionally distinct enzymes (*e.g.* Pol δ, FEN1 and DNA ligase during lagging strand synthesis) might exert their activities by binding to the same PCNA ring is the sequential binding and dissociation of each enzyme. This is often invoked in cases where the binding of one or more of the enzymes is mutually exclusive because of steric hindrance. This is the case, for instance, for Pol δ and DNA ligase I whose binding to PCNA occludes the entire front face of the homo-trimer (Khandagale et al., 2020; Pascal et al., 2004). However, we feel that sequential binding and dissociation of each enzyme is not a viable model for two reasons. This is best illustrated with the roles of Pol δ, FEN1 and DNA ligase I in lagging strand synthesis. The first argument is that any need for Pol δ to dissociate from a single PCNA ring, in order to allow access to FEN1 and DNA ligase I, simply defeats the role of PCNA as a processivity factor for Pol δ. A distributive (binding and dissociation) model for access to

PCNA implies that the affinities of each enzyme for PCNA are sufficiently different to ensure that the enzymes act according to a specific sequence (*e.g.* Pol δ must gain access to PCNA first). This model is flawed for an obvious reason. Assuming that Pol δ has the highest affinity for PCNA, there is no obvious means to prevent it from competing with the enzymes that need to act on DNA synthesized by Pol δ, namely FEN1 and DNA ligase I.

A more plausible, but unproven solution than the "binding and dissociation" model is the "multiple functionally dedicated rings" model. In this case, multiple PCNA rings are loaded sequentially by RF-C and, in the simplest of cases, each PCNA ring becomes functionally specialized by associating with a unique enzyme according to a specific sequence (*e.g.* Pol δ first, then FEN1 and DNA ligase I last). Once the appropriate enzyme has bound to the first ring (*e.g.* Pol δ), functionally dedicating that PCNA ring to DNA synthesis could involve several mechanisms (*e.g.* ring-specific modifications of PCNA and/or the PCNA-binding enzyme) but, in many circumstances, may involve steric occlusion of that PCNA ring from functionally unrelated PCNA-binding enzymes. This is clearly the case for both Pol δ and DNA ligase I because their binding to PCNA completely occludes the front face of PCNA to which functionally different PCNA-binding enzymes might otherwise have access to (Khandagale et al., 2020; Pascal et al., 2004).

Our data shows that the long KER α-helix is in fact a three-helix bundle. Our SEC-MALS and SEC-SAXS data are consistent with the possibility that the three-helix bundle adopts an oblong coiled-coil arrangement. Further work is needed to validate that the three-helix coiled-

coil directly binds PCNA and determine its binding affinity and stoichiometry, which can be determined by isothermal calorimetry. Assuming that the three-helix coiled-coil binds to the PCNA homo-trimer with a 1:1 stoichiometry (1 KER α-helix : 1 PCNA monomer), this may provide a mechanism to dedicate a PCNA ring to CAF1-mediated deposition of H3-H4 onto DNA. We note however that, in order for the three PIPs to simultaneously engage each PCNA monomer, one would likely require splaying of the C-terminal end of the coiled-coil over a sufficiently long distance to enable the three PIPs to reach the PIP-binding surfaces in the three monomers.

It is noteworthy that none of the other canonical DNA replication proteins that we looked at, including p21, FEN1, DNMT1, and DNA ligase I, exhibit the presence of long alpha helices that terminate in their PIPs. (Supplemental Figure 2). Similarly, the error-prone DNA polymerases Pol kappa and Pol iota, which contain non-canonical PIPs, also lack a long a-helix that terminates in their PIPs (Supplemental Figure 3). Thus far, the structure that we identified in CAF-1 p150 is unique, which might have functional significance for regulating CAF-1 binding to DNA and PCNA and, ultimately, chromatin assembly.

Is the long α-helix of CAF-1 p150 acting as a DNA binder, a DNA bender, or a DNA ruler?

In many species ranging from yeast to humans, the KER domain is predicted to form an unusually long α-helix of CAF-1 p150 and these secondary structure predictions were borne out by our circular dichroism experiments with the human p150L protein. A striking feature of the predictions is that, regardless of the species, the long α-helix always ends with the first aromatic residue of the CAF-1 p150 PIP. Because the KER domain of *S. cerevisiae* Cac1 (the orthologue of human p150) has been firmly established as one of the two DNA binding domains of budding yeast CAF-1 (Sauer et al., 2017), the juxtaposition of the KER DNA-binding domain and the PIP

within the same α-helix suggests that DNA and PCNA binding are coordinated. Why might that be the case?

The first possibility is that this may be part of a mechanism to ensure that the nascent DNA immediately behind PCNA is free of protein impediments that might interfere with the formation of $(H3\text{-}H4)_2$ tetramers onto nascent DNA. In this scenario, the KER α-helix would merely serve as a DNA binder that is present immediately behind the PCNA ring to which CAF-1 is associated, which itself must act close to the point where nascent DNA emerges from the replicative polymerases (Smith and Whitehouse, 2012; Yu et al., 2014). Robust DNA binding by the KER α-helix would occlude the freshly synthesized DNA from irrelevant DNA-binding proteins and keep the DNA substrate pristine for deposition of H3-H4 by CAF-1 .

The second possibility stems from the fact that 147bp of DNA have to be wrapped into 1.65 left-handed superhelical turns around histone octamers to form nucleosome core particles (Davey et al., 2002). It turns out that B-form DNA is one of the stiffest known polymers and its persistence length, the length below which a polymer is essentially a rigid rod, is 150bp in 0.1M NaCl. This is a lot longer than the 73bp needed to accommodate the first intermediate in nucleosome assembly, namely the deposition of the $(H3\text{-}H4)_2$ tetramer onto nascent DNA (Dong and van Holde, 1991). The rigidity of DNA against bending stems from electrostatic repulsion among the phosphate groups that necessarily have to come in close proximity as a result of DNA bending. It therefore stands to reason that charge neutralization of the phosphate groups on side of the double helix by a DNA binding protein facilitates deformation (bending) of the DNA double helix. Given this, it seems possible that the function of the KER α-helix may be to prepare the nascent DNA for H3-H4 deposition by bending the DNA substrate.

Several lines of evidence argue that new $(H3\text{-}H4)_2$ tetramers are assembled from two CAF-1 complexes that each bind to an H3-H4 dimer (Sauer et al., 2017). A sufficient length of nascent DNA must be available before CAF-1 deposits two H3-H4 dimers onto DNA to form $(H3\text{-}H4)_2$ tetramers. One can readily calculate the maximal length of DNA that can be covered by the KER α-helix, namely 119 residues of a prototypical Corey-Pauling α-helix (3.6 residues/turn; 5.4 Å/turn for the pitch of the helix). This adds up to 178 Å, which is equivalent to approximately 52bp of B-form DNA (3.4 Å/bp). Fifty-two base pairs is too short to accommodate the 73bp needed to assemble $(H3\text{-}H4)_2$ tetramers onto DNA. However, because two CAF-1 complexes are needed to assemble $(H3\text{-}H4)_2$ tetramers, the maximal amount of DNA contacted by two KER α-helices would be 104bp (2 x 52bp), which is sufficient to accommodate a single $(H3\text{-}H4)_2$ tetramer onto nascent DNA. In this scenario the KER α-helices of two CAF-1 complexes would act in a concerted fashion and serve as "*DNA rulers*" to ensure that H3-H4 are not deposited onto DNA before a sufficient length of freshly synthesized DNA has emerged from the replisome to accommodate the formation of $(H3\text{-}H4)_2$ tetramers. This *DNA ruler* function of the KER α-helices is not mutually exclusive with the aforementioned *DNA binder* and *DNA bender* functions. Lastly, we note that, the fact that the KER DNA-binding domain and the PIP are part of the same α-helix implies that, once the DNA-binding domain is engaged on the DNA substrate, the position of the PCNA ring with respect to DNA is likely fixed, and the PCNA ring to which CAF-1 is bound may no longer slide freely along the DNA. This *bookend* function of the KER DNA-binding domain and PCNA would contribute to ensure that $(H3\text{-}H4)_2$ tetramers are uniformly spaced along the DNA.

In conclusion, the experiments presented in this manuscript have raised many fascinating issues for future research. In particular, the juxtaposition of the KER DNA-binding domain and the PIP within a single higher order oligomeric structure raises the possibility that DNA binding and PCNA binding may be coordinated to bring about efficient H3-H4 deposition onto nascent DNA without functional interference from the numerous other enzymes that need to bind PCNA at replication forks.

Acknowledgments

We wish to thank Dr. Bruce Stillman for providing valuable cell extracts and proteins and Christian Charbonneau for help with confocal microscopy. We are grateful to Drs. Matthew Smith, Chang Hwa Jo, and Mehdi Talebzadeh for help with protein expression and purification. We are indebted to Drs. Tomasso Moschetti and Andrew Thompson for their assistance in the collection of X-ray diffraction data. Research in Dr. Alain Verreault's laboratory was supported by grants from the Canadian Institutes for Health Research (CIHR, FRN 125916) and the Natural Sciences and Engineering Research Council (NSERC, RGPIN - 2019 - 05796).

References Chapter 2

Anthis, N.J., and G.M. Clore. 2013. Sequence-specific determination of protein and peptide concentrations by absorbance at 205 nm. *Protein Sci*. 22:851-858.

Boehm, E.M., M.S. Gildenberg, and M.T. Washington. 2016. The Many Roles of PCNA in Eukaryotic DNA Replication. *Enzymes*. 39:231-254.

Bruning, J.B., and Y. Shamoo. 2004. Structural and thermodynamic analysis of human PCNA with peptides derived from DNA polymerase-delta p66 subunit and flap endonuclease-1. *Structure*. 12:2209-2219.

Casas-Delucchi, C.S., and M.C. Cardoso. 2011. Epigenetic control of DNA replication dynamics in mammals. *Nucleus*. 2:370-382.

Clark, A.B., F. Valle, K. Drotschmann, R.K. Gary, and T.A. Kunkel. 2000. Functional interaction of proliferating cell nuclear antigen with MSH2-MSH6 and MSH2-MSH3 complexes. *J Biol Chem*. 275:36498-36501.

Cohen, C., and D.A. Parry. 1990. Alpha-helical coiled coils and bundles: how to design an alpha-helical protein. *Proteins*. 7:1-15.

Davey, C.A., D.F. Sargent, K. Luger, A.W. Maeder, and T.J. Richmond. 2002. Solvent mediated interactions in the structure of the nucleosome core particle at 1.9 a resolution. *J Mol Biol*. 319:1097-1113.

De March, M., N. Merino, S. Barrera-Vilarmau, R. Crehuet, S. Onesti, F.J. Blanco, and A. De Biasio. 2017. Structural basis of human PCNA sliding on DNA. *Nat Commun*. 8:13935.

Delaglio, F., S. Grzesiek, G.W. Vuister, G. Zhu, J. Pfeifer, and A. Bax. 1995. NMRPipe: a multidimensional spectral processing system based on UNIX pipes. *J Biomol NMR*. 6:277-293.

Dieckman, L.M., B.D. Freudenthal, and M.T. Washington. 2012. PCNA structure and function: insights from structures of PCNA complexes and post-translationally modified PCNA. *Sub-cellular biochemistry*. 62:281-299.

Dong, F., and K.E. van Holde. 1991. Nucleosome positioning is determined by the (H3-H4)2 tetramer. *Proc Natl Acad Sci U S A*. 88:10596-10600.

Fasman, G.D. 1996. Circular dichroism and the conformational analysis of biomolecules. Plenum Press, New York.

Favier, A., and B. Brutscher. 2019. NMRlib: user-friendly pulse sequence tools for Bruker NMR spectrometers. *J Biomol NMR*. 73:199-211.

Gonzalez-Magana, A., and F.J. Blanco. 2020. Human PCNA Structure, Function and Interactions. *Biomolecules*. 10.

Gulbis, J.M., Z. Kelman, J. Hurwitz, M. O'Donnell, and J. Kuriyan. 1996. Structure of the C-terminal region of p21(WAF1/CIP1) complexed with human PCNA. *Cell*. 87:297-306.

Iida, T., I. Suetake, S. Tajima, H. Morioka, S. Ohta, C. Obuse, and T. Tsurimoto. 2002. PCNA clamp facilitates action of DNA cytosine methyltransferase 1 on hemimethylated DNA. *Genes Cells*. 7:997-1007.

Jackson, V. 1988. Deposition of newly synthesized histones: hybrid nucleosomes are not tandemly arranged on daughter DNA strands. *Biochemistry*. 27:2109-2120.

Jimenji, T., R. Matsumura, S. Kori, and K. Arita. 2019. Structure of PCNA in complex with DNMT1 PIP box reveals the basis for the molecular mechanism of the interaction. *Biochemical and biophysical research communications*. 516:578-583.

Kato, Y., T. Miyakawa, and M. Tanokura. 2018. Overview of the mechanism of cytoskeletal motors based on structure. *Biophys Rev*. 10:571-581.

Kaufman, P.D., R. Kobayashi, N. Kessler, and B. Stillman. 1995. The p150 and p60 subunits of chromatin assembly factor I: a molecular link between newly synthesized histones and DNA replication. *Cell*. 81:1105-1114.

Kelch, B.A. 2016. Review: The lord of the rings: Structure and mechanism of the sliding clamp loader. *Biopolymers*. 105:532-546.

Khandagale, P., S. Thakur, and N. Acharya. 2020. Identification of PCNA-interacting protein motifs in human DNA polymerase delta. *Biosci Rep*. 40.

Kim, D., D. Setiaputra, T. Jung, J. Chung, A. Leitner, J. Yoon, R. Aebersold, H. Hebert, C.K. Yip, and J.J. Song. 2016. Molecular Architecture of Yeast Chromatin Assembly Factor 1. *Scientific reports*. 6:26702.

Kontopidis, G., S.Y. Wu, D.I. Zheleva, P. Taylor, C. McInnes, D.P. Lane, P.M. Fischer, and M.D. Walkinshaw. 2005. Structural and biochemical studies of human proliferating cell nuclear antigen complexes provide a rationale for cyclin association and inhibitor design. *Proc Natl Acad Sci U S A*. 102:1871-1876.

Krishna, T.S., X.P. Kong, S. Gary, P.M. Burgers, and J. Kuriyan. 1994. Crystal structure of the eukaryotic DNA polymerase processivity factor PCNA. *Cell*. 79:1233-1243.

Krude, T. 1995a. Chromatin assembly factor 1 (CAF-1) colocalizes with replication foci in HeLa cell nuclei. *Experimental cell research*. 220:304-311.

Krude, T. 1995b. Chromatin. Nucleosome assembly during DNA replication. *Curr Biol*. 5:1232-1234.

Lescop, E., P. Schanda, and B. Brutscher. 2007. A set of BEST triple-resonance experiments for time-optimized protein resonance assignment. *J Magn Reson*. 187:163-169.

Liberti, S.E., S.D. Andersen, J. Wang, A. May, S. Miron, M. Perderiset, G. Keijzers, F.C. Nielsen, J.B. Charbonnier, V.A. Bohr, and L.J. Rasmussen. 2011. Bi-directional routing of DNA mismatch repair protein human exonuclease 1 to replication foci and DNA double strand breaks. *DNA repair*. 10:73-86.

Lupas, A., M. Van Dyke, and J. Stock. 1991. Predicting coiled coils from protein sequences. *Science*. 252:1162-1164.

Maga, G., and U. Hubscher. 2003. Proliferating cell nuclear antigen (PCNA): a dancer with many partners. *Journal of cell science*. 116:3051-3060.

Mertens, H.D., and D.I. Svergun. 2010. Structural characterization of proteins and complexes using small-angle X-ray solution scattering. *J Struct Biol*. 172:128-141.

Moggs, J.G., P. Grandi, J.P. Quivy, Z.O. Jonsson, U. Hubscher, P.B. Becker, and G. Almouzni. 2000. A CAF-1-PCNA-mediated chromatin assembly pathway triggered by sensing DNA damage. *Mol Cell Biol*. 20:1206-1218.

Moldovan, G.L., B. Pfander, and S. Jentsch. 2007. PCNA, the maestro of the replication fork. *Cell*. 129:665-679.

Murzina, N., A. Verreault, E. Laue, and B. Stillman. 1999. Heterochromatin dynamics in mouse cells: interaction between chromatin assembly factor 1 and HP1 proteins. *Mol Cell*. 4:529-540.

Newman, J.R., and A.E. Keating. 2003. Comprehensive identification of human bZIP interactions with coiled-coil arrays. *Science*. 300:2097-2101.

O'Keefe, R.T., S.C. Henderson, and D.L. Spector. 1992. Dynamic organization of DNA replication in mammalian cell nuclei: spatially and temporally defined replication of chromosome-specific alpha-satellite DNA sequences. *J Cell Biol*. 116:1095-1110.

Pascal, J.M., P.J. O'Brien, A.E. Tomkinson, and T. Ellenberger. 2004. Human DNA ligase I completely encircles and partially unwinds nicked DNA. *Nature*. 432:473-478.

Quivy, J.P., P. Grandi, and G. Almouzni. 2001. Dimerization of the largest subunit of chromatin assembly factor 1: importance in vitro and during Xenopus early development. *EMBO J*. 20:2015-2027.

Rolef Ben-Shahar, T., A.G. Castillo, M.J. Osborne, K.L. Borden, J. Kornblatt, and A. Verreault. 2009. Two fundamentally distinct PCNA interaction peptides contribute to chromatin assembly factor 1 function. *Mol Cell Biol*. 29:6353-6365.

Rose, A., and I. Meier. 2004. Scaffolds, levers, rods and springs: diverse cellular functions of long coiled-coil proteins. *Cellular and molecular life sciences : CMLS*. 61:1996-2009.

Sakurai, S., K. Kitano, K. Okada, K. Hamada, H. Morioka, and T. Hakoshima. 2003. Preparation and crystallization of human flap endonuclease FEN-1 in complex with proliferating-cell nuclear antigen, PCNA. *Acta Crystallogr D Biol Crystallogr*. 59:933-935.

Sauer, P.V., J. Timm, D. Liu, D. Sitbon, E. Boeri-Erba, C. Velours, N. Mucke, J. Langowski, F. Ochsenbein, G. Almouzni, and D. Panne. 2017. Insights into the molecular architecture and histone H3-H4 deposition mechanism of yeast Chromatin assembly factor 1. *eLife*. 6.

Shibahara, K., and B. Stillman. 1999. Replication-dependent marking of DNA by PCNA facilitates CAF-1-coupled inheritance of chromatin. *Cell*. 96:575-585.

Smith, D.J., and I. Whitehouse. 2012. Intrinsic coupling of lagging-strand synthesis to chromatin assembly. *Nature*. 483:434-438.

Smith, S., and B. Stillman. 1989. Purification and characterization of CAF-I, a human cell factor required for chromatin assembly during DNA replication in vitro. *Cell*. 58:15-25.

Smith, S., and B. Stillman. 1991a. Immunological characterization of chromatin assembly factor I, a human cell factor required for chromatin assembly during DNA replication in vitro. *J Biol Chem*. 266:12041-12047.

Smith, S., and B. Stillman. 1991b. Stepwise assembly of chromatin during DNA replication in vitro. *EMBO J*. 10:971-980.

Sogo, J.M., H. Stahl, T. Koller, and R. Knippers. 1986. Structure of replicating simian virus 40 minichromosomes. The replication fork, core histone segregation and terminal structures. *J Mol Biol*. 189:189-204.

Taniguchi, Y., B.S. Khatri, D.J. Brockwell, E. Paci, and M. Kawakami. 2010. Dynamics of the coiled-coil unfolding transition of myosin rod probed by dissipation force spectrum. *Biophysical journal*. 99:257-262.

Thiru, A., D. Nietlispach, H.R. Mott, M. Okuwaki, D. Lyon, P.R. Nielsen, M. Hirshberg, A. Verreault, N.V. Murzina, and E.D. Laue. 2004. Structural basis of HP1/PXVXL motif peptide interactions and HP1 localisation to heterochromatin. *EMBO J*. 23:489-499.

Tsurimoto, T. 1999. PCNA binding proteins. *Front Biosci*. 4:D849-858.

Tsutakawa, S.E., A.W. Van Wynsberghe, B.D. Freudenthal, C.P. Weinacht, L. Gakhar, M.T. Washington, Z. Zhuang, J.A. Tainer, and I. Ivanov. 2011. Solution X-ray scattering combined with computational modeling reveals multiple conformations of covalently bound ubiquitin on PCNA. *Proc Natl Acad Sci U S A*. 108:17672-17677.

Verreault, A., P.D. Kaufman, R. Kobayashi, and B. Stillman. 1996. Nucleosome assembly by a complex of CAF-1 and acetylated histones H3/H4. *Cell*. 87:95-104.

Vijayakumar, S., B.R. Chapados, K.H. Schmidt, R.D. Kolodner, J.A. Tainer, and A.E. Tomkinson. 2007. The C-terminal domain of yeast PCNA is required for physical and functional interactions with Cdc9 DNA ligase. *Nucleic Acids Res*. 35:1624-1637.

Yu, C., H. Gan, J. Han, Z.X. Zhou, S. Jia, A. Chabes, G. Farrugia, T. Ordog, and Z. Zhang. 2014. Strand-specific analysis shows protein binding at replication forks and PCNA unloading from lagging strands when forks stall. *Mol Cell*. 56:551-563.

Zhang, K., Y. Gao, J. Li, R. Burgess, J. Han, H. Liang, Z. Zhang, and Y. Liu. 2016. A DNA binding winged helix domain in CAF-1 functions with PCNA to stabilize CAF-1 at replication forks. *Nucleic Acids Res*. 44:5083-5094.

Zhang, Z., K. Shibahara, and B. Stillman. 2000. PCNA connects DNA replication to epigenetic inheritance in yeast. *Nature*. 408:221-225.

Figures

A

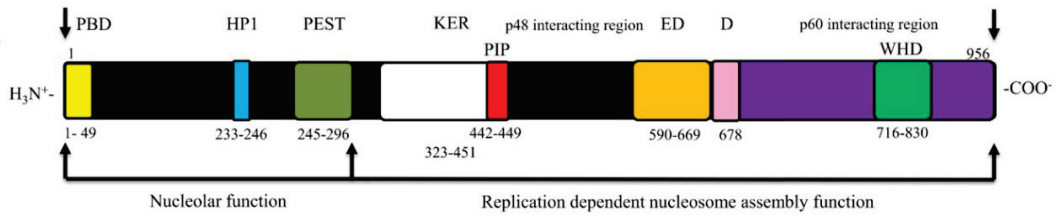

PBD: PCNA binding domain

PIP: PCNA interaction peptide

PEST: Proline Glutamic acid, Serine, Threonine rich domain

HP1: Heterochromatin protein binding motif (PxVxL)

KER: Domain rich in Lysine, Glutamic acid and Arginine residues

ED: Domain rich in Glutamic acid and Aspartic acid residues

D: Dimerization domain

WHD: Winged helix domain

B

Consensus	Q	x	x	h	x	x	F	F	
Canonical PIPs									
H. sapiens p21	Q	T	S	M	T	D	F	Y	
H. sapiens MSH6	Q	S	T	L	Y	S	F	F	
H. sapiens FEN1	Q	G	R	L	D	D	F	F	
H. sapiens LIGASE1	Q	R	S	I	M	S	F	F	
H. sapiens DNMT1	Q	T	T	I	T	S	H	F	

CAF-1 p150 PIPs									Divergence
H. sapiens CAF1	K	A	E	I	T	R	F	F	----
M. musculus CAF1	K	A	E	I	T	R	F	F	89 MYA
X. laevis CAF1	K	A	E	I	T	R	F	F	352
L. chalumnae CAF1	K	A	E	I	T	R	F	L	414
D. rerio CAF1	K	A	E	I	T	R	F	L	433
C. elegans CAF1	S	A	L	F	A	K	F	F	736
D. melanogaster CAF1	A	E	S	F	S	K	F	F	736
S. cerevisiae CAF1	Q	S	R	I	G	N	F	F	1017
S. pombe CAF1	Q	L	K	L	N	N	F	F	1017

C

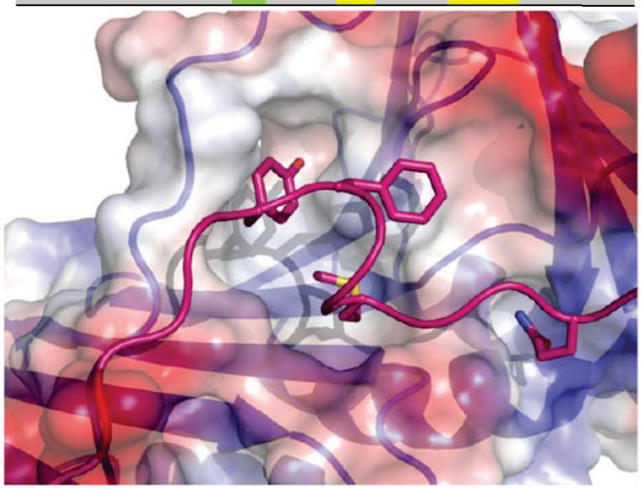

Fig. 1

FIG. 1 Differences between canonical PIPs and the non-canonical CAF-1 p150 PIP

(A). Domains of the human Chromatin Assembly Factor 1 p150 subunit.

(B) Amino acid alignment of canonical PIPs versus evolutionarily conserved CAF-1 p150 PIPs. The evolutionary divergence is shown in the extreme right column (million years = MYA).

(C) Plug and socket mode of binding in the structure of the canonical p21 PIP bound to PCNA (Gulbis *et al*. 2005). The p21 PIP is shown in pink. PCNA hydrophobic surfaces are depicted in white, whereas positively and negatively charged surfaces are respectively in blue and red. Residues of canonical PIP of p21 are shown in stick representation: Q144, M147, F150, and Y151. Q144 occupies the Q pocket of PCNA and M147, F150 and Y151 form the three prongs of the hydrophobic plug that binds to the PCNA socket.

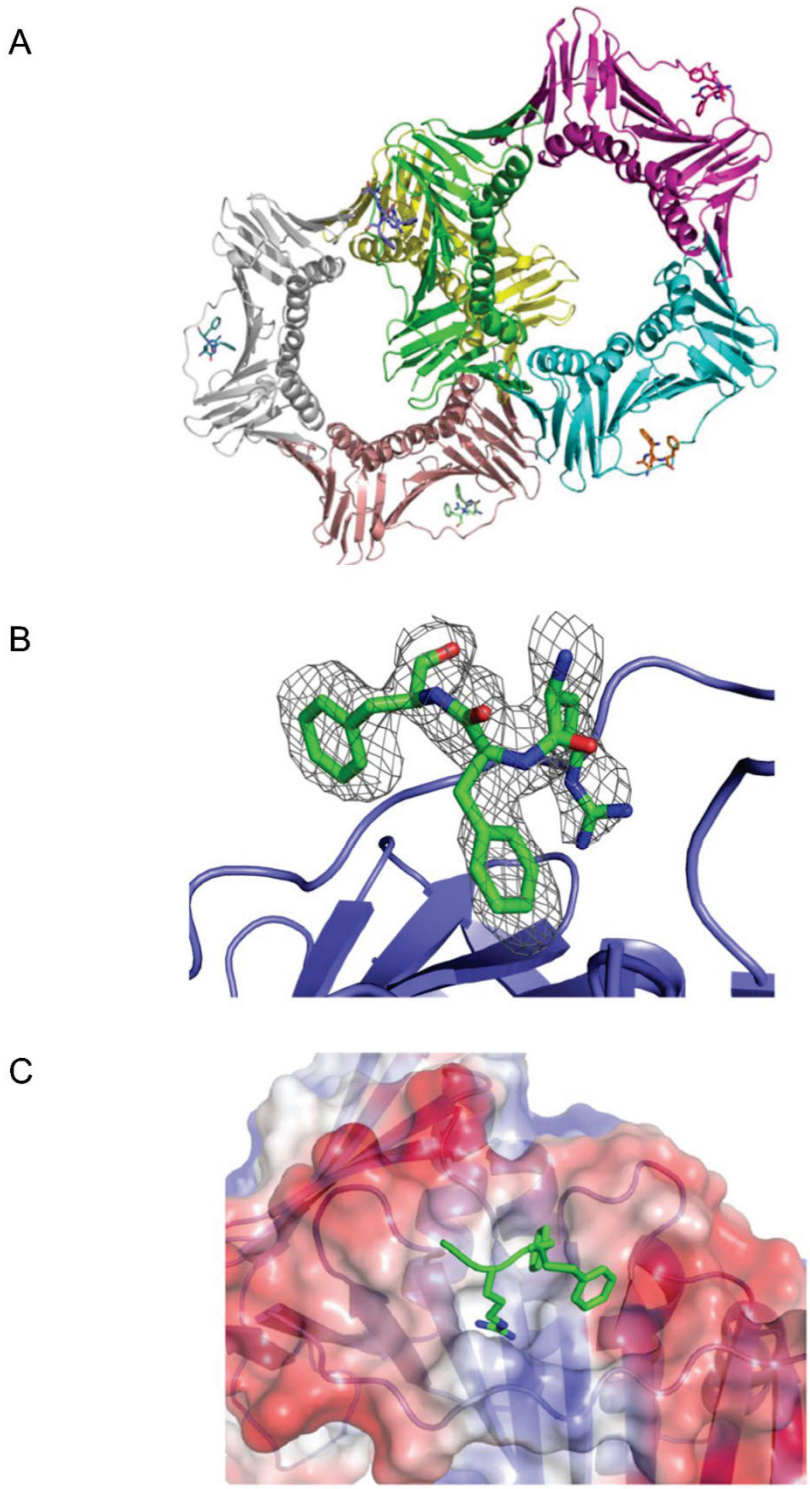

Fig. 2

FIG. 2: CAF-1 p150 PIP binding to PCNA

(A) The two PCNA homo-trimers present in the asymmetric unit. Each PCNA monomer is bound to a PIP. Only three CAF-1 p150 PIP residues (RFF) are depicted in stick representation. PIP binding occurs in a hydrophobic surface located between the interdomain connecting loop (IDCL) and the underlying β-sheet of PCNA.

(B) p150 PIP (green) is shown in stick representation, with F_0- dF_c omit electron density map contoured at 1.0σ covering the p150 residues. Only the RFF residues are shown in the model. PCNA is shown in blue.

(C) The p150 PIP interacts with a hydrophobic surface of PCNA. Three residues of the CAF-1 p150 PIP, Arg 426, Phe 427 and Phe 428 of are shown in stick representation (green). PCNA is represented with surface electrostatics calculated to a solvent radius of 1.5Å. Red corresponds to negatively charged residues, blue to positively charged residues, and white to an uncharged surface.

A

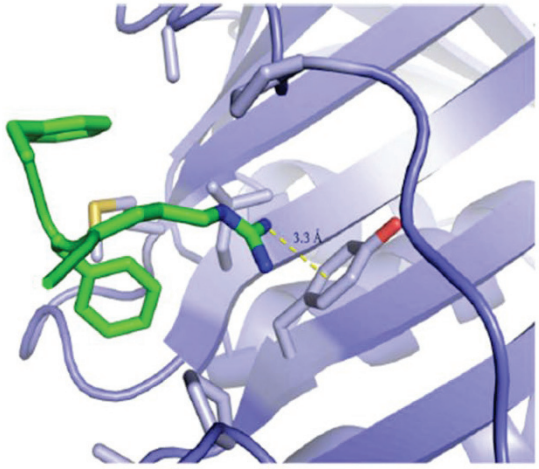

B

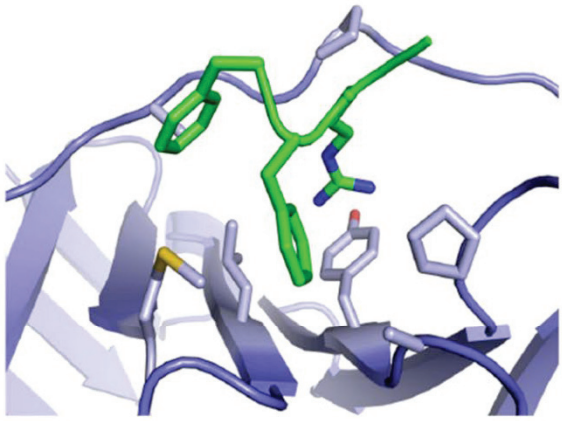

C

Fig. 3

FIG. 3: Cation-π interaction and orientation of PIP binding with respect to PCNA

(A) CAF-1 p150 PIP Arg 426 forms a cation-π interaction with Tyr 250 of PCNA. The side chain of PCNA Pro 234, Tyr 250, Ala 252, Met 40, Ala 126, Pro 129 and Leu 47 are shown in stick representation (light blue). Side chains of p150 PIP are shown in stick representation (green). Arg 426 of PIP extends into the hydrophobic pocket on the surface of PCNA and forms a cation-π interaction with Tyr 250. Bond length is measured between the terminal nitrogen of R426 and the center of the aromatic ring of Tyr 250.

(B) Hydrophobic interaction between PCNA and p150 PIP. The side chains of the PCNA residues listed in (A) are shown in stick representation (light blue). The p150 PIP side chains are shown in stick representation (green). Phe 427 of the p150 PIP nestles into a hydrophobic surface of PCNA composed of Pro 129, Tyr 250, Leu 47, and Met 40 residues. Phe 428 of the p150 PIP is less deeply buried into the hydrophobic surface of PCNA.

(C) Paths of polypeptide chains when the PIPs of different proteins are bound to PCNA. The drawing is derived from the co-crystal structures of PIP peptides bound to PCNA. Pol δ p66-PCNA [dark red] (Bruning and Shamoo 2004), Pol κ-PCNA [red] (Hishiki *et al*. 2009), p21-PCNA [magenta] (Gulbis *et al*. 1998), CAF-1 p150 PIP2- PCNA (green) were aligned to FEN1-PCNA [salmon] (Bruning and Shamoo 2004), with root mean square deviation of < 0.6Å for all alignments. For clarity, PCNA is hidden. All the PIPs adopt a short 3_{10} helix conformation when bound to PCNA, except the CAF-1 p150 PIP which assumes a different orientation with respect to PCNA.

D

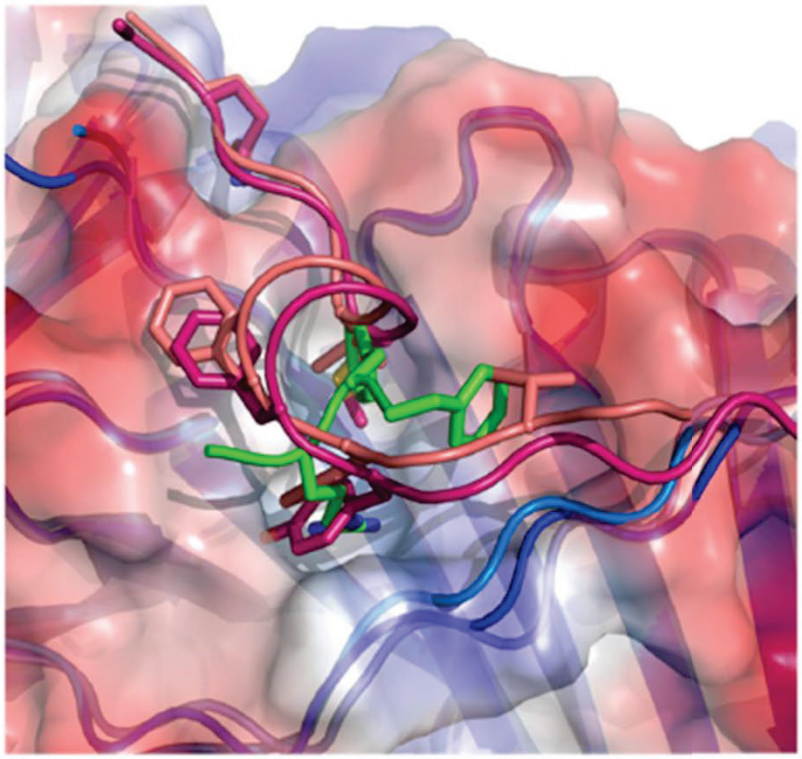

PIP	Sequence
Consensus	**Q**xx**h**xx**(a1)(a2)**
p21	143- **Q**TS**M**TD**FY**-152
FEN1	338- **Q**GR**L**DD**FF**KV-349
P150(PIP2)	420- **K**AE**I**TR**FF**-429

Q = Glutamine
x = any residue
h = hydrophobic residue
(a1) and (a2) = aromatic amino acid residue
Residues in bold are conserved in the consensus PIP
Underlined residues are shown in stick representation
Blue residues deviate from the consensus PIP

Fig. 3

FIG. 3: Cation-π interaction and orientation of PIP binding with respect to PCNA

(D) p150 PIP binding to PCNA compared with the canonical PIPs of p21 and FEN1.

The p21 PIP and p150-PIP were aligned to the FEN1 PIP with root mean square deviation of 0.55 and 0.50. The table shows key residues of the canonical PIPs and the corresponding residues of the CAF-1 p150 PIP in bold. The conserved glutamine replacement by a lysine in the p150 PIP is indicated in dark blue. The underlined residues are those shown in the stick representation. FEN1 bound to PCNA (salmon) ; p21 bound to PCNA (magenta) and p150 PIP bound to PCNA (dark grey).

The glutamines in p21 and FEN1 are interacting with the Q pocket on PCNA (visible in the top left-hand corner). Residues M146, F149 and Y150 in p21 and residues L341, F343 and F344 in FEN1 form 3_{10} helices and occupy the hydrophobic pocket on the surface of PCNA. In contrast, R426 and F427 of CAF-1 p150 both occupy the hydrophobic pocket. Strikingly, R426 (p150) overlaps with Y150 (p21) and F344 (FEN1), which is unusual because R is not a conserved residue in canonical PIPs. F427 and F428 of p150 are both conserved in canonical PIPs, but shown to occupy hydrophobic regions not expected for canonical PIP residues. F427 of p150 overlaps with L341 (FEN1) and M146 (p21) but, given their conservation, not the expected F344 (FEN1) or Y150 (p21). F428 of the p150 RFF occupies a hydrophobic patch with no overlap with conserved residues in canonical PIPs, but instead overlaps with a non conserved residue, V348 (FEN1).

A

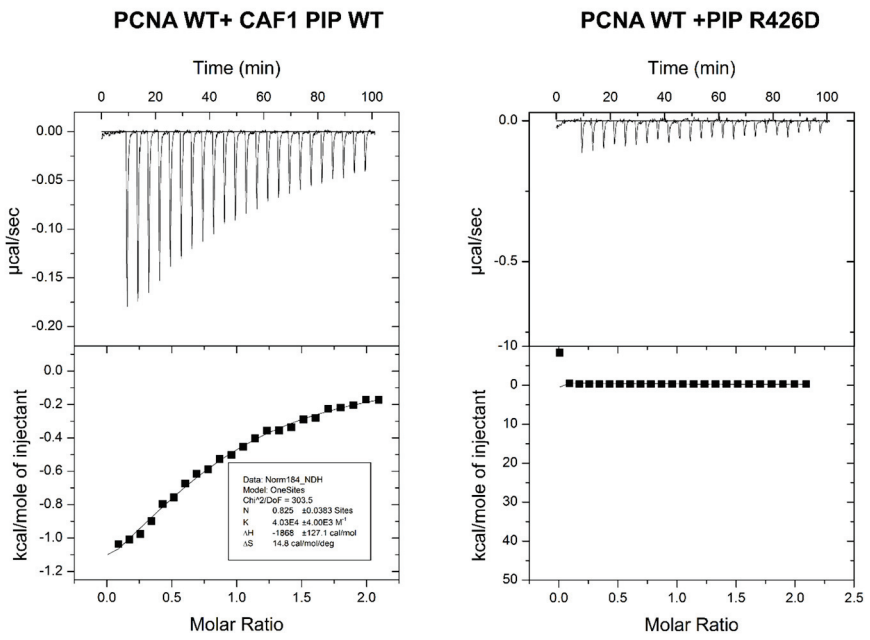
PCNA WT+ CAF1 PIP WT
PCNA WT +PIP R426D
Time (min)
µcal/sec
kcal/mole of injectant
Molar Ratio
Data: Norm184_NDH
Model: OneSites
Chi^2/DoF = 303.5
N 0.825 ±0.0383 Sites
K 4.03E4 ±4.00E3 M^-1
ΔH -1868 ±127.1 cal/mol
ΔS 14.8 cal/mol/deg

B

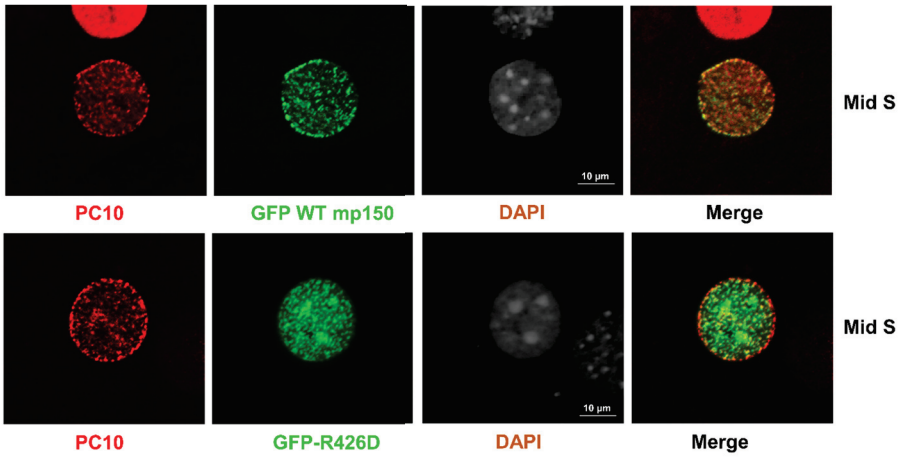
Mid S
PC10
GFP WT mp150
DAPI
Merge
10 µm
Mid S
PC10
GFP-R426D
DAPI
Merge
10 µm

C

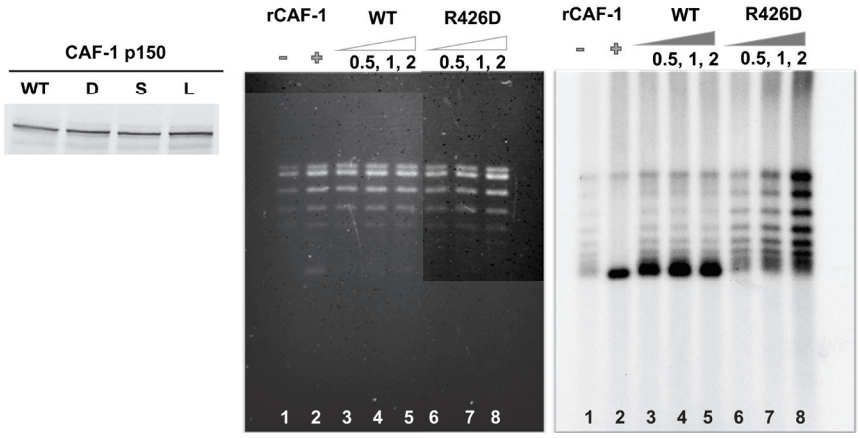
CAF-1 p150
WT
D
S
L
rCAF-1
WT
R426D
0.5, 1, 2
0.5, 1, 2
1 2 3 4 5 6 7 8
rCAF-1
WT
R426D
0.5, 1, 2
0.5, 1, 2
1 2 3 4 5 6 7 8

Fig. 4

FIG. 4: Cellular and molecular consequences of PIP-Arg 426 mutation

(A) In ITC experiments, the CAF-1 PIP wildtype and R426D mutant peptides were progressively titrated into a sample cell containing PCNA-His6. The upper half of each panel shows the measured heat exchanges during each peptide injection. The lower half of each panel shows the enthalpic changes as a function of the molar ratio of peptide to PCNA monomer. The black squares correspond to individual injections. Titrations were performed in 10 mM sodium phosphate, pH 7.0, 10 mM NaCl and at 23°C.

(B) Arg426 mutation causes mislocalization of mouse p150 in mid S-phase cells. Mouse NIH3T3 cells were transduced with constructs for expression of GFP CAF1 p150 WT or R426D mutant and stained with the PC10 monoclonal antibody (PC10) against PCNA to detect DNA replication foci. The mis-localization of the R426D mutant is most evident in mid S-phase cells, where the red PCNA staining is, in part, localized to the periphery of the cell nucleus, whereas the green CAF-1 p150 R426D is more localized to the pericentric heterochromatin (large foci seen with DAPI staining).

(C) Arg426 is required for nucleosome assembly during SV40 DNA replication. *Left panel:* CAF1 p150 wild-type and R426D mutant proteins were expressed in the rabbit reticulocyte lysate in the presence of [^{35}S]-methionine and detected by SDS-PAGE and autoradiography. *Middle panel:* Total DNA from nucleosome assembly reactions was stained with ethidium bromide. *Right panel:* Nucleosome assembly reactions were performed in the presence of increasing amounts of wild type p150 PIP or R426D mutant. Replicated DNA was detected by incorporation of [α-^{32}P] dATP and autoradiography. Lane 1 corresponds to a negative control reaction lacking p150 where there was very little supercoiling observed.

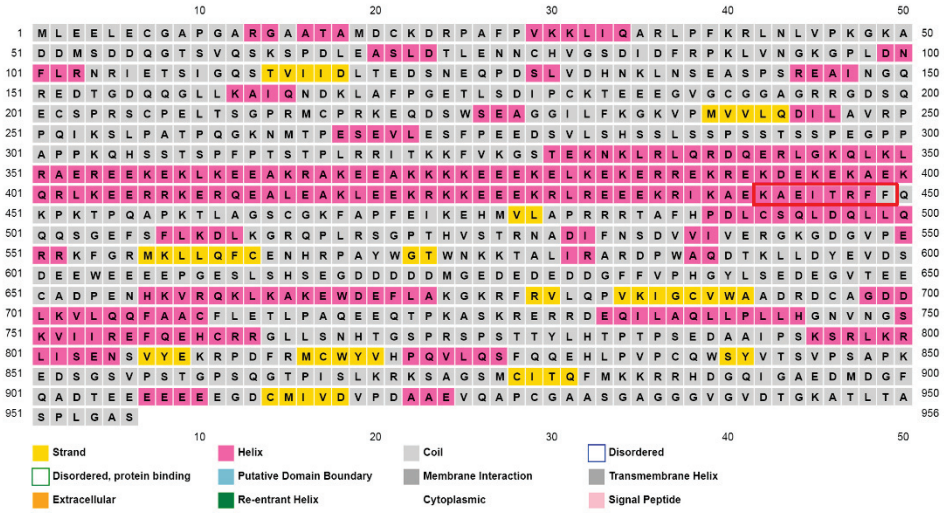
Strand
Helix
Coil
Disordered
Disordered, protein binding
Putative Domain Boundary
Membrane Interaction
Transmembrane Helix
Extracellular
Re-entrant Helix
Cytoplasmic
Signal Peptide

Fig. 5

FIG. 5: Secondary structure prediction analyses of human CAF-1 p150.

An unusually long α-helix (119 amino acids) is predicted to end abruptly in the PIP RFF residues. The CAF-1 p150 PIP is surrounded by a red rectangle.

A

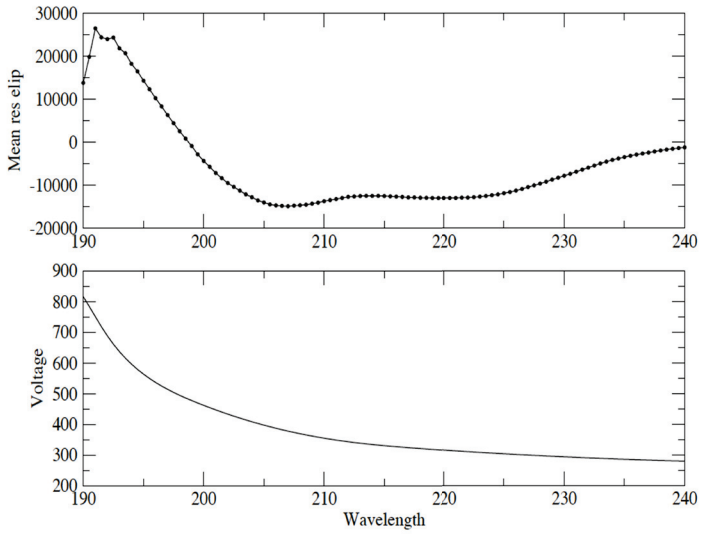

B

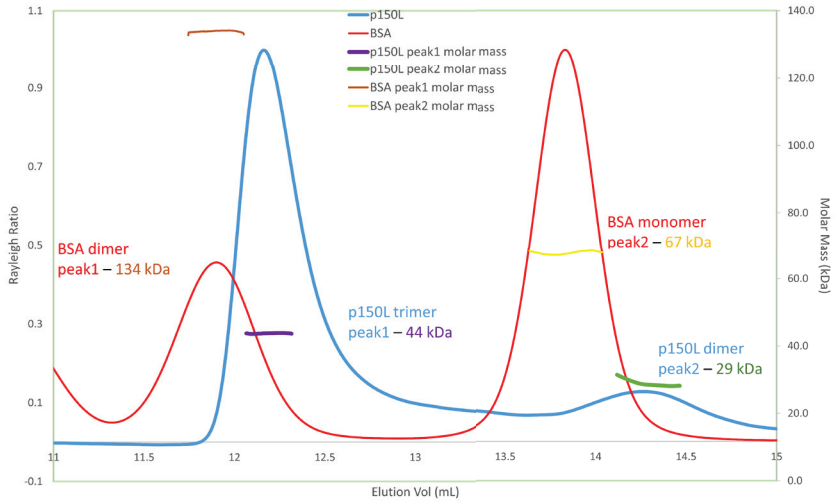

C

Peak Results	Peak 1	Peak 2
Hydrodynamic radius (Q) (nm)		
Rh(Q)z	3.278 (± 6.876%)	61.439 (± 25.677%)
Masses		
Calculated mass (µg)	15.19	4.3
Mass Recovery (%)	n/a	n/a
Mass Fraction (%)	78	22
Molar mass (g/mol)		
Mn	4.391×10^4 (± 0.857%)	2.889×10^4 (± 2.516%)
Mp	4.389×10^4 (± 0.967%)	2.848×10^4 (± 2.422%)
Mw	4.391×10^4 (± 0.856%)	2.891×10^4 (± 2.508%)
Polydispersity		
Mw/Mn	1.000 (± 1.211%)	1.001 (± 3.552%)
rms radius (nm)		
Rz	18.7 (± 7.5%)	14.7 (± 35.2%)

Fig. 6

FIG. 6: Circular dichroism (CD) and SEC-MALS analyses of p150L-His6

(A) CD spectra indicate that CAF-1 p150L-His6 is composed mainly of α-helices. CD spectrum was acquire 10 mM sodium phosphate, pH 7.2, 10 mM NaCl, 0.1 mM TCEP buffer with a data pitch of 0.5 nm over a range from 260 nm to 190 nm.

(B) SEC-MALS analysis. The p150L-His6 protein was injected onto a Superdex 200 Increase 10/300GL column at 0.35 ml/min using an AKTAmicro (GE). Samples were passed through a Dawn HELEOS II MALS and OptiLab T-rEX online refractive index detectors (Wyatt Technology) after calibration with the BSA monomer. Refractive index changes as a function of protein concentration were used to compute the molar mass and oligomerization status of the protein. p150L-His6 eluted from the Superdex 200 column in two peaks. Peak 1 corresponds to a trimer (44 kDa) and peak 2 (29 kDa) corresponds to a dimer of p150L-His6.

(C) The average molecular masses and other parameters of individual peaks are shown.

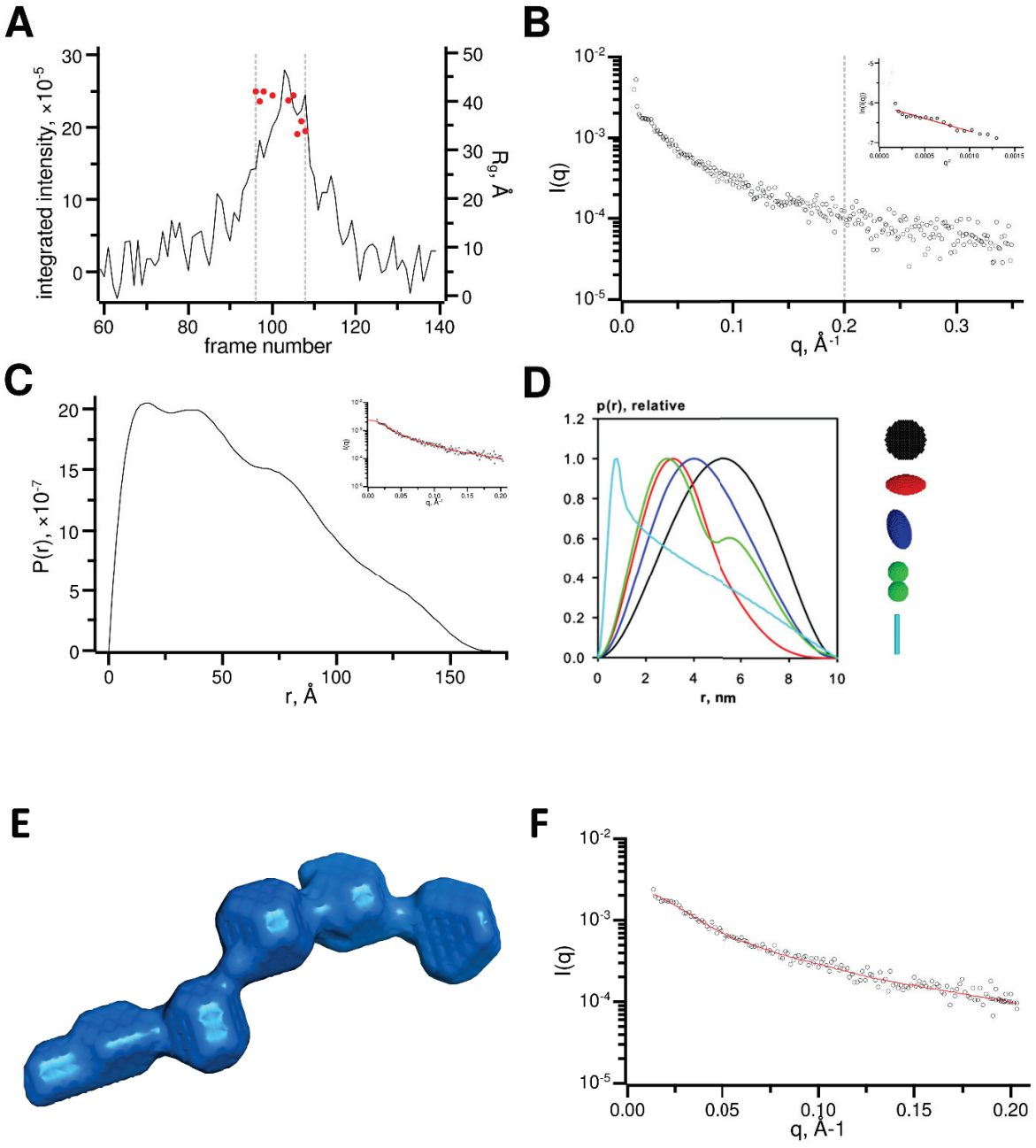
A
integrated intensity, ×10-5
Rg, Å
frame number
B
I(q)
q, Å-1
C
P(r), ×10-7
r, Å
D
p(r), relative
r, nm
E
F
I(q)
q, Å-1

Fig. 7

Figure 7. Study of p150L-His6 by SEC-SAXS.

(A) SEC-SAXS raw data. SAXS frame integrated intensity (buffer subtracted; baseline corrected) was plotted against frame number. Each frame was a 60-second exposure to X-rays performed during SEC elution at 0.05 ml/min. Red dots correspond to the calculated radius of gyration (R_g) for the corresponding frame. The area between the dotted grey lines was used for averaging and further data processing.

(B) Scattering curve corresponding to the averaged scattering from frames 96 to 108, as described in (A). Data beyond q of 0.2 $Å^{-1}$ (grey dotted line) was excluded from the rest of the analysis. The Guinier region is shown in the inset.

(C) The probability distribution function [P(r)] was determined using GNOM and manual adjustments to get the probability function to gradually reach zero at maximum dimension. Fit to experimental data is shown in the inset.

(D) P(r) functions for characteristic shapes (image taken from Mertens and Svergun (2010)).

(E) Dummy atom modeling**.** Surface representation of CAF-1 p150L as calculated by DAMMIF and further refined by DAMMIN.

(F) Fit of the dummy atom model to the experimental data.

A

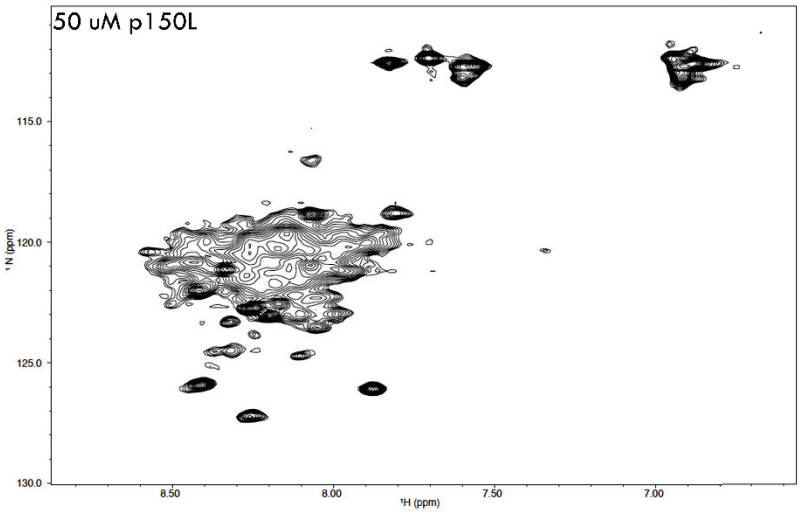
50 uM p150L
115.0
120.0
125.0
130.0
¹⁵N (ppm)
8.50
8.00
7.50
7.00
¹H (ppm)

B

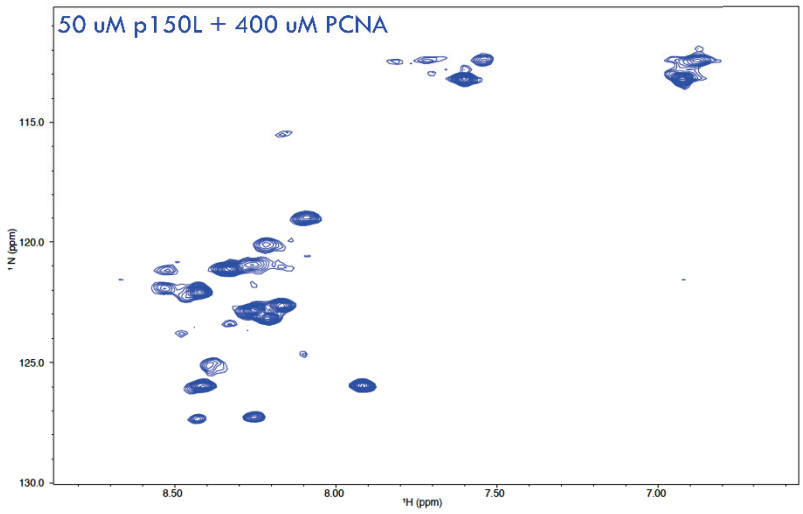
50 uM p150L + 400 uM PCNA
115.0
120.0
125.0
130.0
¹⁵N (ppm)
8.50
8.00
7.50
7.00
¹H (ppm)

C

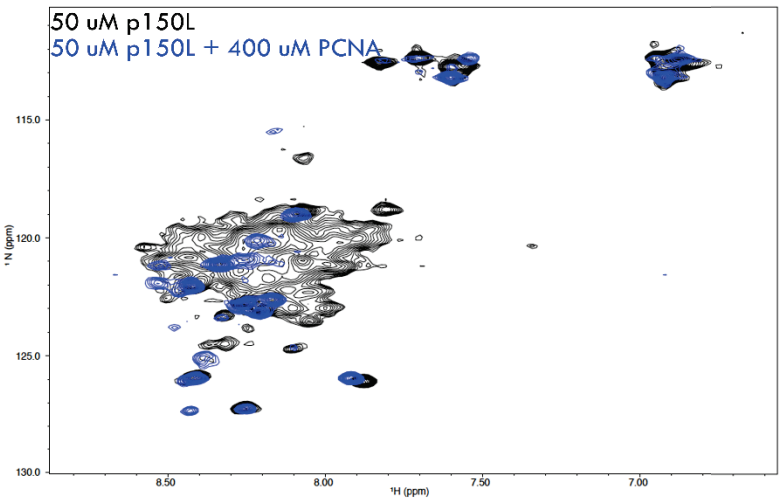
50 uM p150L
50 uM p150L + 400 uM PCNA
115.0
120.0
125.0
130.0
¹⁵N (ppm)
8.50
8.00
7.50
7.00
¹H (ppm)

Fig. 8

FIG. 8: Binding of [15N]-p150L-His6 to PCNA studied by nuclear magnetic resonance

(A) ^{1}H-^{15}N HSQC NMR spectrum of ^{15}N-labelled p150L-His6 shown in black. The signals are not properly dispersed, which is not characteristic of a properly folded globular protein with a single conformation.

(B) Upon addition of a molar excess of PCNA-His6 monomer (spectrum shown in blue, most of the p150L-His6 spectrum disappears, consistent with p150L-His6 binding to a large protein such as PCNA (90 kDa homo-trimer).

(C) Overlay of NMR spectra from ^{15}N-labelled p150L-His6 and a complex of p150L-His6 with PCNA-His6.

A

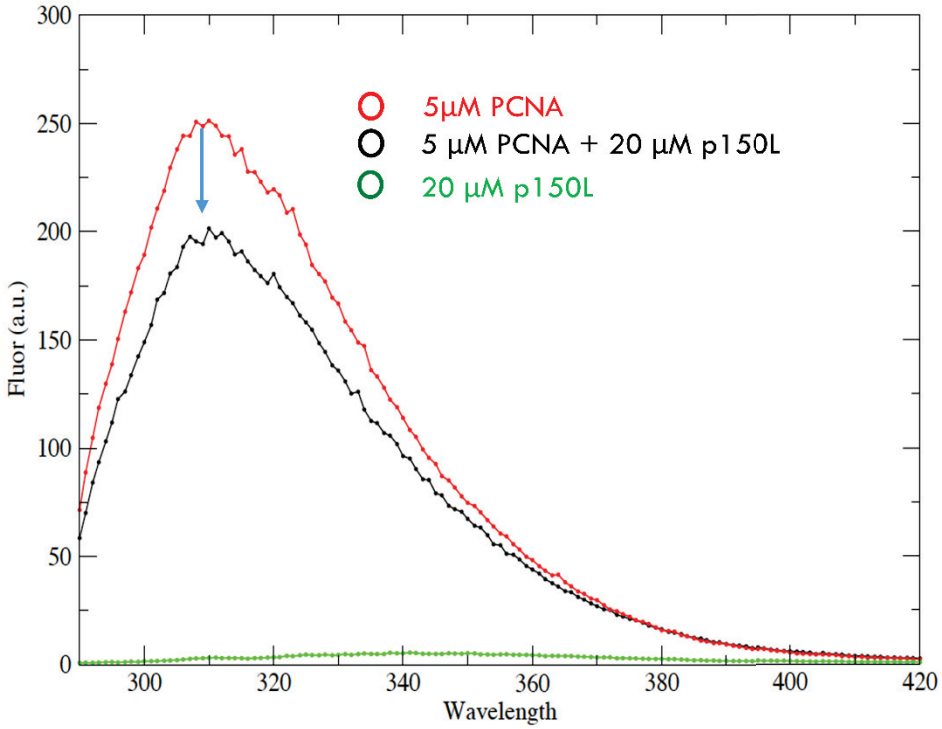

Excitation at 280 nm, showing emission spectra

B

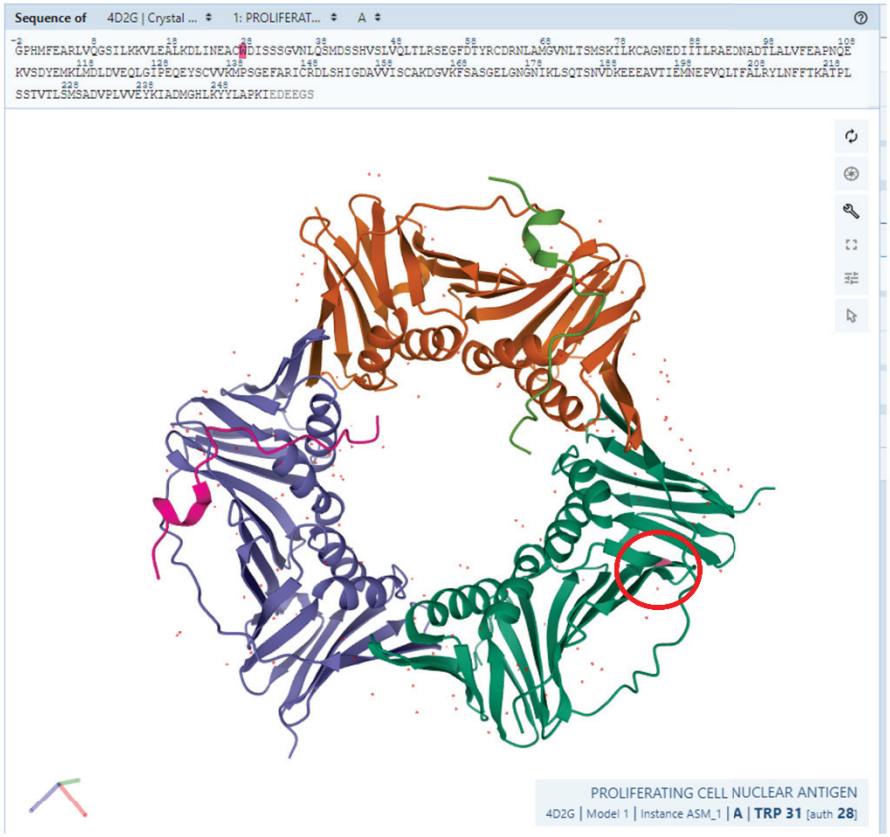

Fig. 9

FIG. 9: p150L-His6 binding to PCNA-His6 studied by fluorescence quenching

(A) Samples were excited at 280 nm and the emission spectra recorded between 295 nm and 420 nm were collected. The buffer used was 10 mM sodium phosphate, pH 7.2, 10 mM NaCl, 0.1 mM TCEP. The red curve shows the emission spectrum for 5 μM PCNA-His6 monomer on its own. The black curve shows the spectrum for a complex containing 5 μM PCNA-His6 monomer and 20 μM p150L-His6. The green curve shows the spectrum for 20 μM p150L-His6 on its own. Due to the absence of tryptophan, the emission spectrum for p150L-His6 is near the baseline.

(B) The figure shows the 3D structure of PCNA. The red circle denotes the location of Trp 28 whose position is quite close to the IDCL and underlying β-sheet, where the PIP was shown to bind in our crystal structure.

Tables

Table 1. Summary of crystallographic statistics

PCNA-p150(PIP2)	
Data Collection	
Space Group	C121
a, b, c (Å)	143.94, 83.24, 145.04
α, β, γ (°)	90.00, 107.32, 90.00
Resolution (Å)	46.2-2.4
Measured Reflections	248112
Unique Reflections	64159
Average Redundancy	3.9
Completeness (%)	100%
R_{merge} (Outer Shell)	0.073 (0.436)
Mean $I/\sigma_{(I)}$ (Outer Shell)	7.9 (2.8)
Refinement	
R_{work}	0.2318
R_{free}	0.3044
No. Reflections (R_{work})	63651
No. Reflections (R_{free})	3223
% R_{free}	5.06

Values in brackets correspond to outer shell, resolution 2.53-2.40 Å
σ(I) is the standard deviations (SD) of the measured intensity (I)
R_{free} is $\Sigma| 1-<I>I/\Sigma|$ where <I> is the mean intensity of all observations
R_{work} is $\Sigma| F_o-F_c I/\Sigma F_o$ for all data excluding data to calculate R_{free}
R_{free} is $\Sigma| F_o-F_c I/\Sigma F_o$ for all data excluded from refinement

Table 2. Thermodynamic parameters of PCNA binding to PIP[a]

Exptl buffer and peptide	Kd(μM)	N[b]	ΔG(kcal mol $^{-1}$)	ΔH(kcal mol $^{-1}$)	ΔS(cal K^{-1} mol $^{-1}$)
10 mM Na-phosphate (pH 7.0), 10 mM NaCl PCNA wild type + CAF-1 PIP wild type	24	0.83	-6.25	-1.868	14.8
PCNA wild type + CAF-1 PIP R426D	No binding				

a Determined by isothermal titration calorimetry at 296 K. All data are derived from Fig. 4C, and the binding curves were fit to one binding site per PCNA monomer, as observed in several crystal structures of PIPs bound to PCNA.
b Stoichiometry of peptide binding per PCNA monomer.

Supplementary figures

A

D. melanogaster CAF-1

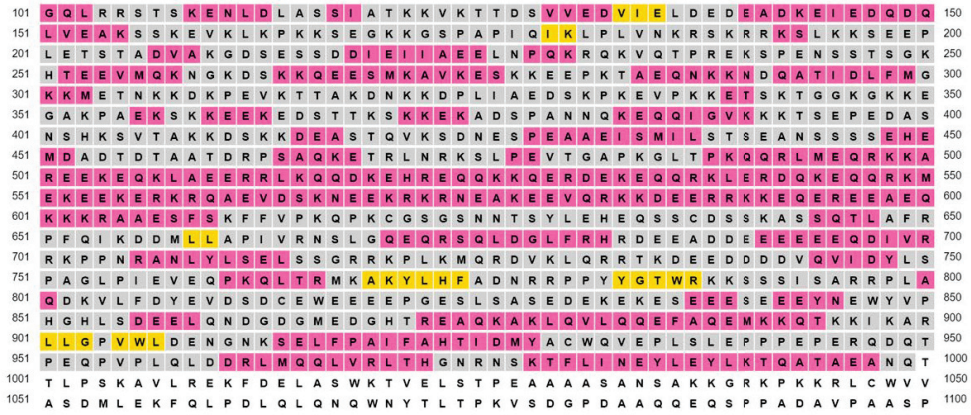

B

S. cerevisiae CAF-1

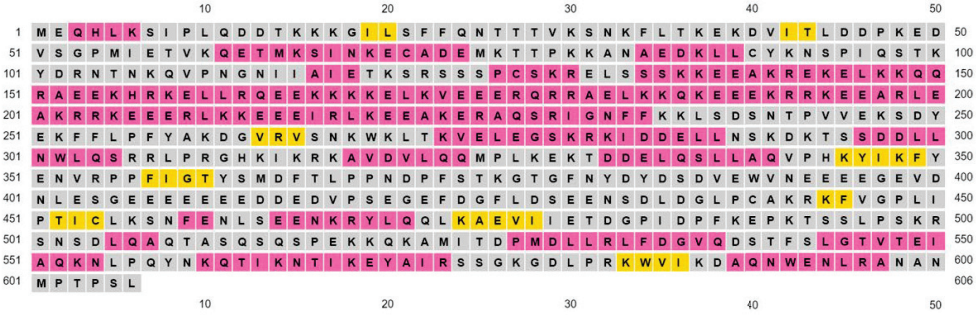

C

S. Pombe CAF-1

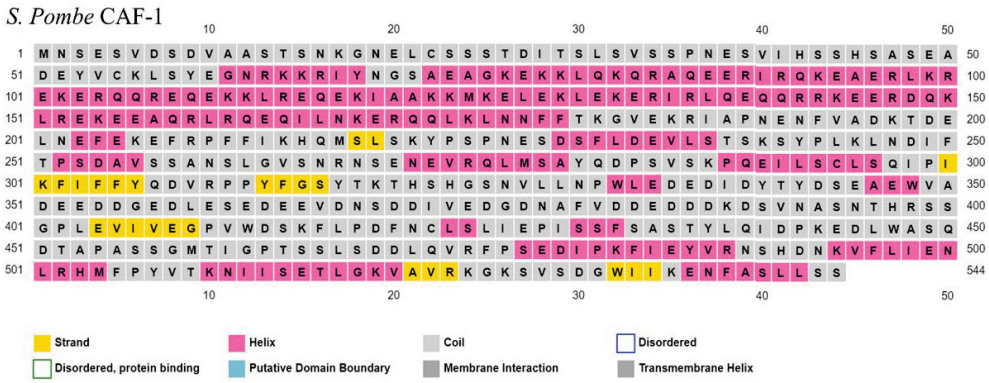

Suppl Fig. 1

Supplemental Fig 1A, 1B, 1C: Secondary structure prediction analyses of CAF-1 p150 homologues.

Even though *D. melanogaster, S. cerevisiae* and *S. pombe are* evolutionarily distant from humans, the large fragment encoding the KER domain of p150 homologues is predicted to form an unusually long α-helix (100-120 amino acids depending on species) that ends abruptly in the PIP residues. It is important to note that in both species of yeast, CAF-1 PIP sequences are canonical.

A *H. sapiens* p21

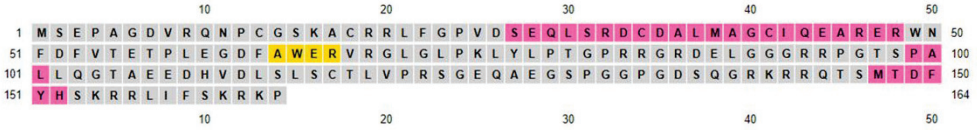

B *H. sapiens* FEN1

C *H. sapiens* DNMT1

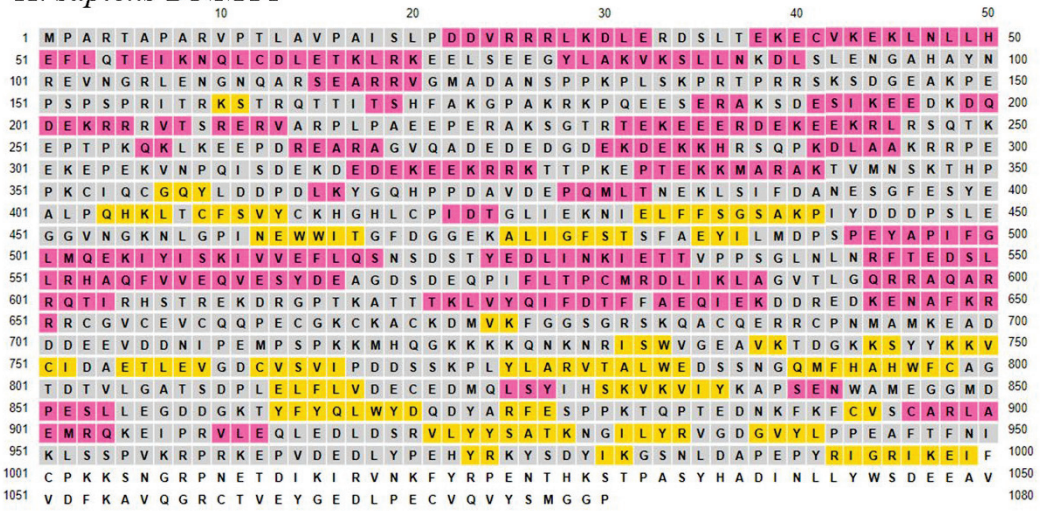

D *H. sapiens* Ligase1

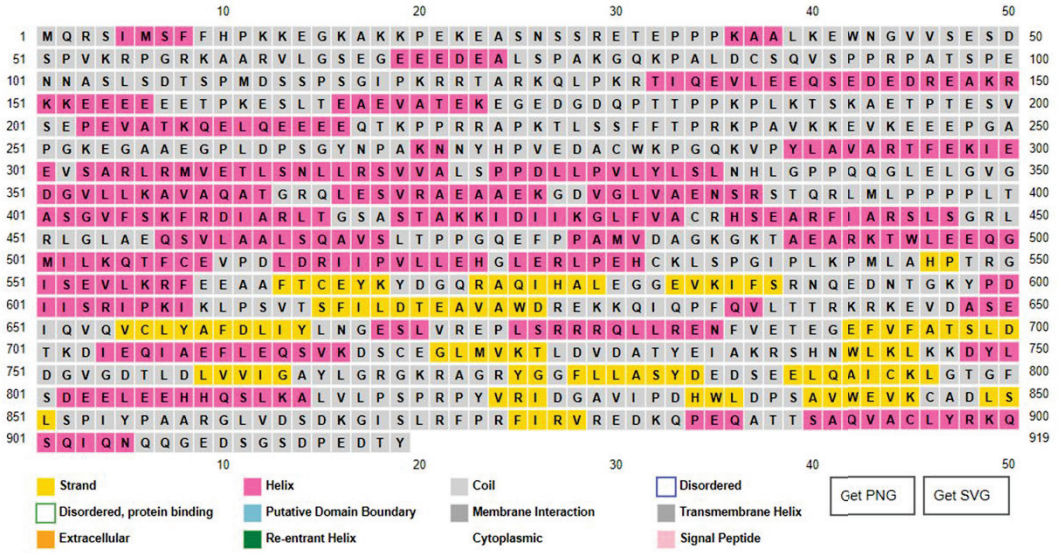

Suppl Fig. 2

Supplemental Fig 2A, 2B, 2C, 2D: Secondary structure prediction analyses of replication enzymes

Secondary structure prediction analyses of several DNA replication enzymes that contain canonical PIPs. None of the proteins (p21, FEN1, DNMT1 and DNA ligase I) are predicted to contain a long α-helix that ends with a PIP, unlike human CAF-1 p150 and its homologues.

A *H. sapiens* pol kappa

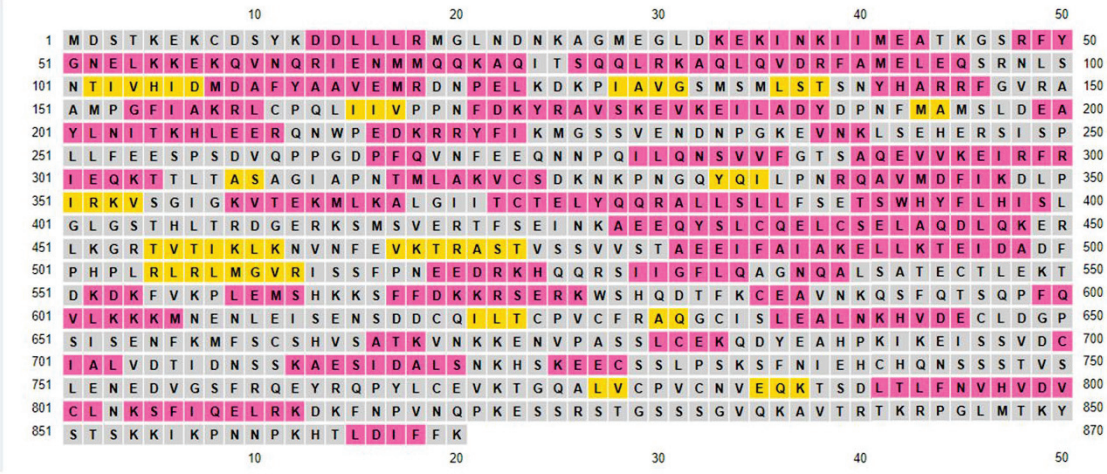

B *H. sapiens* pol iota

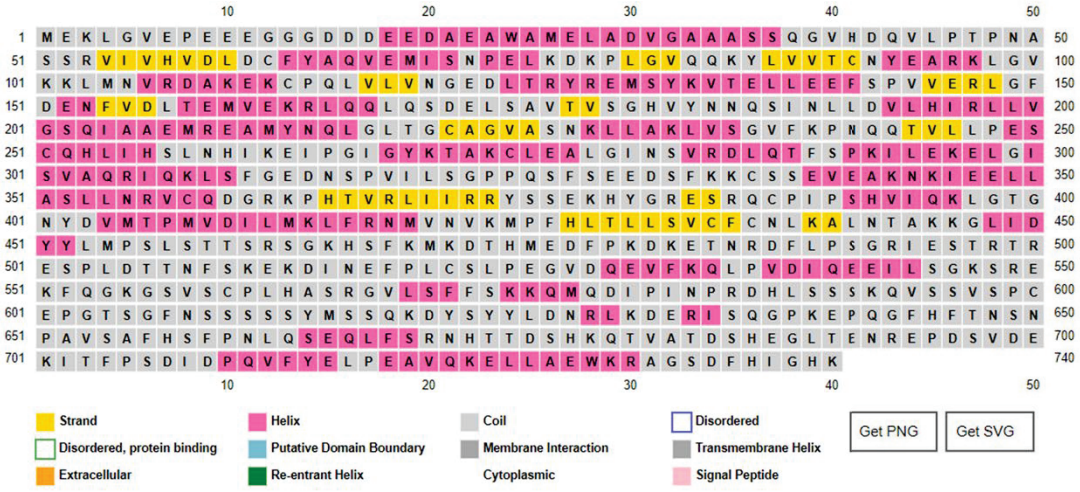

Suppl Fig. 3

Supplemental Fig 3A, 3B:

Secondary structure prediction analyses of non-canonical error prone polymerases Pol kappa and Pol iota. They are not predicted to contain a long α-helix that ends with a non-canonical PIP, unlike human CAF-1 p150 and its homologues.

Chapter 3

DNA Damage Response Kinase-Mediated Histone Gene Repression

Valérie Villeneuve [1,3,§], Amogh Gopinathan Nair [1,3,§], Roch Tremblay [4,5], Ugander Reddy Gajjalaiahvari [7], Marlène Gharib [1,3], Pierre Thibault [1,2], Marie-Hélène Miquel Kabbaj [7], Johanna Paik [7], Hugo Wurtele [4,6], Akash Gunjan [7,*],and Alain Verreault [1,3,*]

[1] Institute for Research in Immunology and Cancer (IRIC), Université de Montréal, Pavillon Marcelle Coutu, 2950 Chemin de Polytechnique, Montréal, H3T 1J4, Canada

[2] Département de Chimie, Université de Montréal

[3] Département de Pathologie et Biologie Cellulaire, Université de Montréal

[4] Centre de recherche de l'Hôpital Maisonneuve-Rosemont, 5415 boulevard de l'Assomption, Montréal, H1T 2M4, Canada

[5] Programme de Biologie Moléculaire, Université de Montréal, Montréal, Canada

[6] Département de Médecine, Université de Montréal, Montréal, Canada

[7] Department of Biomedical Sciences, College of Medicine, Florida State University, West Call Street, Tallahassee, FL 32306, USA

[§] These authors contributed equally to this work. * Corresponding authors:
E-mail: alain.verreault@umontreal.ca, E-mail: akash.gunjan@med.fsu.edu

This manuscript is "under preparation".

Contributions:

A.G.N, V.V, U.R.G, J.P performed experiments and analyzed data. Histone gene repression experiments with Hpc2 wildtype, FID mutants and qRT-PCR experiments were performed by A.G.N. Cycloheximide chase experiments were performed by V.V. Rad53 experiments by J.P and A.G, Mass spectrometry analyses were performed by M.G. A.V, A.G and H.W supervised studies. A.G.N incorporated the section containing histone gene repression experiments into the manuscript written by A.V.

Abstract

In eukaryotic cells, DNA damage during S-phase leads to a rapid decrease in the rates of DNA synthesis that is accompanied by a dramatic reduction in histone mRNA levels. This response helps balance the rates of histone and DNA synthesis, but the underlying molecular mechanisms are poorly understood. Here we show that the *S. cerevisiae* protein kinases involved in the DNA damage response (DDR), namely Rad53 and its upstream activators Mec1/Tel1, are necessary to trigger transcriptional repression of the four core histone genes when S-phase cells are treated with genotoxic agents that interfere with DNA replication. We demonstrate that DDR kinases repress histone gene transcription by extensively phosphorylating the Hpc2 subunit of the HIR complex. In addition, our results suggest that Hpc2 needs to bind histone H3 in order to repress histone gene transcription in G1 and when DNA replication is inhibited by hydroxyurea. Collectively, our results suggest that the repression of histone genes is mediated, at least in part, by a simple negative feedback triggered, at least in part, by binding of excess histones to the Hpc2 subunit of the HIR complex.

Introduction

The bulk of histone synthesis in proliferating cells is restricted to the S-phase of the cell cycle (Osley, 1991). During S-phase, newly synthesized histone H3/H4 form complexes with proteins, such as Asf1 and CAF-1, which promote their deposition behind replication forks almost as soon as enough DNA has emerged from the replisome (Sogo et al., 1986). Coordination of histone and DNA synthesis is important to allow both rapid nucleosome formation behind replication forks and concomitantly prevent the accumulation of excess histones. Because of their highly basic nature, excess histones bind non-specifically to chromatin, leading to mitotic chromosome segregation defects (Meeks-Wagner and Hartwell, 1986; Reis and Campbell, 2007) and sensitivity to a variety of DNA damaging agents (Gunjan and Verreault, 2003). In addition, inappropriate expression of histone mRNAs results in abnormal oogenesis and an early embryonic developmental arrest in *Drosophila* (Berloco et al., 2001; Sullivan et al., 2001). Consistent with this, specialized mechanisms exist to inhibit excessive translation of the large reservoir of histone RNAs present in unfertilized *Xenopus* oocytes (Sánchez and Marzluff, 2004).

Cells have evolved at least three partially redundant strategies to prevent the harmful effects of excess histones. First, yeast cells monitor the presence of excess histone proteins that are not incorporated into chromatin and trigger their degradation (Gunjan and Verreault, 2003; Kumar Singh et al., 2007). Second, conditions that interfere with replication (DNA lesions or shortage of dNTPs) elicit an evolutionarily conserved response that leads to the disappearance of histone mRNAs (Marzluff and Koreski, 2017; Reis and Campbell, 2007). Yeast and human cells have mechanisms that block histone gene

transcription in response to agents that impede replication (Kaygun and Marzluff, 2005; Osley and Lycan, 1987; Sherwood et al., 1993; Xu et al., 1992). In human cells, replication-dependent histone mRNAs end in a stem loop structure, and interference with DNA replication triggers their degradation (Kaygun and Marzluff, 2005). A dedicated exonuclease that recognizes the histone mRNA stem loop has been identified and is likely involved in histone RNA degradation *in vivo* (Dominski et al., 2003; Yang et al., 2006). In *Saccharomyces cerevisiae*, histone mRNAs are polyadenylated and although their stability increases during S-phase (Lycan et al., 1987), their half-life remains relatively short even during normal S-phase progression (Herrick et al., 1990). In spite of this, a post-transcriptional mechanism that senses the presence of excess histone RNAs and triggers their degradation exists in both budding and fission yeast (Campbell et al., 2002). In *S. cerevisiae*, chemicals that interfere with DNA replication also trigger a concerted transcriptional repression of the four gene pairs encoding core histones (Osley, 1991). Three of the four divergent histone gene promoters contain a repressive *cis*-acting element (*NEG*) that is required for histone gene repression outside of S-phase and in response to drugs that interfere with replication (Figure 1A). Four functionally related histone gene regulatory proteins (Hir1, Hir2, Hir3 and Hpc2) form the HIR protein complex that acts, together with the histone H3/H4 chaperone Asf1, to promote histone gene repression through the *NEG* element (Osley, 1991; Sutton et al., 2001). In addition, the four Hir proteins and Asf1 form a complex that mediates replication-independent deposition of histones H3/H4 onto DNA (Green et al., 2005; Prochasson et al., 2005; Tang et al., 2006). The role of Hir proteins in histone gene repression is conserved in fission yeast (Blackwell et al., 2004). Interestingly, a human homologue of *S. cerevisiae* Hir1 and Hir2, known as

HIRA, is also capable of triggering repression of replication-dependent histone genes when overexpressed (Nelson et al., 2002).

Many chemicals that damage DNA, including numerous drugs used in cancer chemotherapy, exert their cytotoxic effects by interfering with DNA replication. For instance, the presence of lesions that impede replication fork progression [*e.g.* those caused by the alkylating agent methyl methane sulfonate, MMS] (Segurado and Tercero, 2009; Tercero et al., 2003). elicits the multi-faceted and evolutionarily conserved intra S-phase DNA damage response [DDR] (Longhese et al., 2003). In *S. cerevisiae*, several features of this response rely on the activation of three protein kinases. In concert with a number of other checkpoint proteins (Longhese et al., 2003) the upstream kinases Mec1 and Tel1 phosphorylate and activate the fork head-associated (FHA) domain protein kinase Rad53 (Sanchez et al., 1996; Sweeney et al., 2005). Mec1 and Rad53 prevent the formation of abnormal DNA structures and irreversible damage to replication forks (Lopes et al., 2001; Sogo et al., 1986; Tercero and Diffley, 2001). In addition, Mec1 and Rad53 also block the firing of new replication origins (Santocanale and Diffley, 1998; Shirahige et al., 1998). Because cells normally deposit new histones very rapidly onto nascent DNA, sudden inhibition of new origin firing causes a decline in the global rate of DNA synthesis (Paulovich and Hartwell, 1995) that, in turn, leads to an accumulation of newly synthesized histones (Gunjan and Verreault, 2003).

A number of studies revealed that DNA damaging agents trigger changes in the abundance of a large number of RNAs (Aboussekhra et al., 1996; De Sanctis et al., 2001; Gasch et al., 2001; Jelinsky et al., 2000). In contrast, little attention has been paid to the

roles of DNA damage response kinases in DNA damage-dependent transcriptional repression. However, following DNA damage in G1, a role for Rad53 in the repression of cyclin genes has been uncovered (Sidorova and Breeden, 1997; Sidorova and Breeden, 2003). In some cases, the changes in gene expression that follow DNA damage are clearly not a mere consequence of the cell cycle delays imposed by checkpoint activation. For instance, *RNR* genes that encode subunits of ribonucleotide reductase, the enzyme that catalyzes the rate-limiting step in deoxyribonucleoside triphosphate (dNTP) synthesis, are induced following DNA damage (Huang et al., 1998). Induction of *RNR* genes in response to DNA damage likely serves as a source of additional dNTPs to promote DNA repair (Huang et al., 1998). Augmenting the abundance of ribonucleoside reductase and dNTP pools may be important even when the damage occurs during S-phase. This is likely the case for the specialized polymerases involved in DNA lesion bypass whose Kms for dNTPs is higher than those of replicative polymerases (Chabes et al., 2003).

In this study, we explored the role of DDR kinases in the repression of histone mRNAs caused by genotoxic agents that interfere with DNA replication. We demonstrate that Mec1 and Tel1, and the downstream kinase Rad53, are necessary for histone gene repression in response to DNA damaging agents that interfere with replication. The kinase activity of Rad53, Hpc2 protein stabilization and extensive phosphorylation of Hpc2 are all pre-requisite for histone gene repression in response to conditions that delay replication. In addition, we show that Hpc2 likely needs to bind histone H3 in order to repress histone gene transcription in G1 and when DNA replication is inhibited by hydroxyurea. Collectively, our results suggest

that the repression of histone genes relies upon a negative feedback triggered, at least in part, by binding of excess histones to the Hpc2 subunit of the HIR complex.

Experimental Procedures

Yeast methods

All the yeast strains used in this study are congenic to W303-1a and are listed in (Supplemental Table S3). Yeast cells were routinely grown at 30°C in either rich (YPD) or synthetic minimal medium lacking uracil to select for the pTS39b plasmid. For experiments involving the temperature-sensitive (ts) strain *cdc7-4*, cells were cultivated at 25°C and blocked at G1/S transition by switching the temperature to a restrictive temperature of 38°C. For experiments involving synchronized yeast cultures, cells were grown to a density of 1×10^7 cells/ml and α-factor was added at a concentration of 20 μg/ml for 2h or until the cells were arrested in the G1 phase of the cell cycle. The α-factor was removed by washing the cells with pre-warmed medium after which the cells were resuspended in pre-warmed medium to allow S-phase progression. Hydroxyurea (0.2M) or methyl methane sulfonate (0.1%) were added for 20 min following α-factor release, which corresponds to early S-phase as judged by FACS analysis. Cell aliquots (10ml) were harvested at 10-min intervals by the addition of sodium azide to 0.1% and centrifugation. The resulting cell pellets were frozen on dry ice and stored at -80°C for subsequent isolation of RNA. For experiments involving exponentially growing yeast cultures, cells were grown to a density of 1×10^7 cells/ml before treating them with or without HU for varying lengths of time, following which they were processed exactly as described above for synchronized cultures.

Generation of *HTA1-neomycin* and Hpc2 expression plasmids

In order to construct a plasmid containing the *HTA1* promoter driving the expression of the *neomycin* reporter gene with a *LEU2* selectable marker, we excised a *Bam*HI fragment from the pTS39b plasmid (Xu et al., 1992). The *Bam*HI fragment comprised the *HTA1* promoter, bacterial *neomycin* resistance gene from the coding region of transposon Tn5, and *CYC1* terminator. This fragment was cloned into the single *Bam*HI site of a centromeric plasmid, YCpIF1, which contains a *LEU2* marker (Foreman and Davis, 1994). Yeast strain W303 *MAT***a** *cdc7-4 hpc2*Δ*::KanMX* was transformed with this plasmid and, following selection on plates of synthetic complete (SC) medium lacking leucine, this resulted in yeast strain YAGN 20-1. This yeast strain was subsequently transformed with plasmids containing a *URA3* selectable marker and encoding the wild-type Hpc2-HA3 (YAGN 21-1), the Hpc2-HA3 FID-AAA mutant (YAGN 22-1) or a YCpIF4 empty vector (YAGN 23-1). Transformants were selected on plates containing SC medium lacking uracil and leucine.

Synchronization of *cdc7-4* mutant cells and exposure to HU

These strains were grown in selective medium for the two plasmids (SC - uracil - leucine) and arrested in G1 phase using 2 μg/ml α-factor added twice during the course of 90 minutes. G1 arrest was monitored by microscopy as the accumulation of non-budded shmoo-shaped cells and the depletion of small- and large-budded cells. The G1-arrested *cdc7-4* cells were then released towards S phase at 37°C (restrictive temperature for the *cdc7-4* mutation) for 60 minutes in medium containing 50μg/ml pronase to degrade α-factor. Microscopy was used to monitor budding as an indication that cells had been released from and reached the

cdc7-4 arrest point. Cells were then returned to the permissive temperature of 25°C for 60 minutes in medium containing 200 mM HU. Cells in G1 (α-factor), at the *cdc7-4* arrest point, and in HU were harvested and aliquots were processed to monitor DNA content by flow cytometry, immunoblotting to detect Hpc2-HA3, and qRT-PCR to determine the abundance of *ACT1* and histone mRNAs.

RNA isolation and northern blotting

Total yeast RNA was isolated from 10 ml of cells at a density of 1-2 × 10^7 cells/ml. RNA was extracted using the RNeasy Kit (Qiagen) according to the manufacturer's instructions. Total RNA (20μg/lane) was resolved in a 1% agarose–formaldehyde gel (Sambrook et al., 1989). The gel was transferred overnight onto a Hybond-XL nylon membrane (Amersham Pharmacia) by upward capillary transfer in 20×SSC (1×SSC is 0.15M NaCl, 15mM sodium citrate). RNA was fixed to the membrane by cross-linking with 0.12J of UV irradiation using a UV Crosslinker (UVP). Membranes were prehybridized for 1h at 68°C in ExpressHyb solution (Clontech). Hybridization was performed in the same buffer at 68°C for 1-2h with [γ-^{32}P] UTP labeled antisense RNA probes transcribed *in vitro* using the MAXIscript kit (Ambion) following the manufacturer's instructions. The DNA fragments used to generate the probes were derived from the 3'-untranslated region of histone genes to enable specific detection of transcripts derived from each gene. Subsequently, the membrane was washed three times with 2×SSC, 0.05% SDS at room temperature, followed by three washes in 0.1× SSC, 0.1% SDS at 50°C. Northern blots were quantitated on a phosphorimager (Molecular Dynamics).

Flow cytometry (FACS) analysis

Samples (1ml) of cultures at a density of 1-2 x 10^7 cells/ml were harvested by centrifugation and fixed for 1 h by resuspending the cells in 1ml of 70% ethanol. Samples were processed for FACS analysis by washing once with 1ml of 50mM Tris-HCl pH 7.8. The cells were resuspended in 500µl of the same buffer containing 10µl of 10mg/ml ribonuclease A and incubated for 5-6 hrs at 37°C. The cells were pelleted and resuspended in 500µl FACS buffer (200mM Tris-HCl pH7.5, 200mM NaCl, 78mM $MgCl_2$) containing 15µl 2mg/ml propidium iodide or Sytox Green. Cell aliquots (100µl) were diluted in 1ml of 50mM Tris-HCl pH7.8, sonicated and analyzed by flow cytometry (FACScan, Becton-Dickinson or BD Biosciences FACS Canto II flow cytometer).

Immunoprecipitation

For immunoprecipitation of tagged proteins, cells were harvested from 1 liter cultures at ~2x10^7 cells/ml. Whole-cell extracts (WCEs) were prepared by grinding cells in liquid nitrogen in a SPEX CertiPrep 6850 Freezer Mill in 20ml lysis buffer containing protease and phosphatase inhibitors (20mM Hepes-KOH pH 7.5, 110Mm potassium acetate, 10% glycerol, 0.1% Tween-20, 1mM sodium vanadate, 50mM sodium fluoride, 50mM sodium β-glycerophosphate, 10mM sodium butyrate, 10mM 2-mercaptoethanol, 1X Roche protease inhibitor cocktail, 5µM MG-132). Extracts from equal amounts of cells were incubated overnight at 4°C with Flag M2 (Sigma), 9E10 or IgG Sepharose (Amersham Biosciences) beads to immunoprecipitate Flag, Myc and TAP-tagged proteins, respectively. The immunoprecipitated material was resolved on 4-12% Bis-Tris Criterion™ XT Pre-cast

polyacrylamide gels run in XT MES buffer (Bio-Rad) and probed for the presence of Flag, Myc or TAP tagged proteins by immunoblotting.

Immunoblotting

For detection of Rad53 or Hpc2 by immunoblotting, $1.5x10^7$ to $3.0x10^7$ cells were harvested and frozen immediately in liquid nitrogen. Whole-cell extracts were prepared using an alkaline method (Kushnirov, 2000). The extracts were analyzed in SDS-7.8% or 10% polyacrylamide gels optimized for the separation of phosphorylated Rad53 or Hpc2, respectively. Rad53 polyclonal antibodies were a generous gift from Dr. John Diffley (Cancer Research UK) and were used at a 1:2000 dilution. Immunoblotting for the detection of immunoprecipitated Flag, HA, Myc or TAP tagged proteins was carried out using Flag M2 (Sigma), HA 12CA5 (Sigma), 4A6 Myc antibodies (Upstate) and peroxidase anti-peroxidase (PAP) complex (Sigma) respectively at 1:2000 dilution. H3-C antibodies (Gunjan and Verreault, 2003) were used at 0.3 μg/ml for the detection of H3 by immunoblotting.

Quantitative reverse transcriptase PCR (qRT-PCR)

Total RNA was extracted and histone and actin (*ACT1*) mRNA abundance were determined by quantitative reverse transcriptase PCR (qRT-PCR). First strand cDNA synthesis was performed using the M-MLV RT kit (Thermo) according to the manufacturer's instructions. RT-qPCR reactions were performed using SYBR Green qPCR Master Mix on a QuantStudio 7 Flex Real-Time PCR system using gene-specific primers (Supplementary Table 3). For each cDNA sample, PCR reactions were carried out in triplicates. Histone mRNA

levels were normalized to those of *ACT1*. Histone mRNA abundance in each sample were expressed relative to the levels observed in *hpc2*Δ G1 cells, which were arbitrarily set to one.

Purification of His-tagged Rad53 and *in vitro* kinase assays with Rad53 and Hpc2

A pET28a^{+} plasmid containing a full length *RAD53-HIS6* gene was expressed and purified from *Escherichia coli* ArticExpress BL21 bacteria. Hpc2 protein was expressed in a shorter form in *Escherichia coli* starting to amino acids 32 to 352 (pET28a^{+} *HPC2-HIS6*). Purification was performed using High-performance liquid chromatography (HPLC) and purified proteins were dialyzed into kinase buffer (25mM HEPES-NaOH pH 7.5, 10Mm MgCl2,10mM MnCl2, 1 mM DTT). 100 μM of cold ATP were used for mass spectrometry detection of Hpc2 phosphorylation sites in the kinase buffer or 10 mM of cold ATP plus 0.1μCi of [γ^{32}P]-ATP were used for hot *in vitro* kinase assays. The radioactive acrylamide gel was dried and assessed by autoradiography. To examine phosphorylation sites, present on Hpc2, Hpc2 band on a 10% acrylamide gel were excised and/or directly trypsin digested and analyzed by LC-MS/MS using the LTQ-Orbitrap XL mass spectrometer.

In-gel trypsin digestion

Coomassie Blue stained protein bands were excised from the gel and incubated by shaking in a 50% acetonitrile (ACN) destaining solution. Proteins were then reduced with dithiothreitol (DTT) and alkylated with iodoacetamide prior to in-gel digestion with 200ng of trypsin for 4h at 37^{o}C. The resulting peptides were extracted from the gel using a solution containing 5% trifluoroacetic acid (TFA) and 50% ACN, dried in a Speed-Vac and redissolved in 0.2% formic acid (FA) for nano-LC-MS/MS analysis.

LC-MS/MS

All MS analyses were conducted using an LTQ-Orbitrap XL hybrid mass spectrometer equipped with a nano electrospray ion source (Thermo Fisher Scientific, San Jose, CA) and coupled to a nano-flow LC system (Eksigent, Dublin, Ireland) and a Finnigan AS autosampler (Thermo Fisher Scientific). The chromatographic separation was performed using a trapping column (4mm length, 360µm i.d.) and an analytical column (10cm length, 150µm i.d.) packed in house with 3µm C18 particles (Jupiter 300Å, Phenomenex, Torrance, CA). Peptides were eluted using a linear gradient of 5-40% ACN containing 0.2% FA for 53 min, followed by a rapid increase to 60% ACN in 3 min. The flow rate was set to 0.6µL/min. Peptides were analyzed in data-dependent mode. For each high-resolution MS scan, the three most abundant ions with intensity above 10,000 counts were selected for MS2 sequencing by the LTQ-Orbitrap XL (60,000 full-width half-maximal resolution; acquisition range of 400-1600 *m/z*). Product ions corresponding to the loss of a phosphate group (*i.e.* a neutral loss of 98 Da) from the precursor peptide were subsequently selected for MS3 fragmentation. For all nano-LC-MS experiments, an internal mass lock (protonated (Si(CH3)2O))6 with *m/z* 445.120025) or an external calibration mixture (Caffeine, MRFA and Ultramark) were used for mass calibration and provided mass accuracy within 5ppm. MS data were analyzed using the Xcalibur software (version 2.0 SR1). Peak lists were then generated using the Mascot distiller software (version 2.1.1, Matrix Science) where MS processing was performed using the LCQ plus zoom script. Searches of the NCBInr database containing 3,310,354 entries (NCBInr March 3, 2006) were conducted using the Mascot search engine (version 2.1, Matrix Science, London, U.K.). The database searches were narrowed to yeast and allowed up to 2 missed cleavage sites for

trypsin. The mass tolerance threshold for experimental MS precursor ions and MS2 fragment ions was set to ±0.02 and ±0.5 Da, respectively. All searches were conducted to allow the following variable modifications: +80 for phosphorylation (Ser, Thr or Tyr), +16 oxidation (Met), +1 for deamidation (Asn and Gln), and + 57 for carbamidomethylation (Cys). Finally, all MS2 and MS3 spectra ascribed to phosphopeptides by the computer search algorithm were manually verified and validated.

Multiple reaction monitoring (MRM)

The Multiple Reaction Monitoring (MRM) assay for Hpc2 tryptic peptides was performed on a 4000 Q-Trap mass spectrometer (AB/MSD Analytical Technologies, Thornhill, ON, Canada), equipped with a Nanospray II interface. The chromatographic separation was performed using a trapping column (4 mm length, 360 µm i.d.) and an analytical column (10 cm length, 150 µm i.d.) packed in-house with 3-µm C18 particles (Jupiter 300Å, Phenomenex, Torrance, CA). The flow rate was set to 0.6µL/min and peptides were eluted using a linear gradient from 5-40% ACN containing 0.2% FA for 53 min, followed by a rapid increase to 80% for 3 min. The 784.90 →735.90 MRM transition was monitored with a 25 ms dwell-time to detect the phosphorylated 328SSSASAILPKPTTTK342 Hpc2 peptide in asynchronous, MMS and MMS + caffeine treated cells. The sequence of the peptide and the site of phosphorylation were confirmed by MRM by triggering an enhance product ion (EPI) scan in data-dependent mode

Results

Cell cycle regulation of histone mRNAs is not affected in *rad53* mutants

We previously showed that Rad53 is involved in degradation of excess histones that are not packaged into chromatin (Gunjan and Verreault, 2003; Singh et al., 2010; Singh et al., 2009c). This housekeeping function of Rad53 promotes normal cell cycle progression and the fidelity of mitotic chromosome segregation (Liang et al., 2012; Singh et al., 2010). Yeast cells lacking Rad53 accumulate abnormally high amounts of newly synthesized histones bound to three distinct chaperones: Asf1, CAF-1 and Hir proteins (Emili et al., 2001; Gunjan and Verreault, 2003). In wild-type cells, it has been reported that histone gene transcription depends on the oscillation of cell cycle stages (Hereford et al., 1982). It was formally possible that part of the accumulation of newly synthesized histones in *rad53* mutant cells that we previously reported (Gunjan and Verreault, 2003) arose as a result of a defect in cell cycle regulation of histone gene transcription. In order to address the contribution of Rad53 to cell cycle regulation of histone mRNAs, we synchronized wild-type and *rad53*Δ *sml1-1* mutant cells (hereafter simply referred to as *rad53* mutants) in G1 phase of the cell cycle using α-factor. The cells were released into S-phase in rich medium at 30°C and 10-min time points were collected to analyze histone mRNA expression using northern blots. FACS analysis in both wild-type and *rad53* mutant cells revealed that S-phase was completed about 30 min after release from α-factor (data not shown). The kinetics of histone mRNA accumulation and disappearance during normal passage through S-phase were very similar in wild-type and *rad53* mutant cells (Figure 1B). However, we consistently observed a delay in histone mRNA disappearance at the end of S-phase in *rad53* mutant cells (Figure 1B, 50 min), which may reflect the slightly longer duration of S-phase that has been reported in *rad53* mutants (Cha

and Kleckner, 2002). This delay was not merely a reflection of slower replication due to limiting dNTP pools because it was observed in *rad53* Δ *sml1-1* cells, which carry a null mutation of the Rnr inhibitor Sml1. In spite of this, histone mRNAs returned to very low levels in G2/M cells (Figure 1B). Thus, *rad53* mutant cells were not defective in the cell cycle-regulated expression of histone RNAs.

The kinase activity of Rad53 is required for histone gene repression triggered by genotoxic agents that impede replication

Drugs that interfere with replication such as MMS and HU result in an accumulation of newly synthesized histones that is more pronounced in *rad53* mutants than in wild-type cells (Gunjan and Verreault, 2003; Singh et al., 2009a). The fact that inhibitors of DNA replication trigger the disappearance of histone mRNAs in both yeast and higher eukaryotes (Marzluff et al., 2008; Osley, 1991), prompted us to determine the role of Rad53 in this response. In order to address whether histone transcripts were downregulated by agents that impede replication, cells were synchronized in G1 with α-factor and released for 20 minutes to allow the cells to reach the beginning of S-phase before adding HU or MMS. In wild-type cells, the abundance of histone *HHT1* or *HHF1* mRNAs declined within 10 minutes following the addition of HU (Figure 2A, 2B). Consistent with its ability to inhibit ribonucleotide reductase and dNTP production, HU slowed down replication in both wild-type and *rad53* cells (Figure 2B, 20-min time points onwards). However, unlike wild-type cells, *rad53* Δ *sml1-1* mutants were deficient in downregulating histone mRNAs in response to HU (Figure 2A). This defect was not due the *sml1-1* mutation because *sml1-1* mutant cells were capable of triggering disappearance of histone mRNAs in response to HU or MMS (data not shown). In addition, *rad53K227A*

mutant cells, which carry a hypomorphic point mutation in the kinase domain of Rad53 and a wild-type *SML1* gene (Pellicioli et al., 1999), were defective in down-regulating histone mRNAs in response to HU (Figure 2A center panel). Thus, the kinase activity of Rad53 was necessary to decrease the abundance of histone RNAs when dNTP depletion induced by HU slowed down replication.

The disappearance of histone mRNAs also occurred when wild-type cells were treated with the alkylating agent MMS at the beginning of S-phase and the kinase activity of Rad53 was required for this response (Figure 2C). The DDR kinases Mec1 and Rad53 are both required to block the firing of late origins in response to MMS (Santocanale and Diffley, 1998; Shirahige et al., 1998; Zegerman and Diffley, 2010). However, we used a dose of MMS (0.1%) that causes a large number of DNA lesions that physically hinder replication fork elongation irrespective of the presence or absence of Rad53 and Mec1 (Tercero et al., 2003). Thus, the failure to repress histone mRNAs in *rad53* mutants treated with MMS was not merely due to defective control of origin firing that would lead to elevated rates of DNA synthesis despite the presence of DNA damage.

We found that the three histone gene pairs repressed by Hir proteins through the *NEG* promoter element (*HHT1-HHF1*, *HHT2-HHF2* and *HTA1-HTB1*) were repressed in a Rad53-dependent manner in response to genotoxic agents that interfere with DNA replication (Figure 2A, C and data not shown). In contrast to these loci, the *HTA2-HTB2* gene pair lacks the *NEG* promoter element (Figure 1A). This is interesting because, unlike the three other histone gene pairs, the repression of *HTA2-HTB2* in response to HU is not impaired by mutations in Hir

proteins (Osley and Lycan, 1987; Xu et al., 1992) or Asf1 (Sutton et al., 2001), a histone chaperone that binds to Rad53 (Agez et al., 2007; Jiao et al., 2012). We therefore investigated whether expression of mRNAs derived from the *HTA2-HTB2* locus was also repressed by Rad53. As observed for RNAs derived from the other three histone gene pairs, we found that the kinase activity of Rad53 was required for downregulation of *HTB2* mRNAs triggered by MMS-induced DNA damage (Figure 2D). This result does not rule out the possibility that Hir proteins may be targets of Rad53 to repress the three other histone gene loci (see below). However, it does suggest the existence of at least one other target whose phosphorylation by Rad53 is involved in repression of *HTA2-HTB2*.

Rad53 triggers histone gene promoter repression in response to replication stress

S. cerevisiae cells have a post-transcriptional mechanism that enhances the stability of histone mRNAs during S-phase to meet the demand for rapid nucleosome assembly behind replication forks (Lycan et al., 1987; Pietrobon et al., 2014; Xu et al., 1990). However, despite the existence of this mechanism, histone RNAs have a relatively short half-life (<5 min) during S-phase (Herrick et al., 1990). In principle, Rad53 could act both by causing destabilization of histone RNAs and triggering histone gene repression. However, it seemed unlikely that the pronounced reduction of histone RNAs triggered by agents that interfere with replication could occur without promoter repression. We therefore sought to determine whether Rad53 contributes to repress histone gene promoters using a construct in which a reporter gene that confers resistance to neomycin was under the control of the *HTA1* promoter (Xu et al., 1992). Unlike natural histone RNAs, mRNAs derived from this reporter gene lack the 3'-untranslated region necessary for post-transcriptional stabilization during S-phase

(Campbell et al., 2002; Xu et al., 1990; Xu et al., 1992). Wild-type and *rad53* null mutant cells carrying the *HTA1-neo* reporter gene were released from G1 arrest and genotoxic agents HU or MMS were added at the beginning of S-phase (20-min time points in Figure 2E). In wild-type cells, the abundance of neomycin transcripts decreased upon addition of either HU or MMS (Figure 2E). In striking contrast, the neomycin transcripts kept accumulating when *rad53* mutant cells were treated with HU or MMS at the beginning of S-phase (Figure 2E). This result demonstrates that Rad53 triggers histone gene promoter repression in response to genotoxic agents that interfere with replication.

Repression of histone mRNAs requires continuous Mec1/Tel1 activity

Passage through S-phase in the absence of histone gene transcription results in cell lethality (Kim et al., 1988a). Therefore, the potential of Rad53 to repress histone gene transcription needs to be carefully controlled to avoid inappropriate repression of histone genes during normal replication. For this reason, we explored the roles of the upstream DDR kinases Mec1/Tel1 in the repression of histone gene expression induced by DNA damage. In response to DNA damage during S-phase, Rad53 is directly phosphorylated in a Mec1/Tel1-dependent manner, which leads to a substantial increase in the kinase activity of Rad53 and its auto-phosphorylation (Gilbert et al., 2001; Sweeney et al., 2005). Although the repression of histone gene promoters following HU treatment was unaffected in either *mec1*Δ or *tel1*Δ single mutants, a *mec1*Δ *tel1*Δ double mutant strain was defective in this response (Figure 3A). We further confirmed this result by treating wild-type cells with caffeine, an inhibitor of PI3-kinases such as Mec1 and Tel1 (Vaze et al., 2002). In wild-type cells, caffeine inhibited the repression of histone gene promoters triggered by HU (Figure 3B). Further, repression of

histone genes in HU requires continuous kinase activity of Mec1/Tel1 because addition of caffeine in the presence of HU resulted in re-activation of histone genes in the absence of normal replication (Figure 3C). This effect of caffeine was associated with rapid dephosphorylation of Rad53 (Figure 3C). This is likely due to the action of phosphatases that dephosphorylate Rad53 during checkpoint recovery (Leroy et al., 2003; O'Neill et al., 2007; Travesa et al., 2008). We also found that, when Rad53 was dephosphorylated and DNA synthesis resumed following removal of HU, histone genes were re-activated (Figure 3D). This is likely important to prevent runaway replication in the absence of histone synthesis. These results clearly demonstrate that the Rad53-dependent repression of histone genes upon replication stress requires activation of the DDR kinases Mec1/Tel1. This ensures that inappropriate Rad53-dependent repression of histone genes does not occur during a normal S-phase.

DDR kinases phosphorylate Hpc2 to repress histone gene transcription.

Based on published data, Hpc2 is phosphorylated in a Rad53 and Mec1/Tel1-dependent manner (Albuquerque et al., 2008; Chen et al., 2007). However, the physiological significance of this phosphorylation is not clear. We hypothesized that DDR kinases might phosphorylate Hpc2 to promote histone gene repression in response to DNA damage that slows down replication. A number of Hpc2 residues are phosphorylated in a Mec1/Tel1 and Rad53-dependent manner *in vivo* (Supplementary Table S1, Figure 4B-D). In contrast, despite the fact that Hir1, Hir2 and Hir3 are much larger than Hpc2, only a few phosphorylation sites have been identified in these proteins. This suggests that phosphorylation of Hpc2 is key to regulation of the HIR complex. None of the Hpc2 sites correspond to the consensus motif for

phosphorylation by Mec1/Tel1 (SQ or TQ dipeptides). In order to address whether Rad53 could directly phosphorylate Hpc2, we purified recombinant Rad53 and a fragment of Hpc2 that was soluble and readily isolated from *Escherichia coli*. When expressed alone in *Escherichia coli*, Rad53 undergoes auto-phosphorylation (Gilbert et al., 2001; Sweeney et al., 2005). When Hpc2 was absent or present at low concentration, Rad53 underwent auto-phosphorylation that led to the appearance of a slow migrating form of [^{32}P]-labeled Rad53 (Figure 4A, lanes 1 and 6). Increasing concentrations of Hpc2 resulted in faster migration of [^{32}P]-labeled Rad53 and robust incorporation of [^{32}P] into Hpc2 (Figure 4A, lanes 3-6), suggesting that Hpc2 phosphorylation competes with auto-phosphorylation of Rad53. In order to identify Hpc2 residues that were directly phosphorylated by Rad53 *in vitro*, we performed assays with non-radioactive ATP and the reaction products were analyzed by mass spectrometry. *In vitro*, Rad53 phosphorylated several Hpc2 residues, including serine 332 (Supplementary Table S1, Supplementary Figure S2) that were identified as DDR kinase-dependent phosphorylation sites *in vivo* (Albuquerque et al., 2008; Smolka et al., 2007). Using multiple reaction monitoring (MRM), we were able to demonstrate that MMS triggered phosphorylation of Hpc2-S332 (Figure 4B-C). This phosphorylation was dependent upon DDR kinases because, even in the continuous presence of MMS, addition of caffeine led to a loss of phosphorylation (Figure 4B-C).

We mutated several Hpc2 phosphorylation sites (Supplementary Table S2) and monitored the abundance of mutant proteins to ensure that their expression was not reduced by the mutations (Figure 5A). To identify residues that were important for histone gene repression, we screened *Hpc2* mutants for defects in HU-induced histone RNA

downregulation. In WT cells, histone mRNA levels increase 20-25-fold in S-phase, but they are strongly reduced following HU treatment (Figure 5B and C). Consistent with previous reports (Amin et al., 2012; Osley, 1991; Vishnoi et al., 2011; Xu et al., 1992), compared with WT cells, *hpc2* mutants contain elevated levels histone RNAs in G1. In spite of this histone RNAs still increased when *hpc2Δ* mutants progressed from G1 into S-phase. However, in striking contrast to WT cells, the abundance of histone RNAs did not decrease when *hpc2Δ* cells were treated with HU (Figure 5B and C). Most of the Hpc2 phosphorylation site mutants analyzed displayed histone transcript downregulation comparable to that observed in WT cells treated with HU (Supplementary Table S2). However, a triple mutant Hpc2 S330,331,332A as well as a quadruple mutant Hpc2 S305A,S307A,S308A,T310V (Val is more closely related to a non-phosphorylated Thr than Ala) showed a strong defect in histone transcript downregulation in response to HU (Figure 5B and C, compare 25' and HU columns for WT cells and cells expressing *Hpc2* mutants). This suggests that Hpc2 residues important for histone gene repression reside in at least two closely spaced clusters. As observed in other proteins (Holt et al., 2009), these multiple serine and threonine residues may form a single acidic surface when phosphorylated. Mutations of individual phosphorylatable residues did not impair HU-induced histone gene repression (Supplementary Table S2), suggesting redundancy among phosphorylation sites. Unlike *hpc2*Δ cells, our two *Hpc2* mutants were significantly, but not completely defective in downregulating histone transcripts. This suggests that additional phosphorylation sites on Hpc2 may also contribute in bringing about histone gene repression in response to HU.

Hpc2 stability is cell cycle and DNA damage regulated.

HIR complex-mediated histone gene repression must be overcome during progression from G1 into S-phase to allow rapid histone synthesis. The molecular switch that inactivates the HIR complex during the G1-S transition is likely critical for cell viability. Without HIR complex inactivation, cells might not be able to express histone genes at sufficiently high levels to support replication-coupled nucleosome assembly. The molecular basis of HIR complex inactivation during the G1-S transition is unknown. In addition, repression must be restored in response to genotoxic agents that interfere with DNA replication. Among the four Hir proteins, Hpc2 was by far the most highly phosphorylated *in vivo*. We therefore focused our attention on Hpc2. For cell synchronization at the onset of S-phase, we used two strains carrying thermosensitive mutant alleles*, cdc7-1 and cdc7-4*. Cdc7 is a protein kinase that is essential for DNA replication origin firing (Bousset and Diffley, 1998). We arrested cells in G1 using α-factor at 25°C, the permissive temperature for the *cdc7-4* mutation. Cells were then released towards the *cdc7* arrest point in pre-warmed medium (38°C) lacking α-factor. As expected, Hpc2 was present when histone genes were repressed in G1 (Figure 6A). However, during the transition from G1 to the *cdc7* arrest point, Hpc2 was degraded (Figure 6A). This is consistent with an earlier report showing that histone gene transcription is activated between G1 and the *cdc7* arrest point (Hereford et al., 1982). We investigated Hpc2 turnover at the cdc7 arrest point. Upon addition of cycloheximide at the cdc7 arrest point, the abundance of Hpc2-FLAG3 decreased approximately 2-fold within 2min (Figure 6A lanes 3-4), residual but readily detectable Hpc2-FLAG3 decayed very slowly from 2 - 10min (Figure 6A lanes 3-7). From 10 - 90min following cycloheximide addition, Hpc2-FLAG3 was barely detectable and eventually was below the threshold for detection (Figure 6A, lanes 7-14). We

further examined the regulation of Hpc2 during the transition from G1 to the cdc7 arrest point in the presence of proteasome inhibitor (MG132) and cycloheximide. In order to enhance the intracellular concentration of MG132 and its efficacy, we deleted the *PDR5* gene encoding a multidrug efflux pump. When G1-arrested cells were shifted to 38°C to inactivate Cdc7 and released towards S-phase at 38°C in the presence of cycloheximide from 30min onwards (to avoid arresting cells during the G1/S transition), Hpc2-TAP was below the threshold for detection (Figure 6B, lanes with cycloheximide but with MG132). In contrast, when MG132 was added at the same time points as cycloheximide a band with an electrophoretic mobility similar to that of Hpc2-TAP (as shown in G1-arrested cells, lane 1) was observed. This indicates that Hpc2-TAP is continuously degraded as cells remain at the cdc7 arrest point for up to 90min. This degradation is sensitive to the proteasome inhibitor MG132. Please note that this result does not rule out the possibility that Hpc2 may be continuously synthesized and degraded at the cdc7 arrest point. The results shown in Figure 6B suggest that, at the cdc7 arrest point, Hpc2 is present but continuously degraded by the proteasome to prevent it from triggering histone gene arrest point. Because we used cycloheximide in Figure 6B, we could not assess whether new Hpc2 molecules were continuously synthesized and degraded. In order to address whether new Hpc2 were synthesized during a normal S-phase, we synchronized cells in G1, inactivated Cdc7 at 38°C and released them to the arrest point at 38°C. After decreasing the temperature to 24°C to ensure that S-phase proceeded slowly (see FACS profiles in Figure 6C), we took time points to monitor the abundance of Hpc2-TAP by immunoblotting. From 10 to 40 min following the temperature shift from 38°C to 24°C, we observed a progressive increase in Hpc2-TAP (Figure 6C). Even after 40min, the cells had only reached about half the DNA content of G2 and Hpc2-TAP was still accumulating in those

cells (Figure 6C). These results suggest that, although Hpc2 is synthesized during S-phase, the control of its abundance and/or regulatory mechanisms contribute to prevent inappropriate repression of histone gene transcription when the demand for histone synthesis is at its peak.

We showed that Rad53 directly phosphorylates Hpc2 *in vitro* (Figure 4A). We naturally wondered whether Rad53's role in repressing histone gene transcription was mediated, directly or indirectly through control of Hpc2 abundance. We synchronized wild-type and r*ad53*Δ *sml1-1* cells expressing Hpc2-FLAG3 in G1 with α-factor. The two strains were then released towards S-phase in the presence of HU for up to 60min at 30°C. At all time points, Hpc2-FLAG3 was more abundant in wild-type cells than in r*ad53*Δ *sml1-1* cells (Figure 7A). This result suggested that the mechanism of repression in response to HU involved Rad53 maintaining, directly or indirectly, higher levels of Hpc2 than they would be during normal passage through S-phase when histone gene transcription needs to be maintained. In order to look more carefully at molecules of Hpc2-FLAG3 present in cells treated with HU, the samples were analyzed through Phos-Tag gels rather than SDS-polyacrylamide gels. The Phos-Tag ligands binds to phosphoproteins in SDS-polyacrylamide gels and greatly retards their mobility compared that observed in conventional SDS-PAGE. In wild-type cells, where Rad53 was present to phosphorylate Hpc2, we noticed that Hpc2-FLAG3 migrated as a broad smear, most likely reflecting the multiple phosphosites identified as Rad53-dependent by mass spectrometry of HU-treated cells (Supplementary Table S1). Consistent with this, HU-treated cells lacking Rad53 (*rad53*Δ) there is a lower abundance of Hpc2-FLAG3 observed (Figure 7B). The smear of Hpc2-FLAG3 molecules derived from

r*ad53*Δ *sml1-1* cells was both less abundant and migrated significantly faster in Rad53-deficient cells than in wild-type cells.

Histone gene repression likely requires histone binding to the Hpc2 subunit of the HIR complex

Clark and colleagues (Eriksson *et al*., 2012) proposed that the repression of histone genes that occurs in G2 might be triggered by a negative feedback triggered by excess histones produced when the total rate of DNA synthesis declines towards the end of S-phase and into G2. We felt this was an elegant hypothesis that also applied to the abrupt and untimely decline in the rate of DNA synthesis that follows from activation of the DDR and the consequent inhibition of origin firing in early S-phase. In order to test this hypothesis, we took advantage of the fact that, among the four subunits of the human HIR complex, the only one that has been shown to bind directly to histone H3.3 is Ubinuclein [human UBN1 / UBN2] (Ricketts *et al*., 2015). The domain of Ubinuclein that binds H3.3 is known as HRD (Hpc2-related domain) because it was originally identified as the domain of *S. cerevisiae* Hpc2 that is most strikingly conserved among organisms that range from the fission yeast *S. pombe* to humans. In humans, Ubinuclein binds specifically to the replication-*independent* variant H3.3, rather than the replication-*dependent* variants H3.1/H3.2. However, in *S. cerevisiae* all the canonical H3 molecules synthesized from the *HHT1* and *HHT2* RNAs possess the amino acid that channels H3.3 towards the replication-independent nucleosome assembly pathway (Figure 9B). Given all this, we felt armed with the tools to ask whether the ability to bind H3 was needed for Hpc2 to repress histone gene transcription.

The structure of Ubinuclein bound to H3.3 revealed three key residues that bind to the H3.3-specific region (Ricketts et al., 2015). Collectively mutating all three residues completely abolished binding of Ubinuclein to H3.3. These residues of Ubinuclein correspond to Hpc2 F585, I586 and D587 (Figure 9A). We generated a triple alanine mutant of Hpc2, F585A, I586A and D587A. Hereafter, this mutant will be referred to as Hpc2 FID-AAA. Simultaneous mutation of these three residues is not expected to destabilize Hpc2 because, rather than being located internally within Hpc2, the three residues are part of a single external surface of the Hpc2 protein. Nevertheless, we verified that Hpc2 FID-AAA tagged at its C-terminus with a triple HA epitope was expressed by immunoblotting of whole-cell lysates. Hpc2 FID-AAA expressed from the natural *HPC2* promoter was readily detected in both proliferating cells and HU-treated cells (Figure 8F) but, unexpectedly, wild-type Hpc2-HA3 was not detected under the same conditions (Figure 8F). This was not because wild-type Hpc2-HA3 was not expressed because, in other experiments, we readily detected the wild-type protein (Figure 5A). Second, despite being below the threshold for detection in this experiment, Hpc2-HA3 was capable of repressing the eight canonicals histone mRNAs and, more specifically, the *HTA1* promoter in response to HU (Figure 8A-8E). The reason why wild-type Hpc2 "appears" to be less abundant than Hpc2 FID-AAA is currently unknown. However, we note that two independent affinity purifications of the HIR complex revealed that, unlike Hir1, Hir2 or Hir3, Hpc2 did not migrate as a single band in SDS-polyacrylamide gels (Green *et al*., 2005 ; Prochasson *et al*., 2005). This suggests that wild-type Hpc2 can be extensively modified even in normally proliferating cells. This requires further investigation, but the fact that Hpc2 FID-AAA gives rise to a sharp band by SDS-PAGE (Figure 8F) suggests that the FID-AAA mutant somehow escapes the regulatory cues that give rise to the

extensive modification of wild-type Hpc2. Regardless, our results indicate that the phenotypes caused by the FID mutation are not due to a lack of expression of Hpc2 FID-AAA.

We used an *hpc2*Δ *cdc7-4* mutant as a control strain that cannot repress histone gene transcription. This strain (W303 *MAT**a** cdc7-4 hpc2*Δ*::KanMX*) was transformed with either an empty plasmid, a plasmid encoding wild-type Hpc2-HA3 or a plasmid encoding Hpc2-HA3 FID-AAA. The *cdc7-4* thermosensitive mutation served to synchronize cells just before the time of replication origin firing (Bousset and Diffley, 1998). Because histone mRNAs are also regulated at the post-transcriptional level, our three strains were also transformed with a second plasmid that contained a reporter for histone gene promoter repression, namely the *HTA1* promoter driving expression of a neomycin resistance gene. The three strains were synchronized in G1 with α-factor (Figure 8G), and the cells released towards the *cdc7-4* arrest point at 37°C, the restrictive temperature for the *cdc7-4* mutation. Wild-type cells activate transcription of histone gene promoters at some point during the transition from G1 [α-factor arrest point] to DNA replication origin firing [*cdc7-4* arrest point] (Hereford *et al*., 1982). Despite the fact that most *cdc7-4* cells at 37°C were clearly arrested with 1C DNA contents (Figure 8G) and, therefore, histone gene transcription should be turned on, we were surprised to see that the abundance of histone mRNAs, normalized to the abundance of actin mRNA, was variable among our three strains (Figure 8A-8E, compare levels of histone mRNAs solely among the three strains at 37°C). Intriguingly, at 37°C in cells expressing wild-type Hpc2, the abundance of the eight canonical histone mRNAs, and even that of the *neomycin* reporter RNA, were always intermediate between the levels of the same RNAs in *hpc2*Δ cells (lowest RNA levels) versus *hpc2*Δ complemented with a plasmid for expression of Hpc2-HA3

FID-AAA (Figure 8A-E). The significance, if any, of this striking pattern, is currently unknown. Because this pattern of mRNA abundance was only observed in *cdc7-4* mutant cells at 37°C, it is not straightforward to compare it with the patterns described below, which were obtained at 25°C, the permissive temperature for the Cdc7-4 protein kinase.

We released the three strains from the *cdc7-4* arrest point by lowering the temperature to 25°C in the presence 200mM of the DNA replication inhibitor hydroxyurea (HU) for 1 h. This allowed very limited synthesis of DNA (Figure 8G) prior to dNTP pools reaching concentrations below the threshold for DNA polymerase activity. Under these conditions, a striking pattern of mRNA abundance was observed among our three strains. The abundance of the eight canonical histone mRNAs, and the *neomycin* reporter RNA normalized to the abundance of actin mRNA, were much higher in the the two mutant strains, *hpc2*Δ and *hpc2*Δ containing a plasmid for expression of Hpc2-HA3 FID-AAA, than in *hpc2*Δ cells expressing wild-type Hpc2-HA3 from a plasmid (Figure 8A-E, compare levels of histone mRNAs solely among the three strains treated with HU). Interestingly, the same pattern was observed when cells were arrested with α-factor in G1 (Figure 8A-E, compare levels of histone mRNAs solely among the three strains arrested in G1). The fact that the *HTA2* and *HTB2* mRNAs were repressed in an Hpc2-dependent manner seems counterintuive because, unlike the other three, the *HTA2-HTB2* promoter region lacks the *NEG* element through which the HIR proteins exert their repressive effect (Figure 1A). However, the *HTA2-HTB2* gene pair was previously shown to be co-repressed with the other three in response to HU, and transcriptional repression of *HTA2-HTB2* was at least partially dependent upon Hpc2 and the other HIR proteins (Osley and Lycan, 1987 ; Xu *et al*., 1992). Collectively, our results indicate that the Hpc2-HA3 FID-

AAA mutant is equivalent to an *hpc2*Δ null mutation in failing to restrict the accumulation of histone mRNAs in G1 or when DNA replication is inhibited by HU. These results suggest, but do not formally prove, that the ability of Hpc2 to bind histone H3 is important to restrict the accumulation of histone mRNAs in G1 or when DNA replication is inhibited by HU, and possibly other genotoxic agents that robustly activate the intra S-phase DNA damage response that inhibits the firing of new replication origins.

Discussion

Excess histones interfere with many cellular processes and, therefore, the amounts of new histones must be tightly regulated during the cell cycle. It is crucial that proliferating cells maintain strict control over the relative abundance of new histones and nascent DNA. This regulatory requirement is further compounded by the fact that the total rate of DNA synthesis abruptly declines in response to DNA damage during S-phase due to the sudden inhibition of new origin firing.

Multiple mechanisms to prevent the accumulation of excess histones

We previously reported that the DDR kinase Rad53 triggers degradation of excess histone proteins (Gunjan and Verreault, 2003; Singh et al., 2009a). Here, we demonstrate that Rad53 is also required to repress transcription of histone genes in response to genotoxic agents that slow down DNA replication. The dual role of Rad53 in histone gene repression and degradation of excess histones raises an interesting issue. At least superficially, these two modes of regulation appear to be redundant with each other. However, early S-phase cells need to synthesize large amounts of histones at very high rates to meet the demand for rapid

histone deposition behind replication forks. The sudden decline in rates of DNA synthesis that follows DNA damage during S-phase therefore results in a substantial accumulation of excess histones (Gunjan and Verreault, 2003; Singh et al., 2009c). Because they form a complex with Rad53 and the multi-functional ubiquitin-conjugating enzymes involved in their degradation (Gunjan and Verreault, 2003; Singh et al., 2012; Singh et al., 2009b), excess histones would eventually saturate the degradation machinery if they were synthesized continuously in the absence of genotoxic agent-induced histone gene repression. This would ultimately interfere with other important functions of Rad53, such as the phosphorylation of target proteins at sites of stalled replication forks.

Regulation of histone gene repression

The fact that Rad53 has the potential to repress histone gene transcription raises an important question. Clearly, the latent potential of Rad53 to repress histone genes needs to be carefully controlled to avoid inappropriate repression during normal progression through S-phase. This is because cells that complete S-phase in the absence of histone gene transcription lose viability (Kim et al., 1988b). There are at least two failsafe molecular mechanisms to ensure that histone gene transcription is not inappropriately interrupted during normal passage through S-phase. The first stems from the fact that the Hpc2 subunit of the HIR repressor complex is unstable at the *cdc7* arrest point, and possibly during early S-phase as well. In fact, Hpc2 is likely synthesized and degraded during that period, which would allow a window of opportunity for new Hpc2 molecules to bind excess histones if there is an impromptu and abrupt decline in the total rate of DNA synthesis. Second, extensive phosphorylation of Hpc2 is needed for HU-induced repression of histone gene transcription. Because of this

requirement, the ability of Rad53 to function as a histone gene repressor is only unmasked in response to replication interference, when the kinase activity of Rad53 is strongly activated by the upstream kinases Mec1/Tel1.

The initial trigger to repress histone genes may depend upon conditions that result in the presence of excess histones and those conditions likely require initiation of DNA replication (*i.e.* passage through the *cdc7-4* arrest point). Although we only tested one mutation that prevents initiation of DNA replication, *cdc7-4* mutant cells failed to repress histone gene transcription even when the mutant was held for long periods of time just before the onset of DNA synthesis. Second, in contrast to the *cdc7-4* mutation, thermosensitive mutations that stall DNA synthesis within S-phase mimic the effects of HU or MMS and trigger histone gene repression (Lycan et al., 1987). Third, this is reminiscent of the requirement for stalled replication forks to activate the kinase activity of Rad53 in the presence of the alkylating agent MMS. Cells held at the *cdc7* arrest point do not activate Rad53 in response to MMS, whereas cells that progress beyond the initiation step of DNA replication readily activate Rad53 (Tercero et al., 2003).

There are at least two non-mutually exclusive reasons why the total rate of DNA synthesis may abruptly decrease in response to DNA damage during early S-phase. At least for some genotoxic agents, the lesions in DNA template strands (*e.g.* 3-methyladenine caused by MMS) may directly interfere with replicative DNA polymerases. However, unless the density of lesions is extremely high, this is not expected to make a major contribution to the abrupt decline in the total rate of DNA synthesis because many forks may not encounter

lesions rapidly. A more likely source of the abrupt decline in the total rate of DNA synthesis is the activation of the intra S-phase DDR, which precludes initiation from many replication origins.

An inevitable consequence of conditions that activate the intra S-phase DDR is the transient accumulation of newly synthesized histones. This was demonstrated by monitoring the amounts of histones bound to several nucleosome assembly factors before and after treatment with drugs that interfere with replication (Emili et al., 2001; Groth et al., 2005; Gunjan and Verreault, 2003; Singh et al., 2009a). Thus, it is conceivable that the signal to repress histone genes is simply the accumulation of newly synthesized histones above a certain threshold. This is consistent with several lines of evidence. Budding yeast cells with reduced levels of H2A/H2B, due to disruption of the *HTA1-HTB1* gene pair, cannot repress transcription of *HTA1-LacZ* in response to HU (Moran et al., 1990). This phenomenon may be conserved because, even in human cells, inhibitors of protein synthesis prevent subsequent repression of histone genes triggered by drugs that slow down replication (Baumbach et al., 1984; Sive et al., 1984). Yeast cells also have a mechanism that downregulates expression of the *HTA1-HTB1* promoter in cells carrying multiple copies of H2A and H2B genes (Moran et al., 1990). This negative feedback is Hir protein-dependent and requires high levels of the H2A/H2B proteins because frameshift mutations that prevent H2A/H2B protein synthesis from the additional gene copies abrogate the repression (Moran et al., 1990).

Mechanism of histone gene repression

Once the decision to repress histone gene transcription has been taken, Rad53 probably activates a series of events that culminates in the coordinate repression of the four core histone gene promoters. One of those events is the recruitment of the ATP-dependent chromatin remodeler RSC to histone gene promoters (Ng et al., 2002). Asf1 is a histone H3-H4 chaperone that is known to function in concert with either replication-*dependent* (CAF-1) and replication-*independent* nucleosome assembly factors such as the HIR complex. In support of the latter, a physical interaction between Asf1 and the HIR complex has been described (Green *et al*., 2005 ; Sutton *et al*., 2001). Histone gene repression is fully dependent on HIR protein and at least partially dependent upon Asf1 (Sutton *et al*., 2001). This raises the intriguing possibility that RSC may cooperate with the Asf1-HIR protein complex (Green *et al*., 2005) to promote nucleosome assembly and positioning over the *UAS* elements of histone gene promoters. Asf1 and HIR were found to promote rapid nucleosome assembly upon phosphate-induced repression of the *PHO5* promoter in G1-arrested cells (Schermer et al., 2005). Thus, it seems likely that complexes of Asf1-Hir proteins bound to H3/H4 (Green et al., 2005) may be recruited to deposit histones and thereby repress transcription of specific promoters, including those of histone genes, via interactions with promoter DNA-bound factors. However, the mechanism of DNA damage-induced histone gene repression is likely to be very complex. Many proteins involved in histone gene regulation, such as the activators SWI/SNF (Dimova et al., 1999), Spt21 (Hess et al., 2004), SBF [Swi4-Swi6] (Eriksson et al., 2011), and Yta7 (Kurat et al., 2011), are all phosphorylated at several sites in response to DNA damage (Albuquerque et al., 2008; Chen et al., 2010; Sidorova and Breeden, 2003; Smolka et al., 2007). Moreover, at least nine of the 15-subunit RSC complex are

phosphorylated at multiple sites by DDR kinases (Albuquerque et al., 2008; Chen et al., 2010; Sidorova and Breeden, 2003; Smolka et al., 2007). Although part of this intricate pattern of phosphorylation may facilitate the action of RSC during DSB repair (Liang et al., 2007; Oum et al., 2011), it is possible that it might also contribute to RSC recruitment and/or its action at histone gene promoters.

Histone gene repression may be under negative feedback triggered by excess histones

In spite of the aforementioned complexity, we feel that we uncovered a key feature of histone gene regulation. Despite being unstable at the *cdc7* arrest point, when histone genes are transcribed, we showed that Hpc2 likely requires binding to excess histones in order to repress histone gene transcription. This is an obvious paradox, which may be resolved if the Hpc2 protein is continuously synthesized and degraded during the G1-S transition and S-phase, and only stabilized when Hpc2 is extensively phosphorylated and/or binds to excess histones in response to conditions that interfere with replication.

As appealing as the negative feedback model for histone gene repression may be, we are missing crucial results to consolidate the model. We have not formally proven that wild-type Hpc2 becomes associated with H3 when cells enter S-phase in the presence of HU or MMS and, conversely, that the Hpc2 FID-AAA mutant fails to bind H3 under the same conditions. Providing this evidence may prove more difficult than it seems. This is because, depending on conditions that are not yet fully understood, wild-type Hpc2 is either detectable by immunoblotting (Figures 5A, 6A-C, 7A-B) or not (Figure 8E). This may be an issue with plasmid retention because Hpc2 was detectable when the sequences encoding TAP and

FLAG3 epitope tags were integrated 3' of the *HPC2* coding region (Figure 6A-C, 7A-B). Alternatively, detection of Hpc2-HA3 during normal cell progression may depend upon the fraction of cells in G1 and G2/M, when histone genes are repressed, as opposed to the G1-S transition and S-phase, when histone genes are transcribed and the Hpc2 protein is unstable. Over and above this problem, it is unclear whether we will be able to show that H3 is bound to Hpc2 in cells where histone genes are repressed. There are two reasons for this concern. The first is that two affinity purifications of the HIR complex from asynchronously growing cells did not show stoichiometric amounts of histones based on Coomassie staining or even sub-stoichiometric amounts of histones based on mass spectrometry (Greene *et al*., 2005 ; Prochasson *et al*., 2005). The second is the possibility that, even in HU-treated cells, only a small subset of HIR complexes may be associated with histones even though HIR is involved in replication-independent nucleosome assembly.

Evolutionary conservation

Metazoans utilize at least two distinct strategies to trigger rapid disappearance of histone mRNAs following replication arrest. They not only repress histone gene transcription (Sittman et al., 1983), but also trigger degradation of histone mRNAs (Baumbach et al., 1984; Kaygun and Marzluff, 2005; Sittman et al., 1983). A potential role of the metazoan HIR complex and its Ubinuclein subunit in histone gene repression has, to our knowledge, never been investigated. Interestingly, the Mec1/Tel1-related protein kinase ATR, a key mediator of the response to DNA damage during S-phase, is needed for degradation of histone RNAs following treatment of human cells with replication inhibitors (Kaygun and Marzluff, 2005). However, several conflicting reports regarding the involvement of additional DNA damage

checkpoint proteins such as DNA-PK and p53 in regulating histone transcript levels in mammalian cells following DNA damage have appeared in the literature (Meador et al., 2011; Muller et al., 2007; Su et al., 2004), suggesting additional complexity and redundancy in mammalian systems (Muller et al., 2007) compared to the clear requirement for the DDR kinases Mec1/Tel1 and Rad53 in the budding yeast. Nevertheless, although the molecular mechanisms may be different, the biological rationale and the role of DDR kinases in genotoxic agent-induced downregulation of histone RNAs is conserved from yeast to human cells.

Acknowledgments

We wish to thank Drs. John Diffley, Michael Grunstein, Steve Jackson, Noel Lowndes, Mary Ann Osley, Rodney Rothstein, Yanchang Wang and Philippe Prochasson for providing strains and plasmids, and Debbie Lyon for constructing the YDL74 strain. We thank Dr. David Brown for critical reading of this manuscript. This work was funded by grants from Cancer Research UK, the Canadian Institutes for Health Research (FRN89928) and the Natural Sciences and Engineering Research Council (NSERC, RGPIN - 2019 - 05796) to A.V., a NIH grant (R15GM079678-01) to J.P. and A.G. and a Bankhead-Coley Cancer Research Program grant (07BN-02) from the Florida Department of Health to A.G.

References Chapter 3

Aboussekhra, A., J.E. Vialard, D.E. Morrison, M.A. de la Torre-Ruiz, L. Cernakov, F. Fabre, and N.F. Lowndes. 1996. A novel role for the budding yeast *RAD9* checkpoint gene in DNA damage-dependent transcription. *EMBO J.* 15:3912-3922.

Agez, M., J. Chen, R. Guerois, C. van Heijenoort, J.Y. Thuret, C. Mann, and F. Ochsenbein. 2007. Structure of the histone chaperone ASF1 bound to the histone H3 C-terminal helix and functional insights. *Structure*. 15:191-199.

Albuquerque, C.P., M.B. Smolka, S.H. Payne, V. Bafna, J. Eng, and H. Zhou. 2008. A multidimensional chromatography technology for in-depth phosphoproteome analysis. *Mol Cell Proteomics*. 7:1389-1396.

Amin, A.D., D.K. Dimova, M.E. Ferreira, N. Vishnoi, L.C. Hancock, M.A. Osley, and P. Prochasson. 2012. The mitotic Clb cyclins are required to alleviate HIR-mediated repression of the yeast histone genes at the G1/S transition. *Biochim Biophys Acta*. 1819:16-27.

Amin, A.D., N. Vishnoi, and P. Prochasson. 2013. A global requirement for the HIR complex in the assembly of chromatin. *Biochim Biophys Acta*. 1819:264-276.

Baumbach, L.L., F. Marashi, M. Plumb, G. Stein, and J. Stein. 1984. Inhibition of DNA replication coordinately reduces cellular levels of core and H1 histone mRNAs: requirement for protein synthesis. *Biochemistry*. 23:1618-1625.

Berloco, M., L. Fanti, A. Breiling, V. Orlando, and S. Pimpinelli. 2001. The maternal effect gene, *abnormal oocyte* (*abo*), of *Drosophila melanogaster* encodes a specific negative regulator of histones. *Proc Natl Acad Sci USA*. 98:12126-12131.

Blackwell, C., K.A. Martin, A. Greenall, A. Pidoux, R.C. Allshire, and S.K. Whitehall. 2004. The *S. pombe* HIRA-like protein, Hip1 is required for the periodic expression of histone genes and contributes to the function of complex centromeres. *Mol. Cell. Biol.* 24:2204-2216.

Bousset, K., and J.F. Diffley. 1998. The Cdc7 protein kinase is required for origin firing during S phase. *Genes Dev*. 12:480-490.

Campbell, S.G., M. Li Del Olmo, P. Beglan, and U. Bond. 2002. A sequence element downstream of the yeast HTB1 gene contributes to mRNA 3' processing and cell cycle regulation. *Mol Cell Biol*. 22:8415-8425.

Cha, R.S., and N. Kleckner. 2002. ATR homolog Mec1 promotes fork progression, thus averting breaks in replication slow zones. *Science*. 297:602-606.

Chabes, A., B. Georgieva, V. Domkin, X. Zhao, R. Rothstein, and L. Thelander. 2003. Survival of DNA damage in yeast directly depends on increased dNTP levels allowed by relaxed feedback inhibition of ribonucleotide reductase. *Cell*. 112:391-401.

Chen, S.H., C.P. Albuquerque, J. Liang, R.T. Suhandynata, and H. Zhou. 2010. A proteome-wide analysis of kinase-substrate network in the DNA damage response. *J Biol Chem*. 285:12803-12812.

Chen, S.H., M.B. Smolka, and H. Zhou. 2007. Mechanism of Dun1 activation by Rad53 phosphorylation in Saccharomyces cerevisiae. *J Biol Chem*. 282:986-995.

De Sanctis, V., C. Bertozzi, G. Costanzo, E. Di Mauro, and R. Negri. 2001. Cell cycle arrest determines the intensity of the global transcriptional response of *Saccharomyces cerevisiae* to ionizing radiation. *Rad Res*. 156:379-387.

Dimova, D., Z. Nackerdien, S. Furgeson, S. Eguchi, and M.A. Osley. 1999. A role for transcriptional repressors in targeting the yeast Swi/Snf complex. *Mol Cell*. 4:75-83.

Dominski, Z., X. Yang, H. Kaygun, M. Dadlez, and W.F. Marzluff. 2003. A 3' exonuclease that specifically interacts with the 3' end of histone mRNA. *Mol. Cell*. 12:295-305.

Emili, A., D.M. Schieltz, J.R. Yates 3rd, and L.H. Hartwell. 2001. Dynamic interaction of DNA damage checkpoint protein Rad53 with chromatin assembly factor Asf1. *Mol Cell*. 7:13-20.

Eriksson, P.R., D. Ganguli, and D.J. Clark. 2011. Spt10 and Swi4 control the timing of histone H2A/H2B gene activation in budding yeast. *Mol Cell Biol*. 31:557-572.

Eriksson, P.R., D. Ganguli, V. Nagarajavel, and D.J. Clark. 2012. Regulation of histone gene expression in budding yeast. *Genetics*. 191:7-20.

Foreman, P.K., and R.W. Davis. 1994. Cloning vectors for the synthesis of epitope-tagged, truncated and chimeric proteins in Saccharomyces cerevisiae. *Gene*. 144:63-68.

Gasch, A.P., M. Huang, S. Metzner, D. Botstein, S.J. Elledge, and P.O. Brown. 2001. Genomic expression responses to DNA damaging agents and the regulatory role of the yeast ATR homolog Mec1p. *Mol Biol Cell*. 12:2987-3003.

Gilbert, C.S., C.M. Green, and N.F. Lowndes. 2001. Budding yeast Rad9 is an ATP-dependent Rad53 activating machine. *Mol Cell*. 8:129-136.

Green, E.M., A.J. Antczak, A.O. Bailey, A.A. Franco, K.J. Wu, J.R. Yates, and P.D. Kaufman. 2005. Replication-independent histone deposition by the HIR complex and Asf1. *Curr Biol*. 15:2044-2049.

Groth, A., D. Ray-Gallet, J.P. Quivy, J. Lukas, J. Bartek, and G. Almouzni. 2005. Human Asf1 regulates the flow of S phase histones during replicational stress. *Mol Cell*. 17:301-311.

Gunjan, A., and A. Verreault. 2003. A Rad53 kinase-dependent surveillance mechanism that regulates histone protein levels in S. cerevisiae. *Cell*. 115:537-549.

Hereford, L., S. Bromley, and M.A. Osley. 1982. Periodic transcription of yeast histone genes. *Cell*. 30:305-310.

Herrick, D., R. Parker, and A. Jacobson. 1990. Identification and comparison of stable and unstable mRNAs in *Saccharomyces cerevisiae*. *Mol. Cell. Biol.* 10:2269-2284.

Hess, D., B. Liu, N.R. Roan, R. Sternglanz, and F. Winston. 2004. Spt10-dependent transcriptional activation in Saccharomyces cerevisiae requires both the Spt10 acetyltransferase domain and Spt21. *Mol Cell Biol*. 24:135-143.

Holt, L.J., B.B. Tuch, J. Villen, A.D. Johnson, S.P. Gygi, and D.O. Morgan. 2009. Global analysis of Cdk1 substrate phosphorylation sites provides insights into evolution. *Science*. 325:1682-1686.

Huang, M., Z. Zhou, and S.J. Elledge. 1998. The DNA replication and damage checkpoint pathways induce transcription by inhibition of the Crt1 repressor. *Cell*. 94:595-605.

Jelinsky, S.A., P. Estep, G.M. Church, and L.D. Samson. 2000. Regulatory networks revealed by transcriptional profiling of damaged *Saccharomyces cerevisiae* cells: Rpn4 links base excision repair with proteasomes. *Mol Cell Biol*. 20:8157-8167.

Jiao, Y., K. Seeger, A. Lautrette, A. Gaubert, F. Mousson, R. Guerois, C. Mann, and F. Ochsenbein. 2012. Surprising complexity of the Asf1 histone chaperone-Rad53 kinase interaction. *Proc Natl Acad Sci U S A*. 109:2866-2871.

Kaygun, H., and W.F. Marzluff. 2005. Regulated degradation of replication-dependent histone mRNAs requires both ATR and Upf1. *Nat Struct Mol Biol*. 12:794-800.

Kim, U.-J., M. Han, P. Kayne, and M. Grunstein. 1988a. Effects of histone H4 depletion on the cell cycle and transcription of *Saccharomyces cerevisiae*. *EMBO J*. 7:2211-2219.

Kim, U.J., M. Han, P. Kayne, and M. Grunstein. 1988b. Effects of histone H4 depletion on the cell cycle and transcription of Saccharomyces cerevisiae. *EMBO J*. 7:2211-2219.

Kumar Singh, R., M.-H. Miquel Kabbaj, J. Paik, A. Verreault, and A. Gunjan. 2007. Histone levels are regulated by phosphorylation and ubiquitylation dependent proteolysis in *S. cerevisiae*. *Cell*. submitted.

Kurat, C.F., J.P. Lambert, D. van Dyk, K. Tsui, H. van Bakel, S. Kaluarachchi, H. Friesen, P. Kainth, C. Nislow, D. Figeys, J. Fillingham, and B.J. Andrews. 2011. Restriction of histone gene transcription to S phase by phosphorylation of a chromatin boundary protein. *Genes Dev*. 25:2489-2501.

Kushnirov, V.V. 2000. Rapid and reliable protein extraction from yeast. *Yeast*. 16:857-860.

Leroy, C., S.E. Lee, M.B. Vaze, F. Ochsenbein, R. Guerois, J.E. Haber, and M.C. Marsolier-Kergoat. 2003. PP2C phosphatases Ptc2 and Ptc3 are required for DNA checkpoint inactivation after a double-strand break. *Mol Cell*. 11:827-835.

Liang, B., J. Qiu, K. Ratnakumar, and B.C. Laurent. 2007. RSC functions as an early double-strand-break sensor in the cell's response to DNA damage. *Curr Biol*. 17:1432-1437.

Liang, D., S.L. Burkhart, R.K. Singh, M.H. Kabbaj, and A. Gunjan. 2012. Histone dosage regulates DNA damage sensitivity in a checkpoint-independent manner by the homologous recombination pathway. *Nucleic Acids Res*. 40:9604-9620.

Longhese, M.P., M. Clerici, and G. Lucchini. 2003. The S-phase checkpoint and its regulation in *Saccharomyces cerevisiae*. *Mut. Res.* 532:41-58.

Lopes, M., C. Cotta-Ramusino, A. Pellicioli, G. Liberi, P. Plevani, M. Muzi-Falconi, C.S. Newlon, and M. Foiani. 2001. The DNA replication checkpoint response stabilizes stalled replication forks. *Nature*. 412:557-561.

Lycan, D.E., M.A. Osley, and L.M. Hereford. 1987. Role of transcriptional and posttranscriptional regulation in expression of histone genes in Saccharomyces cerevisiae. *Mol Cell Biol*. 7:614-621.

Marzluff, W.F., and K.P. Koreski. 2017. Birth and Death of Histone mRNAs. *Trends in genetics : TIG*. 33:745-759.

Marzluff, W.F., E.J. Wagner, and R.J. Duronio. 2008. Metabolism and regulation of canonical histone mRNAs: life without a poly(A) tail. *Nat Rev Genet*. 9:843-854.

Meador, J.A., S.A. Ghandhi, and S.A. Amundson. 2011. p53-independent downregulation of histone gene expression in human cell lines by high- and low-let radiation. *Radiat Res*. 175:689-699.

Meeks-Wagner, D., and L.H. Hartwell. 1986. Normal stoichiometry of histone dimer sets is necessary for high fidelity of mitotic chromosome transmission. *Cell*. 44:43-52.

Moran, L., D. Norris, and M.A. Osley. 1990. A yeast H2A-H2B promoter can be regulated by changes in histone gene copy number. *Genes Dev*. 4:752-763.

Muller, B., J. Blackburn, C. Feijoo, X. Zhao, and C. Smythe. 2007. DNA-activated protein kinase functions in a newly observed S phase checkpoint that links histone mRNA abundance with DNA replication. *J Cell Biol*. 179:1385-1398.

Nelson, D.M., X. Ye, C. Hall, H. Santos, T. Ma, G.D. Kao, T.J. Yen, J.W. Harper, and P.D. Adams. 2002. Coupling of DNA synthesis and histone synthesis in S phase independent of cyclin/cdk2 activity. *Mol Cell Biol*. 22:7459-7472.

Ng, H.H., F. Robert, R.A. Young, and K. Struhl. 2002. Genome-wide location and regulated recruitment of the RSC nucleosome-remodeling complex. *Genes Dev*. 16:806-819.

O'Neill, B.M., S.J. Szyjka, E.T. Lis, A.O. Bailey, J.R. Yates, 3rd, O.M. Aparicio, and F.E. Romesberg. 2007. Pph3-Psy2 is a phosphatase complex required for Rad53 dephosphorylation and replication fork restart during recovery from DNA damage. *Proc Natl Acad Sci U S A*. 104:9290-9295.

Osley, M.A. 1991. The regulation of histone synthesis in the cell cycle. *Annu Rev Biochem*. 60:827-861.

Osley, M.A., and D. Lycan. 1987. Trans-acting regulatory mutations that alter transcription of Saccharomyces cerevisiae histone genes. *Mol Cell Biol*. 7:4204-4210.

Oum, J.H., C. Seong, Y. Kwon, J.H. Ji, A. Sid, S. Ramakrishnan, G. Ira, A. Malkova, P. Sung, S.E. Lee, and E.Y. Shim. 2011. RSC facilitates Rad59-dependent homologous recombination between sister chromatids by promoting cohesin loading at DNA double-strand breaks. *Mol Cell Biol*. 31:3924-3937.

Paulovich, A.G., and L.H. Hartwell. 1995. A checkpoint regulates the rate of progression through S-phase in *S. cerevisiae* in response to DNA damage. *Cell*. 82:841-847.

Pellicioli, A., C. Lucca, G. Liberi, F. Marini, M. Lopes, P. Plevani, A. Romano, P.P. Di Fiore, and M. Foiani. 1999. Activation of Rad53 kinase in response to DNA damage and its effect in modulating phosphorylation of the lagging strand DNA polymerase. *EMBO J.* 18:6561-6572.

Pietrobon, V., K. Freon, J. Hardy, A. Costes, I. Iraqui, F. Ochsenbein, and S.A. Lambert. 2014. The chromatin assembly factor 1 promotes Rad51-dependent template switches at replication forks by counteracting D-loop disassembly by the RecQ-type helicase Rqh1. *PLoS biology*. 12:e1001968.

Prochasson, P., L. Florens, S.K. Swanson, M.P. Washburn, and J.L. Workman. 2005. The HIR corepressor complex binds to nucleosomes generating a distinct protein/DNA complex resistant to remodeling by SWI/SNF. *Genes Dev*. 19:2534-2539.

Reis, C.C., and J.L. Campbell. 2007. Contribution of Trf4/5 and the nuclear exosome to genome stability through regulation of histone mRNA levels in Saccharomyces cerevisiae. *Genetics*. 175:993-991010.

Ricketts, M.D., B. Frederick, H. Hoff, Y. Tang, D.C. Schultz, T. Singh Rai, M. Grazia Vizioli, P.D. Adams, and R. Marmorstein. 2015. Ubinuclein-1 confers histone H3.3-specific-binding by the HIRA histone chaperone complex. *Nat Commun*. 6:7711.

Ricketts, M.D., and R. Marmorstein. 2017. A Molecular Prospective for HIRA Complex Assembly and H3.3-Specific Histone Chaperone Function. *J Mol Biol*. 429:1924-1933.

Sambrook, J., E.F. Fritsch, and T. Maniatis. 1989. Molecular Cloning - A Laboratory Manual. Cold Spring Harbor Laboratory Press, Cold Spring Harbor, New York.

Sánchez, R., and W.F. Marzluff. 2004. The oligo(A) tail on histone mRNA plays an active role in translational silencing of histone mRNA during *Xenopus* oogenesis. *Mol. Cell. Biol.* 24:2513-2525.

Sanchez, Y., B.A. Desany, W.J. Jones, Q. Liu, B. Wang, and S.J. Elledge. 1996. Regulation of *RAD53* by the ATM-like kinases *MEC1* and *TEL1* in yeast cell cycle checkpoints. *Science*. 271:357-360.

Santocanale, C., and J.F. Diffley. 1998. A Mec1- and Rad53-dependent checkpoint controls late-firing origins of DNA replication. *Nature*. 395:615-618.

Schermer, U.J., P. Korber, and W. Horz. 2005. Histones are incorporated in trans during reassembly of the yeast PHO5 promoter. *Mol Cell*. 19:279-285.

Segurado, M., and J.A. Tercero. 2009. The S-phase checkpoint: targeting the replication fork. *Biol Cell*. 101:617-627.

Sherwood, P.W., S.V. Tsang, and M.A. Osley. 1993. Characterization of HIR1 and HIR2, two genes required for regulation of histone gene transcription in Saccharomyces cerevisiae. *Mol Cell Biol*. 13:28-38.

Shirahige, K., Y. Hori, K. Shiraishi, M. Yamashita, K. Takahashi, C. Obuse, T. Tsurimoto, and H. Yoshikawa. 1998. Regulation of DNA replication origins during cell cycle progression. *Nature*. 395:615-621.

Sidorova, J.M., and L.L. Breeden. 1997. Rad53-dependent phosphorylation of Swi6 and down-regulation of *CLN1* and *CLN2* transcription occur in response to DNA damage in *Saccharomyces cerevisiae*. *Genes Dev.* 11:3032-3045.

Sidorova, J.M., and L.L. Breeden. 2003. Rad53 checkpoint kinase phosphorylation site preference identified in the Swi6 protein of *Saccharomyces cerevisiae*. *Mol. Cell. Biol.* 23:3405-3416.

Singh, R.K., M. Gonzalez, M.H. Kabbaj, and A. Gunjan. 2012. Novel E3 Ubiquitin Ligases That Regulate Histone Protein Levels in the Budding Yeast Saccharomyces cerevisiae. *PloS one*. 7:e36295.

Singh, R.K., M.-H.M. Kabbaj, J. Paik, and A. Gunjan. 2009a. Histone levels are regulated by phosphorylation and ubiquitylation-dependent proteolysis. *Nat Cell Biol*. 11:925-933.

Singh, R.K., M.H. Kabbaj, J. Paik, and A. Gunjan. 2009b. Histone levels are regulated by phosphorylation and ubiquitylation-dependent proteolysis. *Nat Cell Biol*. 11:925-933.

Singh, R.K., D. Liang, U.R. Gajjalaiahvari, M.-H.M. Kabbaj, J. Paik, and A. Gunjan. 2010. Excess histone levels mediate cytotoxicity via multiple mechanisms. *Cell cycle*. 9:4236-4244.

Singh, R.K., J. Paik, and A. Gunjan. 2009c. Generation and management of excess histones during the cell cycle. *Front Biosci*. 14:3145-3158.

Sittman, D.B., R.A. Graves, and W.M. Marzluff. 1983. Histone mRNA concentrations are regulated at the level of transcription and mRNA degradation. *Proc. Natl. Acad. Sci. USA*. 80:1849-1853.

Sive, H.L., N. Heintz, and R.G. Roeder. 1984. Regulation of human histone gene expression during the HeLa cell cycle requires protein synthesis. *Mol. Cell. Biol.* 4:2723-2734.

Smolka, M.B., C.P. Albuquerque, S.H. Chen, and H. Zhou. 2007. Proteome-wide identification of in vivo targets of DNA damage checkpoint kinases. *Proc Natl Acad Sci U S A*. 104:10364-10369.

Sogo, J.M., H. Stahl, T. Koller, and R. Knippers. 1986. Structure of replicating simian virus 40 minichromosomes. The replication fork, core histone segregation and terminal structures. *J Mol Biol*. 189:189-204.

Su, C., G. Gao, S. Schneider, C. Helt, C. Weiss, M.A. O'Reilly, D. Bohmann, and J. Zhao. 2004. DNA damage induces downregulation of histone gene expression through the G1 checkpoint pathway. *EMBO J*. 23:1133-1143.

Sullivan, E., C. Santiago, E.D. Parker, Z. Dominski, X. Yang, D.J. Lanzotti, T.C. Ingledue, W.F. Marzluff, and R.J. Duronio. 2001. *Drosophila* stem loop binding protein coordinates accumulation of histone mRNA with cell cycle progression. *Genes Dev*. 15:173-187.

Sutton, A., J. Bucaria, M.A. Osley, and R. Sternglanz. 2001. Yeast ASF1 protein is required for cell cycle regulation of histone gene transcription. *Genetics*. 158:587-596.

Sweeney, F.D., F. Yang, A. Chi, J. Shabanowitz, D.F. Hunt, and D. Durocher. 2005. Saccharomyces cerevisiae Rad9 acts as a Mec1 adaptor to allow Rad53 activation. *Curr Biol*. 15:1364-1375.

Tang, Y., M.V. Poustovoitov, K. Zhao, M. Garfinkel, A. Canutescu, R. Dunbrack, P.D. Adams, and R. Marmorstein. 2006. Structure of a human ASF1a-HIRA complex and insights into specificity of histone chaperone complex assembly. *Nat Struct Mol Biol*. 13:921-929.

Tercero, J.A., and J.F.X. Diffley. 2001. Regulation of DNA replication fork progression through damaged DNA by the Mec1/Rad53 checkpoint. *Nature*. 412:553-557.

Tercero, J.A., M.P. Longhese, and J.F. Diffley. 2003. A central role for DNA replication forks in checkpoint activation and response. *Mol Cell*. 11:1323-1336.

Travesa, A., A. Duch, and D.G. Quintana. 2008. Distinct phosphatases mediate the deactivation of the DNA damage checkpoint kinase Rad53. *J Biol Chem*. 283:17123-17130.

Vaze, M.B., A. Pellicioli, S.E. Lee, G. Ira, G. Liberi, A. Arbel-Eden, M. Foiani, and J.E. Haber. 2002. Recovery from checkpoint-mediated arrest after repair of a double-strand break requires Srs2 helicase. *Mol Cell*. 10:373-385.

Vishnoi, N., K. Flaherty, L.C. Hancock, M.E. Ferreira, A.D. Amin, and P. Prochasson. 2011. Separation-of-function mutation in HPC2, a member of the HIR complex in S. cerevisiae, results in derepression of the histone genes but does not confer cryptic TATA phenotypes. *Biochim Biophys Acta*. 1809:557-566.

Xiong, C., Z. Wen, J. Yu, J. Chen, C.P. Liu, X. Zhang, P. Chen, R.M. Xu, and G. Li. 2018. UBN1/2 of HIRA complex is responsible for recognition and deposition of H3.3 at cis-regulatory elements of genes in mouse ES cells. *BMC Biol*. 16:110.

Xu, H., L. Johnson, and M. Grunstein. 1990. Coding and noncoding sequences at the 3' end of yeast histone H2B mRNA confer cell cycle regulation. *Mol. Cell. Biol.* 10:2687-2694.

Xu, H., U.J. Kim, T. Schuster, and M. Grunstein. 1992. Identification of a new set of cell cycle-regulatory genes that regulate S-phase transcription of histone genes in Saccharomyces cerevisiae. *Mol Cell Biol*. 12:5249-5259.

Yang, X.C., M. Purdy, W.F. Marzluff, and Z. Dominski. 2006. Characterization of 3'hExo, a 3' exonuclease specifically interacting with the 3' end of histone mRNA. *J Biol Chem*. 281:30447-30454.

Zegerman, P., and J.F. Diffley. 2010. Checkpoint-dependent inhibition of DNA replication initiation by Sld3 and Dbf4 phosphorylation. *Nature*. 467:474-478.

Zhao, X., A. Chabes, V. Domkin, L. Thelander, and R. Rothstein. 2001. The ribonucleotide reductase inhibitor Sml1 is a new target of the Mec1/Rad53 kinase cascade during growth and in response to DNA damage. *EMBO J*. 20:3544-3553.

Zhao, X., and R. Rothstein. 2002. The Dun1 checkpoint kinase phosphorylates and regulates the ribonucleotide reductase inhibitor Sml1. *Proc Natl Acad Sci U S A*. 99:3746-3751.

Figures

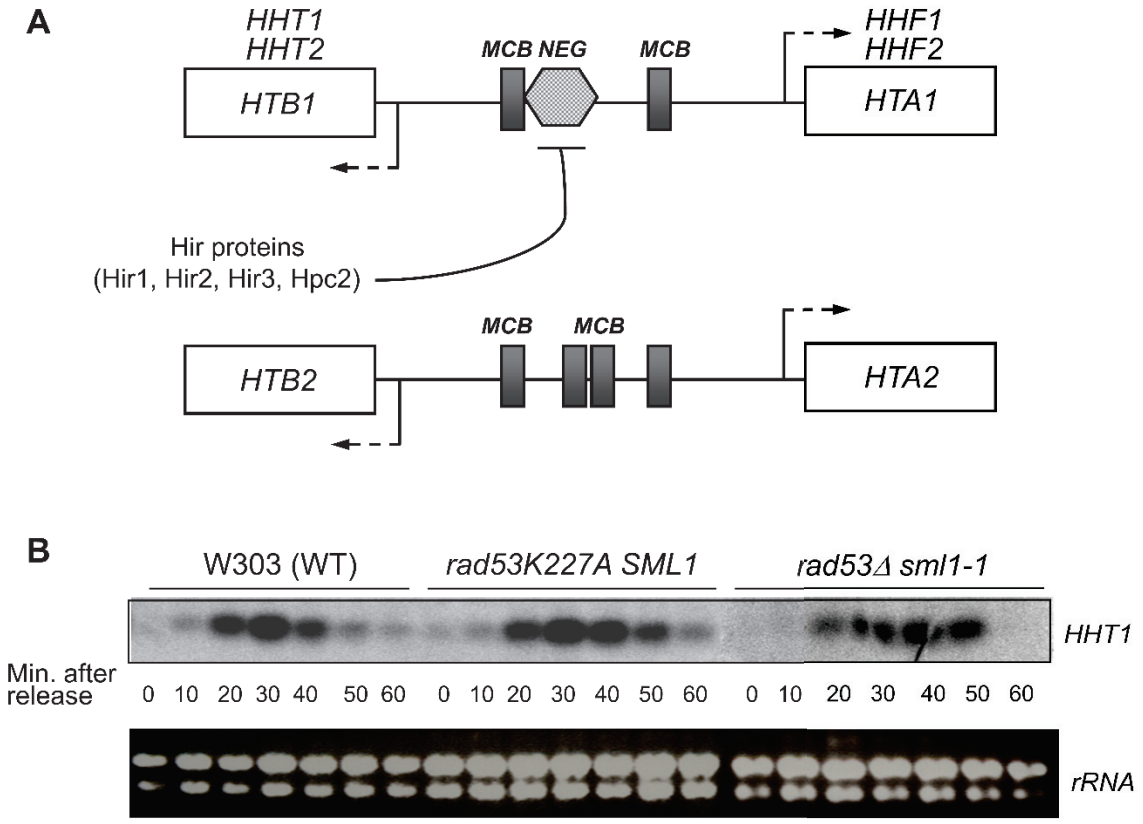

Figure 1

Figure 1. Rad53 is not required for cell cycle regulation of histone gene transcription.

(A) Histone genes are organized as four gene pairs encoding either H3-H4 (*HHT1-HHF1* and *HTT2-HHF2*) or H2A-H2B (*HTA1-HTB1* and *HTA2-HTB2*). Each gene pair is transcribed from a divergent promoter. Three of the four core histone gene promoters are repressed by Hir proteins through a negative *cis*-acting element (*NEG*). The *HTA2-HTB2* promoter lacks the *NEG* element.

(B) Wild-type (W303) and *rad53* mutant cells were synchronized with a-factor in G1 and released into the cell cycle at 30°C in pre-warmed rich medium (YPD). Cells were harvested every 10 minutes after release. Total RNA was isolated and analyzed by northern blotting to detect *HHT1* mRNAs. Ethidium bromide stained 26S and 18S rRNA levels are shown as loading control. *rad53 K227A* is viable despite the presence of wild-type *SML1* because it is a catalytically crippled, but not a null allele of *RAD53*.

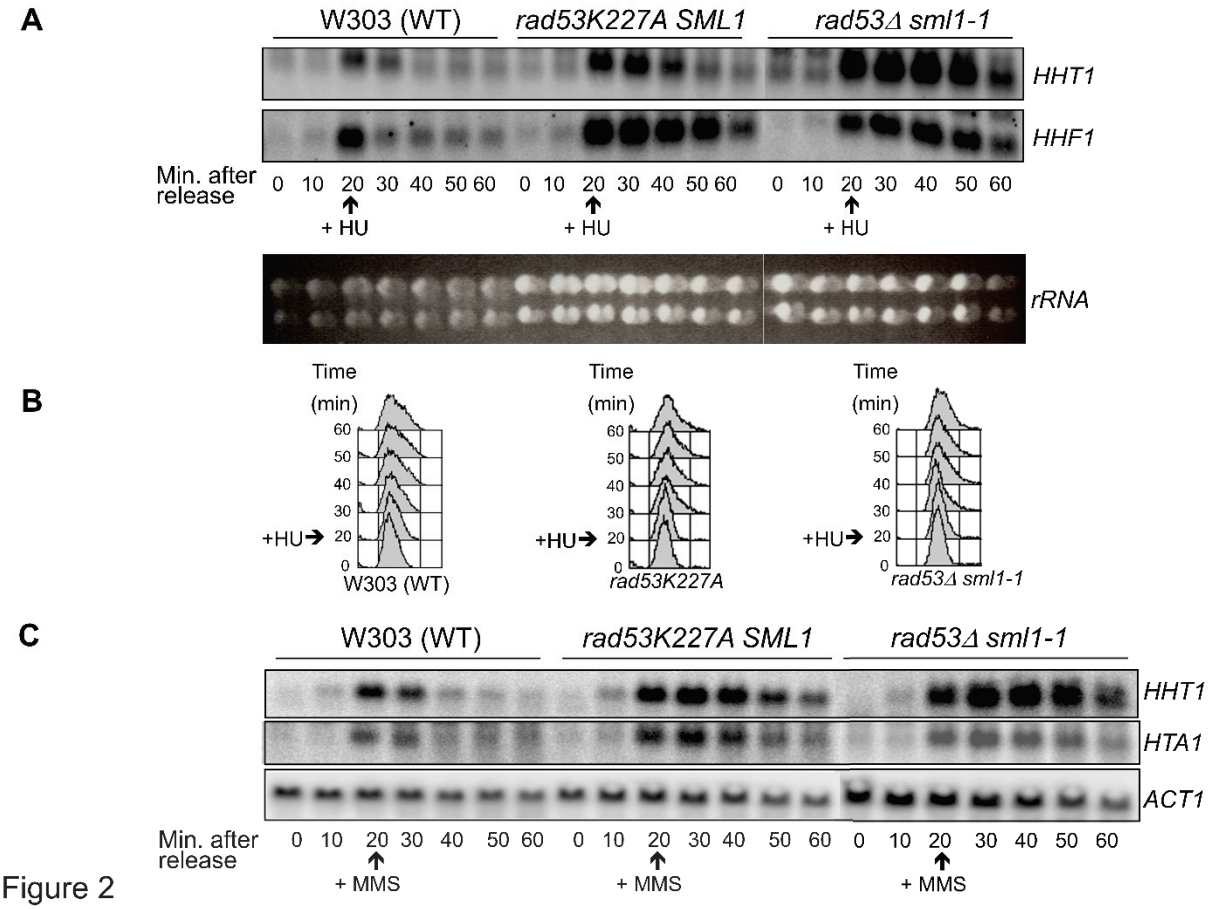
A
W303 (WT)
rad53K227A SML1
rad53Δ sml1-1
HHT1
HHF1
Min. after release
0 10 20 30 40 50 60
+ HU
rRNA
B
Time (min)
+HU
W303 (WT)
rad53K227A
rad53Δ sml1-1
C
HHT1
HTA1
ACT1
+ MMS

Figure 2

Figure 2. Downregulation of histone mRNAs in response to hydroxyurea (HU) and methyl methane sulfonate (MMS) is impaired in *rad53* mutant cells.

(A) Wild-type (W303) and *rad53* mutant cells were released from α-factor arrest and 0.2M HU was added at the beginning of S-phase (20min) to slow down DNA replication by depleting dNTPs. Northern blots were performed to monitor the *HHT1* and *HHF1* transcripts. Ethidium bromide stained 26S and 18S rRNA levels are shown as loading control. The delay in DNA replication caused by HU was monitored by FACS.

(B) Flow cytometric analysis of the DNA content of the cells used in the experiment shown in (A).

(C) Wild-type (W303) and *rad53* mutant cells were released from α-factor arrest and 0.1% MMS was added at the beginning of S-phase (20min) to interfere with DNA replication. Northern blots were performed to detect the *HHT1*, *HTA1* or the *ACT1* transcripts as loading control.

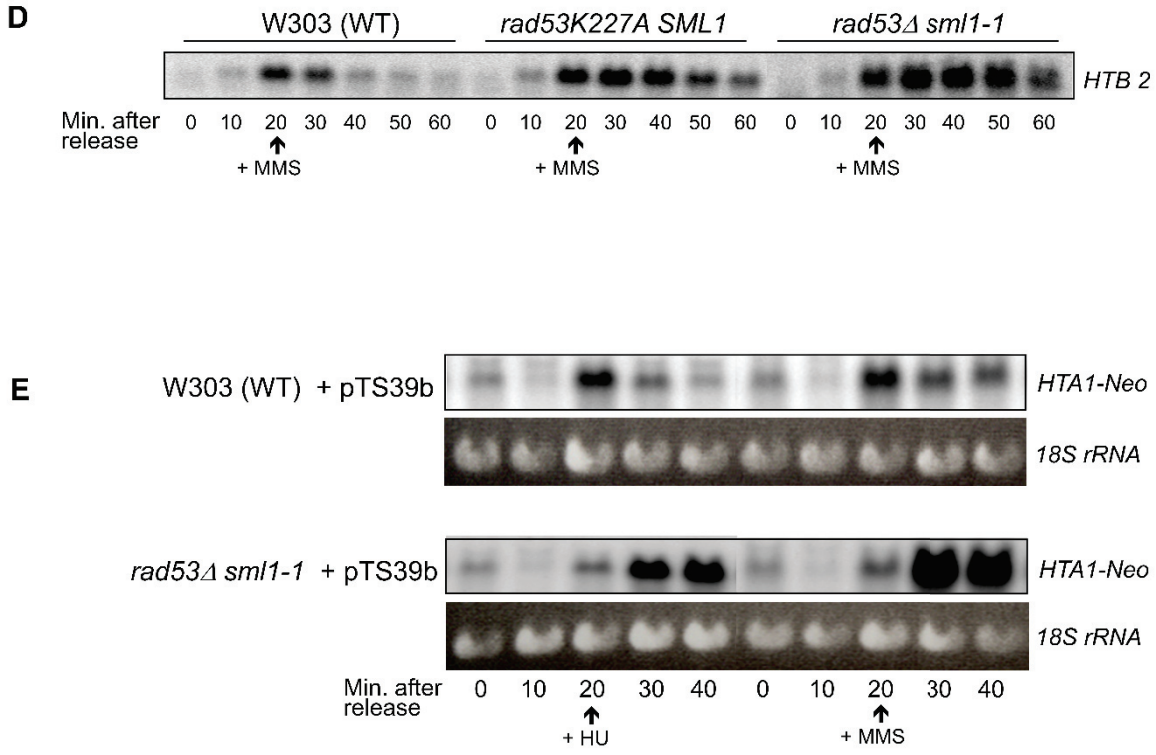
D
W303 (WT)
rad53K227A SML1
rad53Δ sml1-1
HTB 2
Min. after release
0 10 20 30 40 50 60 0 10 20 30 40 50 60 0 10 20 30 40 50 60
+ MMS
+ MMS
+ MMS
E
W303 (WT) + pTS39b
HTA1-Neo
18S rRNA
rad53Δ sml1-1 + pTS39b
HTA1-Neo
18S rRNA
Min. after release
0 10 20 30 40 0 10 20 30 40
+ HU
+ MMS

Figure 2

Figure 2. Downregulation of histone mRNAs in response to hydroxyurea (HU) and methyl methane sulfonate (MMS) is impaired in *rad53* mutant cells.

D) The northern blot was then stripped and re-probed to detect *HTB2* mRNAs.

E) Wild-type and *rad53* null mutant cells carrying the *HTA1-Neo* reporter gene were released from G1 arrest and genotoxic agents HU or MMS were added at the beginning of S-phase (20-min time points). In wild-type cells, the abundance of neomycin transcripts decreased upon addition of either HU or MMS (20 - 40 min time points).

In striking contrast, the neomycin transcripts kept accumulating when *rad53* mutant cells were treated with HU or MMS at the beginning of S-phase. This result demonstrates that Rad53 is needed to trigger histone gene promoter repression in response to genotoxic agents that interfere with replication.

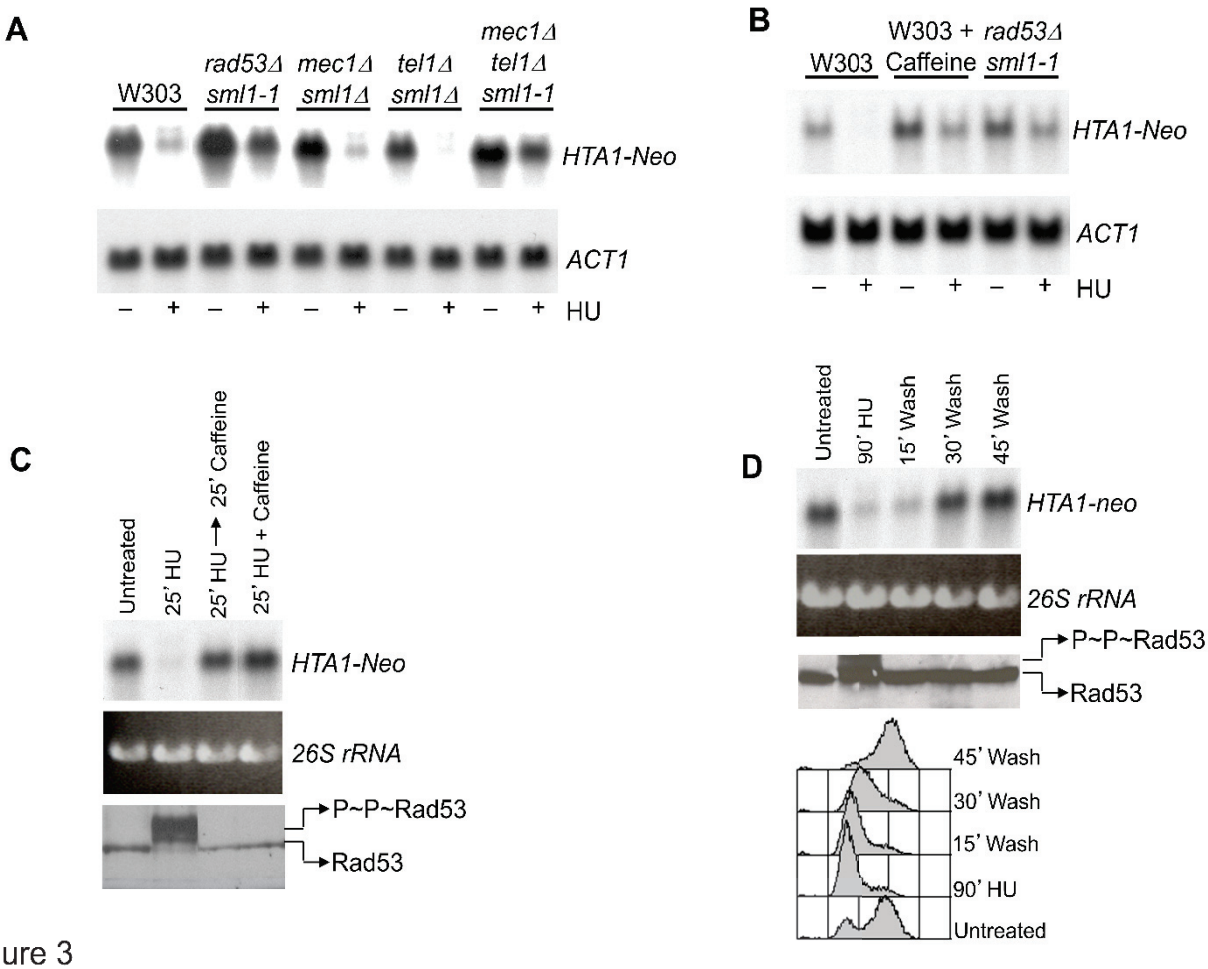
A
W303
rad53Δ sml1-1
mec1Δ sml1Δ
tel1Δ sml1Δ
mec1Δ tel1Δ sml1-1
HTA1-Neo
ACT1
– + – + – + – + – + HU
B
W303
W303 + Caffeine
rad53Δ sml1-1
HTA1-Neo
ACT1
– + – + – + HU
C
Untreated
25' HU
25' HU → 25' Caffeine
25' HU + Caffeine
HTA1-Neo
26S rRNA
P~P~Rad53
Rad53
D
Untreated
90' HU
15' Wash
30' Wash
45' Wash
HTA1-neo
26S rRNA
P~P~Rad53
Rad53
45' Wash
30' Wash
15' Wash
90' HU
Untreated

Figure 3

Figure 3. Histone gene repression in response to hydroxyurea is dependent upon continuous activity of the protein kinases Mec1 and Tel1.

(A) Mec1 and Tel1 are redundant with each other for *HTA1* promoter repression upon HU treatment. Asynchronous populations of the indicated strains expressing the *HTA1-Neo* reporter were either left untreated or incubated with 0.2M HU for 25min. Northern blots were performed to detect the *Neo* mRNAs. *ACT1* transcripts were monitored as loading controls.

(B) Caffeine reduces the HU-induced repression of the *HTA1* promoter. Strains were processed as in (A), except that 0.5% (w/v) caffeine was added 5 minutes prior to the addition of 0.2M HU.

(C) Asynchronously growing wild-type cells expressing the *HTA1-Neo* reporter were treated with 0.5% (w/v) caffeine either after treatment with 0.2M HU (arrow) or simultaneously with HU treatment (+). The upper panel shows *Neo* reporter transcript levels, whereas the middle panel depicts the 26S rRNA levels as loading controls. The bottom panel shows an immunoblot performed to detect Rad53 phosphorylation in the same samples.

(D) Histone gene transcription is reactivated following HU removal, resumption of DNA synthesis and concomitant Rad53 dephosphorylation. Asynchronously growing wild-type (W303) cells expressing the *HTA1-Neo* reporter were treated with 0.2M HU for 90min. HU was then washed away, and cells were grown in the absence of HU for the indicated time periods. The upper three panels are as in (C), while the bottom panel shows the DNA contents of the cells at the time they were harvested.

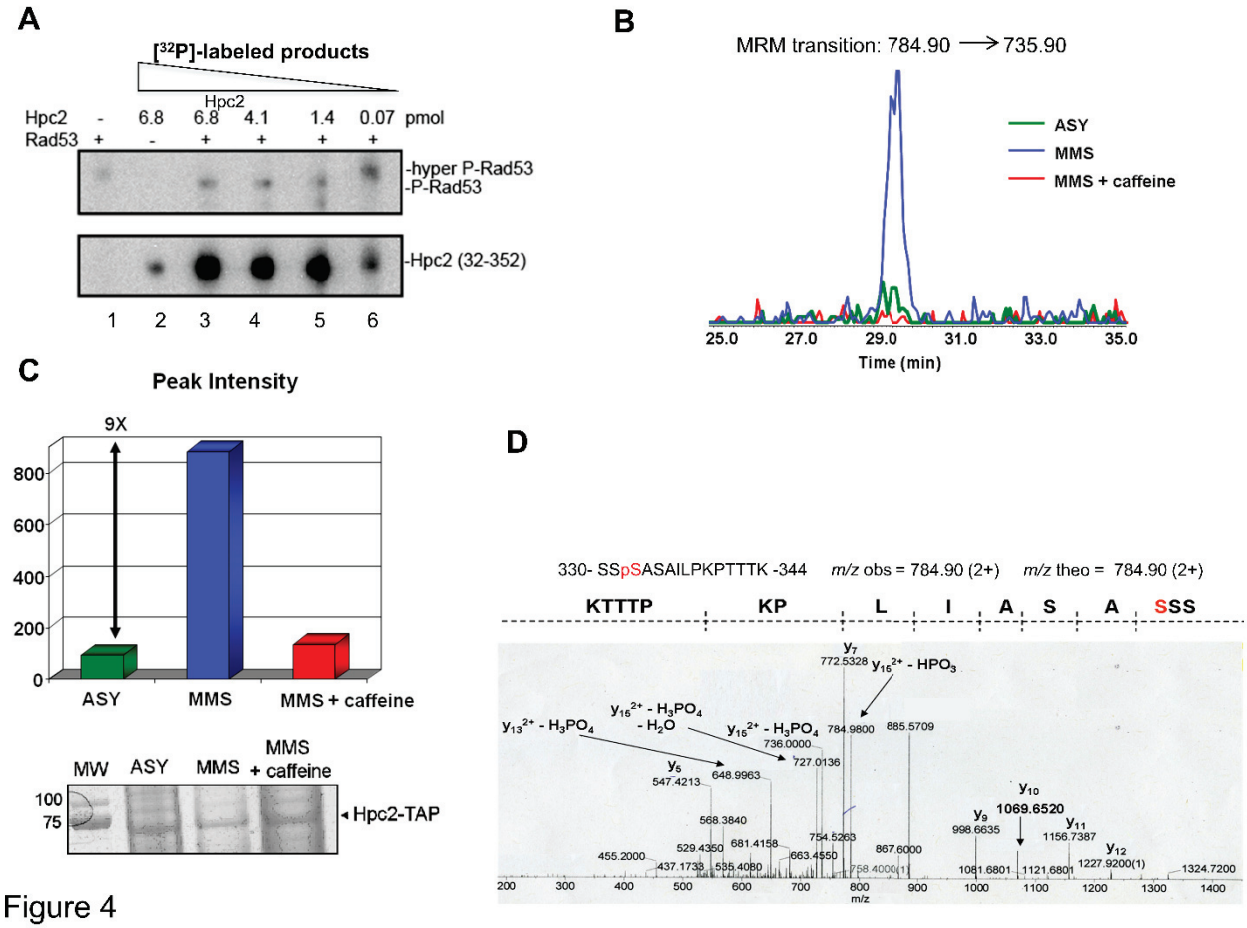
A
[32P]-labeled products
Hpc2
Hpc2 - 6.8 6.8 4.1 1.4 0.07 pmol
Rad53 + - + + + +
-hyper P-Rad53
-P-Rad53
-Hpc2 (32-352)
1 2 3 4 5 6
B
MRM transition: 784.90 → 735.90
ASY
MMS
MMS + caffeine
25.0 27.0 29.0 31.0 33.0 35.0
Time (min)
C
Peak Intensity
9X
800
600
400
200
0
ASY
MMS
MMS + caffeine
MW ASY MMS MMS + caffeine
100
75
Hpc2-TAP
D
330- SSpSASAILPKPTTTK -344 m/z obs = 784.90 (2+) m/z theo = 784.90 (2+)
KTTTP KP L I A S A SSS
y7
772.5328
y16 2+ - HPO3
y15 2+ - H3PO4 - H2O
y13 2+ - H3PO4
y15 2+ - H3PO4
784.9800
885.5709
736.0000
727.0136
y5
547.4213
648.9963
y10
1069.6520
y9
998.6635
y11
1156.7387
y12
1227.9200(1)
568.3840
529.4350
681.4158
754.5263
455.2000
437.1733
535.4080
663.4550
867.6000
758.4000(1)
1081.6801
1121.6801
1324.7200
200 300 400 500 600 700 800 900 1000 1100 1200 1300 1400
m/z

Figure 4

Figure 4. Hpc2 phosphorylation *in vivo* and *in vitro*.

(A) Autoradiogram showing the [^{32}P]-labeled products produced after *in vitro* kinase assays performed with recombinant Rad53 and a fragment of Hpc2 (residues 32-352).

(B-C) MMS-induced phosphorylation of Hpc2-Ser332 is abolished by caffeine. Asynchronous cells were either left untreated or treated for 2h with 0.035% MMS. Half of the MMS-treated culture was then incubated with 0.5% caffeine for 30min to inhibit Mec1/Tel1. Hpc2-TAP was affinity-purified from each cell population and the abundance of Hpc2-Ser332 phosphorylation determined by MRM (see Supplement). Hpc2-TAP was also analyzed by SDS-PAGE and stained with Coomassie Blue. The graph (B) shows the abundance of the Hpc2-Ser332 phosphopeptide as a function of its retention time during liquid chromatography.

(D) Hpc2-Ser332 is phosphorylated *in vivo* in response to MMS. Hpc2-TAP was purified from MMS-treated cells and analyzed by nano LC-MS/MS. The observed and theoretical *m/z* ratio of the non-fragmented precursor peptide are indicated at the top. In the MS/MS spectrum, the sequence from left to right is shown from the C-terminus to the N-terminus relative to that of Hpc2. The fragment with m/z_{obs} 648.9963 is diagnostic of Ser332 phosphorylation and formed by loss of H_3PO_4 from the doubly charged y_{13} fragment ion (y_{13}^{2+} - H_3PO_4): m/z_{theo} 648.87.

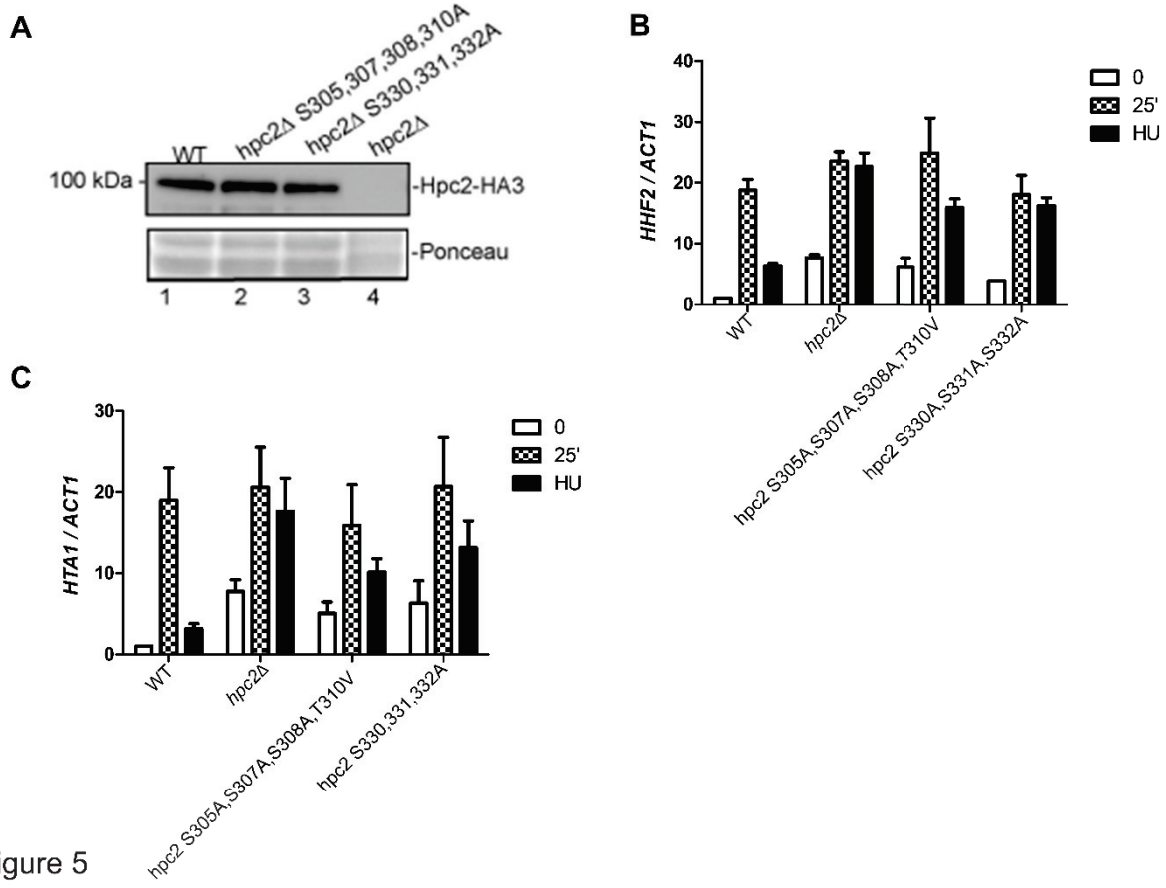
A
WT
hpc2Δ S305,307,308,310A
hpc2Δ S330,331,332A
hpc2Δ
100 kDa
-Hpc2-HA3
-Ponceau
1
2
3
4
B
HHF2 / ACT1
0
25'
HU
WT
hpc2Δ
hpc2 S305A,S307A,S308A,T310V
hpc2 S330A,S331A,S332A
C
HTA1 / ACT1
0
25'
HU
WT
hpc2Δ
hpc2 S305A,S307A,S308A,T310V
hpc2 S330,331,332A

Figure 5

Figure 5. Two clusters of Hpc2 residues contribute to downregulation of histone transcripts upon replication inhibition.

(A) Hpc2 mutations do not destabilize the protein. Hpc2-HA3 levels were determined by immunoblotting of asynchronously growing cell populations. Ponceau S is shown as loading control.

(B) *hpc2* mutants are defective in downregulating *HHF2* transcripts upon HU treatment. Exponentially growing cultures of wild-type or *hpc2* mutant cells were arrested with α-factor for two hours and released towards S-phase for 25 minutes at 30°C prior to addition of 0.2M HU for 20 minutes. Total RNA was extracted from the different samples and histone mRNA levels were determined by qRT-PCR. The abundance of *HHF2* mRNA was normalized to that of *ACT1*. *HHF2* RNA levels in each sample are expressed relative to the levels observed in WT G1 cells, which were arbitrarily set to one.

(C) *hpc2* mutants are defective in downregulating *HTA1* transcripts upon HU treatment. The data were generated as described in (B) but using *HTA1*-specific primers.

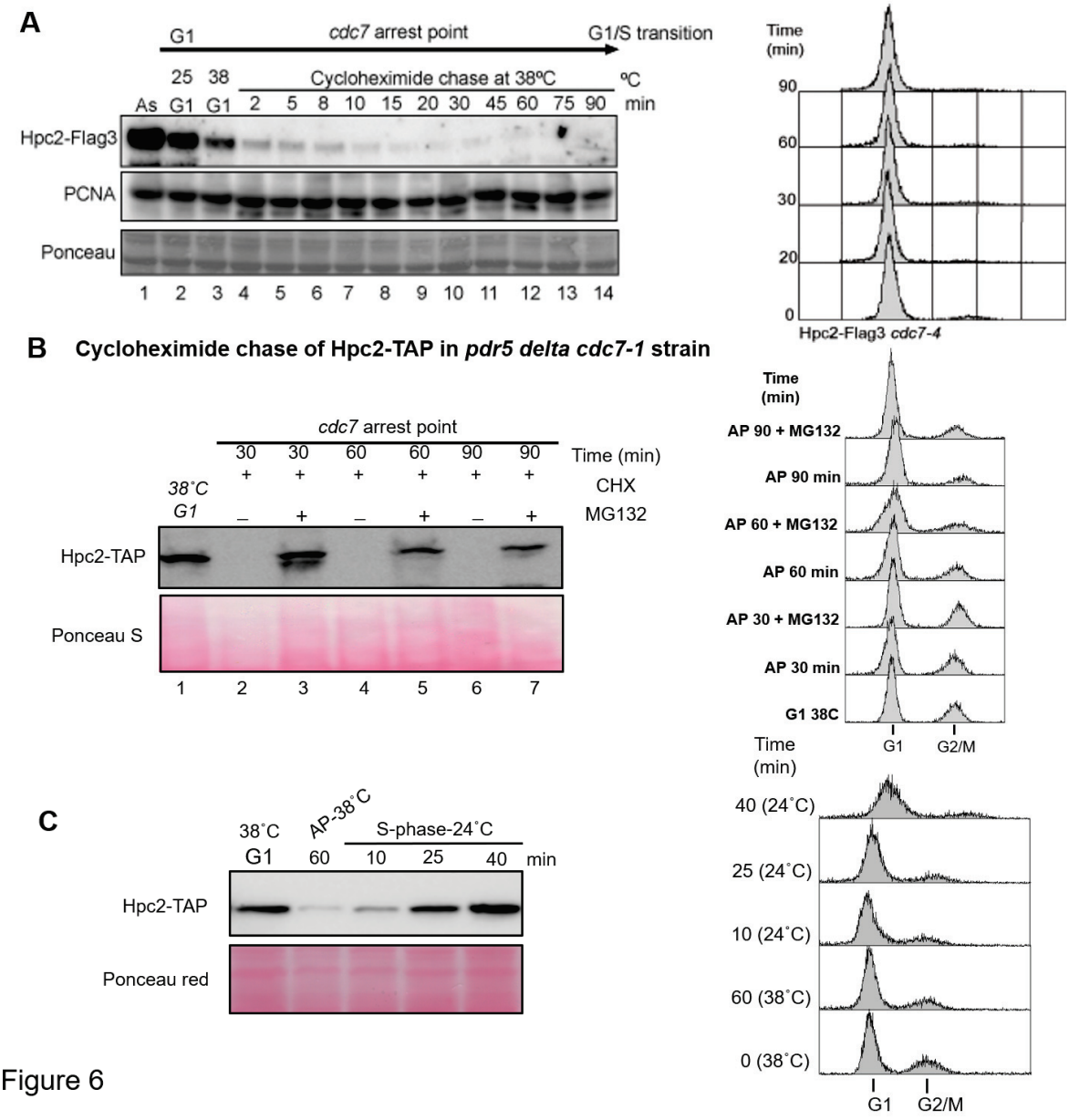
A
G1
cdc7 arrest point
G1/S transition
25 38
Cycloheximide chase at 38ºC
ºC
As G1 G1 2 5 8 10 15 20 30 45 60 75 90 min
Hpc2-Flag3
PCNA
Ponceau
1 2 3 4 5 6 7 8 9 10 11 12 13 14
Time (min)
90
60
30
20
0
Hpc2-Flag3 cdc7-4
B Cycloheximide chase of Hpc2-TAP in pdr5 delta cdc7-1 strain
cdc7 arrest point
30 30 60 60 90 90 Time (min)
38˚C
G1
CHX
MG132
Hpc2-TAP
Ponceau S
1 2 3 4 5 6 7
Time (min)
AP 90 + MG132
AP 90 min
AP 60 + MG132
AP 60 min
AP 30 + MG132
AP 30 min
G1 38C
G1
G2/M
C
38˚C
G1
AP-38˚C
S-phase-24˚C
60 10 25 40 min
Hpc2-TAP
Ponceau red
Time (min)
40 (24˚C)
25 (24˚C)
10 (24˚C)
60 (38˚C)
0 (38˚C)
G1
G2/M

Figure 6

Figure 6. Hpc2 is degraded during the G1-S transition and early S-phase but is stabilized in mid- to late S-phase.

(A) *HPC2-FLAG3 cdc7-4* cells were released from α-factor at 38°C and blocked at the *cdc7* arrest point. Hpc2-FLAG3 was detected by immunoblotting. Ponceau S staining is shown as loading control. Cell synchronization was monitored by FACS.

(B) Cycloheximide chase of *HPC2-TAP pdr5*Δ *cdc7-1* cells that were released from α-factor at 38°C and kept at the *cdc7-4* arrest point for the entire time course. When cells reached the *cdc7-4* arrest point, cycloheximide alone (CHX, 250 μg/ml), MG132 (50μM) or CHX + MG132 were added for 30, 60 or 90 min. Hpc2-TAP was detected by immunoblotting. Ponceau S staining is shown as loading control.

(C) *HPC2-TAP cdc7-1* cells were released from α-factor arrest at 38°C and held at the *cdc7* arrest point (AP - 38°C) for 60 min. Cells were then released in S-phase at 24°C for 10, 25 or 40 min corresponding to early-, mid- and mid/late S-phase monitored by FACS for DNA content. Hpc2-TAP was detected by immunoblotting. Ponceau S staining is shown as loading control.

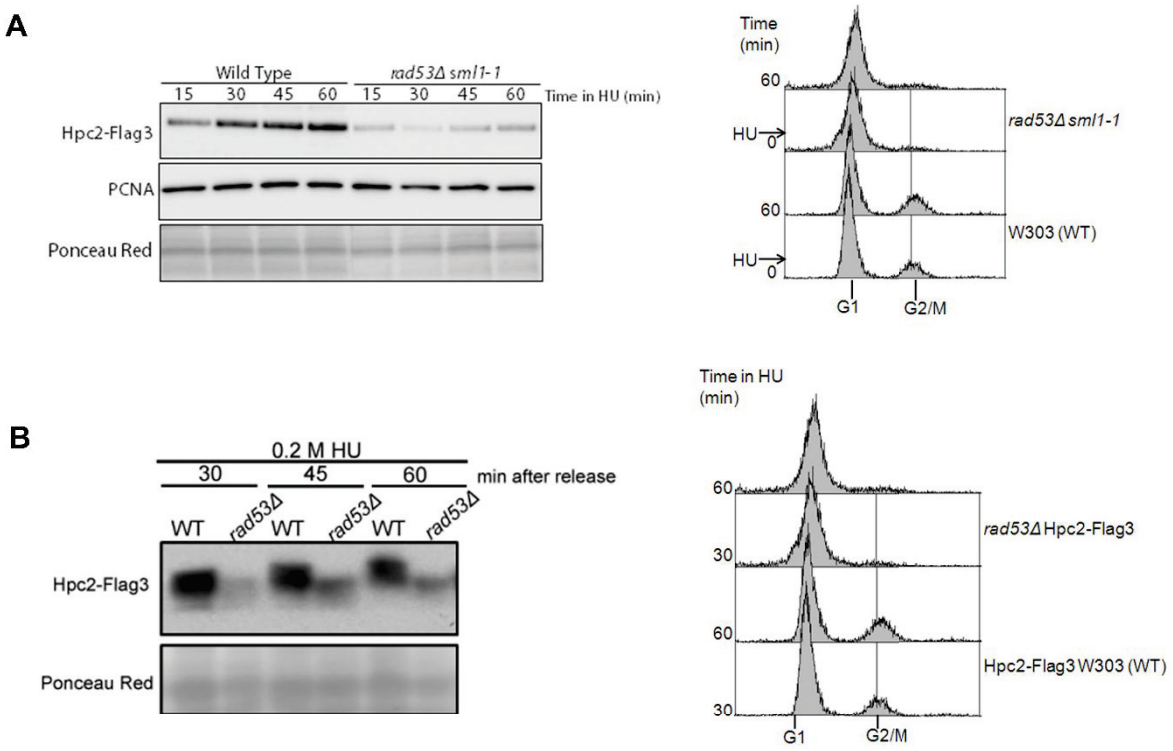
A
Wild Type
rad53Δ sml1-1
15 30 45 60 15 30 45 60
Time in HU (min)
Hpc2-Flag3
PCNA
Ponceau Red
Time (min)
60
HU
0
rad53Δ sml1-1
60
HU
0
W303 (WT)
G1
G2/M
B
0.2 M HU
30 45 60
min after release
WT rad53Δ WT rad53Δ WT rad53Δ
Hpc2-Flag3
Ponceau Red
Time in HU (min)
60
rad53Δ Hpc2-Flag3
30
60
Hpc2-Flag3 W303 (WT)
30
G1
G2/M

Figure 7

Figure 7. Rad53 is required to stabilize Hpc2 in response to hydroxyurea.

(A) Wild-type and *rad53* null mutant cells expressing Hpc2-FLAG3 were released from α-factor arrest at 30°C in medium containing 0.2M HU. Aliquots of the culture were then collected every 15 min for up to 60 min and Hpc2-FLAG3 detected by immunoblotting. Ponceau S staining and a PCNA immunoblot are shown as loading controls. The block in DNA replication caused by HU was monitored by FACS.

(B) Wild-type cells expressing Hpc2-Flag3 were synchronized with α-factor and released towards S-phase at 30°C for up to 60 min in medium containing 0.2M HU. Hpc2-Flag3 protein phosphorylation and mobility were detected by immunoblotting from a Phos-tag gel. Ponceau S is shown shown as loading control.

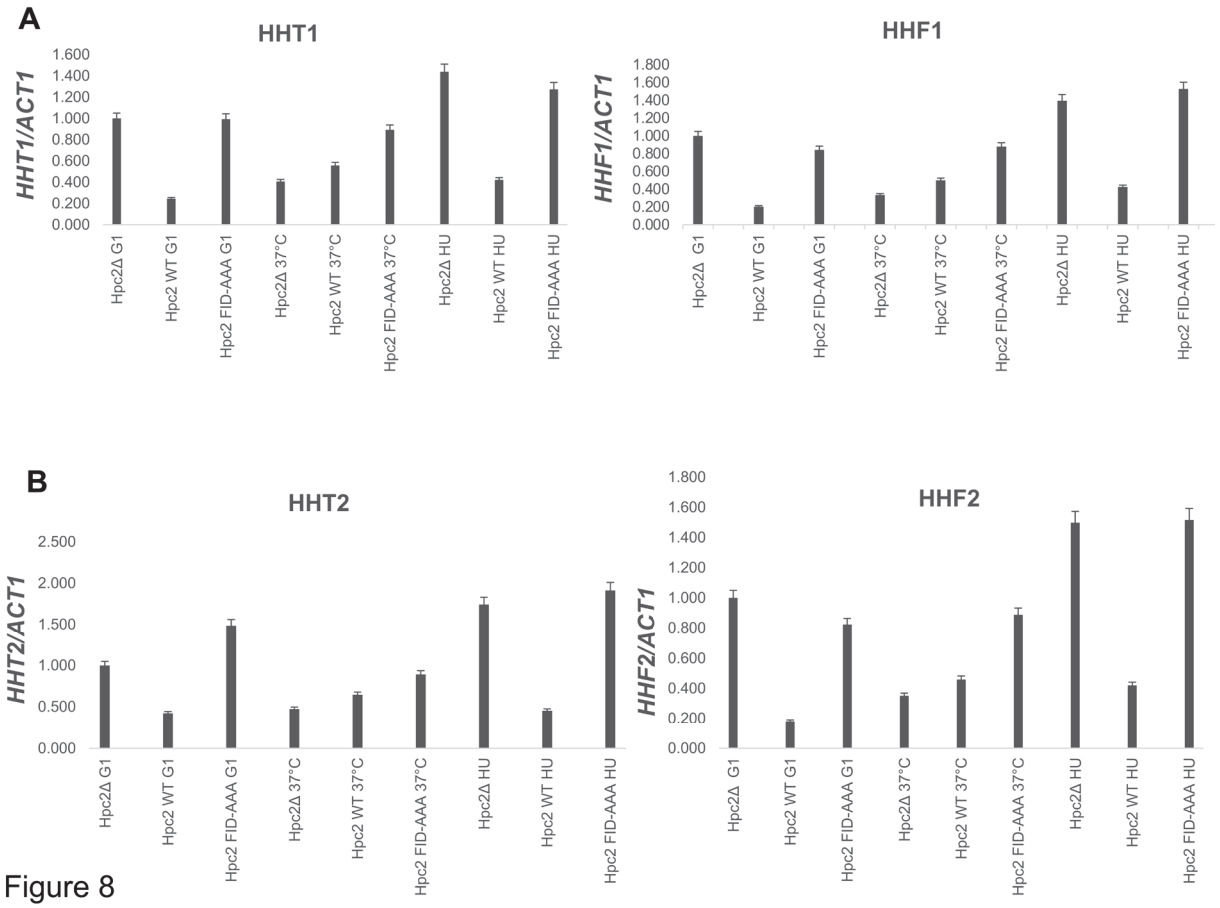
A
HHT1
HHT1/ACT1
1.600
1.400
1.200
1.000
0.800
0.600
0.400
0.200
0.000
Hpc2Δ G1
Hpc2 WT G1
Hpc2 FID-AAA G1
Hpc2Δ 37°C
Hpc2 WT 37°C
Hpc2 FID-AAA 37°C
Hpc2Δ HU
Hpc2 WT HU
Hpc2 FID-AAA HU
HHF1
HHF1/ACT1
1.800
1.600
1.400
1.200
1.000
0.800
0.600
0.400
0.200
0.000
Hpc2Δ G1
Hpc2 WT G1
Hpc2 FID-AAA G1
Hpc2Δ 37°C
Hpc2 WT 37°C
Hpc2 FID-AAA 37°C
Hpc2Δ HU
Hpc2 WT HU
Hpc2 FID-AAA HU
B
HHT2
HHT2/ACT1
2.500
2.000
1.500
1.000
0.500
0.000
Hpc2Δ G1
Hpc2 WT G1
Hpc2 FID-AAA G1
Hpc2Δ 37°C
Hpc2 WT 37°C
Hpc2 FID-AAA 37°C
Hpc2Δ HU
Hpc2 WT HU
Hpc2 FID-AAA HU
HHF2
HHF2/ACT1
1.800
1.600
1.400
1.200
1.000
0.800
0.600
0.400
0.200
0.000
Hpc2Δ G1
Hpc2 WT G1
Hpc2 FID-AAA G1
Hpc2Δ 37°C
Hpc2 WT 37°C
Hpc2 FID-AAA 37°C
Hpc2Δ HU
Hpc2 WT HU
Hpc2 FID-AAA HU

Figure 8

Figure 8. Mutation of Hpc2 FID residues interfere with the downregulation of histone transcripts that follows inhibition of DNA replication.

(A, B) The Hpc2 FID-AAA mutant is defective in downregulating the *HHF1, HHF2* and *HHT1, HHT2* transcripts upon HU treatment. Exponentially growing cultures of wild-type or *hpc2* mutant cells carrying a *cdc7-4* mutation were arrested with α-factor, and released towards S-phase at the restrictive temperature of 38°C for 60 minutes. This was followed by release at 25°C for 60 minutes in 200mM HU. Total RNA was extracted from the different samples and histone mRNA abundance was determined by qRT-PCR. Histone mRNA levels were normalized to those of *ACT1*. The *m*RNA levels in each sample were expressed relative to the levels observed in *hpc2*Δ G1 cells, which were arbitrarily set to one.

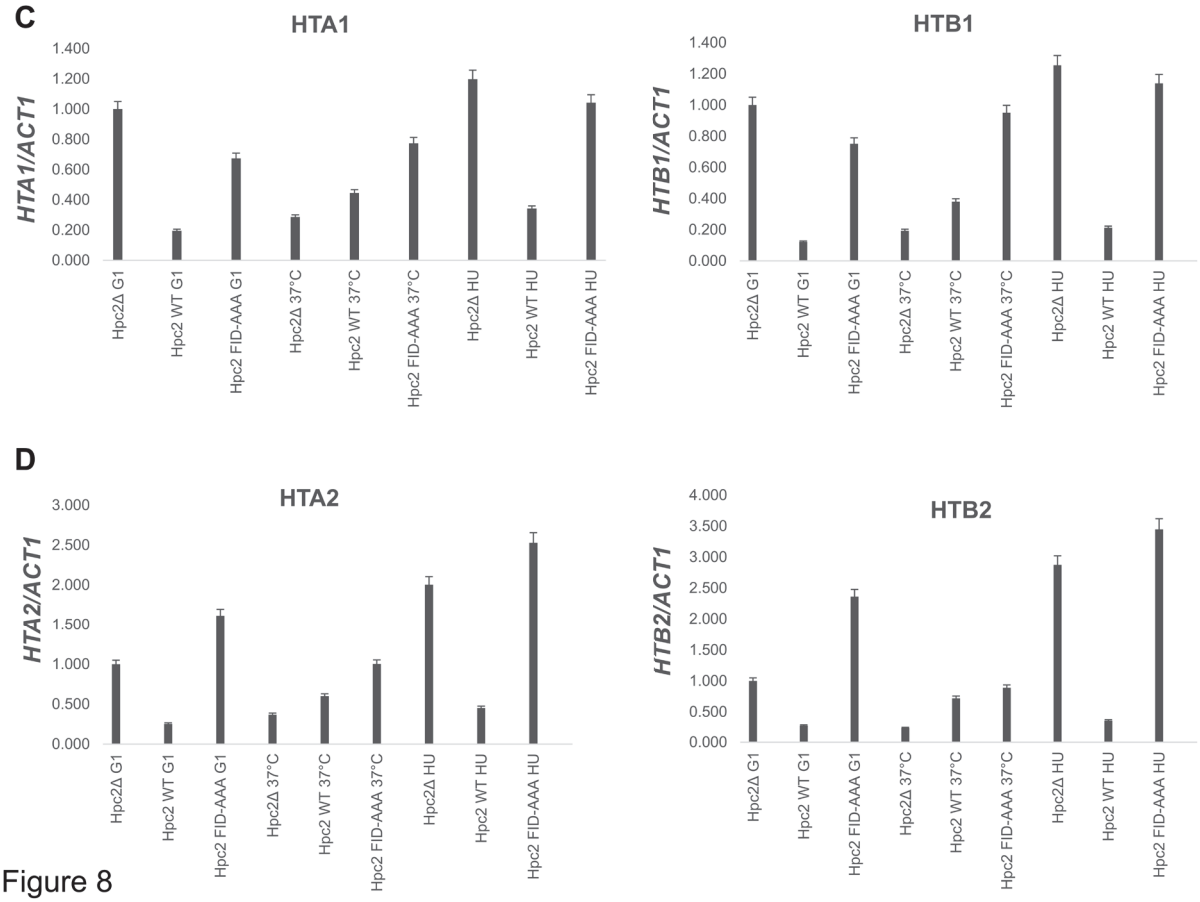
C
HTA1
HTA1/ACT1
1.400
1.200
1.000
0.800
0.600
0.400
0.200
0.000
Hpc2Δ G1
Hpc2 WT G1
Hpc2 FID-AAA G1
Hpc2Δ 37°C
Hpc2 WT 37°C
Hpc2 FID-AAA 37°C
Hpc2Δ HU
Hpc2 WT HU
Hpc2 FID-AAA HU
HTB1
HTB1/ACT1
1.400
1.200
1.000
0.800
0.600
0.400
0.200
0.000
Hpc2Δ G1
Hpc2 WT G1
Hpc2 FID-AAA G1
Hpc2Δ 37°C
Hpc2 WT 37°C
Hpc2 FID-AAA 37°C
Hpc2Δ HU
Hpc2 WT HU
Hpc2 FID-AAA HU
D
HTA2
HTA2/ACT1
3.000
2.500
2.000
1.500
1.000
0.500
0.000
Hpc2Δ G1
Hpc2 WT G1
Hpc2 FID-AAA G1
Hpc2Δ 37°C
Hpc2 WT 37°C
Hpc2 FID-AAA 37°C
Hpc2Δ HU
Hpc2 WT HU
Hpc2 FID-AAA HU
HTB2
HTB2/ACT1
4.000
3.500
3.000
2.500
2.000
1.500
1.000
0.500
0.000
Hpc2Δ G1
Hpc2 WT G1
Hpc2 FID-AAA G1
Hpc2Δ 37°C
Hpc2 WT 37°C
Hpc2 FID-AAA 37°C
Hpc2Δ HU
Hpc2 WT HU
Hpc2 FID-AAA HU

Figure 8

Figure 8. Mutation of Hpc2 FID residues interfere with the downregulation of histone transcripts that follows inhibition of DNA replication.

(C, D) The Hpc2 FID-AAA mutant is defective in downregulating the *HTA1*, *HTB1, HTA2*, and *HTB2* transcripts upon HU treatment.

Exponentially growing cultures of wild-type or *hpc2* mutant cells carrying a *cdc7-4* mutation were arrested with α-factor, and released towards S-phase at the restrictive temperature of 38°C for 60 minutes. This was followed by release at 25°C for 60 minutes in 200mM HU. Total RNA was extracted from the different samples and histone mRNA abundance was determined by qRT-PCR. Histone mRNA levels were normalized to those of *ACT1*. The *m*RNA levels in each sample were expressed relative to the levels observed in *hpc2*Δ G1 cells, which were arbitrarily set to one.

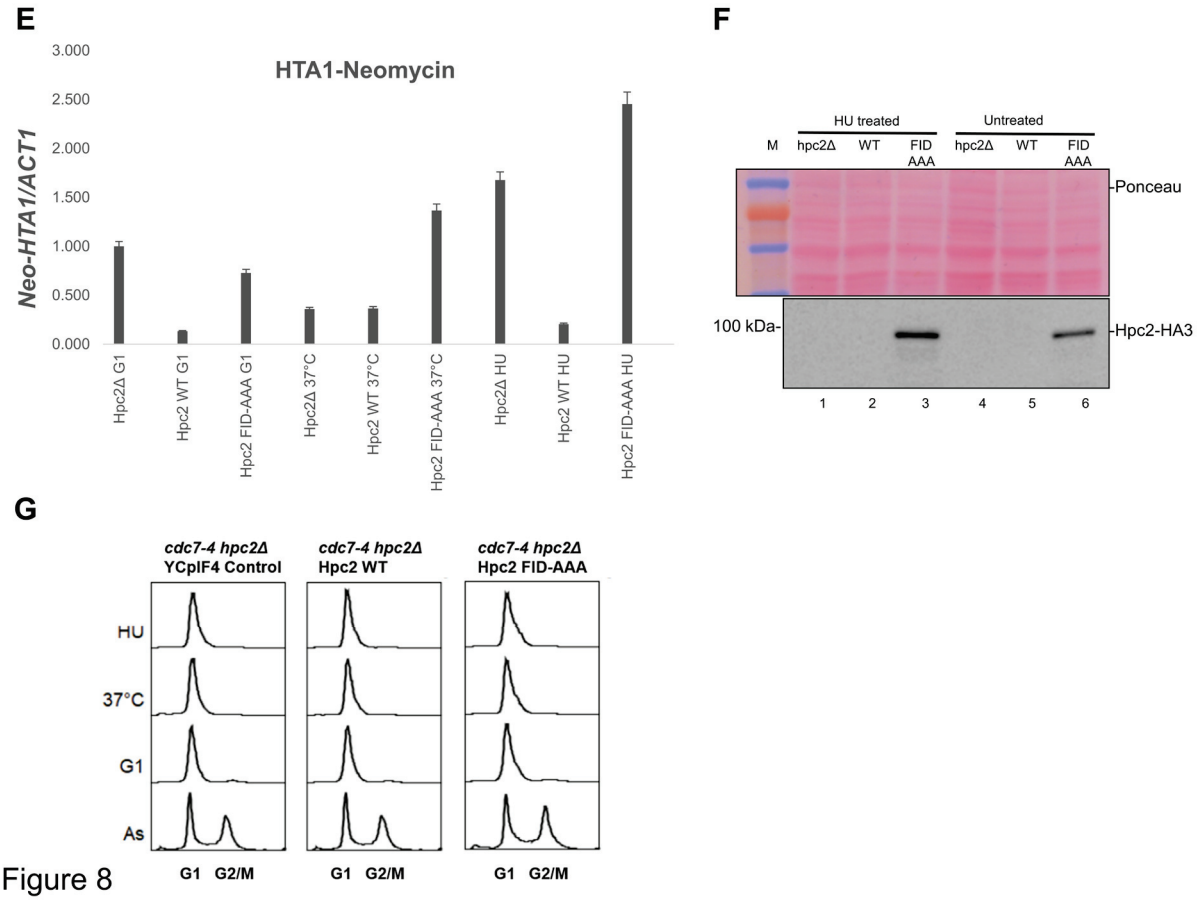
E
HTA1-Neomycin
Neo-HTA1/ACT1
3.000
2.500
2.000
1.500
1.000
0.500
0.000
Hpc2Δ G1
Hpc2 WT G1
Hpc2 FID-AAA G1
Hpc2Δ 37°C
Hpc2 WT 37°C
Hpc2 FID-AAA 37°C
Hpc2Δ HU
Hpc2 WT HU
Hpc2 FID-AAA HU
F
HU treated
Untreated
M
hpc2Δ
WT
FID AAA
hpc2Δ
WT
FID AAA
Ponceau
100 kDa-
Hpc2-HA3
1
2
3
4
5
6
G
cdc7-4 hpc2Δ YCpIF4 Control
cdc7-4 hpc2Δ Hpc2 WT
cdc7-4 hpc2Δ Hpc2 FID-AAA
HU
37°C
G1
As
G1 G2/M
G1 G2/M
G1 G2/M

Figure 8

Figure 8. Mutation of Hpc2 FID residues interfere with the downregulation of histone transcripts that follows inhibition of DNA replication.

(E) The Hpc2 FID-AAA mutant is defective in downregulating an *HTA1* promoter-driven *Neomycin* reporter mRNA upon HU treatment.

(F) The Hpc2-HA3 FID-AAA mutation does not destabilize the protein (lanes 3 and 6). The wild-type Hpc2-HA3 was undetectable under those conditions. Hpc2-HA3 levels was detected by immunoblotting in asynchronously growing cell populations. Ponceau S is shown as loading control.

(G) DNA contents of asynchronous (As) cells, cells arrested in α-factor (G1), cells blocked at the *cdc7-4* arrest point (37°C) and cells released from the *cdc7-4* arrest point in medium containing 0.2M hydroxyurea (HU).

Exponentially growing cultures of wild-type or *hpc2* mutant cells carrying a *cdc7-4* mutation were arrested with α-factor, and released towards S-phase at the restrictive temperature of 38°C for 60 minutes. This was followed by release at 25°C for 60 minutes in 200mM HU. Total RNA was extracted from the different samples and histone mRNA abundance was determined by qRT-PCR. Histone mRNA levels were normalized to those of *ACT1*. The *m*RNA levels in each sample were expressed relative to the levels observed in *hpc2*Δ G1 cells, which were arbitrarily set to one.

A

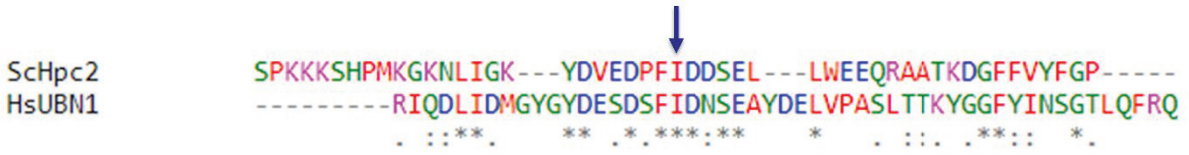
ScHpc2 SPKKKSHPMKGKNLIGK---YDVEDPFIDDSEL---LWEEQRAATKDGFFVYFGP-----
HsUBN1 ---------RIQDLIDMGYGYDESDSFIDNSEAYDELVPASLTTKYGGFYINSGTLQFRQ

B


ScH3 MARTKQTARKSTGGKAPRKQLASKAARKSAPSTGGVKKPHRYKPGTVALREIRRFQKSTE
HsH3.3 MARTKQTARKSTGGKAPRKQLATKAARKSAPSTGGVKKPHRYRPGTVALREIRRYQKSTE
HsH3.1 MARTKQTARKSTGGKAPRKQLATKAARKSAPATGGVKKPHRYRPGTVALREIRRYQKSTE
ScH3 LLIRKLPFQRLVREIAQDFKTDLRFQSSAIGALQESVEAYLVSLFEDTNLAAIHAKRVTI
HsH3.3 LLIRKLPFQRLVREIAQDFKTDLRFQSAAIGALQEASEAYLVGLFEDTNLCAIHAKRVTI
HsH3.1 LLIRKLPFQRLVREIAQDFKTDLRFQSSAVMALQEACEAYLVGLFEDTNLCAIHAKRVTI
ScH3 QKKDIKLARRLRGERS
HsH3.3 MPKDIQLARRIRGERA
HsH3.1 MPKDIQLARRIRGERA

Figure 9

Figure 9. Conservation of the Hpc2-Related Domain (HRD) and H3.3 family members.

(A) Sequences of *S. cerevisiae* Hpc2 (ScHpc2) and the Hpc2-related domain (HRD) of *Homo sapiens* UBN1 (HsUBN1) The FID residues are indicated by an arrow.

(B) Sequence comparison of *S. cerevisiae* H3 (ScH3), *H. sapiens* H3.3 (HsH3.3, replication-*independent*) and *H. sapiens* H3.1 (HsH3.1, replication-*dependent*). The key residue that drives H3.3 towards the replication-*independent* nucleosome assembly pathway is Gly90 (excluding the N-terminal Met) in ScH3 and HsH3.3 (indicated by an arrow), which is a Met in HsH3.1.

Supplementary Figures

44- ETGpSDSEDLFNK -55 pSer47
m/z_{obs} = 711.2769 $^{(2+)}$
m/z_{theo} = 711.2770 $^{(2+)}$

Figure S1a

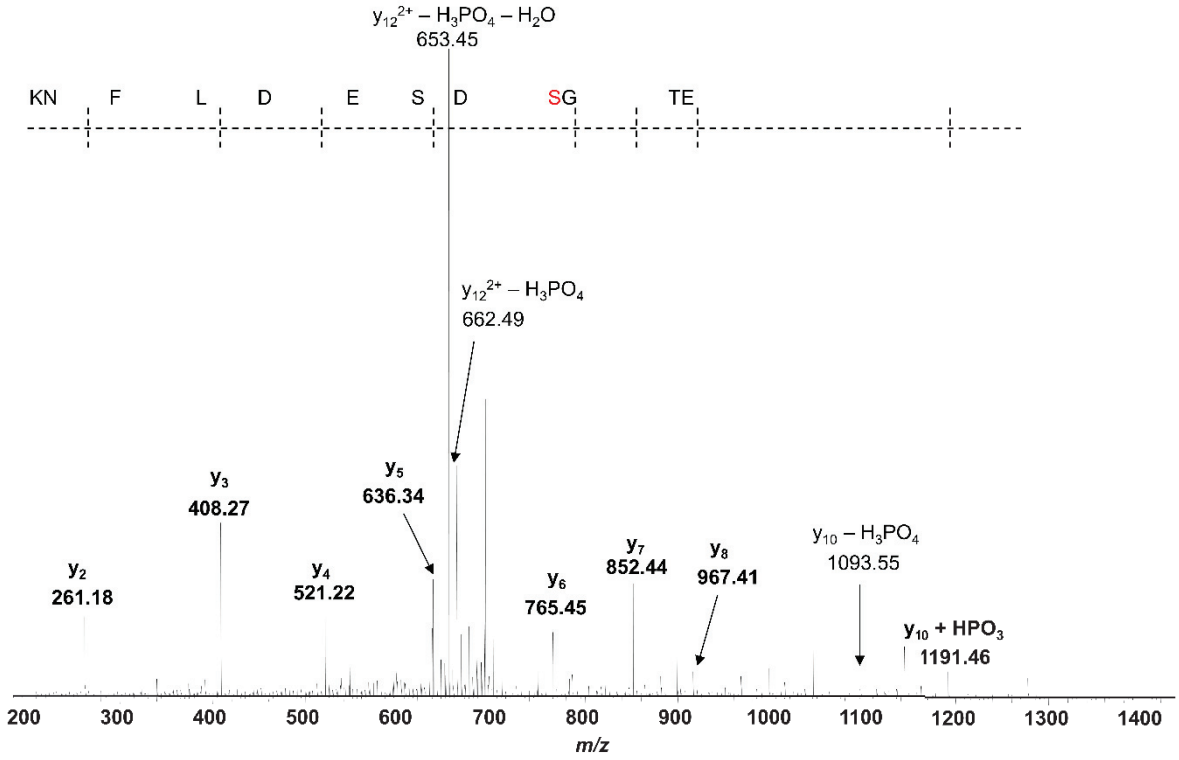

168-ISSLLpTISSNEDSK-181 pThr173
m/z_{obs} = 787.3711 $^{(2+)}$
m/z_{theo} = 787.3715 $^{(2+)}$

Figure S1b

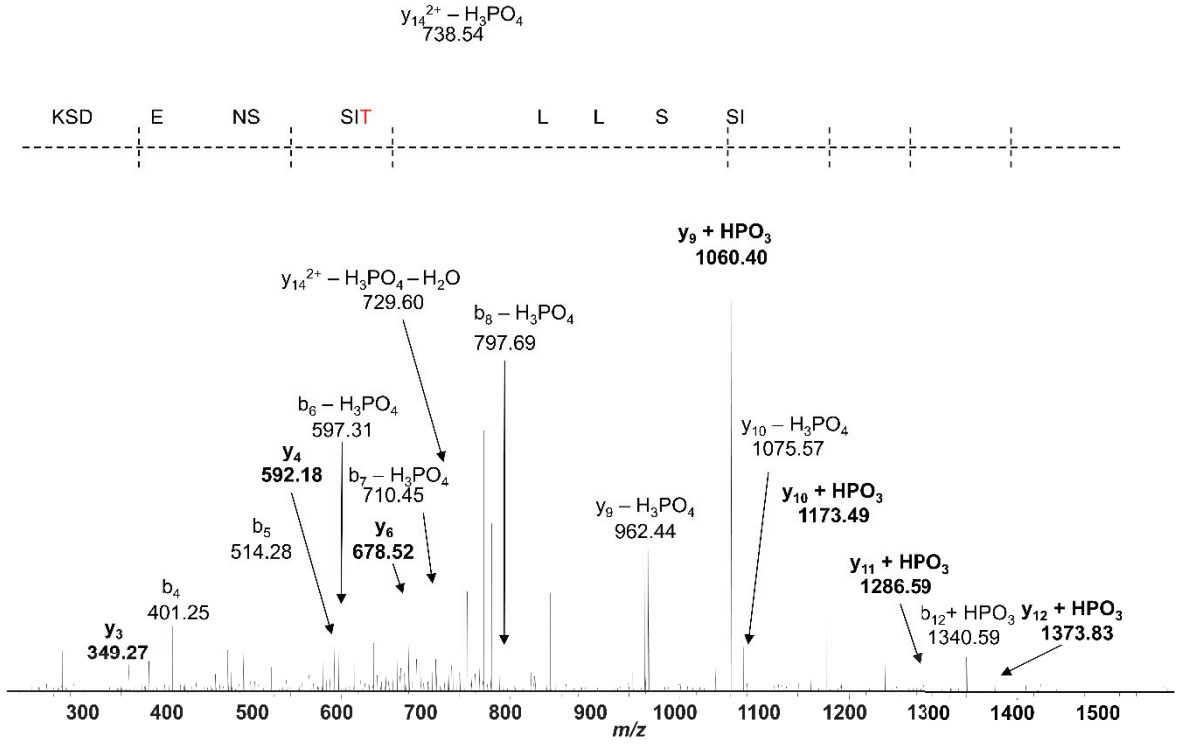

Figure S1c

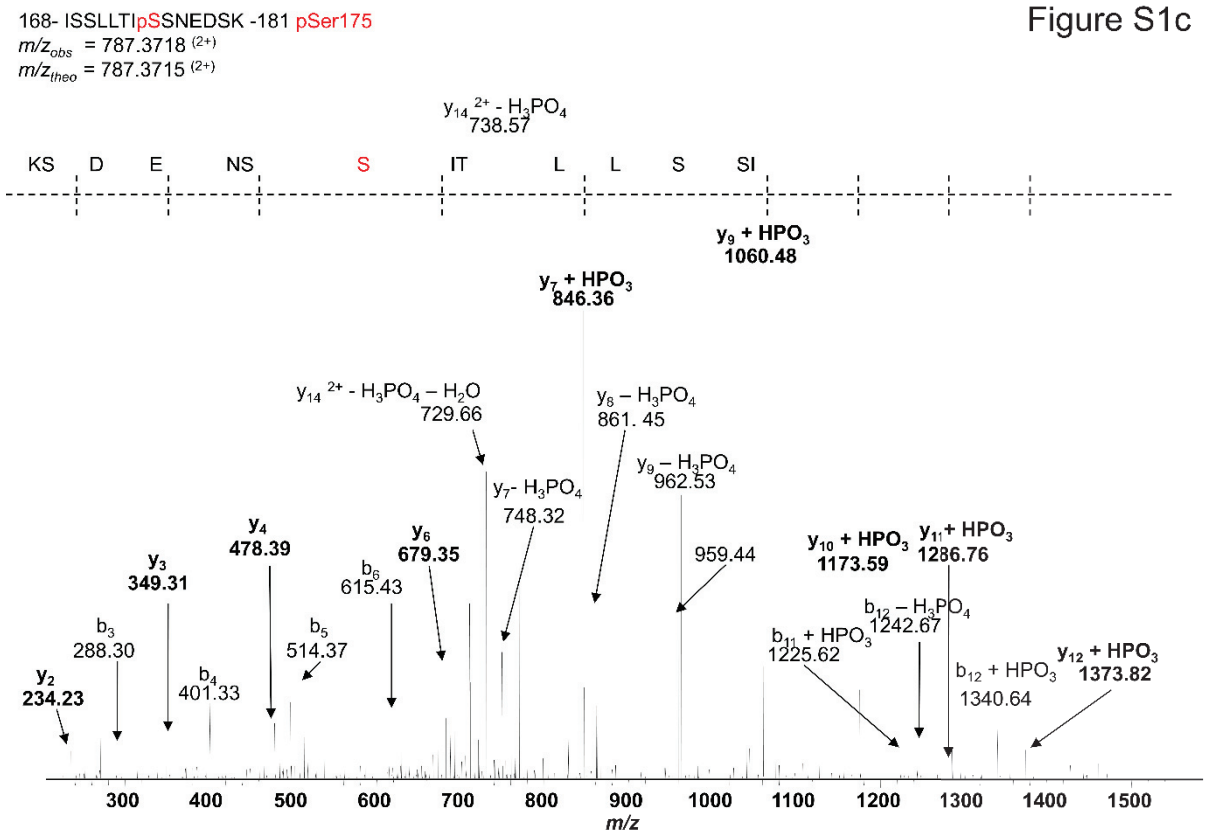
168- ISSLLTIpSSNEDSK -181 pSer175
m/z_obs = 787.3718 (2+)
m/z_theo = 787.3715 (2+)
y14 2+ - H3PO4 738.57
KS D E NS S IT L L S SI
y9 + HPO3 1060.48
y7 + HPO3 846.36
y14 2+ - H3PO4 – H2O 729.66
y8 – H3PO4 861. 45
y9 – H3PO4 962.53
y7- H3PO4 748.32
959.44
y4 478.39
y6 679.35
y3 349.31
b6 615.43
b3 288.30
b5 514.37
b4 401.33
y2 234.23
y10 + HPO3 1173.59
y11+ HPO3 1286.76
b12 – H3PO4 1242.67
b11 + HPO3 1225.62
b12 + HPO3 1340.64
y12 + HPO3 1373.82
300 400 500 600 700 800 900 1000 1100 1200 1300 1400 1500
m/z

263- TSSPVNLDVEpSTAQSLGK -280 pSer273
m/z_{obs} = 956.9479 $^{(2+)}$
m/z_{theo} = 956.9485 $^{(2+)}$

Figure S1d

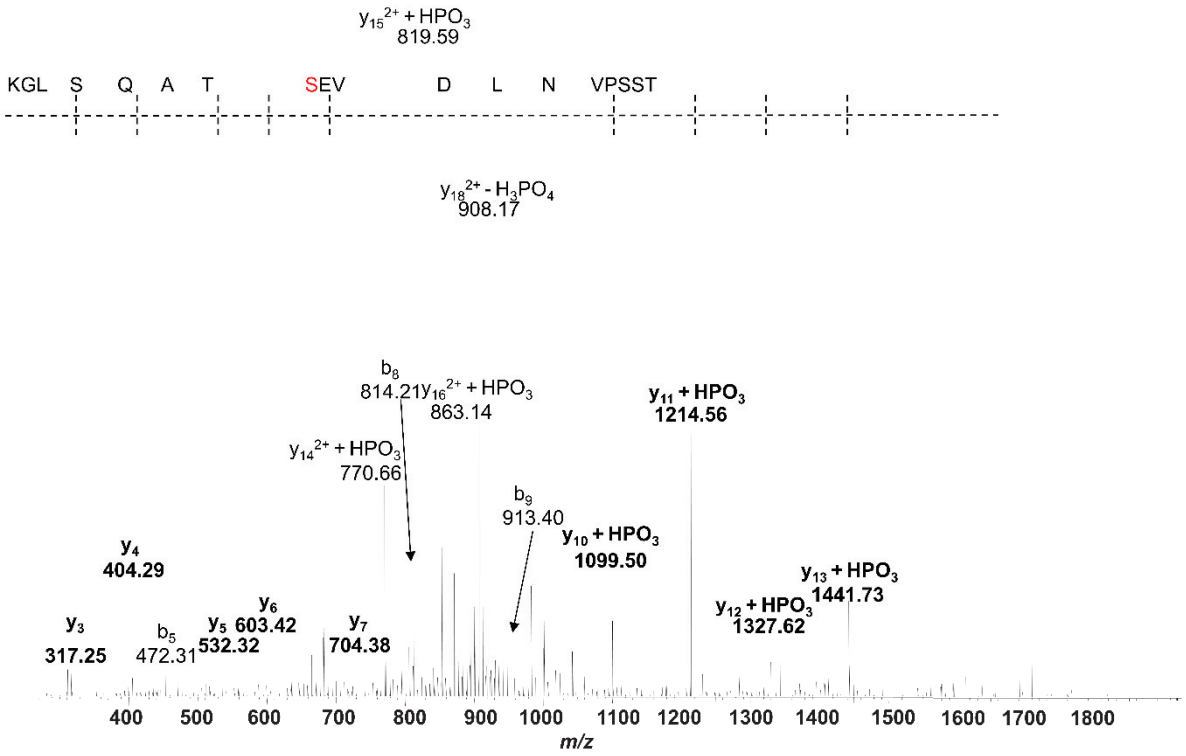

281- FNKp(ST)NSLK -289 pSer284 or pThr285
m/z_{obs} = 559.7657 $^{(2+)}$
m/z_{theo} = 559.7657 $^{(2+)}$

Figure S1e

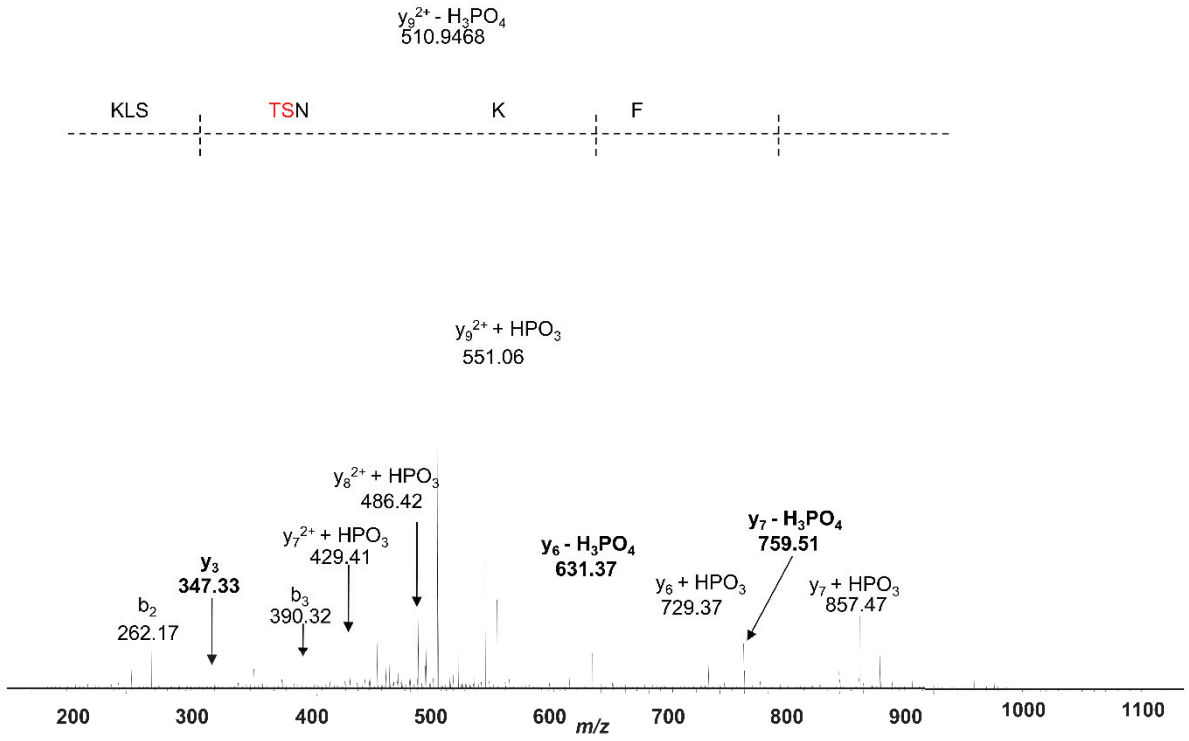

290- AALpTKAPAEK -299 pThr293
m/z_{obs} = 540.2776 $^{(2+)}$
m/z_{theo} = 540.2785 $^{(2+)}$

Figure S1f

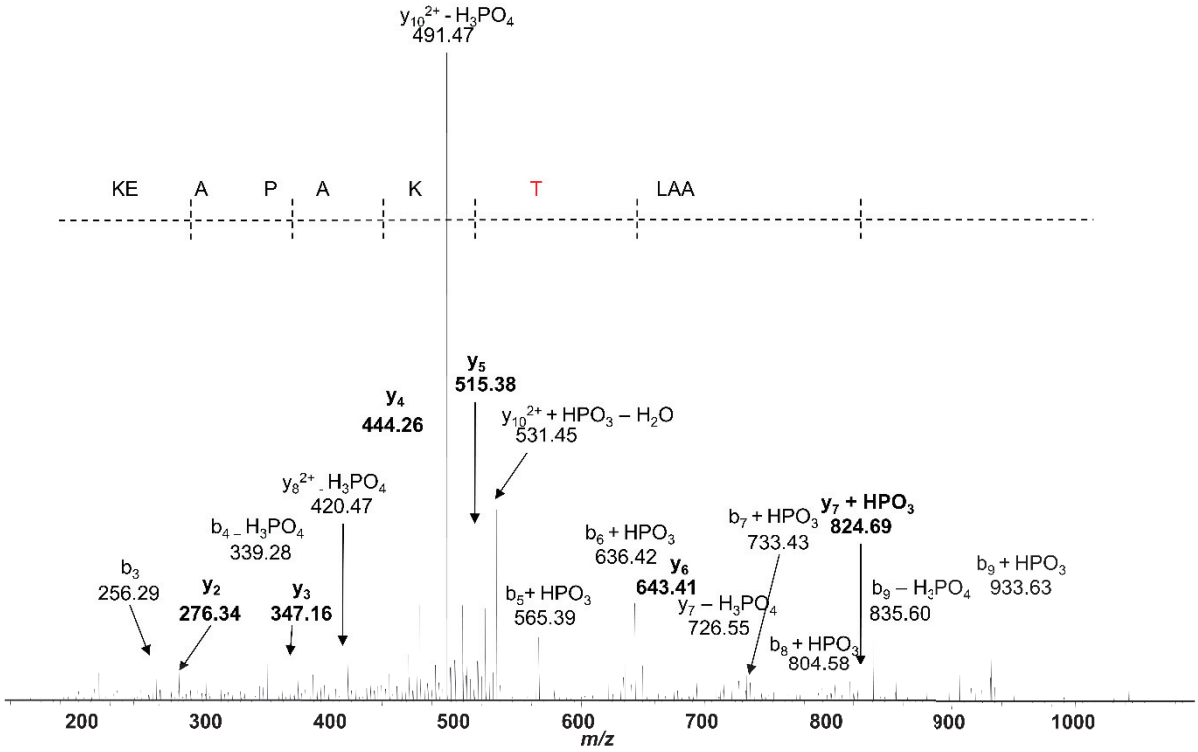

305- SIpSSVTNSDSNISSSK -320 pSer307
m/z_{obs} = 846.8649 $^{(2+)}$
m/z_{theo} = 846.8698 $^{(2+)}$

Figure S1g

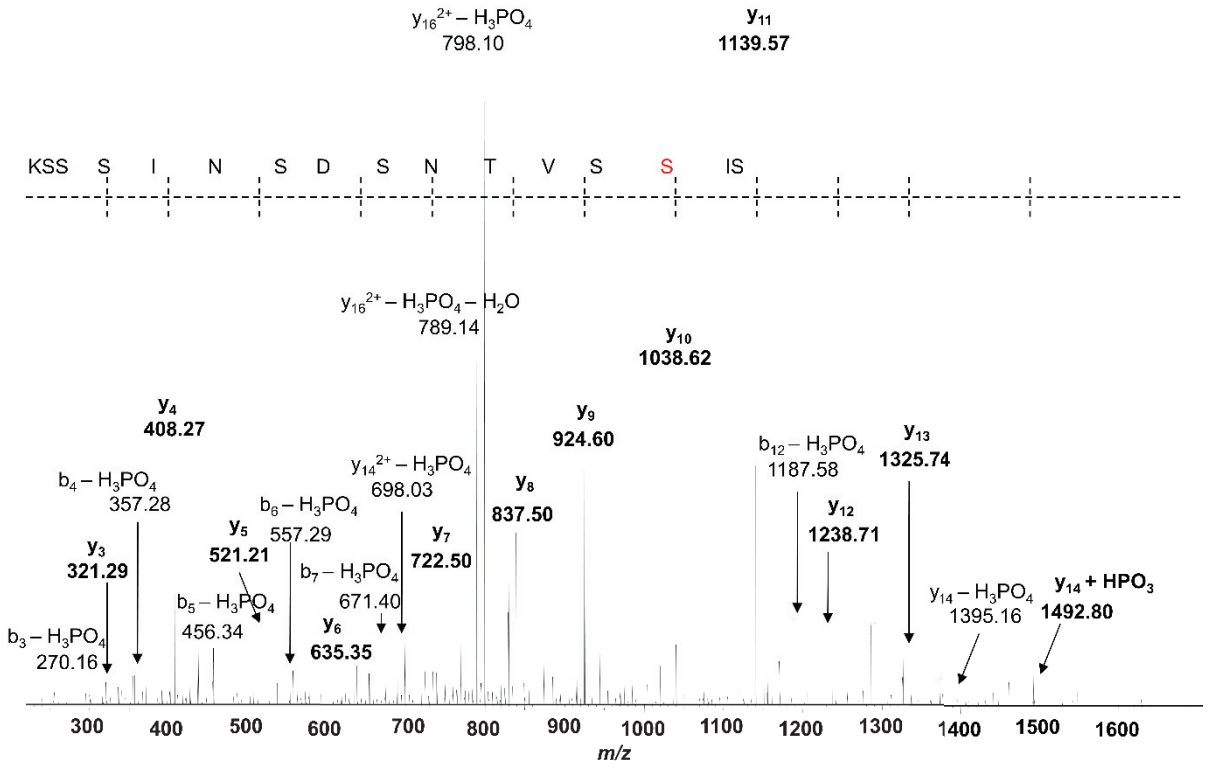

307- SISSVTNpSDSNISSSK -320 pSer314
m/z_{obs} = 846.8701 $^{(2+)}$
m/z_{theo} = 846.8698 $^{(2+)}$

Figure S1h

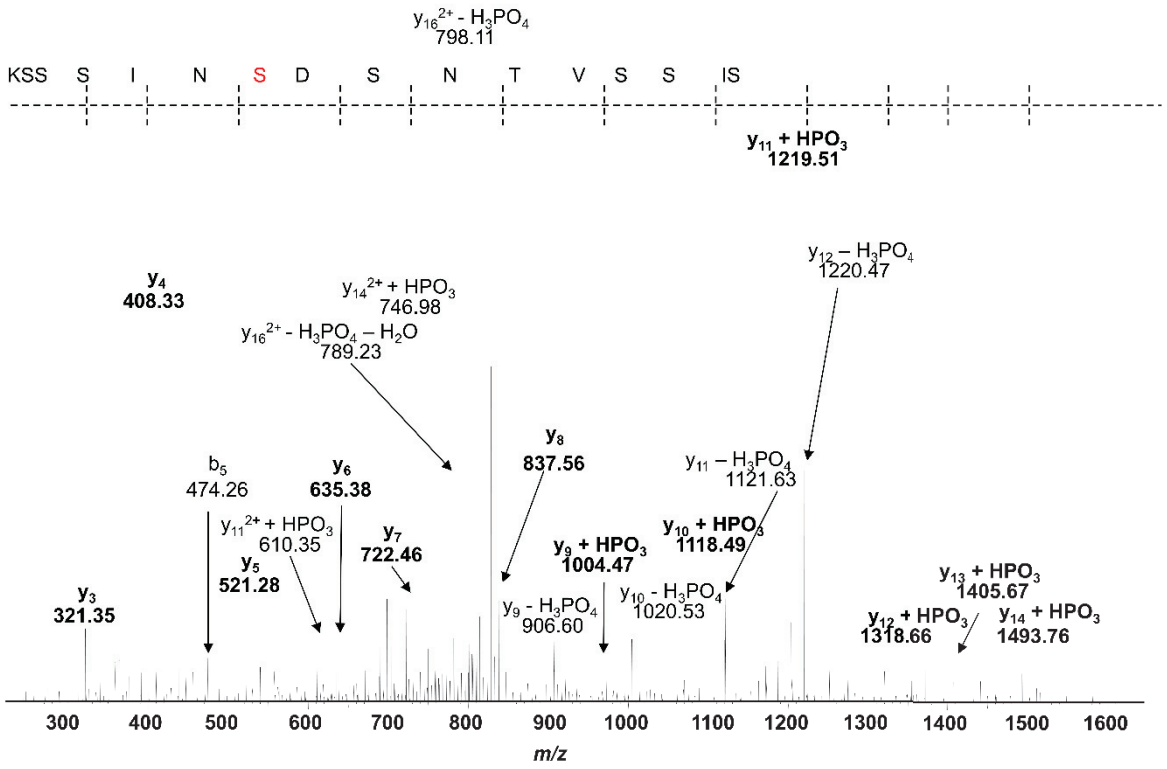

329- KSSpSASAILPKPTTTK -344 pSer332
m/z_{obs} = 566.3009 (3+)
m/z_{theo} = 566.3013 (3+)

Figure S1i

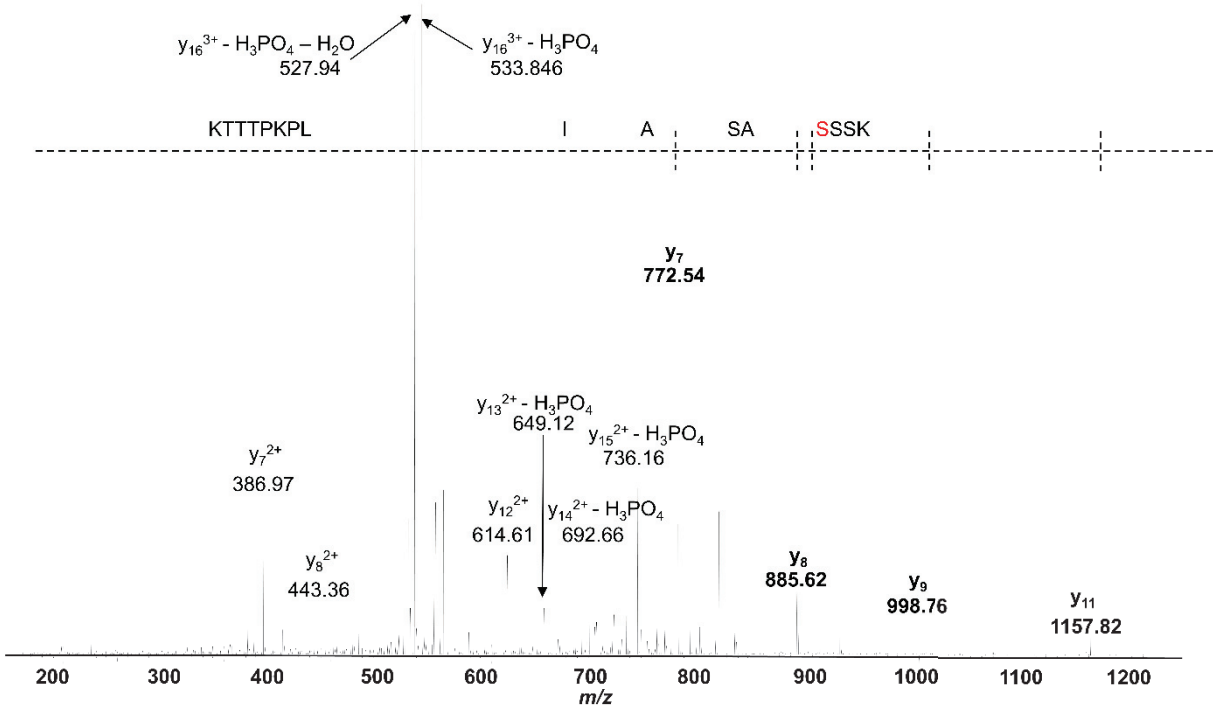

Supplementary Table 1

Hpc2 Phosphorylation sites

Phosphorylated residue	Peptide	Identified	Reference
Ser47	44-ETG**pS**DSEDLFNK-55	*In vitro*	This study
Thr173	168-ISSLL**pT**ISSNEDSK-181	*In vitro*	"
Ser175	168-ISSLLT**pS**SNEDSK-181	*In vitro*	"
Ser273	263-TSSPVNLDVE**pS**TAQSLGK-280	*In vitro*	"
Ser284 or Ser285	281-FNK**p(ST)**NSLK-289	*In vitro*	"
Thr293	290-AAL**pT**KAPAEK-299	*In vitro*	"
Ser307	305-SI**pS**SVTNSDSNISSSK-320	*In vitro*	"
		In vivo	Chen *et al*, 2010
Ser312	305-SISSVTN**pS**DSNISSSK-320	*In vitro*	This study
		In vivo	Chen *et al*, 2010
Ser332	329-KSS**pS**ASAILPKPTTTK-344	*In vitro*	This study
		In vivo	"

Supplementary Table S1

Supplementary Table 2

Hpc2 mutants tested for HU induced histone gene repression *in vivo*

Hpc2 phospho-mutant strain	Defect in HU-induced histone gene repression
S307-308A	No
S305-307-308-310A	Yes
S312-314A	No
S312-314D	No
S317-318-319A	No
S317-318-319D	No
S330-S332A	Yes
S330-S332D	Yes
T45D S47D S49D	No
S83D	No
S223A S224A	No
S223D S224D	No
T263V S264A S265A	No
T263D S264D S265D	No
S338A S389A S391A S392A	No
S338D S389D S391D S392D	No
S435A	No
S435D	No

Supplementary Table S2

Supplementary Table 3

Yeast strains used in the study

Strain	Genotype	Reference
W303-1a	*MATa ho ade2-1 trp1-1 can1-100 leu2-3, 112 his3-11, 15 ura 3-1*	Thomas and Rothstein, 1989
U960-5C	*MATa rad53:: HIS3 sml1-1 RAD5+*	Zhao et al., 1998
CY2034	*MATa rad53K227A:: KanMX4*	Pellicioli et al., 1999
U953-61A	*MATa mec1::TRP1 sml1::HIS3 RAD5+*	Zhao et al., 1998
Y662	*MATa tel1::HIS3*	D'Amours and Jackson, 2001
DDY064	*MATa mec1::TRP1 tel1::HIS3 sml1-1*	D'Amours and Jackson, 2001
YAG126	*MATa hir1::HIR1-FLAG3-HIS3 rad53::RAD53-TAP-TRP1*	This study
YAG127	*MATa hir2::HIR2-FLAG3-HIS3 rad53::RAD53-TAP-TRP1*	This study
YDL74	*MATa hir3::HIR3-FLAG3-LEU2 rad53::RAD53-TAP-TRP1*	This study
YDL79	*MATa hpc2::HPC2-FLAG3-LEU2*	This study
YKB2	*MATa cdc7-4*	Bousset and Diffley, 1998
YVV64	*MATa cdc7-4 hpc2::HIS3*	This study
YDL82	*MATa cdc7-4 hpc2::HPC2-FLAG3-LEU2*	This study
YVV124	*MATa hir2::HIR2-TAP-HIS3 hpc2::KANMX*	This study
YVV120	*W303 MATa hpc2Δ::KanMX his3Δ1 leu2Δ0 met15Δ0 ura3Δ0*	This study
YHW	*W303 MATa cdc7-4 hpc2Δ::KanMX*	This study
YAGN 20-1	*W303 MATa cdc7-4 hpc2Δ:KanMX [HTA1-Neo (Leu 2)]*	This study
YAGN 21-1	*W303 MATa cdc7-4 hpc2Δ:KanMX [HTA1-Neo (Leu 2)] [pRS416 HPC2wt-HA3 URA3]*	This study
YAGN 22-1	*W303 MATa cdc7-4 hpc2Δ:KanMX [HTA1-Neo (Leu 2)] [pRS416 HPC2FID-AAA-HA3 URA3]*	This study
YAGN 23-1	*W303 MATa cdc7-4 hpc2Δ:KanMX [HTA1-Neo (Leu 2)] [YCp1F4-URA3]*	This study

Supplementary Table S3

Supplementary Table 4

Table of DNA Primers

	Gene names	Forward primer sequence (5'-3')	Reverse primer sequence (5'-3')
1	HHF1	AGGTGGTGTCAAGCGTATTT	GTGTTCGGTGTAGGTAACAGAG
2	HHT1	GAAAGTCCACTGGTGGTAAGG	GGCTTATATCTGTGAGGCTTCTT
3	HHF2	CGGTAGAGGTAAAGGTGGTAAAG	CTGATAGCTGGCTTAGTGATACC
4	HHT2	AGACACTAATCTGGCTGCTATTC	TGATCTTTCACCTCTTAGTCTTCTG
5	HTA1	TGACATTCCCAGTCGGTAGA	TTCCAAGACAGCAGTCAAGTAG
6	HTB1	CCACTTCCACTGATGGTAAGAA	GAAATACCAGTGTCAGGGTGAG
7	HTA2	CCGGTGGTAAAGGTGGTAAA	CACTCTACCAACTGGGAATGTTA
8	HTB2	TCCAAACAGCCGTTAGATTGA	GCTTGAGTAGAGGAGGAGTATTTG
9	ACT1	GAGGTTGCTGCTTTGGTTATTG	ACCGACGATAGATGGGAAGA
10	HTA1-Neomycin	ACTGGGCACAACAGACAAT	CTCGTCCTGCAGTTCATTCA

Chapter 4: Discussion

4.1 Chapter 2 Discussion

4.1.1 Choreography of events at DNA replication forks

At each replication fork, there are numerous events that require binding of multiple proteins to PCNA. As an example, at each replication fork, the DNA helicase unwinds the double stranded DNA to create the single-stranded DNA templates necessary for DNA synthesis. The RFC clamp loader opens up the ring-shaped PCNA clamp and closes it around DNA at primer-template junctions, which are junctions between double-stranded and single-stranded DNA. Clamp closure around DNA is referred to as PCNA loading. This is thought to happen only once for leading strand synthesis, but for lagging strand synthesis RFC needs to load at least one PCNA clamp per Okazaki fragment. PCNA loading by RFC requires a PCNA Interaction Peptides (PIP) in RFC. Following PCNA loading, the first proteins that need to bind PCNA are the replicative DNA polymerases: Pol ε for leading strand synthesis and Pol δ for lagging strand synthesis. An evident question emerges at this early stage of DNA synthesis. How does the cell ensure that the first PCNA ring loaded by RFC becomes associated with Pol ε or Pol δ, as opposed to the myriad of functionally unrelated PCNA-binding proteins that are continuously present at DNA replication forks? A related question is the following. Assuming that the primary role of PCNA is to enhance processive DNA synthesis by Pol ε or Pol δ, how does the cell ensure that the polymerases do not frequently dissociate from PCNA? The 8-residue canonical PIPs only confer modest affinity for PCNA with Kds in the micromolar range. Therefore, for proteins such as DNA polymerases that should not dissociate from PCNA, additional surfaces of interaction must contribute to confer high affinity binding. Alternatively, multivalent

engagement of the PCNA homo-trimer would confer an increase in affinity. Remarkably, studies of yeast and human Pol δ showed that at least three subunits of Pol δ can engage PCNA simultaneously (Khandagale et al., 2020). Multivalent engagement of the three PCNA rings by a unique enzyme can also serve the important purpose of functionally dedicating a PCNA ring to a single enzyme.

A number of PCNA-dependent processes need to occur when a sufficient amount of double-stranded DNA has emerged from the replication machinery. For simplicity, we will refer to only three of those "*post-synthetic*" processes, namely mismatch repair (MMR), methylation of the newly synthesized strand catalyzed by DNMT1 and CAF-1-mediated deposition of H3-H4 onto nascent DNA. Those three processes need to occur on the chromatids produced by both leading and lagging strand synthesis. Various lines of evidence argue that the deposition of H3-H4 occurs very quickly onto nascent DNA. For instance, *S. cerevisiae* CAF-1 influences the length of Okazaki fragments (Smith and Whitehouse, 2012), suggesting that lagging strand synthesis is tightly coupled to H3-H4 deposition by CAF-1. This is disconcerting because the repair of errors made by replicative polymerases, known as mismatch repair (MMR), and the methylation of the nascent strands by DNMT1 are, at least *in vitro*, blocked when DNA is wrapped around the surface of histone octamers (Rodriges Blanko et al., 2016) (Felle et al., 2011; Okuwaki and Verreault, 2004). In addition, MMR cannot occur far behind the replication machinery. This is because discrimination between the error-free template strand and the error-containing nascent strand depends upon detection of nicks and/or 3'-ends in the nascent strand. The MMR machinery could not act selectively on the error-containing nascent strand if it were capable of operating at a long distance behind Pol δ and Pol ε. Based on the above, it would seem likely that MMR and DNA methylation need to occur before histone deposition onto

nascent DNA. Furthermore, these three PCNA-dependent processes might need to occur according to a specific sequence (for instance, MMR prior to DNA methylation prior to histone deposition).

This raises fascinating questions, only a handful of which are addressed here. Do PCNA dependent processes need to occur in a specific temporal order? If this has to be the case, would failure to complete an early event in the sequence prevent the execution of subsequent events? Are there multiple PCNA rings that are functionally specialized? More generally, if there are functionally distinct PCNA rings, how does each ring acquire the ability to pair with a specific PIP-containing binding partner given that all the partner proteins with PIPs occupy the same surface of PCNA (*i.e.* the hydrophobic surface located between the inter-domain connector loop and the underlying β-sheet)?

Although they are almost certainly simplistic, we propose three mechanisms to explain how CAF-1 can deposit H3-H4 onto DNA without interfering with replicative DNA polymerases (Pol δ or Pol ε).

4.1.2 Model 1: Multiple PCNA rings with specific and distinct functions

Given the sizes of Pol δ (composed of four subunits known as p125, p60, p50, and p12) and CAF-1 (three subunits known as p150, p60 and p48), it seems unlikely that these two proteins can be bound simultaneously to the same PCNA homo-trimeric ring. Although only two of them are depicted in Figure D.1A, this model therefore presumes that there are multiple PCNA rings present at each replication fork, and onto both the leading strand chromatid and the lagging strand chromatid.

The multiple PCNA rings are each dedicated to a specific function (*e.g.* DNA synthesis, mismatch repair, DNA methylation and nucleosome assembly. Molecular mechanisms to "*dedicate*" a PCNA ring to a specific function have been described (chapter 2, Discussion). In Figure D1.A, only two functionally distinct PCNA rings are depicted. The front ring (PCNA1, Figure D1.A) is the one that binds the DNA polymerase while the rear ring (PCNA2, Figure D1.A). All the PIPs contact the front face of PCNA (*i.e.* the side of the PCNA ring that faces the direction of DNA synthesis, as illustrated in Figure D1.A). Because the KER α-helix and the PIP are juxtaposed within the same α-helix, binding of the PIPs to the front face of PCNA2 would constrain the DNA-binding KER coiled-coil to extend along the DNA that separates the two PCNA rings: PCNA2 and PCNA1. In this scenario, the KER DNA-binding domain may serve as "*DNA length sensor*" that signals to CAF-1 when enough DNA (> 75bp) has emerged from the DNA polymerase to allow the productive deposition of H3-H4 onto nascent DNA and the formation $(H3\text{-}H4)_2$ tetramers that involves the participation of two CAF-1-H3-H4 complexes.

4.1.3 Model 2: Grabbing a PCNA ring from behind

Model 2 (Figure D1.B) is a variation on the theme that multiple PCNA rings with specific and distinct functions are present on both the leading and the lagging strand chromatid. Both rings face the direction of DNA synthesis, but the way in which CAF-1 interacts with PCNA is noticeably different than in model 1 (Figure D1.A). In model 2, the KER coiled-coil extends away from the PCNA2 ring and this is where H3-H4 will be ultimately deposited. Although harder to conceive, model 2 still permits the PIPs to bind to the front side of the PCNA ring provided that the coiled coil crosses through the central cavity of PCNA which, given the diameters of DNA, and that of a three-helix coiled-coil, is physically possible. Bivalent or trivalent engagement of the PCNA ring monomers is possible, but they would require splaying of

the coiled-coil over a suitable length. C-terminal splaying of coiled-coils to expose the constituent α-helices is not unprecedented (McNamara et al., 2008).

This model is different from model 1 in that the DNA-binding KER coiled coil is not located in-between the two rings (Figure D1.A and D1.B). Instead, the coiled-coil is pointing away from the PCNA2 ring dedicated to CAF-1-mediated nucleosome assembly (Figure D.1B). In model 2, the histones are deposited further away from the PCNA ring associated with DNA polymerase than in model (Figure D.1B versus D.1A), which may help in preventing functional interference between H3-H4 deposition onto DNA and DNA synthesis.

4.1.4 Model 3: Back-to-back PCNA rings that face opposite directions

Model 3 is based on a single publication (Naryzhny et al., 2005). The authors showed that formaldehyde, a chemical cross-linking agent, can stabilize the formation of double PCNA trimers (Naryzhny et al., 2005). Second, they showed that PCNA double trimers could not be detected when the PCNA overexpressed into cells carried a specific mutation (PCNA R5A or K110A) on the back side of PCNA (Naryzhny et al., 2005). This result was interpreted as implying that the two PCNA rings are organized in a back-to-back arrangement (Figure D.1C). In other words, the front PCNA ring (PCNA2) would face the direction of DNA synthesis, the rear PCNA ring (PCNA1) would face in the opposite direction. This is an elegant proposal that allows CAF-1 to interact with the front face of the rear PCNA ring (PCNA1, Figure D.1C) and, therefore, the deposition of H3-H4 onto nascent DNA can be physically segregated from DNA synthesis by Pol δ or Pol ε.

To their credit, the authors provided some evidence, not entirely compelling, that wild-type PCNA, but not PCNA-R5A/K110A that, consistent with back-to-back trimer model, Pol δ

was co-precipitated with CAF-1. Although it is not clear why this model has not attracted further attention from the authors or other research groups, their model is compatible with subsequent results, including ours, about CAF-1 and PCNA. Perhaps one of the numerous challenges to this model is that, although the clamp loader function of RFC has been studied for many years there is currently no evidence that RFC can load a PCNA ring facing the direction opposite to that of DNA synthesis. Having said that, it is not known whether researchers have designed experiments that could discriminate the orientation of PCNA rings relative to that of DNA synthesis or the opposite orientation. In addition, it is possible that alternative clamp loaders, Ctf18-RFC, Elg1-RFC or Rad24-RFC may be able to load PCNA clamps backward, *i.e.* facing away from direction of DNA synthesis. In any case, we prefer to keep an open mind, and retain this model as a possibility until further evidence for or against it is obtained.

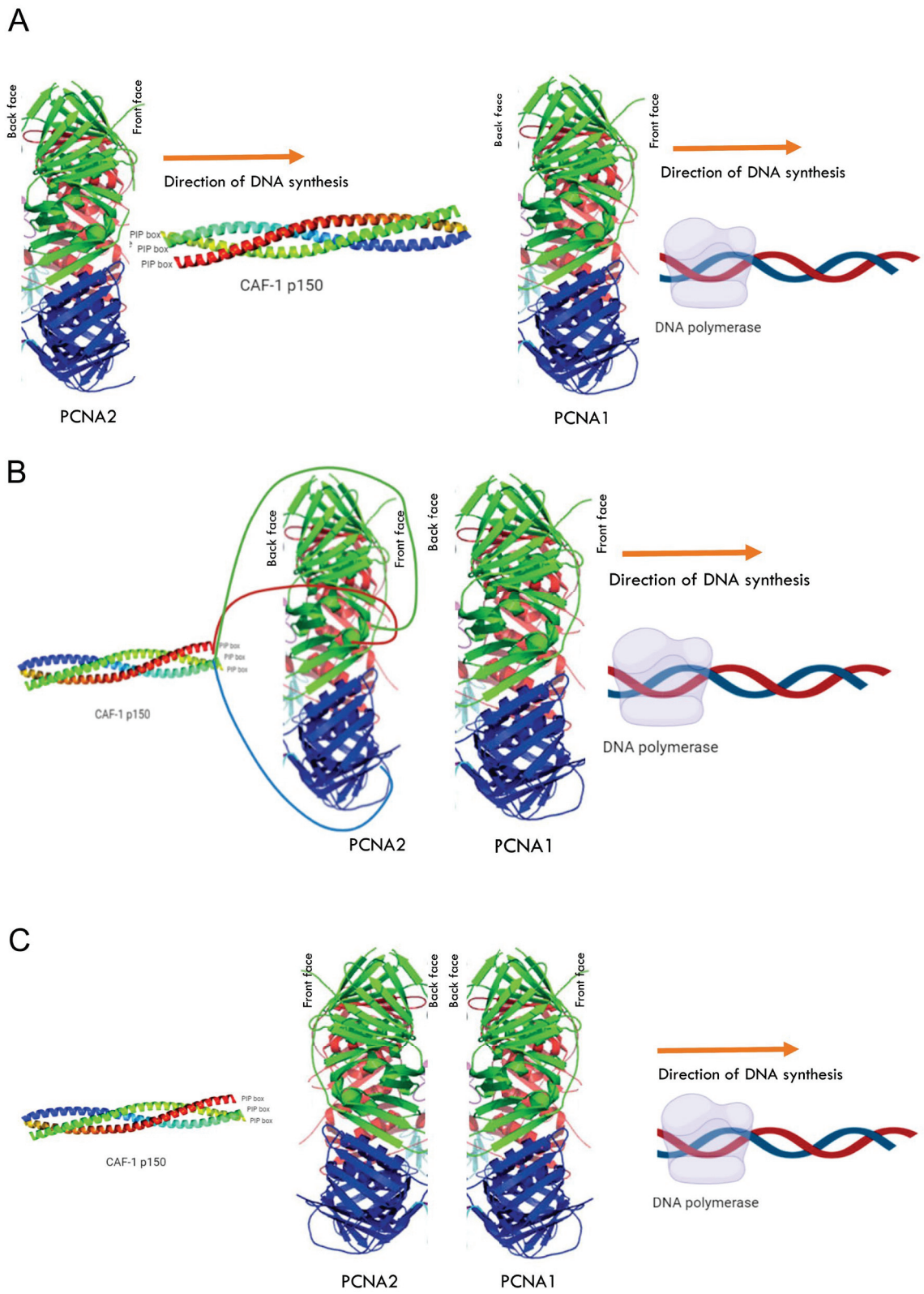
A
Back face
Front face
Direction of DNA synthesis
PIP box
PIP box
PIP box
CAF-1 p150
PCNA2
Back face
Front face
Direction of DNA synthesis
DNA polymerase
PCNA1
B
Back face
Front face
CAF-1 p150
PIP box
PIP box
PIP box
PCNA2
Back face
Front face
Direction of DNA synthesis
DNA polymerase
PCNA1
C
CAF-1 p150
PIP box
PIP box
PIP box
Front face
Back face
PCNA2
Back face
Front face
PCNA1
Direction of DNA synthesis
DNA polymerase

Fig. D.1

Figure D.1 Three models of interaction of chromatin assembly factor 1 with PCNA. Multiple PCNA rings present at each replication fork is indicated. The direction of DNA synthesis is indicated with the arrow pointing to the right.

4.2 Chapter 3 Discussion

Eukaryotic cells need to tightly control the synthesis and supply of new histones with the demand for histones generated by synthesis of new DNA in order to complete nucleosome assembly. While histone synthesis coordinated with passage through S-phase is essential for cell viability, excess histones are toxic to cells because they bind non-specifically to nucleic acids (RNA and DNA). As a result excess histones interfere with many processes that require access to genetic [*e.g.* transcription, DNA repair and mitotic chromosome segregation] (Gunjan and Verreault, 2003; Singh et al., 2010).

Yeast cells have evolved at least three distinct mechanisms to minimize the deleterious consequences of excess histones. These are the degradation of excess histone proteins (Gunjan and Verreault, 2003), the post-transcriptional degradation of histone mRNA (Campbell et al., 2002; Lycan et al., 1987; Reis and Campbell, 2007; Xu et al., 1990) and the transcriptional repression of histone genes (Eriksson et al., 2012)

Chapter 3 was focused on studies of the transcriptional repression of histone genes that is triggered by genotoxic agents that interfere with DNA replication.

4.2.1 Hpc2: "sensor" and/or "effector" of histone gene repression

In an effort to uncover a "sensor" of excess histone proteins produced under conditions that slow down DNA replication, we felt the need to define properties that such a sensor might

be expected to have. Cells that go through S-phase in the absence of histone H4 synthesis lose viability by the time they reach G2 (Kim *et al*., 1988). Thus, the sensor of excess histones should not be capable of triggering histone gene repression during normal passage through S-phase. Second, unless redundant with other proteins, the sensor(s) and downstream effector(s) [*e.g.* the protein(s) that directly act at histone gene promoters] should be essential for HU-induced histone gene repression. In addition, the sensor would be expected to bind histones, but only when they are present in excess (*e.g.* in response to HU, but not during a normal S-phase). We felt that the Hpc2 subunit of the HIR complex met all of these criteria. First, Hpc2 is degraded at the *cdc7* arrest point (prior to replication origin firing, Chapter 3, Figure 6), which might serve to minimize the probability that Hpc2 trigger histone gene repression inappropriately during normal S-phase. Second, untimely histone gene repression by Hpc2 is unlikely to occur because extensive Rad53-dependent phosphorylation of a surface of Hpc2 is required to trigger histone gene repression, and this phosphorylation cannot occur unless the kinase activity of Rad53 is turned on in response to DNA damage. In fact, Hpc2 is the only subunit of the HIR complex that is extensively phosphorylated. Third, S-phase cells contain chromatin assembly factors such as CAF-1 (Cac1, Cac2 and Cac3) whose subunits are 3- to 4-fold more abundant than the subunits of the HIR complex based on mass spectrometry (yeastgenome.org). CAF-1 is not only more abundant than HIR, but CAF-1 binds H3-H4 with very high affinity [Kd approximately 5 nM](Liu et al., 2016; Winkler et al., 2012). In striking contrast, the Kd of the UBN1 Hpc2-related domain (HRD) for H3.3-H4 dimers is approximately 7 μM [1,400-fold higher than the Kd for CAF-1 dissociation from H3-H4](Ricketts et al., 2015).

This is consistent with Hpc2 potentially serving as a sensor of excess histones because its vastly lower affinity for H3-H4 dimers would ensure that, in response to HU or MMS, CAF-1 would likely get saturated with excess histones before Hpc2 has an opportunity to bind excess H3-H4.

The fact that Hpc2 is unstable at the *cdc7* arrest point, and possibly early S-phase, does not rule out the possibility that Hpc2 may serve as a sensor of excess histones. Hpc2 may in fact be continuously synthesized and degraded. A result that may be consistent with this hypothesis is that when cells are released from G1 in the presence of HU, they accumulate high amounts of extensively phosphorylated Hpc2 (Chapter 3, Figure 7B). In addition, progressive synthesis, and accumulation of Hpc2 clearly occur as cells progress from early to late S-phase (Chapter 3, Figure 6C). Although these results are insufficient to conclude that Hpc2 is a likely sensor of excess histones, they make the model more plausible.

4.2.2 A simple model for genotoxic agent-induced histone gene repression

The HIR complex is a DNA replication-independent nucleosome assembly factor that incorporates H3-H4 within the nucleosome free regions commonly found in the promoters of actively transcribed genes (Amin et al., 2013). This is consistent with an alternative, but not mutually exclusive view of the role of Hpc2, namely as an "*effector*" of histone gene repression, rather than a "*sensor*" of excess histone proteins. A plausible, and readily testable model by which Hpc2 may serve as an effector of histone gene repression is depicted in Figure D.2. During normal progression through S-phase in the absence of DNA damage, histone gene transcription has to be active. For histone gene transcription to occur, the *UAS* elements that binds important transcriptional activators such as Spt10 must be accessible (Figure D.2A). When genotoxic agents such as HU or MMS activate the DDR in early S-phase, this causes a decrease

in the total rate of DNA synthesis and, as a result, an accumulation of excess histone proteins. A portion of excess histones H3-H4 may eventually bind to the Hpc2 subunit of the HIR complex (Figure D.2B, lower portion). When Hpc2 is bound to H3-H4, the replication-independent nucleosome assembly activity of the HIR complex, which can be likened to machinery that fills in nucleosome gaps in chromatin, may deposit histone H3-H4 onto histone gene promoters (Figure D.2B). In turn, the histones freshly deposited onto DNA may occlude the DNA binding sites of transcriptional activators, such as Spt10 and/or SBF and MBF, which ultimately might be forced to dissociate from the promoters. The dissociation of a key activator and the incorporation of a general repressor [$(H3\text{-}H4)_2$ tetramers or complete nucleosomes that contain H2A-H2B dimers], would eventually result in HU- or MMS-induced histone gene repression (Figure D.2B). Spt10, for instance, recognizes a 16-bp DNA binding site. Because of this, half of the DNA binding site would necessarily face the surface of the histone octamer or $(H3\text{-}H4)_2$ tetramer because of the superhelical ramp adopted by the DNA wrapped around histones. Under those conditions, the Spt10 binding site would almost certainly be occluded by the presence of histones. In other words, binding of Spt10 and histones are expected to be mutually exclusive.

4.2.3 Experimental approaches to test the model

This model is worth considering because it can be readily tested experimentally using a combination of Chromatin ImmunoPrecipitation (ChIP) and Micrococcal Nuclease (MNase) combined with DNA Sequencing (MNase-Seq). The two techniques can be applied to portions of the same cell population. MNase-Seq relies on the fact that MNase is both an endo- and exonuclease that can processively digest the so-called linker DNA that connects adjacent nucleosomes. Even in cases where certain transcription factors are bound to their DNA binding sites in a static manner, which seems to be the exception rather than the rule, the transcription

factors only protect short DNA fragments against MNase. These short fragments approximately correspond to the lengths of the DNA binding sites of each transcription factor. This is in striking contrast with $(H3\text{-}H4)_2$ tetramers and octamers that robustly protect 73-bp and 147-bp, respectively, against MNase. Based on this, one would expect that, when histone gene promoters are repressed, the *UAS* elements should be part of 73-bp or 147-bp DNA fragments that are strongly protected against MNase digestion (Dong and van Holde, 1991).

Conversely, when histone genes are actively transcribed, the Spt10 recognition sequences should not be part of 73-bp or 147-bp DNA fragments protected against MNase.

Spt10 and subunits of the HIR complex have all been localized to histone gene promoters based on ChIP (Eriksson *et al*, 2012). Therefore, it may be possible to tag Spt10 and a subunit of HIR with different epitopes in the strain used for MNase-Seq. Performing the two techniques on the same population would make it possible to correlate histone gene promoter repression with the presence of histones (tetramers or octamers) onto *UAS* elements, the presence of HIR (even if only transient could be frozen by the formaldehyde used in ChIP assays) and the absence of Spt10. Conversely, when histone genes are transcribed, one would predict that Spt10 will be bound to histone gene promoters, and histones and the HIR complex may be absent.

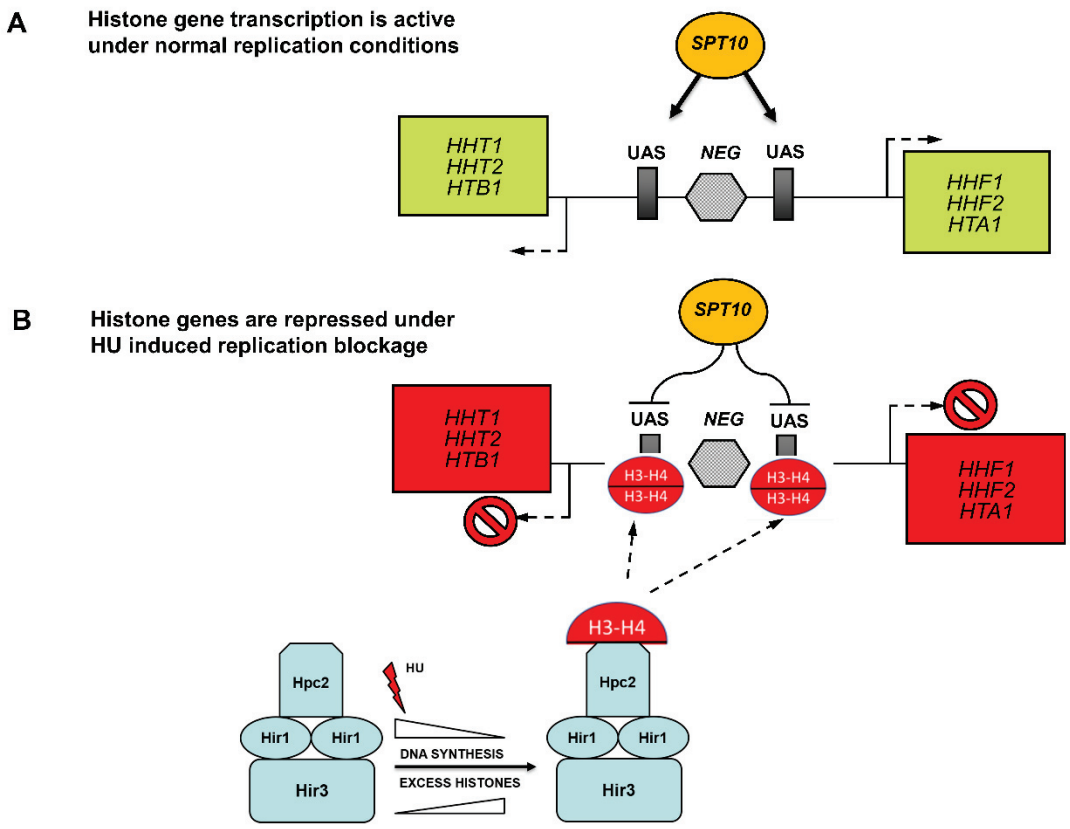

Figure D2

Figure D.2 Simple model for activation and repression of histone gene transcription. Active histone gene transcription indicated by green boxes is represented in A. Histone gene repression blocked under conditions that impede DNA replication is depicted by red boxes in B.

4.2.4 Conclusion and Summary

DNA replication which is fundamental to all the living cells is intimately associated with histone synthesis and chromatin assembly. The passage of replication fork causes duplication of parental DNA strands and subsequent reassembly of newly synthesized DNA, together with the supply of new and pre-existing histones. Any delay or defects affecting DNA replication or the subsequent

chromatin assembly events would eventually compromise the progression of cell cycle regulation and genomic integrity.

As alluded in the introductory chapters, the complexity of events at each DNA replication fork requires the concerted action of multiple replication enzymes. Proliferating cell nuclear antigen (PCNA) in addition to its primary role in increasing the processivity of replicative DNA polymerases, also act as a scaffold that recruits several other proteins involved in DNA replication and repair. For example, as the replication fork progresses; the discontinuously synthesized lagging strand needs to be acted upon by multiple enzymes like DNA polymerase δ, FEN-1 and DNA ligase1 and all these three enzymes need to bind PCNA through their respective PIPs to carry out their function. In addition, most other enzymes at the replication fork like CAF-1, DNMT1 and mismatch repair (MMR) proteins have dual roles on both leading and lagging strands. We were interested in understanding how diverse PCNA binding proteins mediate their interaction in perfect synchrony without functional interference. Through the second chapter of this thesis, we have shown an unprecedented mode of interaction between CAF-1 PIP and PCNA involving a cation-π interaction. We also validated the significance of this interaction through several biochemical and biophysical studies. Through secondary structure prediction algorithms, we also identified that CAF-1 PIP is located within the C-terminus of the KER domain that forms a long alpha helix. We also identified that the arrangement of KER domain followed by the PIP box was capable of forming a three-helix coiled-coil domain organization that can directly bind to PCNA. Our work also highlights the fact that further studies are necessary to clearly understand whether the long alpha helix we identified in CAF-1 p150 has a functional role as a DNA binder, bender, or ruler that brings about efficient histone deposition onto nascent DNA.

As stated earlier, DNA replication and histone synthesis in proliferating cells have to be tightly regulated to allow rapid nucleosome assembly behind the replication forks and also to prevent accumulation of excess histones. Through the third chapter of this thesis we have explored the molecular mechanism through which cells maintain this delicate balance between DNA and histone synthesis. We have uncovered a functional role for DNA damage response (DDR) kinases, namely Rad53 and Mec1/Tel1 in triggering repression of histone gene transcription. We have also shown that Hpc2 subunit of the HIR complex gets extensively phosphorylated upon DNA damage by genotoxic agents. We also propose a novel, elegant and testable negative feedback model for the mechanism of histone gene repression.

In this model, cells treated with genotoxic agents such as HU or MMS activates the DNA damage response (DDR) in early S-phase, which in turn cause a decrease in the total rate of DNA synthesis and as a result leads to an accumulation of excess histone proteins. We suspect that a portion these excess histones (H3-H4) may eventually bind to the Hpc2 subunit of the HIR complex. Subsequently, through the replication-independent nucleosome assembly activity of the HIR complex it deposits these histone onto histone gene promoters. This in turn occludes the DNA binding sites of transcriptional activators, such as Spt10 eventually resulting in an HU or MMS-induced histone gene repression. Though this model needs to be further tested in future experiments to obtain a comprehensive understanding of this regulation. Our studies presented in the Chapter 3 sheds light on the long-standing mechanism of histone gene repression and how cells maintain a fine balance between two biologically important processes of DNA replication and histone synthesis.

References Chapter 4

Amin, A.D., N. Vishnoi, and P. Prochasson. 2013. A global requirement for the HIR complex in the assembly of chromatin. *Biochim Biophys Acta*. 1819:264-276.

Campbell, S.G., M. Li Del Olmo, P. Beglan, and U. Bond. 2002. A sequence element downstream of the yeast HTB1 gene contributes to mRNA 3' processing and cell cycle regulation. *Mol Cell Biol*. 22:8415-8425.

Dong, F., and K.E. van Holde. 1991. Nucleosome positioning is determined by the (H3-H4)2 tetramer. *Proc Natl Acad Sci U S A*. 88:10596-10600.

Eriksson, P.R., D. Ganguli, V. Nagarajavel, and D.J. Clark. 2012. Regulation of histone gene expression in budding yeast. *Genetics*. 191:7-20.

Felle, M., H. Hoffmeister, J. Rothammer, A. Fuchs, J.H. Exler, and G. Langst. 2011. Nucleosomes protect DNA from DNA methylation in vivo and in vitro. *Nucleic Acids Res*. 39:6956-6969.

Gunjan, A., and A. Verreault. 2003. A Rad53 kinase-dependent surveillance mechanism that regulates histone protein levels in S. cerevisiae. *Cell*. 115:537-549.

Khandagale, P., S. Thakur, and N. Acharya. 2020. Identification of PCNA-interacting protein motifs in human DNA polymerase delta. *Biosci Rep*. 40.

Liu, W.H., S.C. Roemer, Y. Zhou, Z.J. Shen, B.K. Dennehey, J.L. Balsbaugh, J.C. Liddle, T. Nemkov, N.G. Ahn, K.C. Hansen, J.K. Tyler, and M.E. Churchill. 2016. The Cac1 subunit of histone chaperone CAF-1 organizes CAF-1-H3/H4 architecture and tetramerizes histones. *eLife*. 5.

Lycan, D.E., M.A. Osley, and L.M. Hereford. 1987. Role of transcriptional and posttranscriptional regulation in expression of histone genes in Saccharomyces cerevisiae. *Mol Cell Biol*. 7:614-621.

McNamara, C., A.S. Zinkernagel, P. Macheboeuf, M.W. Cunningham, V. Nizet, and P. Ghosh. 2008. Coiled-coil irregularities and instabilities in group A Streptococcus M1 are required for virulence. *Science*. 319:1405-1408.

Naryzhny, S.N., H. Zhao, and H. Lee. 2005. Proliferating cell nuclear antigen (PCNA) may function as a double homotrimer complex in the mammalian cell. *J Biol Chem*. 280:13888-13894.

Okuwaki, M., and A. Verreault. 2004. Maintenance DNA methylation of nucleosome core particles. *J Biol Chem*. 279:2904-2912.

Reis, C.C., and J.L. Campbell. 2007. Contribution of Trf4/5 and the nuclear exosome to genome stability through regulation of histone mRNA levels in Saccharomyces cerevisiae. *Genetics*. 175:993-991010.

Ricketts, M.D., B. Frederick, H. Hoff, Y. Tang, D.C. Schultz, T. Singh Rai, M. Grazia Vizioli, P.D. Adams, and R. Marmorstein. 2015. Ubinuclein-1 confers histone H3.3-specific-binding by the HIRA histone chaperone complex. *Nat Commun*. 6:7711.

Rodriges Blanko, E., L.Y. Kadyrova, and F.A. Kadyrov. 2016. DNA Mismatch Repair Interacts with CAF-1- and ASF1A-H3-H4-dependent Histone (H3-H4)2 Tetramer Deposition. *J Biol Chem*. 291:9203-9217.

Singh, R.K., D. Liang, U.R. Gajjalaiahvari, M.-H.M. Kabbaj, J. Paik, and A. Gunjan. 2010. Excess histone levels mediate cytotoxicity via multiple mechanisms. *Cell cycle*. 9:4236-4244.

Smith, D.J., and I. Whitehouse. 2012. Intrinsic coupling of lagging-strand synthesis to chromatin assembly. *Nature*. 483:434-438.

Winkler, D.D., H. Zhou, M.A. Dar, Z. Zhang, and K. Luger. 2012. Yeast CAF-1 assembles histone (H3-H4)2 tetramers prior to DNA deposition. *Nucleic Acids Res*. 40:10139-10149.

Xu, H.X., L. Johnson, and M. Grunstein. 1990. Coding and noncoding sequences at the 3' end of yeast histone H2B mRNA confer cell cycle regulation. *Mol Cell Biol*. 10:2687-2694.